

# **IsoDNA/isoRNA oligomers of the thrombin binding aptamer and 2'-thiopropyl and abasic ethanediol substitutions therein**

by

**Atish A. Wagh**  
**10CC16A26018**

A thesis submitted to the  
Academy of Scientific & Innovative Research  
for the award of the degree of  
**DOCTOR OF PHILOSOPHY**  
in  
**SCIENCE**

Under the supervision of  
**Dr. Moneesha Fernandes**



**CSIR-National Chemical Laboratory, Pune**



Academy of Scientific and Innovative Research  
AcSIR Headquarters, CSIR-HRDC campus  
Sector 19, Kamla Nehru Nagar,  
Ghaziabad, U.P. – 201 002, India

**November 2021**

## Certificate

This is to certify that the work incorporated in this Ph.D. thesis entitled, "IsoDNA/isoRNA oligomers of the thrombin binding aptamer and 2'-thiopropyl and abasic ethanediol substitutions therein", submitted by Atish A.Wagh to the Academy of Scientific and Innovative Research (AcSIR) in fulfillment of the requirements for the award of the Degree of Doctor of Philosophy in Sciences, embodies original research work carried-out by the student. We, further certify that this work has not been submitted to any other University or Institution in part or full for the award of any degree or diploma. Research material(s) obtained from other source(s) and used in this research work has/have been duly acknowledged in the thesis. Image(s), illustration(s), figure(s), table(s) etc., used in the thesis from other source(s), have also been duly cited and acknowledged.

Signature of Student

Atish A. Wagh

Date: 23-Nov-2021


Signature of Supervisor

Dr. Moneesha Fernandes

Date: 23-Nov-2021

## STATEMENTS OF ACADEMIC INTEGRITY

I Atish A.Wagh, a Ph.D. student of the Academy of Scientific and Innovative Research (AcSIR) with Registration No. 10CC16A26018 hereby undertake that, the thesis entitled IsoDNA/isoRNA oligomers of the thrombin binding aptamer and 2'-thiopropyl and abasic ethanediol substitutions therein has been prepared by me and that the document reports original work carried out by me and is free of any plagiarism in compliance with the UGC Regulations on "Promotion of Academic Integrity and Prevention of Plagiarism in Higher Educational Institutions (2018)" and the CSIR Guidelines for "Ethics in Research and in Governance (2020)".

  
**Signature of the Student**

Date : 23-Nov-2021

Place : Pune

---

It is hereby certified that the work done by the student, under my/our supervision, is plagiarism-free in accordance with the UGC Regulations on "Promotion of Academic Integrity and Prevention of Plagiarism in Higher Educational Institutions (2018)" and the CSIR Guidelines for "Ethics in Research and in Governance (2020)".

  
**Signature of the Supervisor**

Name : Dr. Moneesha Fernandes

Date : 23-Nov-2021

Place : Pune

*To*  
*Family*



## *Acknowledgments*

I am incredibly grateful to my research supervisor, Dr. Moneesha Fernandes, for her valuable advice, continuous support, and patience throughout my Ph.D. study. Her vast knowledge and wealth of experience have aided me throughout my doctoral study and daily life. I especially thank her freedom in allowing me to think and plan experiments.

I would like to thank Dr. Vaijayanti Kumar for her valuable guidance during my Ph.D. I am very inspired by her thorough understanding of the subject, which motivates me to keep my knowledge up to date while also remembering the fundamentals.

I would like to thank my Doctoral Advisory Committee Members, Dr. Bhagavatula Prasad, Dr. G. J. Sanjayan, and Dr. Vaijayanti Kumar, for giving me timely feedback on my progress and helpful advice throughout my work.

I gratefully acknowledge Dr. Manisha, and Dr. Namrata for teaching me to operate the DNA synthesizer and other instruments for oligonucleotide study. I am grateful to my seniors and lab mates, Dr. Tanaya, Dr. Govind, Dr. Amit, Dr. Ragini, Harsha, Komal, Aniket, Sanyami, for their kind co-operation in keeping a funny and cheerful atmosphere in the lab. I would also like to thank Mr. Bhumkar and Mr. Gurav for the laboratory assistance, especially Mr. Gurav for helping me shift the lab.

I would especially like to thank Harsha for her help, unconditional support and thank Dr. Manisha and Dr. Ganesh for the encouragement during the challenging periods of Covid 19 lockdown and making the lab a pleasant place to work.

I am very thankful to the NMR group, especially Dr. Sapna, for her oligomer NMR analysis and guidance. I am thankful for the support provided by Dr. Santhakumari and group members for MALDI-TOF and HRMS analysis. I would like to thank Shubhra for her simple way of explaining tedious mathematical calculations and Dr. Pankaj Poddar and Monika for helping with Raman Spectroscopy.

I am thankful to Mr. Gati Nayak, who performed the plagiarism evaluation of my thesis quickly and professionally. I would like to thank the Student Academic Office, particularly Komal, Vijaya, and Vaishali, for support in the time-consuming documentation process required to complete the degrees.

I extend my sincere thanks to the Director, Head of Organic Chemistry Division, for their kind help and encouragement during this work. I am grateful to the UGC, New Delhi for awarding me a research fellowship, as well as the Academy of Scientific and Innovative Research (AcSIR).

I would like to thank my friends Anna, Balu, Navnath, Deepak, Kailash, and Sagar for the peaceful and joyful environment in the room, and my seniors who directly or indirectly supported me during NET, GATE, SET exam preparation. I extend huge thanks to my friends Alok, Dinesh, and my group for their kind presence and support.

I would especially like to thank my parents for always being a source of encouragement. Without knowing much about what I am doing, their good wishes were always there with me. I would like to express my gratitude to my brother, sister and Chandrakant for their support. I would like to thank my wife, Poonam, for understanding the value of my work and for her unwavering patience and support, also thank my son, Aayush, whose cute smile always fills me energetic.

I would like to genuinely thank the efforts of all the people whom I may have missed to acknowledge here. My gratitude to everyone who have inspired me during this doctoral journey.

Lastly, praises and thanks to God, the Almighty, for His showers of blessings that allowed me to carry out my doctoral work smoothly and successfully.

Atish A. Wagh

<b>A</b>			
A	Absorbance	DMF	<i>N, N</i> -dimethylformamide
A	Adenine	DMSO	Dimethyl sulfoxide
Ac <sub>2</sub> O	Acetic anhydride	DNA	Deoxyribonucleic acid
ACN	Acetonitrile	<b>E</b>	
AcOH	Acetic acid	EDTA	Ethylenediaminetetraacetic acid
aq.	Aqueous	EtOH	Ethanol
<b>B</b>		EtOAc	Ethyl acetate
BPB	Bromo phenol blue	<b>G</b>	
<b>C</b>		g	gram
C	Cytosine	G	Guanine
Calc.	Calculated	<b>H</b>	
Cat.	Catalytic/catalyst	h	Hours
CD	Circular Dichroism	HPLC	High Performance Liquid Chromatography
Conc.	Concentrated	Hz	Hertz
CPG	Controlled Pore Glass	HRMS	High Resolution Mass Spectrometry
<b>D</b>		<b>L</b>	
DEPT	Distortion less Enhancement by Polarization Transfer	L	Liter
ds	Double stranded	LNA	Locked nucleic acid
EDTA	Ethylenediaminetetraacetic acid	<b>M</b>	
DCM	Dichloromethane	MALDI-TOF	Matrix Assisted Laser Desorption Ionization-Time Of Flight
DMTr-Cl	4, 4'-dimethoxytrityl chloride	MeOH	Methanol
DIPEA	Diisopropylethylamine	mg	Milligram
DMAP	4',4'-Dimethylaminopyridine	MHz	Megahertz

min	Minutes	ss	Single stranded
M	Molar	s	Second
ml	Milliliter	S-type	South type
mM	Millimolar	SVPD	Snake Venom Phosphodiesterases
mmol	Millimoles		<b>T</b>
MS	Mass spectrometry	T	Thymine
MW	Molecular weight	TBA	Thrombin binding aptamer
	<b>N</b>	TEAA	Triethyl ammonium acetate
N-type	North type	TEA/Et <sub>3</sub> N	Triethylamine
NMR	Nuclear Magnetic Resonance	THAP	2',4',6'-trihydroxyacetophenone
	<b>O</b>	TLC	Thin layer chromatography
Obsd	Observed	TNA	$\alpha$ -L-Threose nucleic acid
ONs	Oligonucleotides	<i>T<sub>m</sub></i>	Melting temperature
	<b>P</b>		<b>U</b>
PO	Phosphodiester-oligomer	U	Uracil
PS	Phosphorothioate-oligomer	UNA	Unlocked nucleic acid
Py	Pyridine	UV-Vis	Ultraviolet-Visible
PNA	Peptide Nucleic Acid		
Pet-ether	Petroleum ether		
	<b>R</b>		
RNA	Ribose Nucleic Acid		
RP	Reversed Phase		
rt	Room temperature		
RP-HPLC	Reversed Phase-HPLC		
	<b>S</b>		



- All the reagents were purchased from Sigma-Aldrich and used without further purification.
- DMF, ACN, were dried over P<sub>2</sub>O<sub>5</sub> and CaH<sub>2</sub> respectively and stored by adding 4 Å Molecular sieves. Pyridine, TEA were dried over KOH and stored on KOH.
- Reactions were monitored by TLC. TLCs were run in either Petroleum ether with appropriate quantity of EtOAc or DCM with an appropriate quantity of MeOH for most of the compounds. TLC plates were visualized with UV light and/or by spraying perchloric acid solution and heating.
- Usual reaction work up involved sequential washing of the organic extract with water and brine followed by drying over anhydrous Na<sub>2</sub>SO<sub>4</sub> and evaporation of the solvent under vacuum.
- Column chromatographic separations were performed using silica gel 60-120 mesh (Merck) or 200- 400 mesh (Merck) and using the solvent systems
- <sup>1</sup>H and <sup>13</sup>C NMR spectra were obtained using Bruker AC-200, AC-400, AC-500 and AC-700 NMR spectrometers. <sup>1</sup>H NMR data are reported in the order of chemical shift, multiplicity (s, singlet; d, doublet; t, triplet; br, broad; m, multiplet and/ or multiple resonance), number of protons.
- Mass spectra were recorded on a Q Exactive Hybrid Quadrupole Orbitrap Massspectrometer (Thermo Fisher Scientific).
- DNA oligomers were synthesized on CPG solid support using Bioautomation MerMade 4 synthesizer. The 2'-deoxy-3'-phosphoramidites were obtained from ChemGenes and 3'-deoxy-2'-phosphoramidites from Glen Research. Universal columns procured from Bioautomation.

- RP-HPLC on C-18 column using Waters system (waters Delta 600e quaternary solvent delivery system, 2998 photodiode array detector and Empower2 chromatography software)
- MALDI-TOF spectra were recorded on a SCIEX TOF/TOF 5800 system, and the matrix used for analysis was THAP (2, 4, 6-trihydroxyacetophenone) /Ammonium citrate (2:1).
- UV experiments were carried out on a Analytik Jena SPECORD® 200 plus spectrometer equipped with a Peltier-controlled cell holder.
- CD spectra were recorded on a Jasco J-815 spectropolarimeter equipped with a Peltier-controlled cell holder.

# Contents

Abbreviations.....	i
General remarks.....	iii

## Chapter 1

### **Introduction to nucleic acids, G-quadruplexes, and the Thrombin binding aptamer**

1. General introduction to nucleic acids .....	1
1.1 Nucleic acid components.....	1
1.2 Structural polymorphism.....	1
1.2.1 Duplex DNA.....	1
1.2.2 Triplex DNA .....	2
1.2.3 Guanine quadruplex (G4) structures.....	2
1.3 Sugar conformation preferences in nucleotides .....	3
1.3.1 Steric effect.....	3
1.3.2 Anomeric effect.....	4
1.3.3 Gauche effect.....	4
1.4 Sugar ring conformations in DNA/RNA vs IsoDNA/IsoRNA.....	5
1.5 G-quadruplex structures .....	5
1.5.1 G-quartets.....	6
1.5.2 G-quadruplex loops.....	6
1.5.3 Alignment of strands.....	6
1.5.4 Inter- and Intra-molecular G-quadruplexes.....	7

1.6 G-quadruplex topology and stability dependence on metal ions.....	7
1.6.1 Monovalent cations and G-quadruplexes.....	8
1.6.2 Divalent cations and G-quadruplexes.....	8
1.7 SELEX .....	8
1.8.1 Aptamers forming G-quadruplexes.....	9
1.8.2 Thrombin binding aptamer.....	9
1.9 Thrombin binding aptamer and its modification.....	10
1.9.1 Modifications in the G tetrads.....	10
1.9.2 Modifications in the loops.....	11
1.9.3 Sugar modification.....	13
1.9.4 Linkage modification.....	15
1.10 TBA- Thrombin interaction.....	16
1.11 Solid-phase synthesis of oligonucleotides.....	17
1.12 Tools and techniques studies of G-quadruplexes.....	19
1.12.1 UV-spectroscopy.....	19
1.12.2 Circular Dichroism (CD) .....	20
1.12.3 Raman Spectroscopy.....	21
1.12.4 Polyacrylamide gel electrophoresis (PAGE) .....	21
1.12.5 MALDI TOF Mass Spectrometry.....	21
1.12.6 High-performance liquid chromatography (HPLC) .....	22
1.13 Present work.....	23
1.14 References .....	25

## Chapter 2

### **Effect of alkali and alkaline earth metal cations on the isoTBA quadruplex: Application to the detection of Sr<sup>2+</sup>**

2.1 Introduction.....	36
2.2 Rationale and objectives of the present work.....	37
2.3 Results and discussion.....	38
2.3.1 Synthesis of TBA, <i>iso</i> TBA oligomers, their purification and characterization. ....	38
2.3.2 Circular dichroism spectroscopy studies of TBA, <i>iso</i> TBA for evaluation of G-quadruplex formation and topology.....	38
2.3.3 Evaluation of G-quadruplex thermal stability.....	40
2.3.4 G-quadruplex topology study by UV-Thermal Difference Spectra.....	41
2.3.5 Molecularity of the <i>iso</i> TBA-Sr <sup>2+</sup> quadruplex.....	42
2.4 Polyacrylamide Gel Electrophoresis (PAGE) study.....	44
2.5 <sup>1</sup> H NMR study.....	44
2.6 CD saturation binding curves for TBA and <i>iso</i> TBA with K <sup>+</sup> and Sr <sup>2+</sup> .....	45
2.7 <i>iso</i> TBA for the detection of Sr <sup>+2</sup> ions.....	46
2.8 Calculation of detection limit.....	47
2.9 Anti-Clotting activity study.....	48
2.10 Conclusions.....	48
2.11 Experimental.....	49
2.11.1 Oligonucleotides synthesis, Purification and characterization.....	49
2.11.2 Gel electrophoresis.....	49
2.11.3 CD experiments.....	49
2.11.4 Calculation of detection limit.....	50
2.11.5 UV experiments.....	50
2.11.6 NMR experiments.....	50

2.11.7 Anti-Clotting activity experiments.....	51
2.12 Appendix A.....	51
2.13 References.....	53

## Chapter 3

### **Iso-rTBA: the 2'-5'-linked functional RNA equivalent of the Thrombin binding aptamer**

3.1 Introduction.....	57
3.2 Rationale and objectives of the present work.....	57
3.3 Synthesis of TBA, iso-rTBA Oligomers, their purification and characterization.....	59
3.4 G-quadruplex formation and topology using circular dichroism spectroscopy.....	59
3.4.1 G-quadruplex thermal stability evaluation by circular dichroism .....	60
3.5 UV-Thermal Difference Spectra (TDS) and TDS factors.....	61
3.6 Hysteresis and concentration-dependence studies.....	62
3.7 NMR Study.....	63
3.8 Thrombin binding study.....	65
3.9 CD saturation binding curves for TBA and iso-r-TBA with thrombin.....	66
3.10 Anti-clotting Study.....	67
3.11 Nuclease stability study.....	68
3.11.1 Stability to RNase A.....	68
3.11.2 Stability to snake venom phosphodiesterase (SVPD) .....	69
3.12 Conclusions.....	70
3.13 Experimental .....	70
3.13.1 Oligonucleotide synthesis, purification and characterization.....	70
3.13.2 HPLC analysis.....	71

3.13.3 CD experiments.....	71
3.13.4 UV experiments .....	71
3.13.5 NMR experiments.....	72
3.13.6 Anticlotting measurements.....	72
3.13.7 Stability of oligonucleotides to cleavage by RNase A.....	72
3.13.8 SVPD stability study.....	72
3.14 Appendix B.....	73
3.15 References.....	75

## Chapter 4

### **Replacement of loop residues in TBA by an abasic ethylene glycol spacer: Effect on stability, structure and function**

4.1 Introduction.....	78
4.2 Rationale and objectives of the present work.....	78
4.3 Synthesis of ethylene glycol spacer phosphoramidite.....	79
4.4 Synthesis of TBA, and modified TBA oligomers, their purification and characterization.....	80
4.5 G-quadruplex formation and stability by circular dichroism spectroscopy.....	80
4.6 Raman spectroscopy.....	82
4.7 G-quadruplex thermal stability using UV and CD spectroscopy.....	83
4.8 Evaluation of G-quadruplex topology by UV-Thermal Difference Spectra (TDS) .....	84
4.9 Nuclease stability study.....	85
4.9.1 Endonuclease stability.....	85
4.9.2 Serum stability study.....	86
4.10 Thrombin binding and inhibition.....	86
4.11 Conclusions.....	88

4.12 Experimental section .....	88
4.12.1 Synthetic procedures and spectral data.....	88
4.12.2 Synthesis of oligonucleotides.....	90
4.12.3 CD Experiments.....	90
4.12.4 Raman measurements.....	90
4.12.5 UV experiments .....	91
4.12.6 Nuclease stability study.....	91
4.12.7 Thrombin time assay.....	92
4.13 Appendix C.....	92
4.14 References.....	98

## Chapter 5

### **Synthesis of 2'-thiopropyl thymidine nucleoside, conformation studies, and incorporation into the Thrombin binding aptamer (TBA)**

5.1 Introduction.....	101
5.2 Rationale, design and objectives of the present work.....	102
5.3 Synthesis of 2'-thiopropyl-thymidine phosphoramidite .....	103
5.4 Study of sugar pucker using $^1\text{H}$ NMR $J_{1'2'}$ coupling constant.....	104
5.5 Synthesis of TBA and modified TBA variants, their purification and characterization.....	105
5.6 G-quadruplex formation and stability.....	106
5.6.1 G-quadruplex topology .....	106
5.6.2 G-quadruplex thermal stability using UV Spectroscopy .....	106
5.6.3 G-quadruplex in the presence of thrombin .....	107
5.7 Antithrombin effect of modified aptamers.....	108



5.8 Snake venom phosphodiesterase (SVPD) stability.....	109
5.9 Conclusions.....	110
5.10 Experimental section.....	110
5.10.1 Experimental procedures and spectral data.....	110
5.10.2 Oligonucleotide synthesis.....	113
5.10.3 Purification and characterization.....	113
5.10.3.1 High-performance liquid chromatography.....	113
5.10.3.2 MALDI-TOF characterization.....	113
5.10.4 CD spectroscopy experiments.....	114
5.10.5 UV experiments .....	114
5.10.6 SVPD stability experiments.....	114
5.10.7 Thrombin time measurements for antithrombin effect.....	115
5.11 Appendix D .....	115
5.12 References.....	126

<b>Appendix</b>
-----------------

Abstract.....	129
List of Posters.....	130
List of Publications.....	131

**ABSTRACT****Name of the Student:** Atish A Wagh**Registration No.:** 10CC16A26018**Faculty of Study:** Chemical Science**Year of Submission:** 2021**AcSIR academic centre/CSIR Lab:****Name of the Supervisor:** Dr. Moneesha Fernandes

CSIR-National Chemical Laboratory, Pune

**Title of the thesis:** IsoDNA/isoRNA oligomers of the thrombin binding aptamer and 2'-thiopropyl and abasic ethanediol substitutions therein

The Thrombin Binding Aptamer (TBA), a 15mer DNA sequence was reported in 1992 that folds into a quadruplex containing two G(syn): G(anti): G(syn): G(anti) quartets and three lateral loops. It was identified through the SELEX procedure and preferentially binds to thrombin (an enzyme involved in blood coagulation). TBA is a potent anticoagulant in vitro, with a short half-life in vivo. Its anticoagulant properties make it an excellent choice for surgeries. Currently used anticoagulants such as Heparin, Warfarin (Coumadin), Rivaroxaban (Xarelto), Dabigatran (Pradaxa), Enoxaparin (Lovenox), etc., cause side effects such as red or pink-colored urine, stools that are bloody, more bleeding than average during a menstrual period, blackish areas in fingers, toes, hands or feet, that can be avoided with the use of TBA as an anticoagulant. Chapter 1 gives a quick overview of nucleic acids, nucleosides structural preference, types of G-quadruplexes, TBA and topology of TBA. It also mentions the research being done to produce novel TBA derivatives by modification of the sugar, nucleobase, phosphate or inter-nucleoside linkage, to result in better thermal- and enzymatic stability and anticoagulant activity. In Chapter 2, the effect of various alkali and alkaline earth metal cations on the G-quadruplex-forming ability of isoTBA is studied, and its ability to detect Sr<sup>2+</sup> ions is elucidated. In Chapter 3, we show that iso-rTBA, with a 2'-5'-linked backbone, is able to fold into an antiparallel G-quadruplex, unlike most RNA quadruplexes (including rTBA), that adopt a parallel topology. Further, this stable unimolecular antiparallel iso-rTBA quadruplex is able to inhibit clotting, similar to TBA, and also resist degradation by nucleases. In Chapter 4, a 2-carbon E- spacer is reported, and we show that single replacements of loop residues by this E-spacer in TBA are tolerated better than two. Although a beneficial effect on the nuclease stability and half-life of the oligomers was observed, and anti-coagulant activity was reasonably good, the thermal stability of the resulting quadruplexes was adversely affected. In Chapter 5 we describe the synthesis of 2'-thiopropyl thymidine phosphoramidite, and incorporation into selected loop positions of TBA. TBA variants were found to be able to form antiparallel G-quadruplexes, with a beneficial effect on the nuclease stability and half-life. Moderate anti-clotting activity was observed, though lower than TBA.

# **Chapter 1**

**Introduction to**

**Nucleic acids, G-quadruplexes**

**and**

**the Thrombin binding aptamer**

## 1.1 General introduction to nucleic acids

### 1.1.1 Nucleic acid components

Nucleotides are fundamental units that are interconnected by phosphodiester covalent bonds and make up nucleic acids. Nucleotides in turn comprise a nucleobase which is covalently linked by a glycosidic bond, a phosphate group and pentose sugar (Figure 1). DNA and RNA are the two classes of nucleic acids present that contain purine and pyrimidine nitrogenous bases Adenine (A), Thymine (T), Cytosine (C), and Guanine (G) in case of DNA, whereas, for RNA, Thymine is replaced by Uracil (U). Although both DNA and RNA contain a pentose sugar, it is 2'-deoxy-D-ribose in the case of DNA, and D-ribose in RNA.

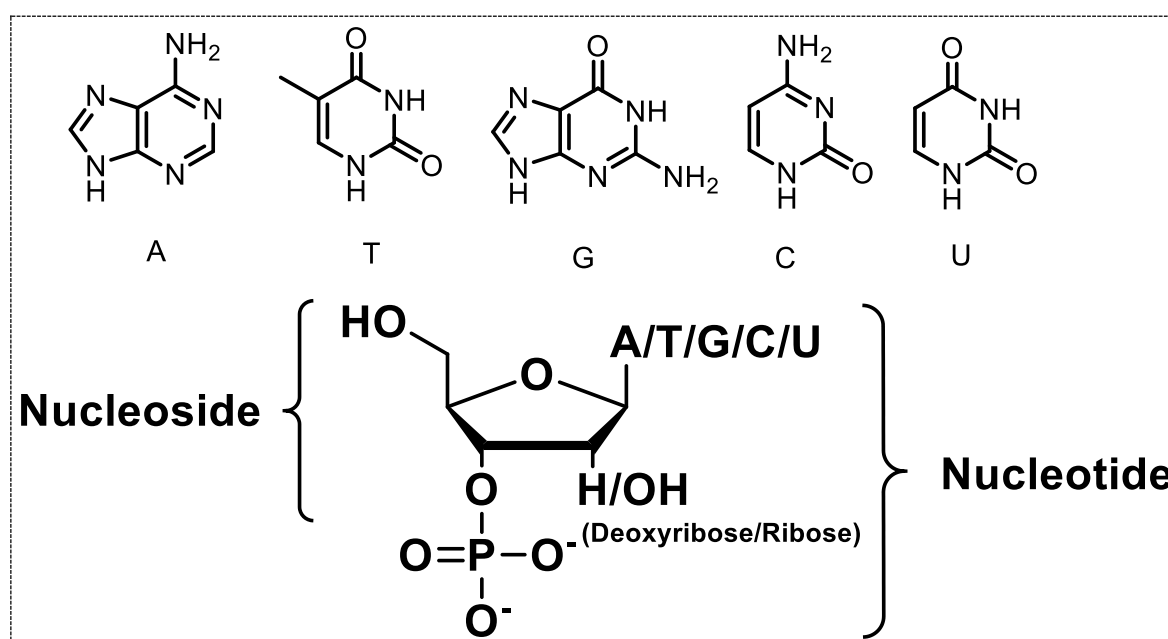


Figure 1: Nucleic acid components.

## 1.2 Structural polymorphism

### 1.2.1 Duplex DNA

DNA as a double-helical structure was elucidated by J. Watson and F. Crick in 1953.<sup>1</sup> Two anti-parallel strands that are held together by complementary base pairing *via* hydrogen bonds give rise to this double-helical nature of DNA. Complementary base pairing is seen between C-G and A-T bases, and base-pairs are stacked on top of each other due to  $\pi$ - $\pi$  interaction (Figure 2). Additionally, the sugar is puckered in two major conformations- *C2'*- and *C3'*-*endo*. In the *C2'*-*endo* conformation, the nucleobase adopts an *anti*-conformation arrangement, while the *C3'*-*endo* conformation usually implies a *syn* conformation about the glycosidic bond.

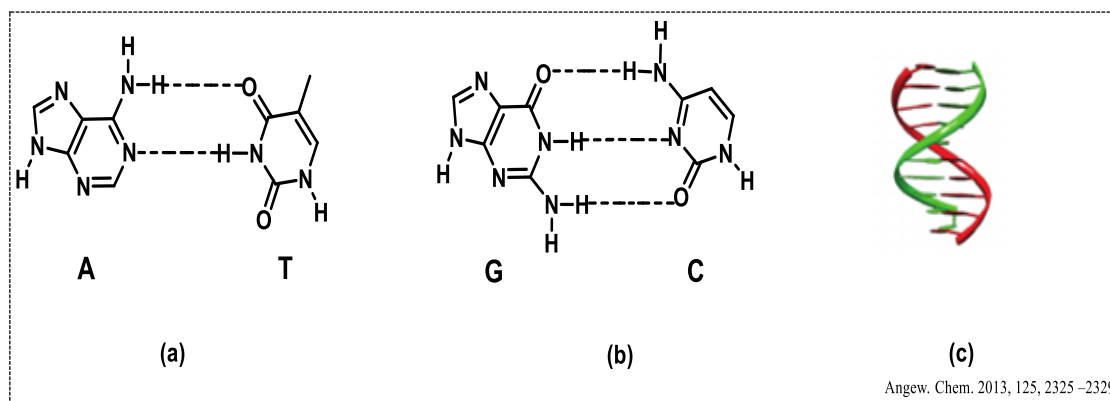


Figure 2: a) A: T and b) G: C base pairing of nucleotides within a DNA duplex, c) Duplex DNA.<sup>2</sup>

### 1.2.2 Triplex DNA

A triple helix form of DNA was first observed by Felsenfeld *et al.*<sup>3</sup> in 1957 (Figure 3c). This form of DNA is seen when a third strand gets incorporated in the major groove of a duplex. An uneven double helix where one strand is pyrimidine-rich while the other is purine-rich, favors the formation of a triple-helical DNA as the third strand, via H-bonding, and recognizes the purine-rich strand through non-canonical base pairing. This non-canonical base pairing was first explained by Karst Hoogsteen through X-ray diffraction and came to be known as ‘Hoogsteen’ hydrogen bonding<sup>4</sup> (Figure 3a-b).

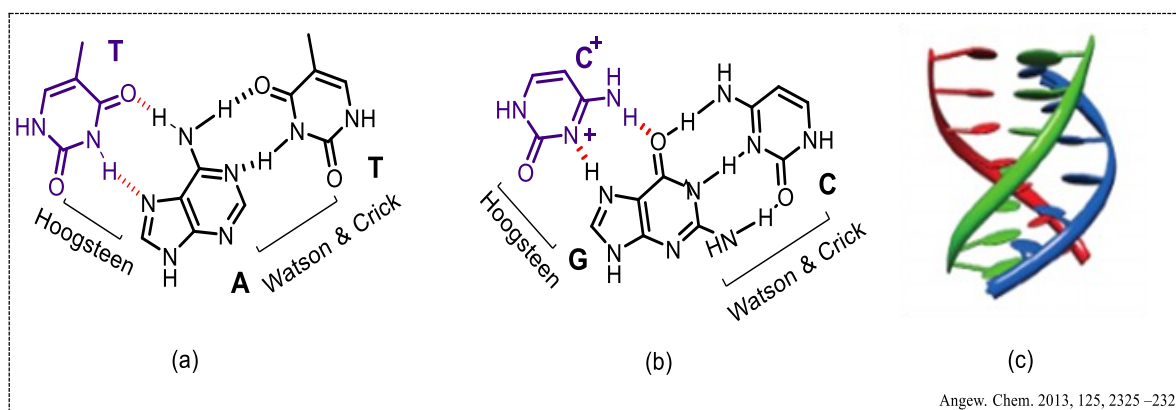


Figure 3: a) T:A:T and b) C:G:C Base pairing of nucleotides within a DNA triplex c) Triplex DNA.<sup>2</sup>

### 1.2.3 Guanine quadruplex (G4) structures

Guanine-rich DNA sequences can undergo another type of non-canonical base pairing involving 4 guanine nucleobases and 8 hydrogen bonds via both Watson-Crick and Hoogsteen hydrogen bonding, resulting in a planar structure known as a G-quartet.<sup>5</sup> The formation of G-quadruplex structures are seen when these G-quartets stack over each other<sup>6</sup> (Figure 4).

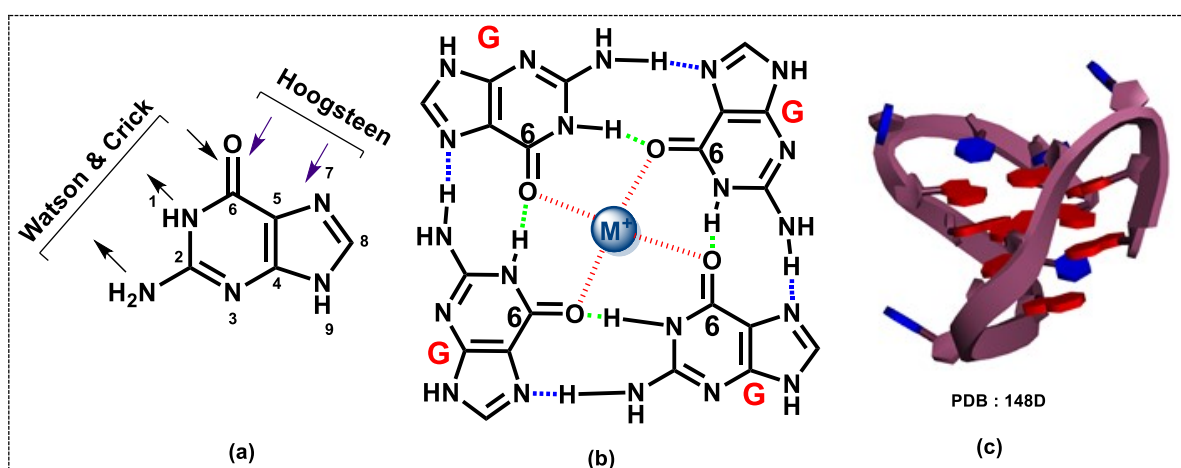


Figure 4: (a) Schematic structure of guanine with the Hoogsteen and Watson-Crick faces (b) Presentation of a G-quartet formed by the association of four guanines (c) The TBA G-quadruplex.

### 1.3 Sugar conformation preferences in nucleotides

Minimization of non-bonded stereoelectronic interactions between substituents occur in the pentafuranose ring, that does not exist in a planar form. Pseudorotational cycle was explain different conformations mainly four North and South (twist), East and West (envelope) conformations. Purine nucleosides prefer *C2'-endo* form whereas the pyrimidine nucleosides prefer the *C3'-endo* form, and as defined by the pseudorotational cycle, an equilibrium is seen between the two conformations with a low energy barrier between them<sup>7</sup> (Figure 5). Anomeric and *gauche* effects give rise to the prevalence of a single type of conformation.<sup>8</sup>

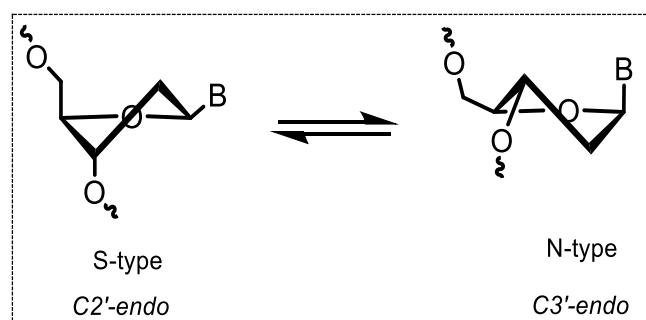


Figure 5: *C2'-endo* (South, S) and *C3'-endo* (North, N) sugar pucker in 2'-deoxy-D-ribose.

#### 1.3.1 Steric effect

The *C2'-endo* sugar conformation is preferred in  $\beta$ -D-nucleosides. This is because the nucleobase, in this case, is pseudo-equatorial to the sugar ring, causing less steric clashes, whereas in the case of *C3'-endo* sugar conformation, the nucleobase is pseudo-axially oriented,

causing more steric clashes. Hence between the two states  $N \leftrightarrow S$ , the pseudorotational equilibrium shifts towards the  $C2'$ -endo conformation (Figure 6).

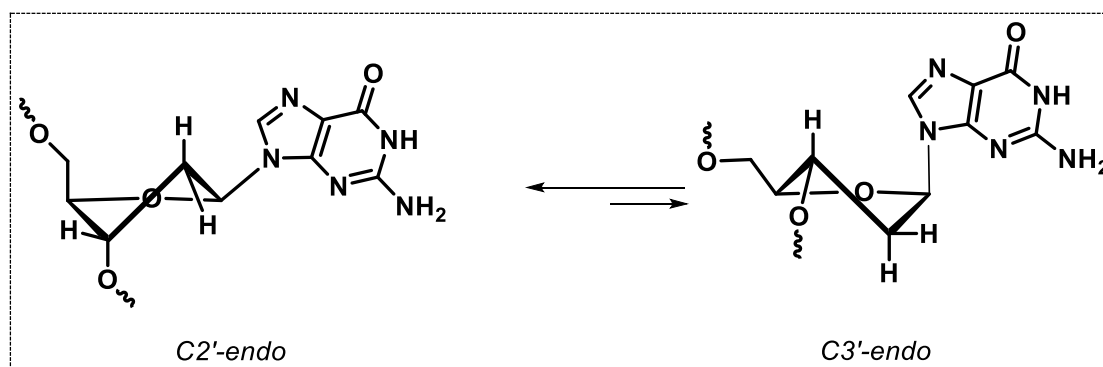


Figure 6: The steric interactions of nucleobase in the ( $C2'$ -endo)  $\leftrightarrow$  ( $C3'$ -endo) equilibrium in DNA.

### 1.3.2 Anomeric effect

The anomeric effect, also known as the Edward-Lemieux effect, describes the tendency of heteroatomic substituents next to a heteroatom within a ring to favor the axial orientation over the less hindered equatorial orientation, that would be expected based on steric considerations. Nucleosides and nucleotides prefer the  $C3'$ -endo conformation when an anomeric effect is more prevalent than the steric effect caused due to stabilizing interaction between the exocyclic glycosidic C-N bond and the lone pair of endocyclic oxygen of the sugar ring<sup>8</sup> (Figure 7). Likewise, electrostatic repulsive forces between dipoles caused by ring oxygen lone pairs and the exocyclic C-N bond may contribute for some of the occurring nucleotides prefer the  $C3'$ -endo conformation.

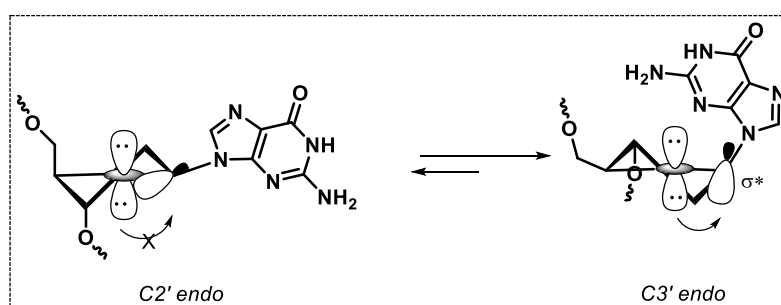


Figure 7: Anomeric effect in nucleobase molecular orbital overlap.

### 1.3.3 Gauche effect

The gauche effect is a typical situation that arises in conformational isomers differing by a torsion angle. A torsional angle between two vicinal groups of  $60^\circ$  gives rise to the 'gauche effect' which influences the sugar conformation. A more substantial gauche effect of fragment ( $O3'-C3'-C4'-O4'$ ) favors S-type conformation in deoxyribonucleotides, whereas in the case

of ribonucleotides, the gauche effect of fragment ( $O2'-C2'-C1'-O4'$ ) favors the N-type conformation.<sup>9</sup>

#### 1.4 Sugar ring conformations in DNA/RNA vs IsoDNA/IsoRNA

In this thesis, isoDNA or isoRNA refers to DNA or RNA respectively, with regioisomeric 2'-5'-phosphodiester links rather than 3'-5'-phosphodiester. They are not the same as native DNA or RNA (Figure 8). These constitutional isomers form duplexes via Watson–Crick base-pairs and do not encode genetic information.<sup>10</sup> The 2'-5' linkage and not the 3'-5' linkage is the primary product obtained during the non-enzymatic oligonucleotide synthesis due to the higher reactivity of the 2'-OH group. Therefore during evolution, the 2'-5' linkage might have been a primary substitute of the natural 3'-5' linkage, but instead, the natural synthesis is 3'-5' linked due to the slower rate of hydrolysis than the 2'-5' linkage.<sup>11</sup>

Another reason for the natural selection of the 3'-5' linkage is the low ability of 2'-5'-linked oligonucleotides to form a helical structure, and the internucleotide linkage changing from  $C3'$  to  $C2'$  leading to increased internucleotide bonds from six (3'-5') to seven (2'-5') respectively.

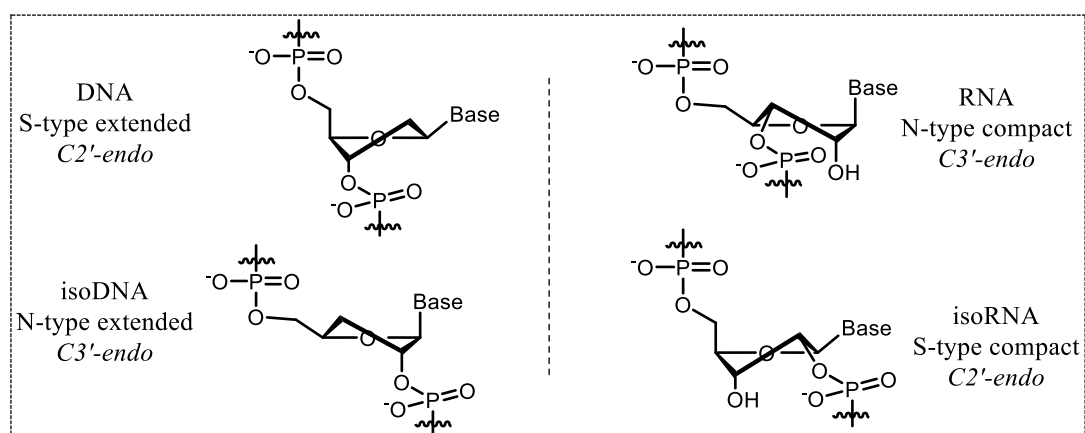


Figure 8: 3'-5'-DNA/RNA in comparison to 2'-5'-DNA/RNA.

#### 1.5 G-quadruplex structures

Although being guanine-rich is important for forming quadruplexes, not all guanine-rich sequences tend to form quadruplex structures. When formed, quadruplex structures involve precise strand alignment and contain G-quartets, loops, and cations.





**Figure 9: G-quadruplex.** Cell Chem Biol. 2021; 28:436–55

### 1.5.1 G-quartets

G quartets arise from the association of four guanines in planar structures (Section 1.2.3, Figure 4b) with the hydrogen bonds correlating with guanines. The quartets that are formed are held together generally by monovalent metal cations such as  $K^+$ ,  $Na^+$ ,  $NH_4^+$ ,  $Li^+$  or divalent cations such as  $Sr^{+2}$ ,  $Ca^{+2}$ ,  $Pb^{+2}$  or  $Ba^{+2}$ . Hydrogen bonds are formed between O6 and the hydrogen at N1, while another hydrogen bond is formed between N7 and hydrogen at N2 position of the guanines involved in the quartet formation.<sup>12-14</sup> The oxygen at O6 additionally interacts with the cations stabilizing the quartets formed.<sup>15</sup> Usually a *C2'-endo* or *C3'-exo* conformation of the sugar is seen in DNA quadruplexes, and the glycosidic bond angle could either adopt a *syn* or *anti*-conformation. Depending on the alignment of the adjacent guanines and their conformation, the quartets mainly have two wide and two narrow grooves,<sup>16</sup> with the phosphate backbone being the common core.<sup>17</sup>

### 1.5.2 G-quadruplex loops

The guanine nucleobases that are involved in the formation of G quartets are linked by simple strings of nucleotides called loops such as diagonal loop joining two anti-parallel strands, lateral loop joining two anti-parallel adjacent strands, propeller loop joining two adjacent parallel strands. These loops play a crucial role in the conformational polymorphism of quadruplexes and their stability. Loop length is also essential in deciding whether the quadruplex formation would be parallel (short loops, stable conformation) or anti-parallel type (long loops, less stable conformation).<sup>18-21</sup>

### 1.5.3 Alignment of strands

All the strands in a quadruplex are aligned and labeled by the 5'-3' directionality of the phosphate backbone. *Syn*- and *anti*-conformations and the guanine glycosidic bond angle usually decide the alignment and conformations of the strands. In cases where all the guanines are present in only one conformation (*syn* or *anti*), the quadruplex adopts a parallel structure.

Therefore, in theory, sixteen different structural alignments are possible for a given quadruplex structure.<sup>22</sup> Most commonly seen and important quadruplex structures are parallel structures, where all the four strands that make up a quadruplex are oriented in one direction, and anti-parallel structures, where adjacent strands are aligned in opposite direction<sup>23</sup>. Another type of conformation seen is the hybrid conformation, where among the four strands that make up a quadruplex, three are aligned in one direction while the fourth one is aligned in the opposite direction (Figure10).

#### 1.5.4 Inter- and Intra-molecular G-quadruplexes

G-quadruplexes are of two types- inter- and intramolecular, depending on the number of nucleic acid oligomers involved in the formation of the quadruplex. Intermolecular quadruplexes can further be tetramolecular, trimolecular, or bimolecular, where four, three, or two different strands come together to form a quadruplex, respectively.<sup>23,24</sup> An intramolecular quadruplex is formed when one single long guanine rich nucleic acid sequence with a minimum of four blocks of guanines with two or more than two guanines for each block separated by nucleotides folds in a manner to form the quadruplex structure<sup>25</sup> (Figure 10).

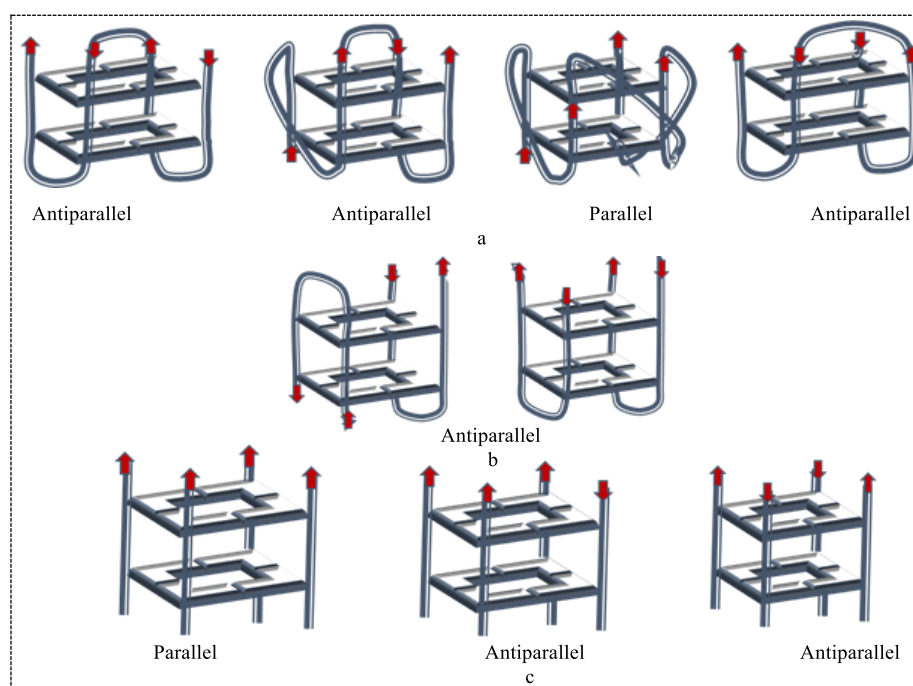


Figure 10: G-quadruplex: a) Unimolecular; b) bimolecular; c) tetramolecular topology.

#### 1.6 G-quadruplex topology and stability dependence on metal ions

Eight O6 atoms of two stacked quartets of a quadruplex structure form coordination sites with metal cations. Monovalent and divalent cations such as  $K^+$ ,  $Na^+$ ,  $Li^+$ ,  $Rb^+$ ,  $Cs^+$ ,  $NH_4^+$ ,

and  $\text{Mg}^{2+}$ ,  $\text{Ba}^{2+}$ ,  $\text{Ca}^{2+}$ ,  $\text{Sr}^{2+}$ ,  $\text{Pb}^{2+}$ ,  $\text{Co}^{2+}$ ,  $\text{Mn}^{2+}$ ,  $\text{Zn}^{2+}$ ,  $\text{Mg}^{2+}$ ,  $\text{Ni}^{2+}$  respectively stabilize and impact the topology of quadruplexes.<sup>26</sup>

### 1.6.1 Monovalent cations and G-quadruplexes

Ion-dependent polymorphism depends on the charge and size of the ions that influence the topology of G-quadruplex.<sup>27</sup> This can be best exemplified by the triplet repeat sequence d(TG<sub>2</sub>CG<sub>2</sub>C), which forms a tetramolecular parallel quadruplex in  $\text{K}^{+}$  ions and an anti-parallel quadruplex in the presence of  $\text{Na}^{+}$  ions at neutral pH.<sup>28</sup> Similarly, in sodium phosphate buffer, telomeric DNA repeats of *Tetrahymena* d(T<sub>2</sub>G<sub>4</sub>)<sub>4</sub> form a unimolecular structure, while in potassium phosphate buffer, it adopts a multi-strand structure.<sup>29</sup> Both bimolecular and tetramolecular quadruplex structures can be seen for sequences d(G<sub>3</sub>T<sub>4</sub>G<sub>3</sub>) and d(G<sub>4</sub>T<sub>4</sub>G<sub>4</sub>) in the presence of  $\text{K}^{+}$  ions, whereas with  $\text{Na}^{+}$  ions, they fold into bimolecular structures only.<sup>30,31</sup>

### 1.6.2 Divalent cations and G-quadruplexes

Sen and co-workers in 1993 explained the switch in quadruplex polymorphism from parallel to anti-parallel in the presence of divalent cations like  $\text{Mg}^{2+}$  and  $\text{Ba}^{2+}$ .<sup>32</sup> Sequences such as d(G<sub>4</sub>T<sub>4</sub>G<sub>4</sub>), and (GTG<sub>3</sub>TAG<sub>3</sub>CG<sub>3</sub>T<sub>2</sub>G<sub>2</sub>) exhibited parallel, anti-parallel, unimolecular, or multimolecular quadruplex structures in the presence of different ions, including  $\text{K}^{+}$  and  $\text{Pb}^{2+}$ , providing evidence that cations are capable of inducing polymorphism in quadruplexes.<sup>33,34</sup>

## 1.7 SELEX

Single-stranded DNA or RNA or a modified sequence that can fold into unique three-dimensional structures and bind to different targets such as proteins, small molecules, ions, whole cell bacteria, or viruses are known as aptamers. These aptamers, also known as chemical antibodies, have high affinity, selectivity, and specificity towards the target. Similar to chemical antibodies, riboswitches contain natural aptamers that bind to their targets by shape complementarity via van der Waals forces, electrostatic interactions and hydrogen bonding.<sup>35</sup> Aptamers can distinguish between minor structural variations probably arising due to differing chirality or presence and absence of a small functional group. Ellington and Szostak first introduced the term 'aptamer'.<sup>36</sup> In the 1990s, the groups of Szostak<sup>36</sup> and Gold<sup>37</sup> independently demonstrated an *in vitro* selection and amplification technique for the isolation of oligonucleotides able to bind non-nucleic acid targets with high affinity and specificity from a large pool of random sequences. This process of selection is known as Systematic Evolution of Ligands by Exponential enrichment (*SELEX*, Figure 11). Due to advantages such as smaller size (~10 fold than antibodies), the possibility of chemical modifications, and longer shelf-life,

make aptamers attractive in various diagnostic, therapeutic, and imaging applications. More than a hundred extraordinarily potent and selective aptamers have been developed in the past 30 years. Pegaptanib sodium (Macugen) was the first aptamer-based drug approved by the US FDA in 2004 to treat age-related macular degeneration.<sup>38</sup>

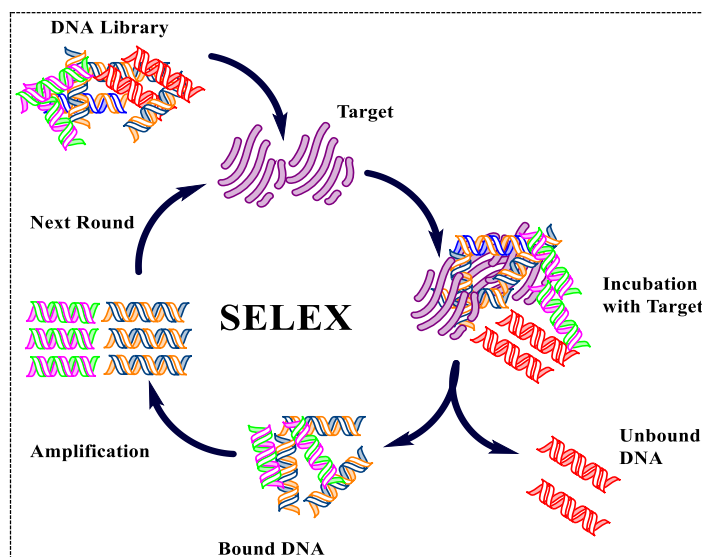


Figure 11: Schematic representation of SELEX

### 1.8.1 Aptamers forming G-quadruplexes

SELEX has resulted in a wide variety of G-quadruplex aptamers specific to many different proteins and targets. Some of the protein target sequences include the thrombin binding aptamer, an anti-parallel  $d(G_2T_2G_2TGTG_2T_2G_2)$  monomer,<sup>39</sup> a nucleolin-targeting, anti-parallel dimer  $d(G_2TG_2TG_2TG_2T_2GTG_2TG_2TG_2TG_2)$ ,<sup>40</sup> signal transducer and activator of transcription (STAT3)-targeting  $d(G_3CG_3CG_3CG_3C)$ , etc.<sup>41</sup>

Some examples of non-protein targeted DNA G-quadruplex aptamers include hematoporphyrin IX-targeting antiparallel G-quadruplex  $d(ATG_4TCG_3CG_3C_2G_3TGTC)$  monomer,<sup>42</sup> hemin-targeting  $d(GTG_3TAG_3CG_3T_2G_2)$ ,<sup>43</sup> potassium ion-targeting anti-parallel G-quadruplex  $d(G_3T_2AG_3T_2AG_3TAG_3)$  monomer,<sup>44</sup> and ATP-targeting antiparallel G-quadruplex  $d(C_2TG_5AGTAT_2GCG_2AG_2A_2G_2)$  monomer.<sup>45</sup>

### 1.8.2 Thrombin binding aptamer

Bock and co-workers discovered the thrombin binding aptamer (TBA), a 15mer DNA sequence in 1992<sup>39</sup> that folds into a quadruplex (Figure 12) containing two G(syn): G(anti): G(syn): G(anti) quartets and three lateral loops. Such quadruplex structures are referred to as chair structures where each of the G2 repeats is 5'-syn – anti-3', and all the thymines are in the anti-conformation. Two wide and two narrow grooves are present in this quadruplex structure

with a T:T base pair seen due to the thymine at the 3' end of the short T2 loops (T4 and T13) are stacked over the neighboring G-quartet while some degree of flexibility is seen for thymine present at the 5'-end of the loops T3 and T12. The 5' thymine (T7) of the longer TGT lateral loop is positioned in the wide groove while the other two bases in the loop (G8 and T9) are more or less stacked over the G-quartet.<sup>46</sup> Although TBA is a sequence that inhibits human thrombin, in literature, many other sequences of different lengths have also been reported to bind to thrombin.<sup>39</sup>

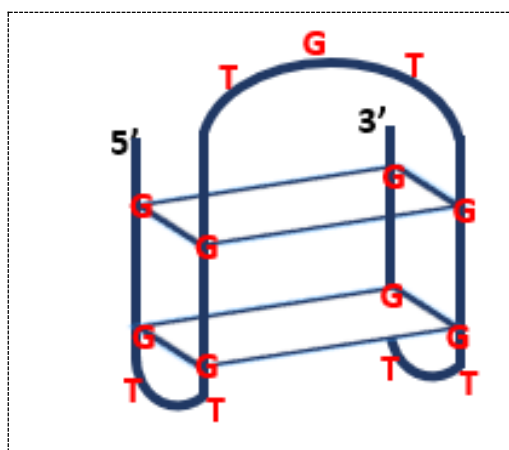


Figure 12: Schematic representation of TBA.

## 1.9 Thrombin binding aptamer and its modification

Currently used anticoagulants such as Heparin, Warfarin (Coumadin), Rivaroxaban (Xarelto), Dabigatran (Pradaxa), Apixaban (Eliquis), Edoxaban (Savaysa), Enoxaparin (Lovenox), Fondaparinux (Arixtra), etc., cause side effects such as red or pink-colored urine, stools that are bloody or look like coffee grounds, more bleeding than average during a menstrual period, blackish areas in fingers, toes, hands, or feet that can be avoided with the use of TBA as an anticoagulant. However, the poor stability of TBA<sup>47</sup> can be overcome by introducing different modifications in different positions such as the loop, the quartet, sugar, or phosphate backbone.<sup>48</sup>

### 1.9.1 Modifications in the G tetrads

Important modifications such as N2- and C8-alkyl substituted guanine nucleosides and their incorporation at different positions in TBA have been reported in literature.<sup>49</sup> Different modifications at different positions bring out a wide range of effects; for benzyl/naphthyl substituents, the best anticoagulant effect was seen when there was a benzyl group at the N2 of G6 or G11, and a naphthyl methyl moiety at the N2 of G6 (Figure 13a); the use of small groups like methyl and propynyl at C8 positions in G1, G5, G10, and G14 increased the antithrombotic activity of the analogues while larger substituents caused a decrease in the activity (Figure

13b).<sup>49</sup> Improved thrombin inhibitory activity was reported by Goji and co-workers by simultaneous substitution with 8-bromoguanine at G1 and G10 (Figure 13c).<sup>50</sup>

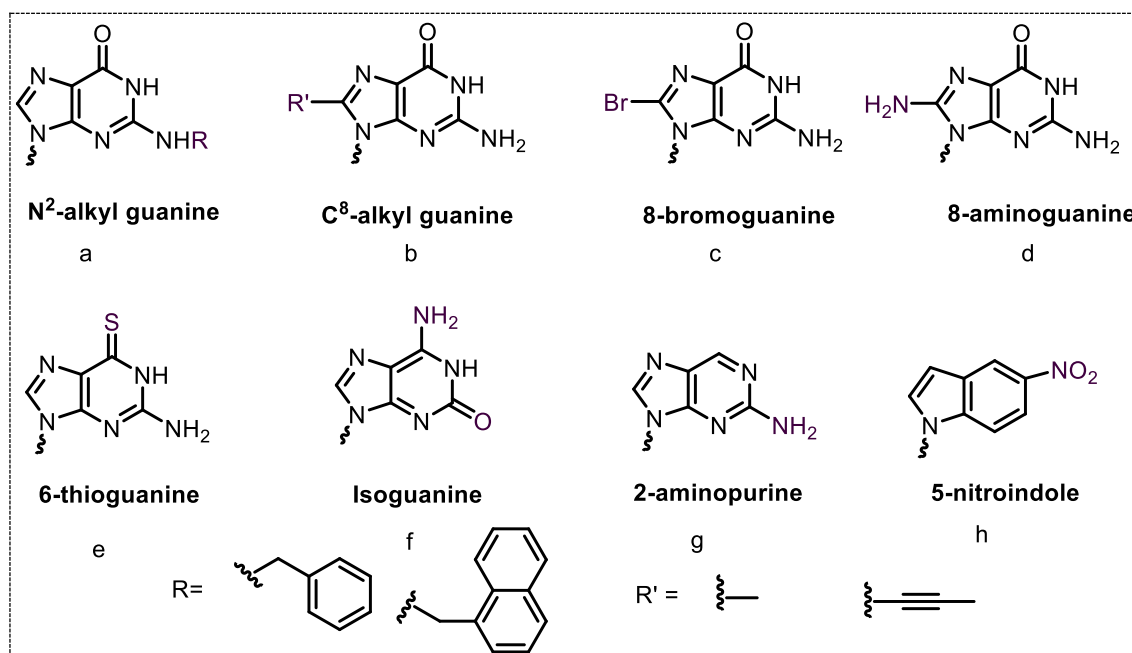


**Figure 13: Modified guanines reported in the G-quartet region of TBA.**

The TBA G-quadruplex was destabilized by 8-aminoguanine substitution at G2 (Figure 13d).<sup>51</sup> NMR studies confirmed complete inhibition of the G-quadruplex formation, due to the decreased electronegativity of sulfur vs. oxygen, which led to weaker interactions with cations and water molecules when 6-thioguanine was incorporated at G2 position (Figure 13e).<sup>52</sup> A single isoguanine substitution at positions G1, G8 and G10 showed a slightly higher thrombin affinity than unmodified TBA (Figure 13f).<sup>53</sup> Lower thermal stability was seen with the 2-aminopurine substitution<sup>54</sup> (Figure 13g), while 5-nitroindole (Figure 13h) substitution at G8 gave a similar  $T_m$  value as TBA, with higher clotting time and thrombin binding affinity.<sup>55</sup>

### 1.9.2 Modifications in the loops

Similar to G-quartet modifications, the guanines and thymines in the loops of TBA have also been modified by different modifications, leading to either favorable or unfavorable outcomes. Replacement of the nucleobase by alternative nucleobases, such as the T→U substitution resulted in a higher  $T_m$  value than the unmodified counterpart. In another modification, when G8 was replaced by uracil producing a UUU central loop, a decrease in thermal stability was seen.<sup>54</sup> When a simultaneous substitution of T → U at T7 and T9, T3 and T4 or T4 and T13 was carried out, the modification at the central loop caused enhanced quadruplex stability.<sup>56</sup> When cytosine was substituted for each thymine in the TT loops, no

difference in the thermal stability was seen but a lower thermal stability was observed when replacement at T4 or T13 was carried out.<sup>57</sup>

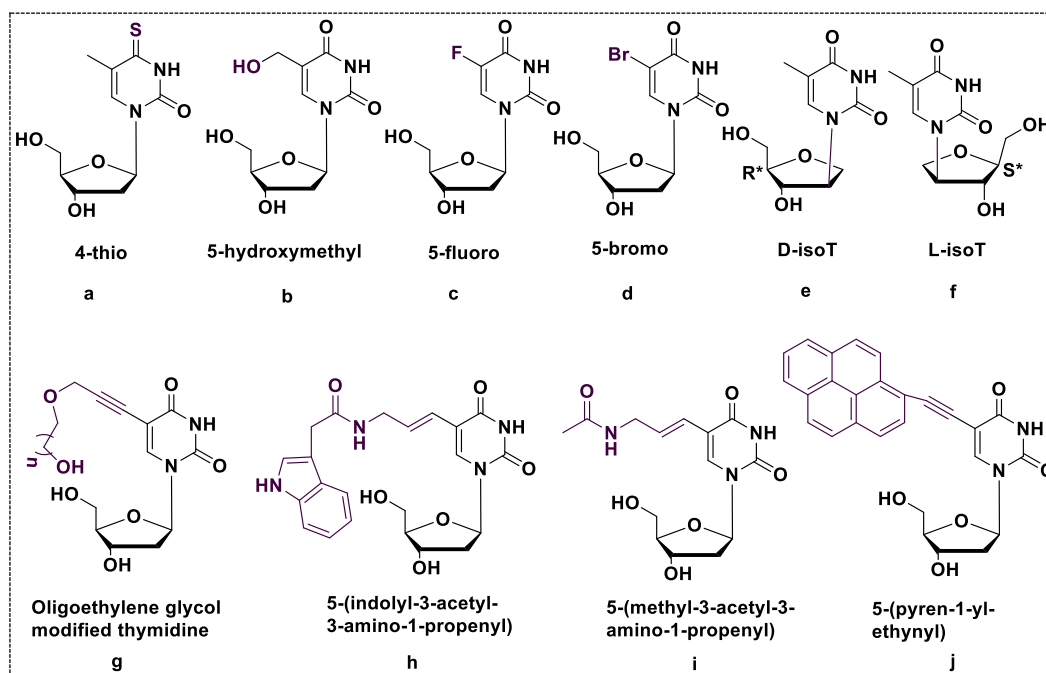


**Figure 14: Modified thymidine in loop region.**

When each thymine was replaced with adenine, it led to a less stable quadruplex except when the substitution was carried out at T4 or T13 which gave aptamers as stable as the parent TBA. A higher thermal stability and a drastic change in the quadruplex topology to the intermolecular parallel structure was seen when TBA was modified with multiple T  $\rightarrow$  G substitutions.<sup>58</sup> Enzymatic stability was seen to increase when  $\alpha$ -nucleosides were incorporated into both G tetrads and loops. Substitutions at T4 or T13 in sequences exhibited higher thermal stability but exhibited lower clotting time than unmodified TBA.<sup>59</sup> But 2-fold increased efficiency in inhibiting thrombin was seen when all thymidines of TBA or positions T3, T7, T9, and T13 in the lateral loops were replaced with thio-2'-deoxyuridine (Figure 14a).<sup>60</sup> Derivatives with higher thermal stability were obtained when thymidine residues were one by one replaced by 5-hydroxymethyl-2'-deoxyuridine (Figure 14b), especially when the replacement was at position T9. Although all the TBA analogues in this case showed decreased thrombin affinities, in Prothombin Time assays, T3, T7, and T9 exhibited more efficient anticoagulant properties than TBA. Similarly, when thymidine at positions T4 or T13 only were replaced by 5-fluoro-2'-deoxyuridine (Figure 14c), it gave analogues with better thermal stability and anticoagulant activity.<sup>61</sup>

Increased thermal stability and anticoagulant activity was seen when 5-bromo-2'-deoxyuridine (Figure 14d) was introduced at positions T4 or T13 of TBA.<sup>61</sup> Anti-parallel

quadruplexes with low thermal stability were obtained when D- and L-iso thymidine were incorporated at either position T4 or T13 while modifications at T3 and T12 led to better stable analogues. Depending on the isoT configuration, substitution at T7 and T9 gave analogues with either good or low thermal stability. Similar serum stability was seen in all isoT (Figure 14e-f) analogues. Replacement at positions T3, T9, or T12 with L-isoT and at T7 with D-isoT resulted in both enhanced anticoagulant activity and thrombin affinity.<sup>62</sup> Modified 2'-deoxythymidine oligoethylene glycol functionality (Figure 14g) with varying ethylene glycol lengths were also substituted in TBA at positions T4, T7 and T13. With increasing length of the chain and increasing number of modifications, higher thermal stability was seen for substitutions at the same site.<sup>63</sup> However, thrombin interaction was not reported for these analogues. Improved thrombin affinity was seen due to additional interactions when C-5 of thymine was modified with end derivatization with an indole moiety<sup>55</sup> (Figure 14h). A 3-fold and a 9-fold improved binding affinity was seen when substitutions were made at T4 and T4-T12, respectively. To confirm the importance of the indole moiety, an analogue without the indole moiety was studied (Figure 14i), that showed a 7-fold increase in the affinity towards thrombin. Altogether, similar behavior was seen in analogues with or without the indole moiety,<sup>64</sup> that indicated no special role of the indole moiety in thrombin binding. Pyrene-modified (Figure 14j) TBA showed increased resistance to nuclease degradation, while thermal stability and thrombin affinity was site-dependent.<sup>65</sup>

### 1.9.3 Sugar modification

Sugar ring modifications in TBA have been studied, of which, some have led to improved biological activity and stability. Topology of TBA RNA (rTBA) has also been studied and it was found that when rG (Figure 15a) was introduced at *syn* position of TBA (DNA), a parallel structure was seen and when rG was introduced at *anti*-position, and antiparallel structure was seen. Similarly, an antiparallel structure was seen when dG was introduced at *anti*-position of TBA(RNA) with good thermal stability, while a less stable parallel structure was seen when dG was introduced at *syn* position.<sup>66</sup> TBA sequence were replaced with 2'-O-4'-C-methylene-linked bicyclic locked nucleic acid (Figure 15b) at G5 and G8 positions, a higher quadruplex thermal stability than TBA was observed. Replacements at G2 and T7 resulted in lower  $T_m$  values, while those at G5, T7, and G8 resulted in decreased anticoagulant activity, although G2 and T4 had similar activity to TBA.<sup>67,68</sup> When compared to a single substitution by unlocked nucleic acid (UNA, Figure 15c) in TBA, substitutions improved thermal stability and clotting time.<sup>69,70</sup>



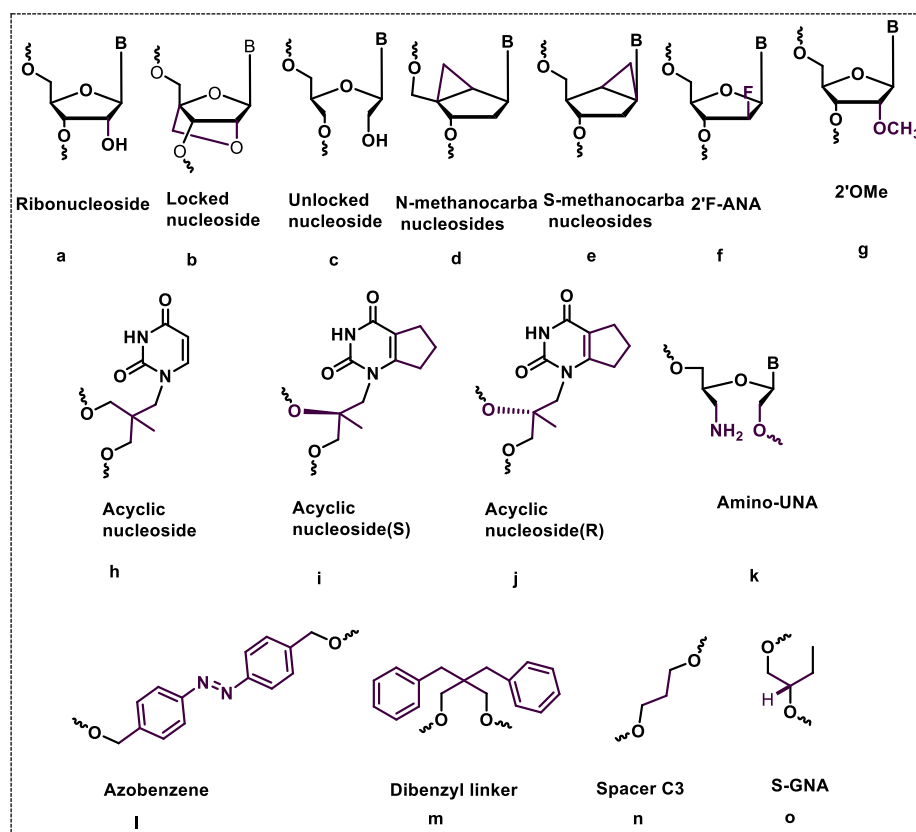


Figure 15: Modifications of the sugar ring

Carbocyclic bicyclo [3.1.0] (Figure 15d-e) 2'-deoxyguanosines (*N*- or *S*-type pseudo-sugars, hexane locked nucleosides) substitutions in TBA were also reported.<sup>71</sup> In TBA-dG5*S* and TBA-dG14*S*, the substitution of *syn* dGs at positions G5, G10, and G14 resulted in modified ODNs with significantly reduced G-quadruplex thermal stability and lower  $T_m$  values than unmodified TBA. The G-quadruplex structure was dramatically destabilized by TBA-dG14*N*. Notably, decreased  $T_m$  values were obtained for both replacements at position 15, with more significant effects using *S*(*syn*)dG, implying that the *N*-glycosyl conformation is more important for TBA stability than the sugar puckering conformation. The insertion of *N*-methanocarba nucleosides in the loop regions at positions T7 and T9 or T4 and T13, resulted in TBA derivatives with significantly lower G-quadruplex thermal stability than their unmodified counterparts in both cases.<sup>71,72</sup>

Sugar modifications like 2'-F-ANA (Figure 15f) in singly- or fully-modified TBA sequences resulted in parallel or antiparallel topologies, the antiparallel form having better nuclease and thermal stability.<sup>73,74</sup> The 2'OMe (Figure 15g) modification was found to be not well suited to the quartet region, but it is well suited to the loop region.<sup>75,76</sup> All acyclic (Figure 15 h-j) modifications in the loop area had an antiparallel structure, with T3, T4, and T7 replacements clotting better than TBA.<sup>77,78</sup> Replacements at these same positions by amino

UNA (Figure 15k) resulted in almost the same clotting time and thermal stability as TBA.<sup>79</sup> Azobenzene (Figure 15l) derivatives replacements<sup>80</sup> of the TGT loop resulted in the well-known TBA G-quadruplex topology. Scutto *et al.* synthesized TBA-based sequences by replacing one residue at a time of the TT or TGT loops with a 2,2-dibenzylpropane-1,3-diol linker (Figure 15m).<sup>81</sup> A reduced G-quadruplex thermal stability was observed only when this modification occurred at positions G8 or T9, almost same thermal stability was observed compared to TBA at other loop positions T3, T4, T7, T12 and T13. The presence of a C3-spacer (Figure 15n) in the single loop region conferred T3, T7 or T12 replacements with the same thermal stability as compared to TBA.<sup>79</sup> The optically pure acyclic nucleotide S-GNA (Figure 15o), which is a propylene glycol-thymine derivative with a three carbon atom scaffold connecting the phosphodiester linkages, was used as single or multiple substitutes for thymidine at various positions of TBA.<sup>82</sup> Only the insertion at position T7 resulted in raised  $T_m$  values, whereas the rest of the modified TBAs had much lower G-quadruplex thermal stability than TBA.

#### 1.9.4 Linkage modification

Replacement of the phosphate backbone of TBA by modified linkages or by an alternate moiety have been reported. The presence of phosphorothioate (Figure 16a) modification in the loop region was tolerated better than in the quartet region, with all sequences exhibiting the antiparallel topology like TBA.<sup>83</sup> The inclusion of methyl phosphonate (Figure 16b) in the backbone resulted in a completely unstructured oligonucleotide with a flat thermal denaturation curve.<sup>84</sup> He *et al.* investigated the use of neutral formacetal bonds (Figure 16c) to replace negatively charged phosphodiester groups. The anticoagulant action was reduced in all cases, particularly in analogues where one or both phosphodiester groups between T4 and G5 or T13 and G14 were changed.<sup>85</sup>

3'-5'-linkage replacement by 2'-5'- in isoTBA (Figure 16d) resulted in lower thermal stability but comparable clotting time and increased nuclease stability.<sup>86</sup> TBA analogues with a single internal 3'-3' or 5'-5' IPS (inversion of polarity site, Figure 16 e, f) at different positions in the TBA sequence were reported.<sup>87</sup> Analogues with 5'-5' IPS at the level of the G2-T3, T3-T4, and T4-G5 internucleotide bonds were revealed to form a unimolecular antiparallel G-quadruplex by NMR. Also, when compared to unmodified TBA, CD-derived  $T_m$  values were higher. In comparison to native TBA, a comprehensive calorimetric investigation revealed improved thrombin binding affinity.<sup>88</sup>

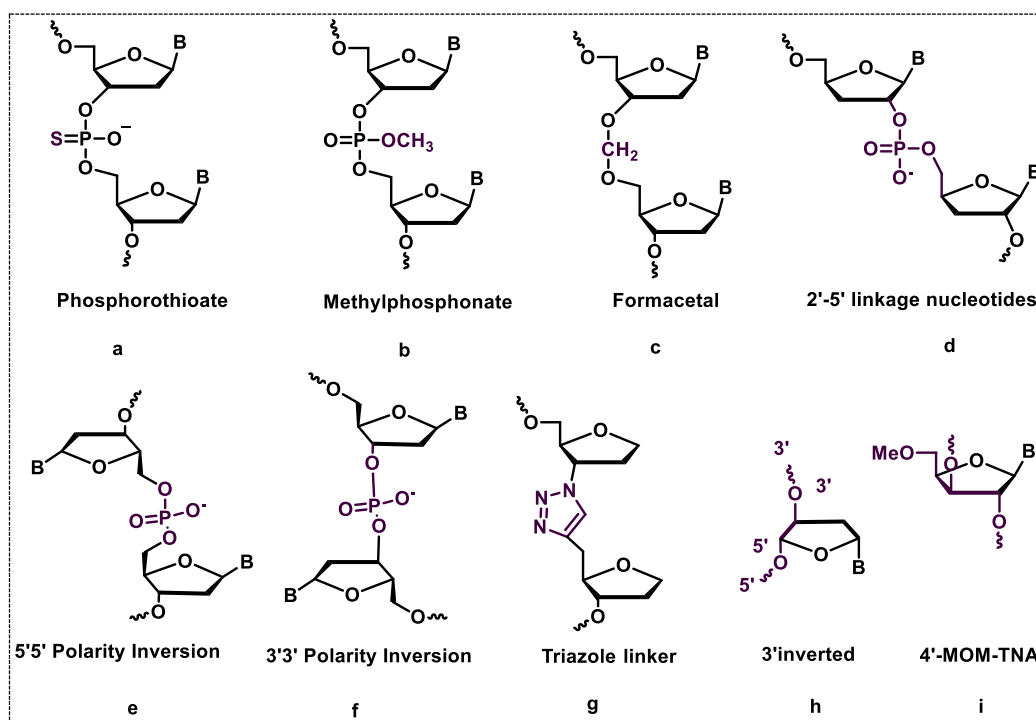


Figure 16: Modifications in the backbone linkage

A single inter-nucleoside triazole (Figure 16g) modification at position T3-T4, T12-T13, T7-T8 (G8 replaced by T) and double inter-nucleoside modification at positions T3-T4, T12-T13 were found to have better nuclease stability than parent TBA, with comparable thermal stability, but a shorter clotting time.<sup>89</sup> 3'-3' and 5'-5' IPS (Figure 16h) were used to increase TBA resistance to both 3'- and 5'-exonuclease digestion. Extra residues were added at one or both TBA edges.<sup>90</sup> With two IPS, almost all of the modified aptamers formed antiparallel G-quadruplex structures similar to parent TBA and showed enhanced  $T_m$  values compared to unmodified TBA, notably when 3'-3' IPS were inserted at the 3'-end of TBA.<sup>90</sup> In the case of 4'-MOM-TNA (Figure 16i), the T7 position modification improved thermal stability and clotting time, together with offering increased nuclease resistance.<sup>91</sup>

### 1.10 TBA- Thrombin interaction

Thrombin is a serine protease that serves as both a procoagulant and an anticoagulant, similar to trypsin. It accelerates the transformation of fibrinogen to fibrin. It also stimulates the blood coagulation factors V and VIII, which are required for blood clotting. The catalytic site, two electropositive domains, and a fibrinogen-recognition exosite are among the structural domains of the thrombin protein. TBA binds to thrombin; the two lateral TT loops (T3-T4 and

T12-T13) of TBA are essential for the interaction with exosite I of  $\alpha$  thrombin, and act as a pincer-like system<sup>92</sup> (Figure 17).

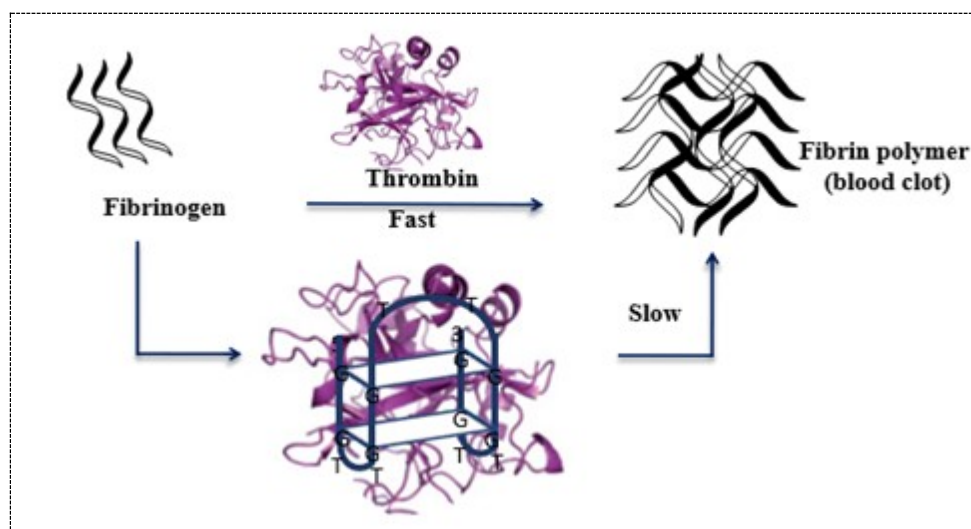


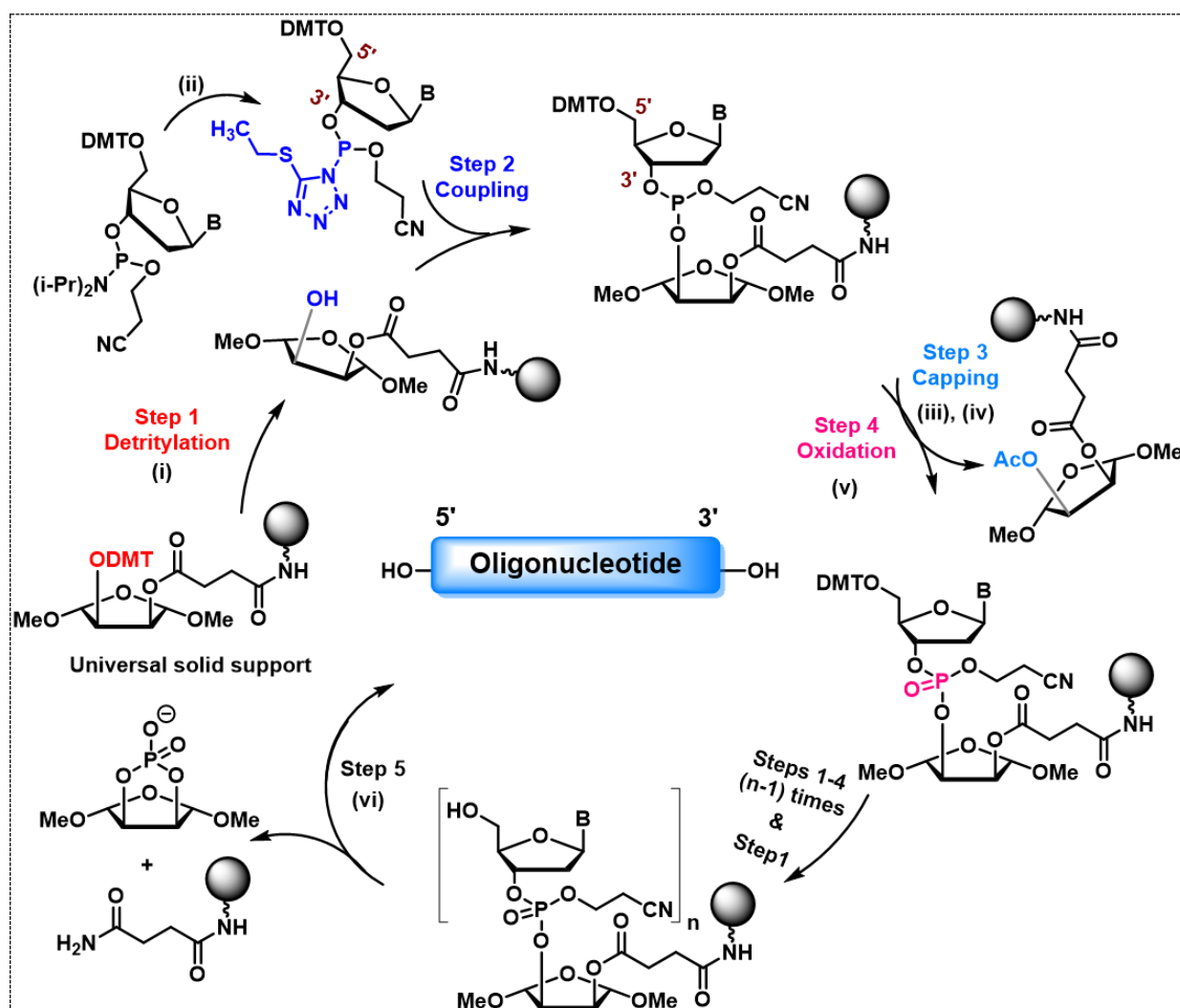
**Figure 17: Schematic representation of inhibition of clotting activity by TBA.**

T4 and T13 have mainly polar interactions, while T3 and T12 are associated with amino acid residues His71, Arg75, Tyr76, Arg77, Asn78, Ile79, and Tyr117 in the exosite I of thrombin through hydrophobic interactions. Studies done by Yeates and co-workers suggested that the TGT loop is in the vicinity of the exosite II of an adjacent thrombin molecule.<sup>93</sup> The thrombin protein binds to fibrinogen to cause clot formation in a normal clotting process. This is a quick reaction, but in the presence of TBA, the two TT loops bind to thrombin exosite I rather than fibrinogen, delaying clot formation.

### 1.11 Solid-phase synthesis of oligonucleotides

Oligonucleotides and peptides are frequently synthesized via solid-phase synthesis. Bruce Merrifield, who won the Nobel Prize in 1984, invented it in 1960. On a solid support, such as controlled pore glass or polystyrene, this synthesis is carried out. In the solution phase, several methods for oligonucleotide synthesis have been established. In the early 1950s, Michelson and Todd<sup>94</sup> pioneered the H-phosphonate and phosphate triester approach. Later, Har Govind Khorana's group<sup>95</sup> developed the phosphodiester method. In the 1960s, the phosphotriester<sup>96</sup> approach was developed by a group led by R. Letsinger, and in the 1970s, a reinvestigation of the phosphotriester method was done by the same group and they developed the phosphite triester<sup>97</sup> approach. Each of these approaches has its own set of disadvantages. Marvin Caruthers made a breakthrough in the early 1980s when he pioneered the phosphoramidite approach,<sup>98</sup> which was later improved with solid support and automation to become the gold standard method for oligonucleotide synthesis.

Oligonucleotide synthesis can be done on two different types of solid support. The standard support, which contains a nucleoside unit that forms the 3'-end residue as the synthesis proceeds in the 3'-5' direction, and the universal solid support, which has an abasic sugar unit instead of the 3'-nucleoside unit and does not form part of the final oligonucleotide. The benefit of using the universal support is that four different supports (depending on whether the desired oligonucleotide has A/ T/ G or C at the 3'-end) for DNA synthesis are not necessary, and another key benefit is that 3'-end modified oligomer synthesis can be done only on a universal solid support which is not feasible on conventional standard supports. Synthesis of phosphoramidite oligonucleotides takes place in the 3'-5' direction, as shown in Scheme 1.



Reagents and conditions: (i) 3% TCA in  $\text{CH}_2\text{Cl}_2$  (ii) 0.25 M 5-(S-ethyltetrazole) in  $\text{CH}_3\text{CN}$  (iii) 10% N-methylimidazole in THF 0.1 M (iv)  $\text{Ac}_2\text{O}/\text{Py}$  (v)  $\text{I}_2/\text{Py}/\text{H}_2\text{O}/\text{THF}$  (vi) aq.  $\text{NH}_3$ , 55 °C.

**Scheme 1:** The sequence of chemical reactions involved in the solid phase synthesis of oligonucleotides

The synthesis is carried out by adding protected nucleotide residues one by one. Detritylation, coupling, capping, and oxidation is all part of the four-step process. Treatment with 3 % trichloroacetic acid removes the 4,4'-dimethoxytrityl group of the support-bound

nucleoside at the start of conventional oligonucleotide synthesis (step 1). The activated phosphoramidite monomer is added after the DMT group is removed. Activation of the phosphoramidite monomer is achieved by treatment with solution of 5-(S-ethyltetrazole) in CH<sub>3</sub>CN (step 2). The activated phosphoramidite moiety of this added monomer reacts with the free 5'-hydroxy group on the solid support to produce a one-nucleotide-extended oligonucleotide on the support bound by a phosphotriester linkage. Using acetic anhydride and N-methylimidazole in pyridine, the unreacted 5'-OH groups of nucleosides on the support are blocked by capping as their acetate derivatives (step 3). Because the newly generated phosphotriester (P(III)) is acid unstable, it must be converted to a stable P (V) state by oxidation with iodine, water, and pyridine (step 4). The target oligonucleotide sequence is obtained by repeating this cycle once for each nucleotide. Aqueous ammonia treatment is used to cleave the solid support during the post-synthesis procedure. Aqueous ammonia treatment also removes the protective groups of exocyclic amino groups of nucleobases and inter-nucleoside  $\beta$ -cyanoethyl phosphate protection. The crude oligomers are purified using RP-HPLC and characterized using MALDI-TOF mass spectrometry.

## 1.12 Tools and techniques in the study of G-quadruplexes

### 1.12.1 UV-spectroscopy

The heterocyclic bases of nucleic acids absorb ultraviolet light. Because of the  $\pi$ - $\pi^*$  transitions associated with purine and pyrimidine bases, the  $\lambda$  max for all nucleobases is between 250 and 280 nm. As a result, measuring the absorbance at 260 nm in an aqueous solution can be used to estimate nucleic acid concentration. The concentration can then be determined using the Beer-Lambert law,  $A = \epsilon cl$  Where,  $\epsilon$  = extinction coefficient,  $c$  = the concentration, and  $l$  = the cuvette length. The folding and unfolding patterns of nucleic acids in solution are commonly monitored using UV absorption spectroscopy. A rise in absorbance at 295 nm coincides with the creation of the G-quadruplex structure. Thermal denaturation assays can determine the thermal stability of DNA/RNA complexes such as duplexes, triplexes, and quadruplexes. At different temperatures, the denaturation/renaturation of quadruplexes can be tracked by monitoring absorbance at 295 nm. Melting studies for G-quadruplexes<sup>12</sup> can be performed on a UV-visible spectrophotometer by recording the absorbance at 295 nm with increasing temperature. The melting temperatures ( $T_m$ ) can be obtained from the absorbance versus temperature curves. Recording a UV absorbance scan at different temperatures can be used to generate a thermal difference spectrum (TDS). The TDS is calculated by subtracting the spectral scan of the sample below the melting temperature from that above the melting

temperature.<sup>99</sup> TDS is a simple, and quick approach for obtaining structural understanding of nucleic acid structures.

### 1.12.2 Circular Dichroism (CD)

Circular dichroism is a differential absorption spectroscopic technique widely utilized to explore structural characteristics of optically active chiral compounds, biological molecules, and their interactions with metal ions and other molecules. The ability to display conformational changes in molecules gives CD a significant value. The spectrum produced by an organized arrangement can contain both positive and negative signals; in the absence of a stable structure, the CD amplitude is zero. Because the phenomena of CD are sensitive to the secondary structures of biomolecules such as proteins, DNA, and RNA, it is extremely useful in biomolecule characterization. The asymmetric sugar, the helicity of the nucleic acid's secondary structure, and the long-range tertiary ordering of DNA in specific conditions are all sources of chirality in nucleic acids. The heterocyclic bases in nucleic acids are achiral, but they are the primary chromophores.<sup>100</sup> CD spectroscopy is one of the most effective tools for studying G-quadruplexes and is a widely used method. It's a well-known method for investigating G-quadruplex polymorphism. The source of spectra in CD spectroscopy is one of two defining criteria in the case of G-quadruplexes- 1) differential folding geometry and 2) G-tetrad polarity, that can be defined in terms of strand orientation and stacking orientation. In parallel quadruplexes, all nucleobases are either *syn* oriented or *anti* oriented and have the same stacking polarity (head-to-head). However, in antiparallel quadruplexes, nucleobases are alternately *syn*- and *anti*-oriented and have the opposite stacking polarity (head-to-tail). In the case of G-quadruplexes, the characteristic differences in the CD spectra are very much dependent on the folding topology related to *syn*- or *anti*-glycosidic bond angles and orientation of nucleobases.

The topology of strands can be parallel, mixed parallel-antiparallel, or antiparallel, depending on their orientation. Parallel quadruplexes have significant positive CD maxima at 260 nm, whereas antiparallel quadruplexes have a distinctive signal that is positive at 295 nm and negative at 260 nm, allowing them to be distinguished. In addition to the topology, denaturation/ renaturation of quadruplexes at different temperatures can be monitored by recording the amplitude at 295 nm in CD spectroscopy.<sup>101</sup> CD melting analyses can be performed on G-quadruplexes by measuring the differences as the temperature rises. Ellipticity versus temperature curves can provide the melting temperature ( $T_m$ ) of the quadruplex. Hysteresis is not seen in the majority of intramolecular quadruplexes. Most bimolecular quadruplexes fold much quicker than unimolecular quadruplexes, resulting in hysteresis in the

melting and annealing profiles. CD spectroscopy has been used to investigate the G-quadruplex structure of DNA and RNA. This is a handy tool in this area.<sup>102</sup>

### 1.12.3 Raman Spectroscopy

Raman spectroscopy is a non-destructive chemical examination technique that can provide details about chemical properties, polymorphs, crystallinity, and complex interactions. It is based on the interaction of light with a material's chemical bonds. Raman spectroscopy is a tool for analyzing the secondary structure of nucleic acids that is particularly useful for studying G-quadruplexes. The formation of H-bonds between O6 and H1 is indicated by the characteristic marker peaks at  $1580\text{ cm}^{-1}$ ,  $1670\text{ cm}^{-1}$  for G-quadruplexes, as well as the band around  $1480\text{ cm}^{-1}$  for N7–H2.<sup>103</sup>

### 1.12.4 Polyacrylamide gel electrophoresis (PAGE)

There are several methods for purifying oligonucleotides; polyacrylamide gel electrophoresis (PAGE) is one of the most extensively utilized for purification and studying complex formation in DNA/RNA. It classifies molecules according to their electrical charge, size, and secondary or tertiary structure. When a denaturing agent like urea is used, denaturing gel electrophoresis is used to purify DNA. Using PAGE, an oligonucleotide of 'n' base pairs can be separated and purified from a failure sequence of 'n-1' base pairs or others. Denaturing polyacrylamide gels can separate oligonucleotides ranging in length from 2 to 300 bases depending on the proportion of polyacrylamide used. Molecules can be run in their native state on the gel, preserving their higher-order structure. To differentiate structural changes in oligomers, a non-denaturing or native gel can be used. Under native conditions, it is simple to distinguish between folded and unfolded single-stranded DNA forms.

### 1.12.5 MALDI TOF Mass Spectrometry

MALDI-TOF mass spectrometry (matrix-assisted laser desorption/ionization time-of-flight) can be used to analyze biomolecules such as DNA, RNA, proteins, and peptides due to its ease and speed of analysis. It is a two-step soft ionization process in which the matrix is vaporized by desorption induced by laser light pulses (nitrogen laser, 337 nm). The oligomer molecules are ionized in a heated cloud in the second stage. The electric field accelerates ionized oligomer molecules to the same kinetic energy, and the time it takes them to reach the detector is measured in time-of-flight (TOF). Their velocities and TOF are solely dependent on their masses when they have the same charge and kinetic energy, and lighter ions travel quicker while larger ions travel slowly. The mass spectrum is recorded as ion flux versus time. The



matrix is a low-molecular-weight crystalline substance; standard matrices include 3, 5-dimethoxy-4-hydroxycinnamic acid, 2', 4', 6' trihydroxy acetophenone (THAP), and 2, 5 dihydroxybenzoic acids. MALDI-TOF analysis can be used to confirm the identity and integrity of a synthesized oligonucleotide sequence and at multiple stages throughout synthesis to indicate potential problems.

### **1.12.6 High-performance liquid chromatography (HPLC)**

HPLC (high-performance liquid chromatography) is an effective method for analyzing and purifying synthesized oligonucleotides. Reverse phase RP-HPLC and anion exchange chromatography are commonly used to purify oligonucleotides. Anion exchange HPLC separates oligonucleotides based on charge differences using ion exchange resin containing positively charged groups. The cationic resin binds to negatively charged molecules, and raising the ionic strength of the mobile phase lowers the interaction between ONs and the cationic stationary phase, allowing shorter ONs to elute first and longer, more highly charged ONs to elute later. RP-HPLC separates oligonucleotides based on hydrophobicity differences. Crude oligonucleotides contain terminated shorter sequences that differ from the desired oligonucleotide in hydrophobicity. RP-HPLC uses a nonpolar stationary phase. The mobile phase for elution is a mixture of organic solvents and aqueous buffers. The purification of oligonucleotides was accomplished using RP-HPLC in the current work of this thesis. The elution solvents were aqueous ammonium acetate and acetonitrile. Molecules with a higher hydrophobicity are eluted more slowly, while polar components are eluted first in an aqueous buffer with a gradient of increasing acetonitrile. RP-HPLC can also be used to evaluate the degradation of single-stranded nucleic acid oligomers. The area under the peak can be used to determine the relative amount of intact oligonucleotides. A plot of the amount of intact oligonucleotide vs. time can be used to estimate the oligonucleotide's half-life under the given experimental conditions.

### 1.13 Present work

The research described in this thesis focuses on various alterations of the thrombin binding aptamer. The backbone is crucial to the quadruplex's structure, which is a key component dictating its functionalities. The effect on anticoagulant activity and stability that occur as a result of modifying the backbone and employing different cations are also described.

#### **Chapter 1: Introduction to nucleic acids, G-quadruplexes, and the Thrombin binding aptamer**

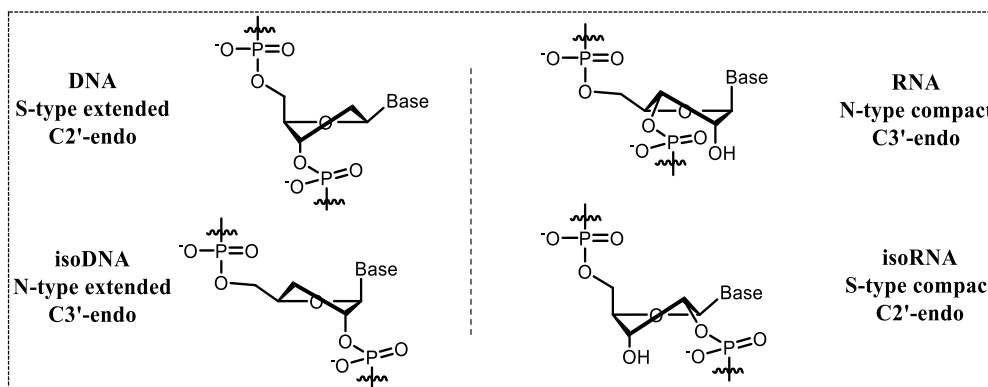
Bock and co-workers discovered the Thrombin Binding Aptamer (TBA), a 15mer DNA sequence in 1992 that folds into a quadruplex containing two G(*syn*): G(*anti*): G(*syn*): G(*anti*) quartets and three lateral loops. It was identified through the SELEX procedure and preferentially binds to thrombin (an enzyme involved in blood coagulation) to prevent it from acting. TBA is a potent anticoagulant in vitro with a short half-life in vivo. Its anticoagulant properties make it an excellent choice for surgeries. Currently used anticoagulants such as Heparin, Warfarin, Rivaroxaban, Edoxaban, Enoxaparin, Fondaparinux, etc., cause side effects such as red or pink-colored urine, stools that are bloody or look like coffee grounds more bleeding than average during a menstrual period, blackish areas in fingers, toes, hands, or feet that can be avoided with the use of TBA as an anticoagulant. However, the poor stability of TBA can be overcome by introducing different modifications. This chapter gives a quick overview of the research being done to produce novel TBA derivatives with better anticoagulant characteristics and also improving thermal and nuclease stability.

#### **Chapter 2: Effect of alkali and alkaline earth metal cations on the isoTBA quadruplex: Application to the detection of Sr<sup>2+</sup>**

The presence of cations stabilizes G-quadruplex structures, and various cations result in distinct polymorphs. G-quadruplex structural polymorphism occurs not only in monovalent but also in divalent cations. A change in the quadruplex topology can either increase or reduce the function of the aptamer. The structure of TBA in the presence of different cations has been studied and reported to show only unimolecular antiparallel kind of quadruplexes. In this chapter, the effect of various alkali and alkaline earth metal cations on the G-quadruplex-forming ability of isoTBA is studied. In contrast to all the other cations studied, Sr<sup>2+</sup> was found to bind to isoTBA with high affinity and specificity and led to a parallel intramolecular quadruplex formation. This is unique behavior of isoTBA in the presence of Sr<sup>2+</sup> ions.

### Chapter 3: Iso-rTBA: the 2'-5'-linked functional RNA equivalent of the thrombin-binding aptamer

In isoTBA, the 2'-5' backbone results in an extended backbone with sugars preferring the N-type pucker, whereas in iso-rTBA, it results in a compact backbone with sugars preferring the S-type pucker.



We demonstrated in this chapter that iso-rTBA, with a 2'-5' linked backbone, folded into an antiparallel G-quadruplex, in contrast to most RNA quadruplexes (including rTBA), which adopt a parallel topology. In addition, like TBA and isoTBA, this unimolecular antiparallel iso-rTBA quadruplex inhibited clotting and resisted nuclease degradation. This demonstrates the 2'-5'-backbone's flexibility and versatility, as well as its ability to adopt functional topologies, regardless of whether the sugar is ribose or deoxyribose.

### Chapter 4: Replacement of loop residues in TBA by an abasic ethylene glycol spacer: Effect on stability, structure and function

The synthesis of abasic spacer units produced from ethylene glycol, as loop residue replacements, in an attempt to further simplify and arrive at a minimal spacer unit that would ideally retain or improve TBA's stability and anticoagulant characteristics. Studies with a 2-carbon E spacer in this chapter reveal that a single E spacer replacement of loop residues is tolerated better than two. Although the 2-carbon E spacer had a positive influence on the nuclease stability and half-life of the oligomers, it had a poorer thermal stability and anti-clotting function than the 3-carbon spacer unit, suggesting that this shorter backbone is not so well-tolerated in TBA.

### Chapter 5: Synthesis of 2'-thiopropyl thymidine nucleoside, conformation studies, and incorporation into TBA

Substitutions at the 2'-position of the sugar in nucleosides have been explored in literature for various applications, including increasing the thermal stability, binding to

ligands/protein nuclease resistance properties of the derived oligonucleotides. The 2'-SCF<sub>3</sub> modification destabilized RNA duplexes, probably as a result of the S-type sugar pucker. However, when the 2'-SCF<sub>3</sub>-modified nucleoside was incorporated in the loop region of an RNA hairpin, it increased thermal stability compared to the unmodified RNA hairpin. Evidence has accumulated over the past few years to support the premise that structural alterations such as modifications, are known to confer resistance to nucleolytic cleavage. Only the 2'-SCF<sub>3</sub> substituents at the oligonucleotide level, and none of these modifications being included in G-quadruplexes. The 2'-thiopropyl derivative of thymidine was synthesized, and its effect on TBA at the structural and functional levels was studied. The sugar pucker in 2'-thiopropyl thymidine was found to be C2'-endo and ~100 % S-type, even more than that observed in native DNA (C2'-endo, 58 % S-type). TBA variants bearing this unit at selected loop positions were found to be able to form antiparallel G-quadruplexes, with a beneficial effect on the nuclease stability and half-life, although the thermal stability of the quadruplexes formed was lower than that of TBA. Some of the TBA variants, viz., TBA-t7, TBA-t9, and TBA-t12 showed moderate anti-clotting activity, though lower than TBA.

#### 1.14 References

- (1) Watson, J. D.; Crick, F. H. C. Genetical Implications of the Structure of Deoxyribonucleic Acid. *Nature* **1953**, *171* (4361), 964–967.
- (2) Limongelli, V.; De Tito, S.; Cerofolini, L.; Fragai, M.; Pagano, B.; Trotta, R.; Cosconati, S.; Marinelli, L.; Novellino, E.; Bertini, I.; Randazzo, A.; Luchinat, C.; Parrinello, M. The G-Triplex DNA. *Angew. Chem* **2013**, *125* (8), 2325–2329.
- (3) G. Felsenfeld, David R. Davies, and A. R. Formation of a Three-Stranded Polynucleotide Molecule. *J. Am. Chem. Soc.* **1957**, *79* (8), 2022–2023.
- (4) Hoogsteen, K. The Crystal and Molecular Structure of a Hydrogen-Bonded Complex between 1-Methylthymine and 9-Methyladenine. *Acta Crystallogr.* **1963**, *16*, 907–916.
- (5) Gellert, M.; Lipsett, M. N.; Davies, D. R. Helix Formation by Guanylic Acid. *Proc. Natl. Acad. Sci. U. S. A.* **1962**, *48* (12), 2013–2018.
- (6) Arnott, S.; Chandrasekaran, K.; Marttila, C. M. Structures for Polyinosinic Acid and Polyguanylic Acid. *Biochem. J.* **1974**, *141* (2), 537–543.

- (7) Mathe, C.; Perigaud, C. Recent Approaches in the Synthesis of Conformationally Restricted Nucleoside Analogues. *European J. Org. Chem.* **2008**, *9*, 1489–1505.
- (8) Plavec, J.; Tong, W.; Chattopadhyaya, J. How Do the Gauche and Anomeric Effects Drive the Pseudorotational Equilibrium of the Pentofuranose Moiety of Nucleosides. *J. Am. Chem. Soc.* **1993**, *115* (21), 9734–9746.
- (9) Thibaudeau, C.; Acharya, P.; Chattopadhyaya, J. Stereoelectronic Effects in Nucleosides and Nucleotides and Their Structural Implications. *Uppsala University Press, Uppsala.* **1999**, 91-506.
- (10) Dougherty, J. P.; Rizzo, C. J.; Breslow, R. Oligodeoxynucleotides That Contain 2',5' Linkages: Synthesis and Hybridization Properties. *J. Am. Chem. Soc.* **1992**, *114* (10), 6254–6255.
- (11) Dhingra, M. M.; Sarma, R. H. Why Do Nucleic Acids Have 3'5' Phosphodiester Bonds? *Nature.* **1978**, 798–801.
- (12) Mergny, J.; Phan, A.; Lacroix, L. Following G-Quartet Formation by UV-Spectroscopy. *FEBS Lett.* **1998**, *435*, 74–78.
- (13) Wong, A.; Wu, G. Selective Binding of Monovalent Cations to the Stacking G-Quartet Structure Formed by Guanosine 5'-Monophosphate: A Solid-State NMR Study. *J. Am. Chem. Soc.* **2003**, *125* (45), 13895–13905.
- (14) Włodarczyk, A.; Grzybowski, P.; Patkowski, A.; Dobek, A. Effect of Ions on the Polymorphism, Effective Charge, and Stability of Human Telomeric DNA. Photon Correlation Spectroscopy and Circular Dichroism Studies. *J. Phys. Chem. B* **2005**, *109* (8), 3594–3605.
- (15) Pinnavaia, T. J.; Marshall, C. L.; Mettler, C. M.; Fisk, C. L.; Miles, H. T.; Becker, E. D. Alkali Metal Ion Specificity in the Solution Ordering of a Nucleotide, 5'-Guanosine Monophosphate. *J. Am. Chem. Soc.* **1978**, *100* (11), 3625–3627.
- (16) Smith, F. W.; Feigon, J. Quadruplex Structure of Oxytricha Telomeric DNA Oligonucleotides. *Nature* **1992**, *356*, 164–168.
- (17) Davis, J. T. G-Quartets 40 Years Later: From 5'-GMP to Molecular Biology and Supramolecular Chemistry. *Angew. Chemie - Int. Ed.* **2004**, *43* (6), 668–698.
- (18) Crnugelj, M.; Sket, P.; Plavec, J. Small Change in a G-Rich Sequence, a Dramatic

- Change in Topology: New Dimeric G-Quadruplex Folding Motif with Unique Loop Orientations. *J. Am. Chem. Soc.* **2003**, *125* (26), 7866–7871.
- (19) Guedin, A.; Alberti, P.; Mergny, J. L. Stability of Intramolecular Quadruplexes: Sequence Effects in the Central Loop. *Nucleic Acids Res.* **2009**, *37* (16), 5559–5567.
- (20) Rachwal, P. A.; Brown, T.; Fox, K. R. Sequence Effects of Single Base Loops in Intramolecular Quadruplex DNA. *FEBS Lett.* **2007**, *581* (8), 1657–1660.
- (21) Rachwal, P. A.; Findlow, I. S.; Werner, J. M.; Brown, T.; Fox, K. R. Intramolecular DNA Quadruplexes with Different Arrangements of Short and Long Loops. *Nucleic Acids Res.* **2007**, *35* (12), 4214–4222.
- (22) Webba Da Silva, M. Geometric Formalism for DNA Quadruplex Folding. *Chem. Eur. J.* **2007**, *13* (35), 9738–9745.
- (23) Burge, S.; Parkinson, G. N.; Hazel, P.; Todd, A. K.; Neidle, S. Quadruplex DNA: Sequence, Topology and Structure. *Nucleic Acids Res.* **2006**, *34* (19), 5402–5415.
- (24) Jing, H.; Fu, W.; Hu, W.; Xu, S.; Xu, X.; He, M.; Liu, Y.; Zhang, N. NMR Structural Study on the Self-Trimerization of d(GTTAGG) into a Dynamic Trimolecular G-Quadruplex Assembly Preferentially in Na<sup>+</sup> solution with a Moderate K<sup>+</sup> tolerance. *Nucleic Acids Res.* **2021**, *49* (4), 2306–2316.
- (25) Guedin, A.; Gros, J.; Alberti, P.; Mergny, J. L. How Long Is Too Long? Effects of Loop Size on G-Quadruplex Stability. *Nucleic Acids Res.* **2010**, *38* (21), 7858–7868.
- (26) Bhattacharyya, D.; Arachchilage, G. M.; Basu, S. Metal Cations in G-Quadruplex Folding and Stability. *Front. Chem.* **2016**, *4* (38), 1–14.
- (27) Chen, F. M. Sr<sup>2+</sup> Facilitates Intermolecular G-Quadruplex Formation of Telomeric Sequences. *Biochemistry* **1992**, *31* (15), 3769–3776.
- (28) Patel, P. K.; Bhavesh, N. S.; Hosur, R. V. Cation-Dependent Conformational Switches in d-TGGCGGC Containing Two Triplet Repeats of Fragile X Syndrome: NMR Observations. *Biochem. Biophys. Res. Commun.* **2000**, *278* (3), 833–838.
- (29) Hardin, C. C.; Henderson, E.; Watson, T.; Prosser, J. K. Monovalent Cation Induced Structural Transitions in Telomeric DNAs: G-DNA Folding Intermediates. *Biochemistry* **1991**, *30*, 4460–4472.

- (30) Balagurumoorthy, P.; Brahmachari, S. K.; Mohanty, D.; Bansal, M.; Sasisekharan, V. Hairpin and Parallel Quartet Structures for Telomeric Sequences. *Nucleic Acids Res.* **1992**, *20* (15), 4061–4067.
- (31) Strahan, G. D.; Keniry, M. A.; Shafer, R. H. NMR Structure Refinement and Dynamics of the  $K^+$ -[d(G<sub>3</sub>T<sub>4</sub>G<sub>3</sub>)]<sub>2</sub> Quadruplex via Particle Mesh Ewald Molecular Dynamics Simulations. *Biophys. J.* **1998**, *75*, 968–981.
- (32) Venczel, E. A.; Sen, D. Parallel and Antiparallel G-DNA Structures from Complex Telomeric Sequence \*. *Biochemistry* **1993**, *32*, 6220–6228.
- (33) Miyoshi, D.; Nakao, A.; Sugimoto, N.; Technology, H. Structural Transition of (G<sub>4</sub>T<sub>4</sub>G<sub>4</sub>) from Antiparallel to Parallel G-Quartet Induced by Divalent Cations. *Nucleic Acids Res.* **2001**, *2* (1), 259–260.
- (34) Majhi, P. R.; Shafer, R. H. Characterization of an Unusual Folding Pattern in a Catalytically Active Guanine Quadruplex Structure. *Biopolymers* **2006**, *82* (6), 558–569.
- (35) Ku, T.; Zhang, T.; Luo, H.; Yen, T. M.; Chen, P.; Han, Y.; Lo, Y. Nucleic Acid Aptamers: An Emerging Tool for Biotechnology and Biomedical Sensing. *sensors* **2015**, *15*, 16281–16313.
- (36) Ellington, A. D.; Szostak, J. W. In Vitro Selection of RNA Molecules That Bind Specific Ligands. *Nature* **1990**, *346* (6287), 818–822.
- (37) Tuerkt, C.; Gold, L. Systematic Evolution of Ligands by Exponential Enrichment: RNA Ligands to Bacteriophage T4 DNA Polymerase. *Science* **1990**, *249* (4968), 505–510.
- (38) Viores, S. A. Pegaptanib in the Treatment of Wet, Age-Related Macular Degeneration. *Int. J. Nanomedicine* **2006**, *1* (3), 263–268.
- (39) Bock, L.; Griffin, L.; Lantham, J.; Vermass, E.; Toole, J. Selection of Single-Stranded DNA Molecules That Bind and Inhibit Human Thrombin. *Nature* **1992**, *355*, 564–566.
- (40) Ireson, C. R.; Kelland, L. R. Discovery and Development of Anticancer Aptamers. *Mol. Cancer Ther.* **2006**, *5* (12), 2957–2962.
- (41) Zhu, Q.; Jing, N. Computational Study on Mechanism of G-Quartet Oligonucleotide T40214 Selectively Targeting Stat3. *J. Comput. Aided. Mol. Des.* **2007**, *21*, 641–648.

- (42) Li, Y.; Geyer, C. R.; Sen, D. Recognition of Anionic Porphyrins by DNA Aptamers. *Biochemistry* **1996**, *35* (21), 6911–6922.
- (43) Travascio, P.; Li, Y.; Sen, D. DNA-Enhanced Peroxidase Activity of a DNA Aptamer-Hemin Complex. *Chem. Biol.* **1998**, *5* (9), 505–517.
- (44) Ueyama, H.; Takagi, M.; Takenaka, S. A Novel Potassium Sensing in Aqueous Media with a Synthetic Oligonucleotide Derivative. Fluorescence Resonance Energy Transfer Associated with Guanine Quartet-Potassium Ion Complex Formation. *J. Am. Chem. Soc.* **2002**, *124* (48), 14286–14287.
- (45) Huizenga, D.; Szostak, J. A DNA Aptamer That Binds Adenosine and ATP. *Biochemistry* **1995**, *34* (2), 656–665.
- (46) Schultze, P.; Macaya, R.; Feigon, J. Three-Dimensional Solution Structure of the Thrombin-Binding DNA Aptamer d(GGTTGGTGTGGTTGG). *J. Mol. Biol.* **1994**, *235* (5), 1532–1547.
- (47) Lancellotti, S.; De Cristofaro, R. Nucleotide-Derived Thrombin Inhibitors: A New Tool for an Old Issue. *Cardiovasc. Hematol. Agents Med. Chem.* **2009**, *7* (1), 19–28.
- (48) Goodchild, J. Conjugates of Oligonucleotides and Modified Oligonucleotides: A Review of Their Synthesis and Properties. *Bioconjug. Chem.* **1990**, *1* (3), 165–187.
- (49) He, G.; Krawczyk, S.; Swaminathan, S.; Shea, R.; Dougherty, J.; Terhorst, T.; Law, V.; Griffin, L.; Coutre, S.; Bischofberger, N. N<sup>2</sup>- and C<sup>8</sup>-Substituted Oligodeoxynucleotides with Enhanced Thrombin Inhibitory Activity in Vitro and in Vivo. *J. Med. Chem.* **1998**, *41* (13), 2234–2242.
- (50) Goji, S.; Matsui, J. Direct Detection of Thrombin Binding to 8-Bromodeoxyguanosine-Modified Aptamer: Effects of Modification on Affinity and Kinetics. *Journal of Nucleic Acids* **2011**, 316079.
- (51) Lopez De La Osa, J.; Gonzalez, C.; Gargallo, R.; Rueda, M.; Cubero, E.; Orozco, M.; Avino, A.; Eritja, R. Destabilization of Quadruplex DNA by 8-Aminoguanine. *ChemBioChem* **2006**, *7* (1), 46–48.
- (52) Marathias, V.; Sawicki, M.; Bolton, P. 6-Thioguanine Alters the Structure and Stability of Duplex DNA and Inhibits Quadruplex DNA Formation. *Nucleic Acids Res.* **1999**, *27* (14), 2860–2867.



- (53) Nallagatla, S.; Heuberger, B.; Haque, A.; Switzer, C. Combinatorial Synthesis of Thrombin-Binding Aptamers Containing Iso-Guanine. *J. Comb. Chem.* **2009**, *11* (3), 364–369.
- (54) Olsen, C.; Lee, H.; Marky, L. Unfolding Thermodynamics of Intramolecular G-Quadruplexes: Base Sequence Contributions of the Loops. *J. Phys. Chem. B* **2009**, *113* (9), 2587–2595.
- (55) Tsvetkov, V.; Varizhuk, A.; Pozmogova, G.; Smirnov, I.; Kolganova, N.; Timofeev, E. A Universal Base in a Specific Role: Tuning up a Thrombin Aptamer with 5-Nitroindole. *Sci. Rep.* **2015**, *5*, 1–11.
- (56) Avino, A.; Fabrega, C.; Tintore, M.; Eritja, R. Thrombin Binding Aptamer, More than a Simple Aptamer: Chemically Modified Derivatives and Biomedical Applications. *Curr. Pharm. Des.* **2012**, *18* (14), 2036–2047.
- (57) Smirnov, I.; Shafer, R. Effect of Loop Sequence and Size on DNA Aptamer Stability. *Biochemistry* **2000**, *39* (6), 1462–1468.
- (58) Portella, G.; Ferreira, R.; Gargallo, R.; Mazzini, S.; Avi, A. Specific Loop Modifications of the Thrombin-Binding Aptamer Trigger the Formation of Parallel Structures. *FEBS J.* **2014**, *281* (4), 1085–1099.
- (59) Kolganova, N.; Varizhuk, A.; Novikov, R.; Florentiev, V.; Pozmogova, G.; Borisova, O.; Shchyolkina, A.; Smirnov, I.; Kaluzhny, D.; Timofeev, E. Anomeric DNA Quadruplexes. *Artif. DNA PNA XNA* **2014**, *5* (2), e28422-1- e28422-8.
- (60) Mendelboum Raviv, S.; Horvath, A.; Aradi, J.; Bagoly, Z.; Fazakas, F.; Batta, Z.; Muszbek, L.; Harsfalvi, J. 4-Thio-Deoxyuridylate-Modified Thrombin Aptamer and Its Inhibitory Effect on Fibrin Clot Formation, Platelet Aggregation and Thrombus Growth on Subendothelial Matrix. *J. Thromb. Haemost.* **2008**, *6* (10), 1764–1771.
- (61) Esposito, V.; Russo, A.; Amato, T.; Vellecco, V.; Bucci, M.; Mayol, L.; Russo, G.; Virgilio, A.; Galeone, A. The “Janus Face” of the Thrombin Binding Aptamer: Investigating the Anticoagulant and Antiproliferative Properties through Straightforward Chemical Modifications. *Bioorg. Chem.* **2018**, *76*, 202–209.
- (62) Cai, B.; Yang, X.; Sun, L.; Fan, X.; Li, L.; Jin, H.; Wu, Y.; Guan, Z.; Zhang, L.; Zhang, L.; Yang, Z. Stability and Bioactivity of Thrombin Binding Aptamers Modified with D-

- /I-Isothymidine in the Loop Regions. *Org. Biomol. Chem.* **2014**, *12* (44), 8866–8876.
- (63) Tateishi-Karimata, H.; Ohyama, T.; Muraoka, T.; Podbevsek, P.; Wawro, A. M.; Tanaka, S.; Nakano, S. I.; Kinbara, K.; Plavec, J.; Sugimoto, N. Newly Characterized Interaction Stabilizes DNA Structure: Oligoethylene Glycols Stabilize G-Quadruplexes CH- $\pi$  Interactions. *Nucleic Acids Res.* **2017**, *45* (12), 7021–7030.
- (64) Dolot, R.; Lam, C. H.; Sierant, M.; Zhao, Q.; Liu, F.; Nawrot, B.; Egli, M.; Yang, X. Crystal Structures of Thrombin in Complex with Chemically Modified Thrombin DNA Aptamers Reveal the Origins of Enhanced Affinity. *Nucleic Acids Res.* **2018**, *46* (9), 4819–4830.
- (65) Kovacic, M.; Podbevsek, P.; Tateishi-Karimata, H.; Takahashi, S.; Sugimoto, N.; Plavec, J. Thrombin Binding Aptamer G-Quadruplex Stabilized by Pyrene-Modified Nucleotides. *Nucleic Acids Res.* **2020**, *48* (7), 3975–3986.
- (66) Tang, C.; Shafer, R. Engineering the Quadruplex Fold: Nucleoside Conformation Determines Both Folding Topology and Molecularity in Guanine Quadruplexes. *J. Am. Chem. Soc.* **2006**, *128*, 5966–5973.
- (67) Opalinska, J.; Gewirtz, A. Nucleic-Acid Therapeutics: Basic Principles and Recent Applications. *Nat. Rev. Drug Discov.* **2002**, *1* (7), 503–514.
- (68) Randazzo, A.; Esposito, V.; Ohlenschlager, O.; Ramachandran, R.; Virgilio, A.; Mayol, L. Structural Studies on LNA Quadruplexes. *Nucleosides, Nucleotides and Nucleic Acids* **2005**, *24* (5–7), 795–800.
- (69) Pasternak, A.; Hernandez, F. J.; Rasmussen, L. M.; Vester, B.; Wengel, J. Improved Thrombin Binding Aptamer by Incorporation of a Single Unlocked Nucleic Acid Monomer. *Nucleic Acids Res.* **2011**, *39* (3), 1155–1164.
- (70) Jensen, T.; Henriksen, J.; Rasmussen, B.; Rasmussen, L.; Andresen, T.; Wengel, J.; Pasternak, A. Thermodynamic and Biological Evaluation of a Thrombin Binding Aptamer Modified with Several Unlocked Nucleic Acid (UNA) Monomers and a 2'-C-Piperazino-UNA Monomer. *Bioorg. Med. Chem.* **2011**, *19* (16), 4739–4745.
- (71) Saneyoshi, H.; Mazzini, S.; Avino, A.; Portella, G.; Gonzalez, C.; Orozco, M.; Marquez, V.; Eritja, R. Conformationally Rigid Nucleoside Probes Help Understand the Role of Sugar Pucker and Nucleobase Orientation in the Thrombin-Binding Aptamer. *Nucleic*

- Acids Res.* **2009**, 37 (17), 5589–5601.
- (72) Saneyoshi, H.; Mazzini, S.; Avino, A.; Portella, G.; González, C.; Orozco, M.; Marquez, V. E.; Eritja, R. The Use of Conformationally Rigid Nucleoside Probes to Study the Role of Sugar Pucker and Nucleobase Orientation in the Thrombin Binding Aptamer. *Nucleic Acids Symp. Ser. (Oxf)*. **2009**, No. 53, 109–110.
- (73) Avino, A.; Mazzini, S.; Ferreira, R.; Gargallo, R.; Marquez, V.; Eritja, R. The Effect on Quadruplex Stability of North-Nucleoside Derivatives in the Loops of the Thrombin-Binding Aptamer. *Bioorg. Med. Chem.* **2012**, 20 (14), 4186–4193.
- (74) Peng, C. G.; Damha, M. J. G-Quadruplex Induced Stabilization by 2'-Deoxy-2'-Fluoro-d-Arabinonucleic Acids (2'F-ANA). *Nucleic Acids Res.* **2007**, 35 (15), 4977–4988.
- (75) Zhao, X.; Liu, B.; Yan, J.; Yuan, Y.; An, L.; Guan, Y. Structure Variations of TBA G-Quadruplex Induced by 2'-O-Methyl Nucleotide in  $K^+$  and  $Ca^{2+}$  Environments. *Acta Biochim. Biophys. Sin.* **2014**, 46 (10), 837–850.
- (76) Awachat, R.; Wagh, A.; Aher, M.; Fernandes, M.; Kumar, V. Favorable 2'-Substitution in the Loop Region of a Thrombin-Binding DNA Aptamer. *Bioorg. Med. Chem. Lett.* **2018**, 28 (10), 1765–1768.
- (77) Coppola, T.; Varra, M.; Oliviero, G.; Galeone, A.; D'Isa, G.; Mayol, L.; Morelli, E.; Bucci, M. R.; Vellecco, V.; Cirino, G.; Borbone, N. Synthesis, Structural Studies and Biological Properties of New TBA Analogues Containing an Acyclic Nucleotide. *Bioorg. Med. Chem.* **2008**, 16 (17), 8244–8253.
- (78) Borbone, N.; Bucci, M.; Oliviero, G.; Morelli, E.; Amato, J.; D'Atri, V.; D'Errico, S.; Vellecco, V.; Cirino, G.; Piccialli, G.; Fattorusso, C.; Varra, M.; Mayol, L.; Persico, M.; Scuotto, M. Investigating the Role of T7 and T12 Residues on the Biological Properties of Thrombin-Binding Aptamer: Enhancement of Anticoagulant Activity by a Single Nucleobase Modification. *J. Med. Chem.* **2012**, 55 (23), 10716–10728.
- (79) Aaldering, L.; Poongavanam, V.; Langkjær, N.; Murugan, N. A.; Jorgensen, P. T.; Wengel, J.; Veedu, R. N. Development of an Efficient G-Quadruplex-Stabilised Thrombin-Binding Aptamer Containing a Three-Carbon Spacer Molecule. *ChemBioChem* **2017**, 18 (8), 755–763.
- (80) Mo, M.; Kong, D.; Ji, H.; Lin, D.; Tang, X.; Yang, Z.; He, Y.; Wu, L. Reversible

- Photocontrol of Thrombin Activity by Replacing Loops of Thrombin Binding Aptamer Using Azobenzene Derivatives. *Bioconjug. Chem.* **2019**, *30* (1), 231–241.
- (81) Scuotto, M.; Rivieccio, E.; Varone, A.; Corda, D.; Bucci, M.; Vellecco, V.; Cirino, G.; Virgilio, A.; Esposito, V.; Galeone, A.; Borbone, N.; Varra, M.; Mayol, L. Site Specific Replacements of a Single Loop Nucleoside with a Dibenzyl Linker May Switch the Activity of TBA from Anticoagulant to Antiproliferative. *Nucleic Acids Res.* **2015**, *43* (16), 7702–7716.
- (82) Avino, A.; Mazzini, S.; Fabrega, C.; Penalver, P.; Gargallo, R.; Morales, J. C.; Eritja, R. The Effect of L-Thymidine, Acyclic Thymine and 8-Bromoguanine on the Stability of Model G-Quadruplex Structures. *Biochim Biophys Acta Gen Subj.* **2017**, *1861* (5), 1205–1212.
- (83) Zaitseva, M.; Kaluzhny, D.; Shchyolkina, A.; Borisova, O.; Smirnov, I.; Pozmogova, G. Conformation and thermostability of oligonucleotide d(GGTTGGTGTGGTTGG) containing thiophosphoryl internucleotide bonds at different positions. *Biophys. Chem.* **2010**, *146* (1), 1–6.
- (84) Saccà, B.; Lacroix, L.; Mergny, J. L. The Effect of Chemical Modifications on the Thermal Stability of Different G-Quadruplex-Forming Oligonucleotides. *Nucleic Acids Res.* **2005**, *33* (4), 1182–1192.
- (85) He, G. X.; Williams, J. P.; Postich, M. J.; Swaminathan, S.; Shea, R. G.; Terhorst, T.; Law, V. S.; Mao, C. T.; Sueoka, C.; Coutre, S.; Bischofberger, N. In Vitro and in Vivo Activities of Oligodeoxynucleotide-Based Thrombin Inhibitors Containing Neutral Formacetal Linkages. *J. Med. Chem.* **1998**, *41* (22), 4224–4231.
- (86) Gunjal, A. D.; Fernandes, M.; Erande, N.; Rajamohanam, P.; Kumar, V. A. Functional IsoDNA Aptamers: Modified Thrombin Binding Aptamers with a 2'-5'-Linked Sugar-Phosphate Backbone (IsoTBA). *Chem. Commun.* **2014**, *50* (5), 605–607.
- (87) Esposito, V.; Galeone, A.; Mayol, L.; Randazzo, A.; Virgilio, A.; Virno, A. A Mini-Library of TBA Analogues Containing 3'-3' and 5'-5' Inversion of Polarity Sites. *Nucleosides, Nucleotides and Nucleic Acids* **2007**, *26* (8–9), 1145–1149.
- (88) Pagano, B.; Martino, L.; Randazzo, A.; Giancola, C. Stability and Binding Properties of a Modified Thrombin Binding Aptamer. *Biophys. J.* **2008**, *94* (2), 562–569.

- (89) Varizhuk, A.; Tsvetkov, V.; Tatarinova, O.; Kaluzhny, D.; Florentiev, V.; Timofeev, E.; Shcholykina, A.; Borisova, O.; Smirnov, I.; Grokhovsky, S.; Aseychev, A.; Pozmogova, G. Synthesis, Characterization and in Vitro Activity of Thrombin-Binding DNA Aptamers with Triazole Internucleotide Linkages. *Eur. J. Med. Chem.* **2013**, *67*, 90–97.
- (90) Esposito, V.; Scuotto, M.; Capuozzo, A.; Santamaria, R.; Varra, M.; Mayol, L.; Virgilio, A.; Galeone, A. A Straightforward Modification in the Thrombin Binding Aptamer Improving the Stability, Affinity to Thrombin and Nuclease Resistance. *Org. Biomol. Chem.* **2014**, *12* (44), 8840–8843.
- (91) Varada, M.; Aher, M.; Erande, N.; Kumar, V. A.; Fernandes, M. Methoxymethyl Threofuranosyl Thymidine (4'-MOM-TNA-T) at the T7 Position of the Thrombin-Binding Aptamer Boosts Anticoagulation Activity, Thermal Stability, and Nuclease Resistance. *ACS Omega* **2020**, *5* (1), 498–506.
- (92) Krauss, I. R.; Merlino, A.; Randazzo, A.; Novellino, E.; Mazzarella, L.; Sica, F.; Ii, F.; Cintia, V.; Napoli, I.; Istituto, I.; Chimiche, S.; Bioimmagini, B.; Mezzocannone, V.; Napoli, I.; Chimica, D. High-Resolution Structures of Two Complexes between Thrombin and Thrombin-Binding Aptamer Shed Light on the Role of Cations in the Aptamer Inhibitory Activity. *Nucleic Acids Res.* **2012**, *40* (16), 8119–8128..
- (93) Kelly, J.; Feigon, J.; Yeates, T. Reconciliation of the X-Ray and NMR Structures of the Thrombin-Binding Aptamer d(GGTTGGTGTGGTTGG). *J. Mol. Biol.* **1996**, *256* (3), 417–422.
- (94) Michelson, A. M.; Todd, A. Synthesis of a Dithymidine Dinucleotide Containing a 3': 5'-Internucleotidic Linkage. *J. Label. Comp. Radiopharm.* **1955**, *2206*, 2632–2636.
- (95) Gilham, P.; Khorana, H. Studies on Polynucleotides I. A New and General Method for the Chemical Synthesis of the C5'-C3' Internucleotidic Linkage. Syntheses of Deoxyribo-Dinucleotides. *J. Am. Chem. Soc.* **1958**, *80* (23), 6212–6222.
- (96) Letsinger, R. L.; Mahadevan, V. Stepwise Synthesis of Oligodeoxyribonucleotides on an Insoluble Polymer Support. *J. Am. Chem. Soc.* **1966**, *88* (22), 5319–5324.
- (97) Letsinger, R.; Finnan, J.; Heavner, G. A.; Lunsford, W. B. Phosphite Coupling Procedure for Generating Internucleotide Links. *J. Am. Chem. Soc.* **1975**, *97* (11), 3278–3279.

- 
- (98) Matteucci, M. D.; Caruthers, M. H. Synthesis of Deoxyoligonucleotides on a Polymer Support. *J. Am. Chem. Soc.* **1981**, *103* (11), 3185–3191.
- (99) Mergny, J.; Li, J.; Lacroix, L.; Amrane, S.; Chaires, J. Thermal Difference Spectra: A Specific Signature for Nucleic Acid Structures. *Nucleic Acids Res.* **2005**, *33* (16), 1–6.
- (100) Elzagheid, M. I.; Viazovkina, E.; Damha, M. J. Synthesis of Protected 2'-Deoxy-2'-Fluoro- $\beta$ -D-Arabinonucleosides. *Curr. Protoc. Nucleic Acid Chem* **2002**, *10* (1), 1–19.
- (101) Gray, D.; Wen, J.; Gray, C.; Repges, R.; Repges, C.; Raabe, G.; Fleischhauer, J. Measured and Calculated CD Spectra of G-Quartets Stacked with the Same or Opposite Polarities. *Chirality* **2008**, *20*, 431–440.
- (102) Paramasivan, S.; Rujan, I.; Bolton, P. H. Circular Dichroism of Quadruplex DNAs: Applications to Structure, Cation Effects and Ligand Binding. *Methods* **2007**, *43* (4), 324–331.
- (103) Pagba, C. V.; Lane, S. M.; Wachsmann-Hogiu, S. Raman and Surface-Enhanced Raman Spectroscopic Studies of the 15-Mer DNA Thrombin-Binding Aptamer. *J. Raman Spectrosc.* **2010**, *41* (3), 241–247.

## **Chapter 2**

**Effect of alkali and alkaline earth  
metal cations**

**on the isoTBA quadruplex:**

**Application**

**to the detection of Sr<sup>2+</sup>**

## 2.1 Introduction

G-quadruplexes have attracted increasing attention in recent years because of their importance in key cellular regulatory processes, aptamers towards macromolecular drugs, and the development of nanostructures for varied applications. Within the cell, they are found to be present in widely distributed locations<sup>1</sup> apart from telomeric regions, where they were first found, including other regions such as promoters, where they carry out critical roles in controlling gene expression through regulation of transcription and translation. They also form an important class of aptamers and display improved cellular uptake properties and increased resistance to nuclease degradation due to their remarkable kinetic and thermodynamic stability.<sup>2</sup> G-quadruplexes are formed as a consequence of stacking of successive G-quartets, that are in turn stabilized by hydrogen bonding of four guanine residues.<sup>3</sup> The G-quartets are further stabilized by the presence of metal ions, that are typically located between two successive G-quartets and are tightly associated through coordination to the guanine O6-carbonyl groups of the neighboring planes.<sup>4</sup>

The thrombin-binding pentadecameric aptamer (TBA), d(G<sub>2</sub>T<sub>2</sub>G<sub>2</sub>TGTG<sub>2</sub>T<sub>2</sub>G<sub>2</sub>) is widely studied and is known to fold into a unimolecular anti-parallel G-quadruplex in the presence of K<sup>+</sup> ions.<sup>5</sup> This quadruplex comprises two G-quartets stacked on each other, connected by three edge-wise loops: two TT loops and one central TGT loop. The role of different cations Li<sup>+</sup>, Na<sup>+</sup>, K<sup>+</sup>, Rb<sup>+</sup>, Cs<sup>+</sup>, Mg<sup>2+</sup>, Ca<sup>2+</sup>, Sr<sup>2+</sup>, Ba<sup>2+</sup> in the formation of this structure was earlier reported.<sup>6</sup> Although several monovalent and divalent cations were studied, in all cases, the unimolecular anti-parallel quadruplex topology was observed.<sup>6</sup> The stability of the resulting TBA G-quadruplexes was rationally explained as a consequence of the ionic radii, with cations possessing an ionic radius in the range of 1.3 Å to 1.5 Å leading to stabler quadruplexes compared to others, owing to a favorable fit between the two G-quartets. Several modifications in the sugar-phosphate backbone of TBA have been reported with a view to enhancing its properties.<sup>7-10</sup> An isoTBA oligomer wherein the natural 3'-5'-phosphodiester backbone linkages were replaced by the isomeric 2'-5'-phosphodiester (Figure 1), showed that it could fold into a unimolecular anti-parallel G-quadruplex structure, similar to that observed for TBA and also effect anti-coagulation.<sup>11</sup>

The isomeric backbone in this oligomer leads to further enhancement in the nuclease resistance properties of the G-quadruplex and is, therefore, attractive in the context of application in biological systems. Further, studies on loop-edited isoTBA oligomers<sup>12</sup> led to the observation that even oligomers containing the shortest loops (only one T per loop and three-loop residues) retained the unimolecular anti-parallel quadruplex fold, completely in



contrast to the TBA oligomers, where shorter loop lengths (total number of loop residues less than 6) were found to result in multimolecular parallel quadruplexes, as reported for several other G-quadruplex sequences as well.<sup>13</sup>

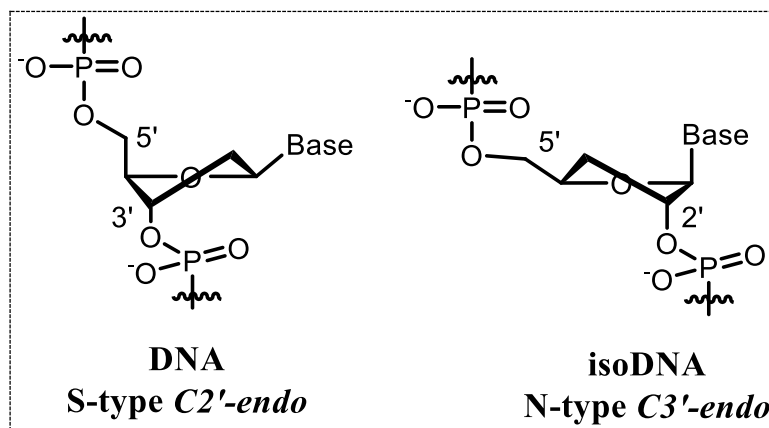


Figure 1: Backbone geometry in DNA and isoDNA

## 2.2 Rationale and objectives of the present work

G-quadruplex structures are stabilized due to the presence of cations, and different cations can give rise to different polymorphs. Some examples illustrating this are described here. The triplet repeat sequence d(TG<sub>2</sub>CG<sub>2</sub>C) forms a tetramolecular parallel G-quadruplex in the presence of K<sup>+</sup> ions. Interestingly, under similar conditions, when Na<sup>+</sup> ions replace the K<sup>+</sup>, it forms an anti-parallel G-quadruplex.<sup>14</sup> The telomeric DNA repeats of *Tetrahymena* d(T<sub>2</sub>G<sub>4</sub>)<sub>4</sub> form a unimolecular structure in sodium phosphate buffer, while adopting a multi-strand G-quadruplex structure in potassium phosphate buffer.<sup>15</sup> The sequences d(G<sub>3</sub>T<sub>4</sub>G<sub>3</sub>) and d(G<sub>4</sub>T<sub>4</sub>G<sub>4</sub>) folded in bimolecular G-quadruplex structures in the presence of Na<sup>+</sup> ions, although with K<sup>+</sup> ions, both bimolecular and tetramolecular G-quadruplexes were observed.<sup>16,17</sup>

The structural polymorphism of the G-quadruplex is not only observed with monovalent cations, but also divalent cations. In 1993, Sen and coworkers reported that the G-quadruplex-forming *Saccharomyces* telomeric consensus sequence d(TGTG<sub>3</sub>TGTGTGTG<sub>3</sub>) switches from a parallel to an antiparallel topology in the presence of divalent cations.<sup>18</sup> The sequence d(G<sub>4</sub>T<sub>4</sub>G<sub>4</sub>) also showed antiparallel to parallel G-quadruplex transformation in the presence of different divalent cations.<sup>19</sup> Another sequence, d(GTG<sub>3</sub>TAG<sub>3</sub>CG<sub>3</sub>T<sub>2</sub>G<sub>2</sub>), showed structural polymorphism with K<sup>+</sup> and Pb<sup>2+</sup> ions; both unimolecular antiparallel and multi-stranded parallel structures were formed with K<sup>+</sup> ions, but with Pb<sup>2+</sup> ions, only an antiparallel unimolecular G-quadruplex structure was observed.<sup>20</sup> Collectively, these studies provide evidence for structural polymorphisms of G-quadruplexes induced by mono- and divalent cations.

Likewise, the structure of TBA in the presence of different cations has been studied and is reported to show only unimolecular antiparallel kind of quadruplex folding topology.<sup>6</sup> The TBA sequence, but with a 2'-5'-phosphodiester backbone linkage (isoTBA) was previously reported by our group,<sup>11</sup> but extensive studies on the structural preference in the presence of different cations was not undertaken. These studies are reported here. A change in the topology can either increase or decrease the function of the aptamer; therefore, topology and cations play a significant role in the functions of the quadruplexes.

## 2.3 Results and discussion

### 2.3.1 Synthesis of TBA, isoTBA oligomers, their purification and characterization

3'-5'-phosphodiester-linked TBA and 2'-5'-phosphodiester-linked isoTBA oligonucleotides were synthesized using commercially available protected 2'-deoxyguanosine-3'-phosphoramidite, 2'-deoxythymidine-3'-phosphoramidite, 3'-deoxythymidine-2'-phosphoramidite, and 3'-deoxyguanosine-2'-phosphoramidite by standard  $\beta$ -cyanoethyl phosphoramidite chemistry.<sup>21</sup> The general scheme for solid-phase oligonucleotide synthesis is explained in Chapter 1, Scheme 1. Post-synthesis, reverse-phase HPLC purification of the oligomers was carried out, and their identity was confirmed by MALDI-TOF mass analysis (Table 1).

Table 1. TBA and isoTBA oligomers.

Sr.No.	Sequence	Sequence name	MALDI TOF Mass (Da)	
			M <sub>calcd.</sub>	M <sub>obsd.</sub>
1	<b>TBA</b>	5'-GGTTGGTGTGGTTGG-3'	4726	4731
2	<b>IsoTBA</b>	5'-GGTTGGTGTGGTTGG-2'	4726	4727

### 2.3.2 Circular dichroism spectroscopy studies of TBA, isoTBA for evaluation of G-quadruplex formation and topology

CD spectroscopy is a valuable and widely-used technique to evaluate the formation and topology of G-quadruplexes. A maximum at ~ 260 nm with a minimum at ~ 240 nm may be attributed to the stacking of successive guanines with the same (both *syn* or both *anti*) glycosidic bond angle and is thus a characteristic of parallel quadruplexes.<sup>22, 23</sup> There is thus, no clear signal at ~ 290 nm in these quadruplexes. On the other hand, antiparallel quadruplexes

display a maximum at  $\sim 290$  nm and a minimum at  $\sim 260$  nm, which arises as a result of guanosines with different glycosidic bond angles stacking on each other.<sup>23</sup>

In the presence of  $\text{Na}^+$  and  $\text{K}^+$  ions, the typical anti-parallel topology was observed for both TBA and isoTBA, as reported earlier.<sup>6,11</sup> Both displayed maxima centered at 292 nm and minima near 260 nm. In the presence of  $\text{Sr}^{2+}$ , however, starkly contrasting spectra were observed with TBA and isoTBA. TBA displayed a CD spectrum corresponding to an antiparallel G-quadruplex, as reported earlier,<sup>6</sup> with a maximum at 300 nm, while the CD spectrum of isoTBA suggested a parallel G-quadruplex, with a strong maximum at 260 nm and a minimum at 240 nm (Figure 2b). Some differences were also observed with the other ions studied, but these were not so remarkable.

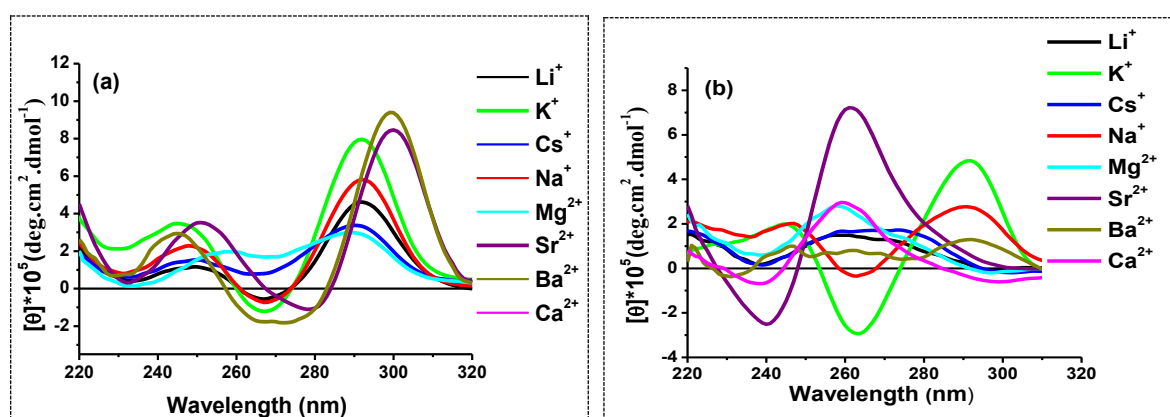


**Figure 2.** CD spectra at 4°C in the presence of different mono- and divalent cations, of (a) TBA and (b) isoTBA.

The CD spectra of TBA in the presence of  $\text{Li}^+$ ,  $\text{Cs}^+$ ,  $\text{Mg}^{2+}$ , and  $\text{Ba}^{2+}$  indicated the presence of antiparallel quadruplexes, as reported earlier, with the 292 nm maximum red-shifted to 300 nm in the presence of  $\text{Ba}^{2+}$  (Figure 2a).<sup>6</sup> The CD signals of isoTBA in the presence of  $\text{Li}^+$ ,  $\text{Cs}^+$ ,  $\text{Mg}^{2+}$  and  $\text{Ba}^{2+}$ , on the other hand, were inconclusive and of very low intensity (Figure 2 b). The amplitude of the maximum was found to vary with the cation, consistent with earlier reports.<sup>6</sup> The observed differences in the strength of the CD signal, apparent as differential CD amplitude, could be a consequence of differences in the coordination number of the metal ions and the strength of the complex formed, which in turn also depends on the charge and ionic radius.<sup>6</sup> Thus, a decreased CD amplitude could result from partially unfolded structures, owing to the low thermal stability of the quadruplex. Although the magnitude of the CD band at a particular wavelength could differ, depending on the cation, all CD spectra with a typical maximum showed an isoelliptic point at 275 nm for TBA and 280 nm for isoTBA, indicating the formation of similar types of complexes in terms of molecularity.

### 2.3.3 Evaluation of G-quadruplex thermal stability

The thermal stability of the observed quadruplexes was assessed by temperature-dependent changes that were followed by CD and UV spectroscopy. The melting data are indicated in Table 2, and the CD-melting plots are shown in Figure 3.

Table 2. CD- and UV-melting data for the TBA/isoTBA quadruplexes in the presence of different cations.

Sr. No.	Cation	TBA		isoTBA	
		CD- $T_m$ (°C)	UV- $T_m$ (°C)	CD- $T_m$ (°C)	UV- $T_m$ (°C)
1	Li <sup>+</sup>	20 ± 1	14 ± 2	nd	nd
2	Na <sup>+</sup>	22 ± 1.5	21 ± 1	19 ± 0.5	21 ± 1
3	K <sup>+</sup>	49 ± 0.5	51 ± 0.5	29 ± 1	29 ± 1
4	Cs <sup>+</sup>	20 ± 0.5	18 ± 1	nd	nd
5	Mg <sup>2+</sup>	16 ± 1	14 ± 1	nd	nd
6	Sr <sup>2+</sup>	63 ± 1	61 ± 1	62 <sup>a</sup> ± 1	63 ± 1
7	Ba <sup>2+</sup>	57 ± 1.5	53 ± 1.5	26 ± 1	28 ± 1

<sup>a</sup>measured at 260 nm. nd = not detected. Measurements were carried out using TBA/isoTBA at 5 μM concentration, in Tris buffer (10 mM), pH 7.2, containing the respective cation (100 mM) in the form of its chloride. Experiments were repeated at least three times, and the average values are listed with the standard deviations.

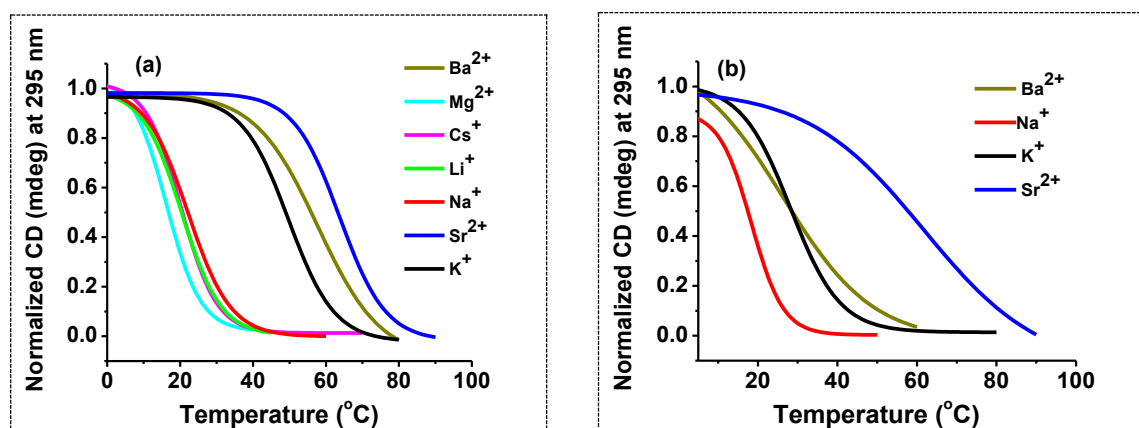


Figure 3. CD melting plots of (a) TBA and (b) isoTBA in the presence of the different cations of the study. The CD amplitude at 295 nm was monitored with increasing temperature for all plots, except Sr<sup>2+</sup>-isoTBA, which was monitored at 260 nm.

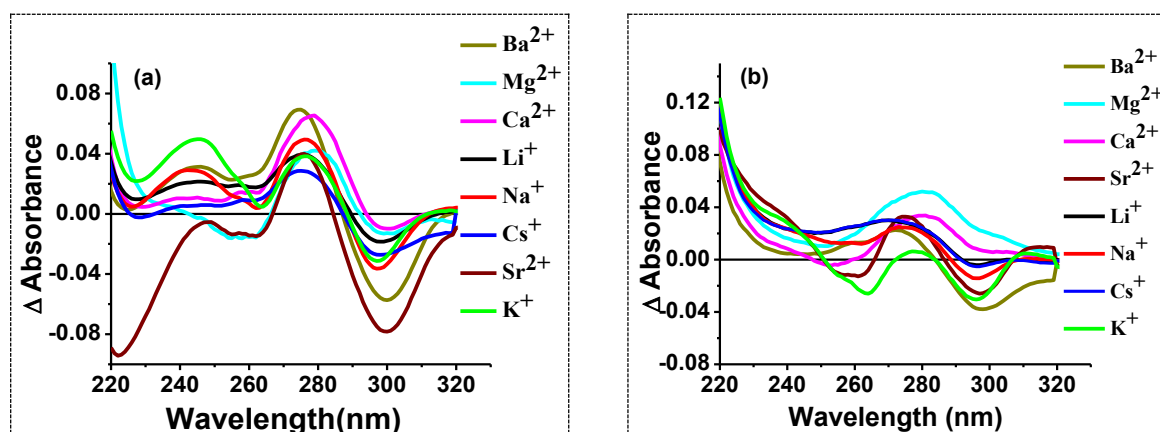
Among the monovalent ions studied, the most stable quadruplexes were formed in the presence of K<sup>+</sup>, where TBA melted at 49 °C and isoTBA at 29 °C. On the whole, the quadruplexes formed were the most stable in the presence of Sr<sup>2+</sup> ( $T_m$  = 63 °C and 62 °C for TBA and isoTBA, respectively). The  $T_m$  values of TBA in the presence of the other ions followed the trend as reported earlier, with Ba<sup>2+</sup> also leading to stable quadruplex formation

( $T_m = 57\text{ }^\circ\text{C}$ ) while the quadruplexes of isoTBA in the presence of the other cations were comparatively unstable; with  $\text{Ba}^{2+}$ , the  $T_m$  was  $26\text{ }^\circ\text{C}$ , while it was  $19\text{ }^\circ\text{C}$  with  $\text{Na}^+$  and not clearly detectable with  $\text{Li}^+$ ,  $\text{Cs}^+$  or  $\text{Mg}^{2+}$ .

UV-spectroscopy can conveniently monitor the thermal stability of G-quadruplexes by measuring the temperature-dependent change in absorbance at  $295\text{ nm}$ ,<sup>24</sup> where transitions of other structures such as duplexes and triplexes do not interfere. The trend observed in the  $T_m$  of the quadruplexes when monitored by UV-spectroscopy remained the same as that observed from the CD studies, and the values were in agreement with CD- $T_m$  (Table 2). Thus, TBA and isoTBA formed the most stable complexes in the presence of  $\text{Sr}^{2+}$  ions, with a  $T_m$  of  $61\text{ }^\circ\text{C}$  and  $63\text{ }^\circ\text{C}$ , respectively.

### 2.3.4 G-quadruplex topology study by UV-Thermal Difference Spectra

The G-quadruplex formation was further confirmed by the UV-thermal difference spectra (TDS), which are obtained by recording the difference in UV absorption spectra above and below the melting temperature of the nucleic acid and are helpful in the characterization of nucleic acid structures. The UV-TDS complements data obtained by UV, and each nucleic acid structure has its own unique TDS. Accordingly, G-quadruplexes are characterized by a negative peak at  $295 \pm 1\text{ nm}$  and positive peaks at  $273 \pm 2\text{ nm}$  and  $243 \pm 1\text{ nm}$ .<sup>25</sup>



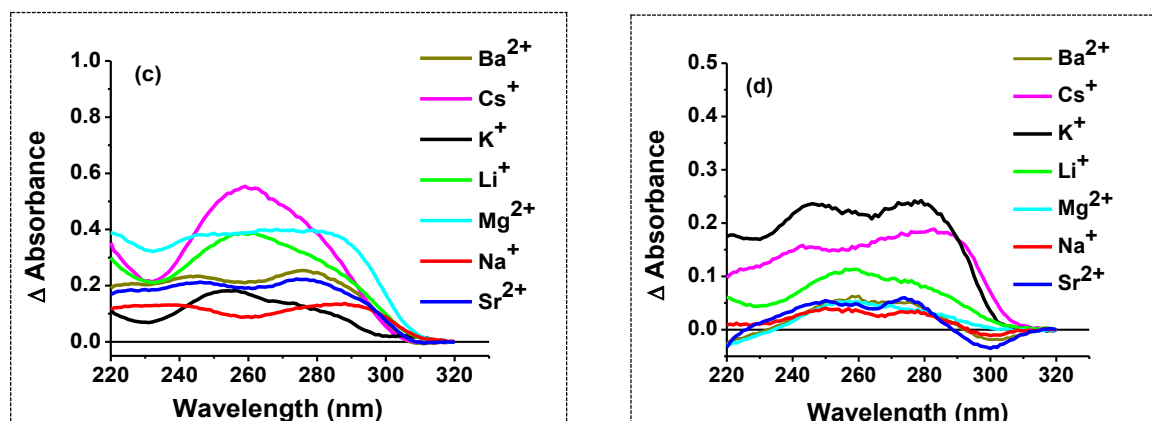


Figure 4. UV-thermal difference spectra for (a) TBA and (b) isoTBA in the presence of  $Li^+$ ,  $K^+$ ,  $Cs^+$ ,  $Na^+$ ,  $Mg^{2+}$ ,  $Sr^{2+}$ ,  $Ba^{2+}$ ,  $Ca^{2+}$  ions.; UV-isothermal difference spectra for (c) TBA and (d) isoTBA in presence of the different cations, recorded at 10 °C.

The UV-TDS for TBA and isoTBA in the presence of  $Li^+$ ,  $Na^+$ ,  $K^+$ ,  $Cs^+$ ,  $Mg^{2+}$ ,  $Ca^{2+}$ ,  $Sr^{2+}$  and  $Ba^{2+}$  are shown in Figure 4a, b. Except in the presence of  $Mg^{2+}$ , where no negative at 295 nm was observed with isoTBA, all the UV-TDS were found to conform to the G-quadruplex signature and displayed negative peaks near 295 nm and positive peaks near 273 nm. The positive peak near 243 nm was not as obvious for isoTBA as compared to TBA, possibly indicative of a slight change in the stacking of nucleobases in the quadruplex as a consequence of the 2'-5'-backbone and the nature of the different cations. Thus, all the other ions led to a quadruplex formation with TBA and isoTBA, albeit low thermal stability, as evident from the CD and UV melting studies. This was also apparent from the isothermal difference spectra (IDS) Figure 4c, d. Isothermal difference spectra (IDS) were obtained by subtracting the UV spectra of TBA or isoTBA at 10°C in the absence or presence of cations (0 mM or 100 mM). Because the absorbance spectra of the unfolded and folded species are temperature-dependent, IDS are not strictly equivalent to TDS. As a result, IDS better reflects the folded species' absorbance properties.<sup>26</sup>

### 2.3.5 Molecularity of the isoTBA- $Sr^{2+}$ quadruplex

Since stable parallel G-quadruplex formation was observed with isoTBA in the presence of  $Sr^{2+}$  ions, to confirm the molecularity of the complex, the UV plots during heating and subsequent cooling were analyzed for hysteresis, in comparison to TBA and to the complexes in the presence of  $K^+$  ions. Negligible hysteresis ( $\Delta T_m \approx 0$  °C, Table 3 and Figure 5) was observed, in agreement with a unimolecular complex with  $Sr^{2+}$  for TBA and isoTBA.

Table 3. UV- $T_m$  data for TBA and isoTBA at 5  $\mu\text{M}$  and 20  $\mu\text{M}$  concentrations.

Cation	Strand conc ( $\mu\text{M}$ )	TBA ( $^{\circ}\text{C}$ )				isoTBA ( $^{\circ}\text{C}$ )			
		$T_m$ (heat)	$T_m$ (cool)	$\Delta T_m$ (20 $\mu\text{M}$ -5 $\mu\text{M}$ )	$\Delta T_m$ (heat-cool)	$T_m$ (heat)	$T_m$ (cool)	$\Delta T_m$ (20 $\mu\text{M}$ -5 $\mu\text{M}$ )	$\Delta T_m$ (heat-cool)
$\text{Sr}^{2+}$	5	61	61	+2	0	63	63	-2	0
$\text{Sr}^{2+}$	20	63	63		0	61	62		-1
$\text{K}^+$	5	51	50	-2	+1	29	27	+3	+2
$\text{K}^+$	20	49 <sup>[6]</sup>	-		-	32	30		+2

Further, when the UV- $T_m$  measurements were carried out at a higher strand concentration, including a ten-fold excess (Figure 5), no appreciable differences were observed ( $\Delta T_m = +2$  to  $-2$   $^{\circ}\text{C}$ ), as observed earlier for TBA and isoTBA with  $\text{K}^+$ ,<sup>11</sup> again suggesting the unimolecularity of the quadruplex. The data are listed in Table 3. This is the first report of a unimolecular parallel G-quadruplex for TBA with an isomeric backbone, which implies three propeller loops- two TT loops and one TGT loop.

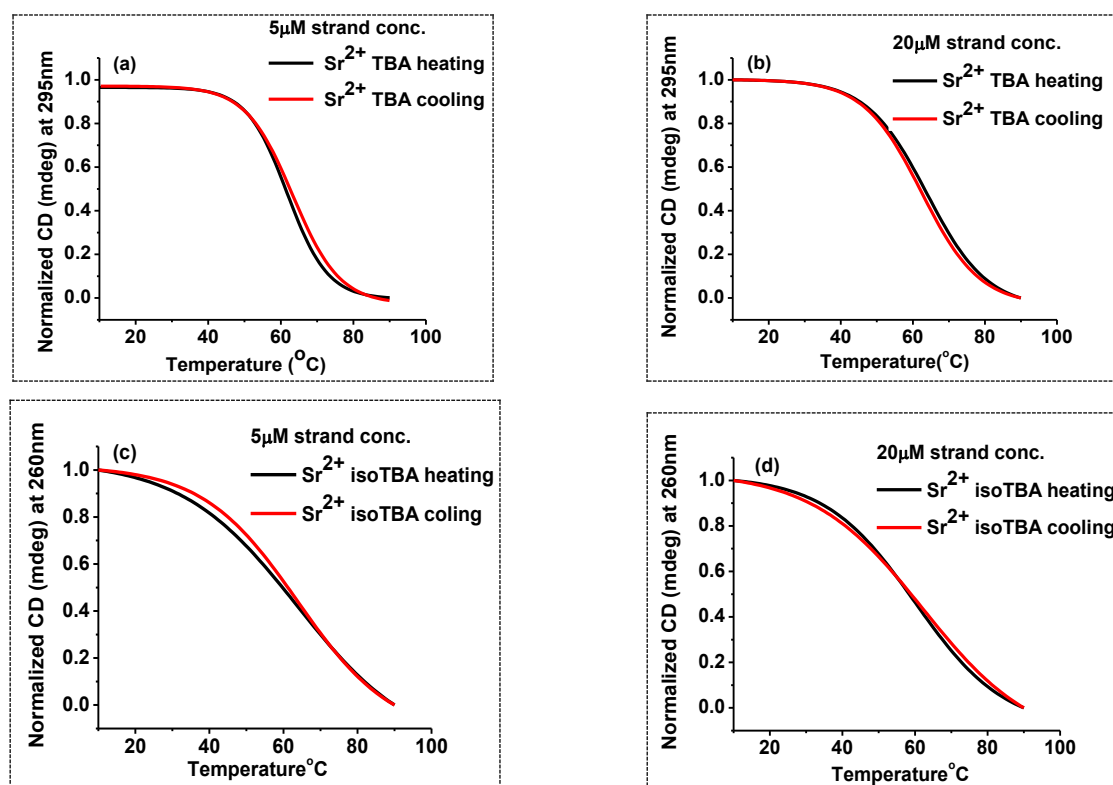
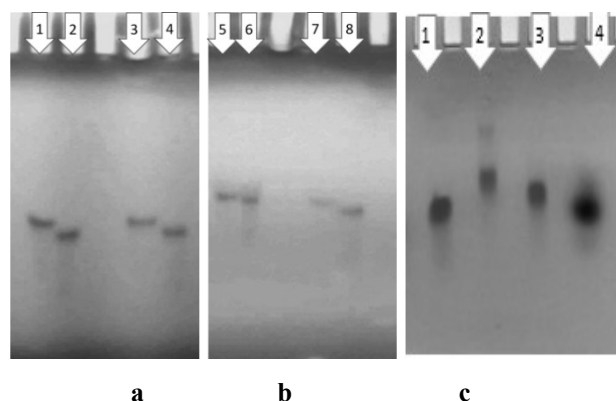


Figure 5. Heating and cooling profiles of TBA and isoTBA at 5 and 20  $\mu\text{M}$  concentrations in the presence of  $\text{Sr}^{2+}$  ions.

This is probably more easily accommodated in the case of the 2'-5'-linked isoTBA because the extended 7-atom backbone allows an optimum fit of the  $\text{Sr}^{2+}$  cation between the two G-tetrads. Additional stabilization of the G-quadruplex structure through extended stacking interactions or other interactions with the loop residues cannot be ruled out and requires more extensive evaluation through further NMR studies to be confirmed.

## 2.4 Polyacrylamide Gel Electrophoresis (PAGE) study

The comparative quadruplex-forming ability of TBA and isoTBA in the presence of  $\text{K}^+$  and  $\text{Sr}^{2+}$  ions was assessed by polyacrylamide gel electrophoresis. The complexes formed by isoTBA were of slightly higher mobility than their TBA counterparts (Figure 6a,b). However, no retarded bands were observed, as might be expected in the case of multimolecular complexes.<sup>12</sup> This further suggests that TBA and isoTBA form unimolecular quadruplexes with all the cations of the study.



**Figure 6 (a, b).** Non-denaturing polyacrylamide gel mobility assays of TBA and isoTBA in the presence of cations (100mM). Lane 1 -  $\text{Na}^+$  TBA, lane 2 -  $\text{Na}^+$  isoTBA, lane 3 -  $\text{K}^+$  TBA, lane 4 -  $\text{K}^+$  isoTBA, lane 5 -  $\text{Sr}^{2+}$  TBA, lane 6 -  $\text{Sr}^{2+}$  isoTBA, lane 7 -  $\text{Ba}^{2+}$  TBA, lane 8 -  $\text{Ba}^{2+}$  isoTBA.; (c). Lane 1 -  $\text{K}^+$  isoTBA, lane 2 -  $\text{Sr}^{2+}$  TBA, lane 3 -  $\text{Sr}^{2+}$  isoTBA, lane 4 - BPB dye. The gel was visualized by UV-shadowing

Further, both TBA and isoTBA are retarded to the same relative extent in the gel, suggesting complexes of the same molecularity. The complexes with  $\text{Sr}^{2+}$  were found to be slightly retarded in comparison to those in the presence of  $\text{K}^+$  ions (Figure 6c); this difference may be attributed to differences in mass and charge of the two ions.

## 2.5 $^1\text{H}$ NMR study

The  $^1\text{H}$  NMR spectrum of isoTBA in the absence of any added cations (Figure 7a) is devoid of any signals in the guanine imino proton region (10 to 12 ppm), where guanine residues typically hydrogen-bonded in a G-quadruplex are expected to appear.<sup>27, 28</sup> In the



presence of  $\text{Sr}^{2+}$  ions, broad imino proton signals were observed (Figure 7b), that have been reported in parallel G-quadruplexes.<sup>27, 29</sup>

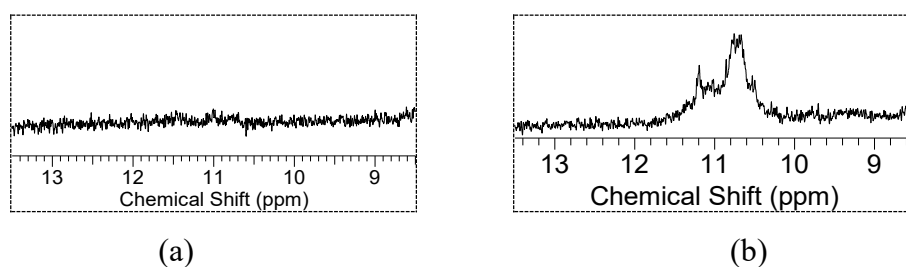


**Figure 7.** (a) Imino proton region of the  $^1\text{H}$  NMR spectrum of isoTBA in the absence of cations and (b) in the presence of  $\text{Sr}^{2+}$  ions. Spectra were recorded at  $5^\circ\text{C}$  for a strand concentration of  $200\ \mu\text{M}$  in  $90:10\ \text{v/v}$   $\text{H}_2\text{O}:\text{D}_2\text{O}$ .

These are in contrast to the sharp resonance signals observed for the anti-parallel isoTBA G-quadruplex in the presence of  $\text{K}^+$  ions.<sup>11</sup> Further, the imino proton signals of isoTBA were observed between 10.5 to 11.5 ppm in the presence of  $\text{Sr}^{2+}$ , while in the presence of  $\text{K}^+$ , they appeared between 11.5 to 12.5 ppm.<sup>11</sup> This is similar to the observations with  $d(\text{G}_4\text{C}_2)_2$  quadruplexes, where the imino protons in the parallel quadruplex fold appeared between 10.5 to 11.0 ppm, while those in the anti-parallel quadruplex fold appeared between 11.0 and 12.0 ppm.<sup>30</sup> This data further supports the existence of a parallel quadruplex fold for isoTBA in the presence of  $\text{Sr}^{2+}$ .

## 2.6 CD saturation binding curves for TBA and isoTBA with $\text{K}^+$ and $\text{Sr}^{2+}$

The  $K_d$  for complexes of  $\text{K}^+$  and  $\text{Sr}^{2+}$  with TBA and isoTBA were calculated from the CD saturation binding curves (Figure 8) obtained by titrating solutions of the TBA/isoTBA oligomers with the respective cations. The  $K_d$  value for  $\text{Sr}^{2+}$  with TBA and isoTBA was found to be one order of magnitude lower than for  $\text{K}^+$  (Table 4), indicating the higher affinity of this ion for binding to TBA/isoTBA.

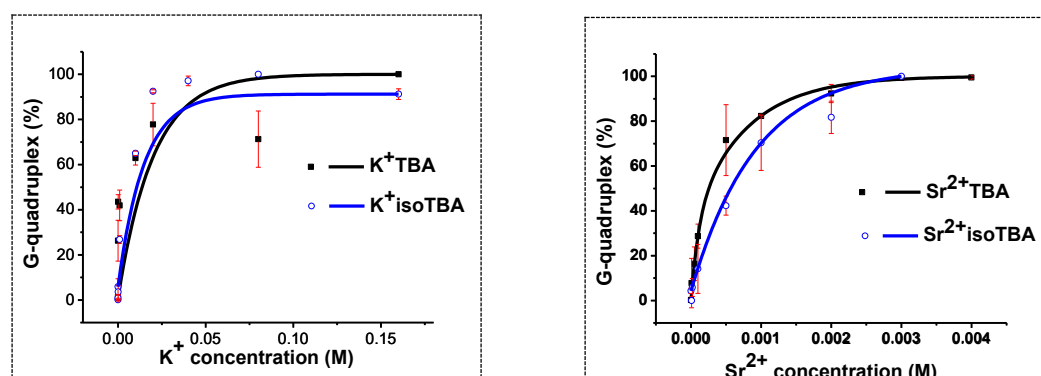


**Figure 8.** CD saturation binding curves for TBA and isoTBA with  $\text{K}^+$  and  $\text{Sr}^{2+}$ . The standard deviation is indicated by error bars.

$K_d$  was calculated using the formula

$$\theta = \frac{[L]}{[L] + K_d}$$

Where,  $\theta$  is the normalized CD amplitude at 260 nm (for  $\text{Sr}^{2+}$ ) or 295 nm (for  $\text{K}^+$ ),  $[L]$  is the ligand ( $\text{Sr}^{2+}$  or  $\text{K}^+$ ) concentration, and  $K_d$  is the dissociation constant, which is equivalent to  $1/K_a$ .

**Table 4. Dissociation constants for  $\text{K}^+$  and  $\text{Sr}^{2+}$  complexes with TBA/isoTBA**

Oligomer	cation	$K_d$ (M)	cation	$K_d$ (M)
TBA	$\text{K}^+$	$9.54 \times 10^{-3}$	$\text{Sr}^{2+}$	$1.94 \times 10^{-4}$
isoTBA	$\text{K}^+$	$3.37 \times 10^{-3}$	$\text{Sr}^{2+}$	$9.82 \times 10^{-4}$

$K_d$  values in the table are averages that were calculated from two independent experiments

## 2.7 IsoTBA for the detection of $\text{Sr}^{2+}$ ions

The unique ability of isoTBA to fold into a parallel G-quadruplex in the presence of  $\text{Sr}^{2+}$  ions, and bind to it with high affinity, may be exploited in the detection of this cation. The detection limit was found to be  $\sim 55 \mu\text{M}$  (Figure 9). Although this is not as low as that possible by inductively coupled plasma atomic emission spectroscopy (ICP-AES),<sup>31</sup> Energy-dispersive X-ray fluorescence (EDXRF)<sup>32,33</sup> or Zeeman atomic absorption spectrometry (Zeeman AAS),<sup>34</sup> which are the methods reported for strontium detection, and where the detection limit is in the sub-micromolar range,<sup>35</sup> it offers a fairly sensitive alternative method for detection. Although G-quadruplexes are known to bind many different metal ions and some metal-binding aptamers, including TBA,<sup>36, 37</sup> have also been reported,<sup>38</sup> there are no aptamers so far reported for  $\text{Sr}^{2+}$ , although  $\text{Sr}^{2+}$ -binding G-quadruplexes are known.<sup>26, 39 - 41</sup>

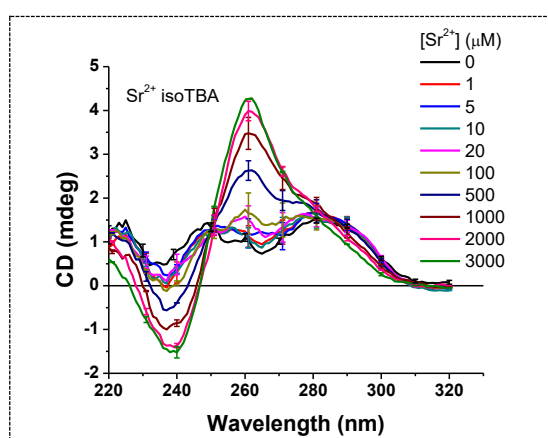


**Figure 9. CD spectra recorded at 37 °C for a solution of isoTBA (5  $\mu\text{M}$ ) in PBS with increasing (1  $\mu\text{M}$  to 3  $\text{mM}$ ) concentration of  $\text{Sr}^{2+}$  ions.**

It is worth noting that the plots shown in Figure 9 were obtained by successively increasing  $\text{Sr}^{2+}$  ion concentrations in a solution of isoTBA taken in phosphate-buffered saline that contained both  $\text{Na}^+$  (137 mM) and  $\text{K}^+$  (2.7 mM) ions, both in sufficiently large excess compared to  $\text{Sr}^{2+}$  (1  $\mu\text{M}$   $\text{Sr}^{2+}$  ions, in the first case); in spite of this, the characteristic CD signature of a parallel G-quadruplex (of isoTBA  $\text{Sr}^{2+}$ ) starts appearing. This is indicative of the selectivity and affinity of isoTBA for  $\text{Sr}^{2+}$ .

## 2.8 Calculation of detection limit

For calculating the detection limit, strontium ions were added to a solution of isoTBA (5  $\mu\text{M}$  in PBS) at 37 °C, at concentrations ranging from 1  $\mu\text{M}$  to 3 mM, and the CD at 260 nm was recorded. This CD amplitude was plotted as a function of the  $\text{Sr}^{2+}$  ion concentration (Figure 10). The slope of the linear part of the graph (k) was used in the following formula to calculate the detection limit.<sup>42</sup>

Detection limit =  $3.3\sigma/k$  where  $\sigma$  is the standard deviation obtained from twenty blank measurements. The data are listed in Table 5.

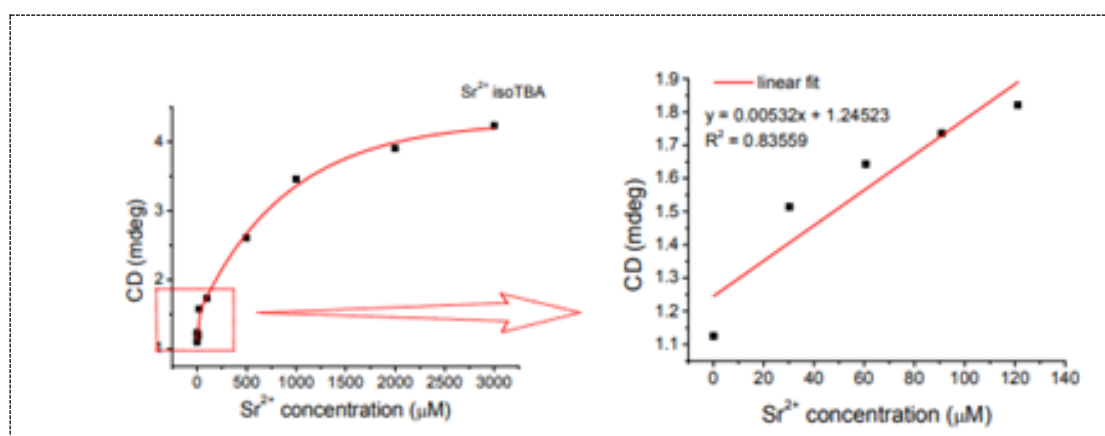


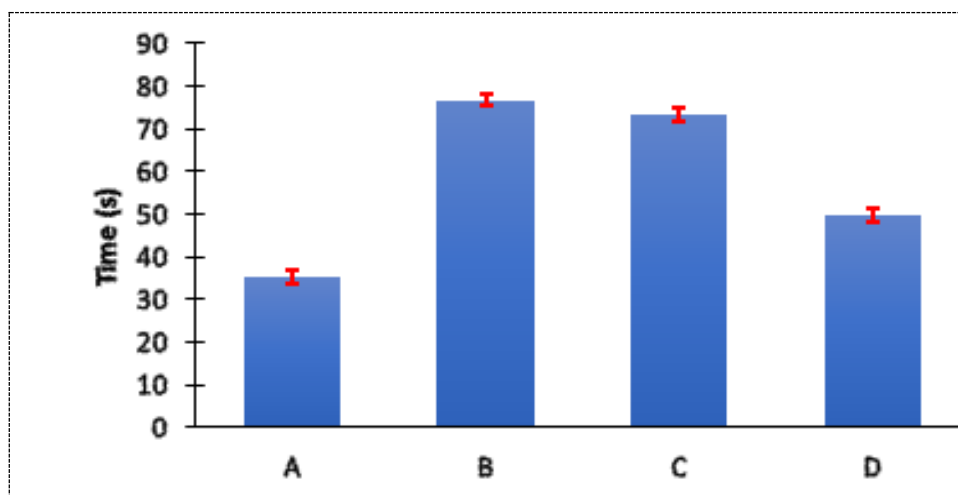
Figure 10. CD amplitude at 260 nm observed upon addition of  $\text{Sr}^{2+}$  to a solution of isoTBA (5  $\mu\text{M}$ ), in PBS.

Table 5. Detection limit for  $\text{Sr}^{2+}$  with isoTBA.

Sr. No.	Slope (k) of graph of CD amplitude (mdeg) at 260 nm Vs. $[\text{Sr}^{2+}]$	Standard deviation ( $\sigma$ )	Detection limit ( $\mu\text{M}$ )
1	0.00532	0.08875	55

## 2.9 Anti-clotting activity study

The anti-clotting activity of  $\text{Sr}^{2+}$  isoTBA was assessed in relation to TBA and isoTBA, in terms of inhibition of the thrombin-catalyzed fibrin polymerization. The anti-clotting effect was measured in terms of the additional time required for clotting in the presence of TBA/isoTBA when thrombin was added to the fibrinogen. As shown in Figure 11, the anti-clotting activity of isoTBA was severely reduced (clotting time 49 s) in the presence of  $\text{Sr}^{2+}$  ions, in comparison to TBA (clotting time 76 s) or isoTBA in the absence of  $\text{Sr}^{2+}$  ions (73 s). This may be expected, considering that the TT loops that are mainly implicated in thrombin binding in the antiparallel TBA G-quadruplex are not readily available for this interaction in the  $\text{Sr}^{2+}$  isoTBA unimolecular parallel G-quadruplex, as these TT loops would be propeller type. This reduced anti-clotting activity of  $\text{Sr}^{2+}$  isoTBA would be advantageous when considering the usefulness of isoTBA in  $\text{Sr}^{2+}$  detection in body fluids such as blood.



**Figure 11.** Clotting time measured as the time required for fibrin polymerization upon addition of thrombin to fibrinogen A. in the absence of TBA or isoTBA (control), B. in the presence of TBA (Standard 1), C. in the presence of isoTBA (Standard 2), and D. in the presence of  $\text{Sr}^{2+}$  isoTBA

## 2.10 Conclusions

In conclusion, we have studied the effect of various alkali and alkaline earth metal cations on the G-quadruplex-forming ability of isoTBA. In contrast to all the other cations studied,  $\text{Sr}^{2+}$  was found to bind to isoTBA with high affinity and specificity and led to a parallel intramolecular quadruplex formation. This unique behavior of isoTBA in the presence of  $\text{Sr}^{2+}$  together with its already reported higher resistance to nuclease-mediated degradation, may be utilized in the detection of this cation in the micromolar range, which it senses with a detection limit of  $\sim 55 \mu\text{M}$

## 2.11 Experimental

### 2.11.1 Oligonucleotide synthesis, Purification and characterization

3'-5'- (TBA) and 2'-5'-(isoTBA) linked oligonucleotides were synthesized in-house on a Bioautomation Mermade-4 DNA synthesizer employing  $\beta$ -cyanoethyl phosphoramidite chemistry. The 2'-deoxy-3'-phosphoramidites were obtained from ChemGenes and 3'-deoxy-2'-phosphoramidites from Glen Research. Universal columns procured from Bioautomation were used for 2'-5'-linked oligomer synthesis. Oligonucleotides were cleaved from the solid support by treating with aqueous ammonia at 60° C for 6 h and then concentrated. Oligonucleotides were purified by RP-HPLC on a C18 column using a Waters system (Waters Delta 600e quaternary solvent delivery system, 2998 photo-diode array detector and Empower2 chromatography software). An increasing gradient of acetonitrile in 0.1 M triethyl ammonium acetate (pH 7.0) was used.

### 2.11.2 Gel electrophoresis

Experiments to evaluate G-quadruplex formation were carried out on a 20 % native polyacrylamide gel with 1 X Tris-Borate-EDTA (TBE) buffer (pH 8.0) as the running buffer. TBA and isoTBA samples were prepared by annealing at 320  $\mu$ M concentration in 10 mM Tris buffer (pH 7.0) in the presence of 100 mM concentration of the appropriate salt (NaCl, KCl, BaCl<sub>2</sub>, or SrCl<sub>2</sub>). The gel was run at 10 °C and 150 V till the bromophenol blue indicator had migrated to half the gel length. After electrophoresis, the gel was transferred to a GF254 pre-coated silica gel chromatographic plate (Merck 5554) and visualized by UV-shadowing.

### 2.11.3 CD experiments

CD spectra were recorded on a Jasco J-815 CD spectrometer equipped with a Jasco PTC-424S/15 Peltier system. 5 mm path-length quartz cuvettes were used for a sample volume of 2 ml and strand concentration of 5  $\mu$ M in tris buffer (10 mM, pH 7.2) containing 100 mM Na<sup>+</sup>, Li<sup>+</sup>, K<sup>+</sup>, Cs<sup>+</sup>, Mg<sup>+2</sup>, Ca<sup>+2</sup>, Sr<sup>+2</sup>, Ba<sup>+2</sup>. Oligomers in buffer were annealed by heating at 95 °C for 5 min, then slowly cooled to room temperature followed by refrigeration for 3 to 4 h before use. Spectral scans over a range of 320 nm to 200 nm were collected as accumulations of 3 scans at a scanning rate of 100 nm min<sup>-1</sup>. CD melting was performed by monitoring CD intensity at 295 nm against temperature over a range of 5–90 °C at a heating rate of 3 °C per min. To determine K<sub>d</sub>, TBA and isoTBA were taken at a concentration of 5  $\mu$ M in water and phosphate-buffered saline (PBS), respectively. DNA was denatured at 90 °C for 5 min and

allowed to cool slowly to room temperature. Spectra were acquired at 20 °C for K<sup>+</sup> and 37 °C for Sr<sup>2+</sup> and data were buffer subtracted. Titrations were performed with KCl and SrCl<sub>2</sub> and the changes in the CD spectra recorded. The data is plotted as an average of two independent measurements and the standard deviation is indicated by error bars. The CD saturation binding curves were obtained by applying an exponential association fit using OriginPro 8 SRO v8.0725 (B725) software.

#### 2.11.4 Calculation of Detection Limit

For calculation of the detection limit, the standard deviation was calculated from 20 blank measurements. CD spectra were recorded at 37 °C after the incremental addition of Sr<sup>2+</sup> ions to a 5 μM solution of isoTBA taken in PBS (10 mM sodium phosphate buffer containing 137 mM NaCl and 2.7 mM KCl, pH 7.2), till saturation was observed in the CD signal.

#### 2.11.5 UV experiments

UV-absorbance scans of the TBA and isoTBA oligomers were recorded using 10 mm path-length quartz cells on an Analytik Jena SPECORD® 200 plus spectrometer equipped with a Peltier-controlled temperature controller and at a scanning speed of 5 nm sec<sup>-1</sup>. The TBA oligomers (5 μM strand concentration) were annealed in tris buffer (10 mM, pH 7.2), containing 100 mM of the appropriate cations. The concentration was calculated based on absorbance from molar extinction co-efficients of the corresponding nucleobases of DNA. Thermal difference spectra (TDS) were obtained by subtracting the UV-absorbance spectral scan of the sample at temperatures below (i.e., 10 °C) from that above (i.e., 90 °C) the melting temperature ( $T_m$ ). Isothermal difference spectra (IDS) were recorded at 10 °C.

#### 2.11.6 NMR experiments

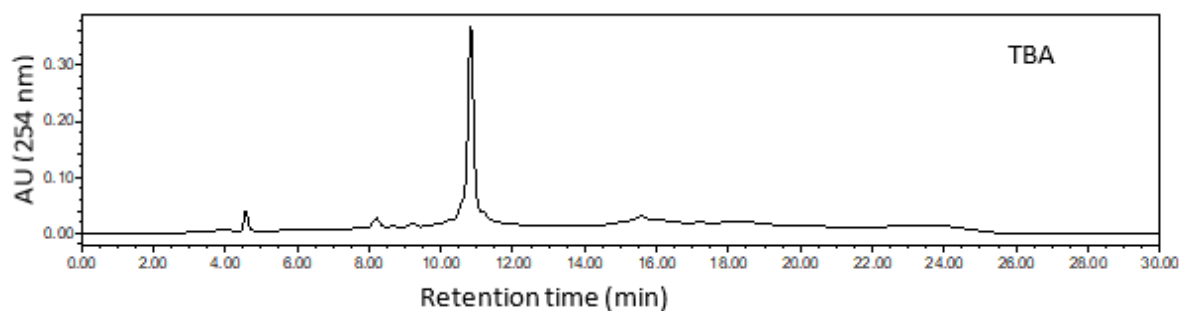
<sup>1</sup>H NMR spectra were acquired at 700 MHz and 4°C using a Bruker AV 700 NMR spectrometer operating at 700.13 MHz for <sup>1</sup>H using a 5 mm BBFO probe. The raw data were processed with a Gaussian function for the improvement of the signal-to-noise ratio. The temperature during the measurements was controlled using a Bruker BVT 3000 unit. HPLC-purified isoTBA was taken at 200 μM concentration in 90:10 v/v H<sub>2</sub>O:D<sub>2</sub>O with or without 100 mM SrCl<sub>2</sub>. The presence of imino protons in the region between 11.0 to 12.5 δ indicate quadruplex formation.

### 2.11.7 Anti-Clotting activity experiments

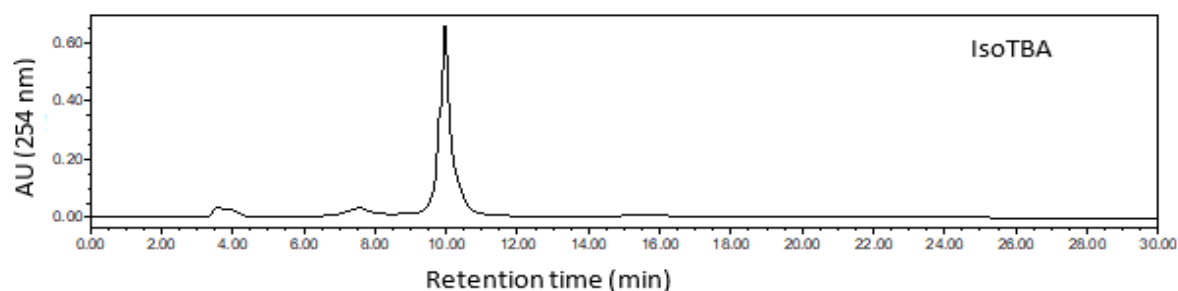
Clotting time experiments were performed at 37 °C on a Start-Max (Stago) coagulation analyzer. Each experiment was repeated at least thrice; the standard deviation was  $\pm 1$  s. Each commercial reagent was reconstituted according to the manufacturer's protocol. Bovine Thrombin (Tulip Diagnostics, 0.1 NIH unit) was incubated with TBA or isoTBA as applicable and specified at 0.25  $\mu\text{M}$  oligomer concentration for 1.5 min before adding fibrinogen from human plasma (Aldrich, 3.5  $\mu\text{M}$ ). The clotting time (s) was measured as the time taken upon addition of thrombin till the polymerization of fibrin.

### 2.12 Appendix A

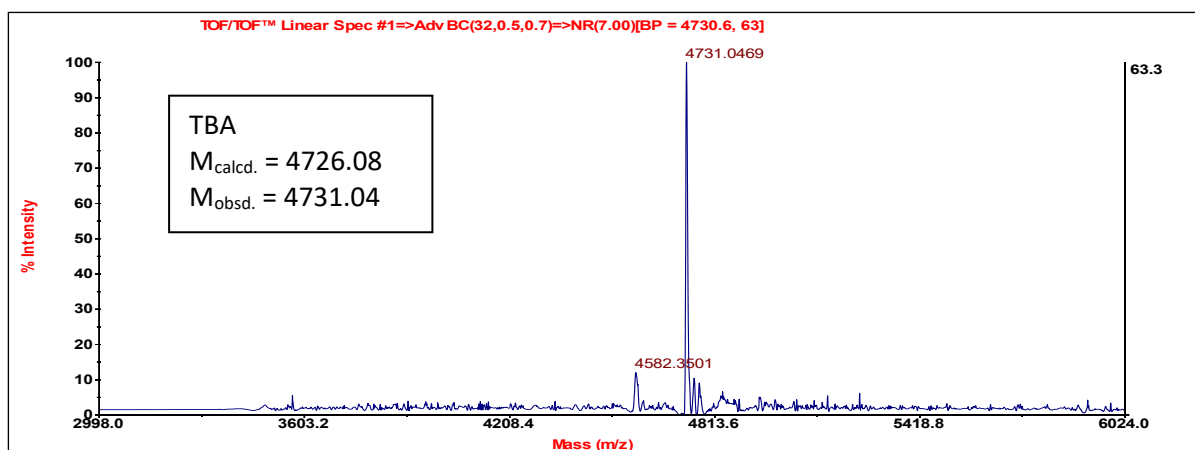
Description	Page No.
HPLC chromatogram of TBA oligomer	51
HPLC chromatogram of <i>iso</i> TBA oligomer	51
MALDI-TOF spectra of TBA oligomer	52
MALDI-TOF spectra of <i>iso</i> TBA oligomer	52
$^1\text{H}$ NMR spectrum of <i>iso</i> TBA (200 $\mu\text{M}$ ) in 90:10 $\text{H}_2\text{O}:\text{D}_2\text{O}$ v/v	52
$^1\text{H}$ NMR spectrum <i>iso</i> TBA (200 $\mu\text{M}$ ) in the presence of $\text{Sr}^{2+}$ ions (100 mM)	53



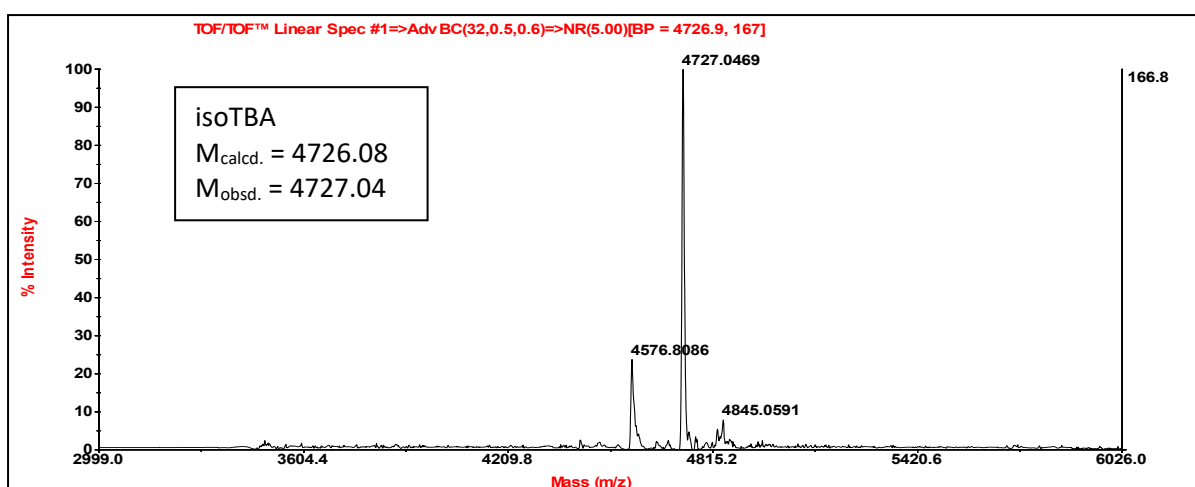
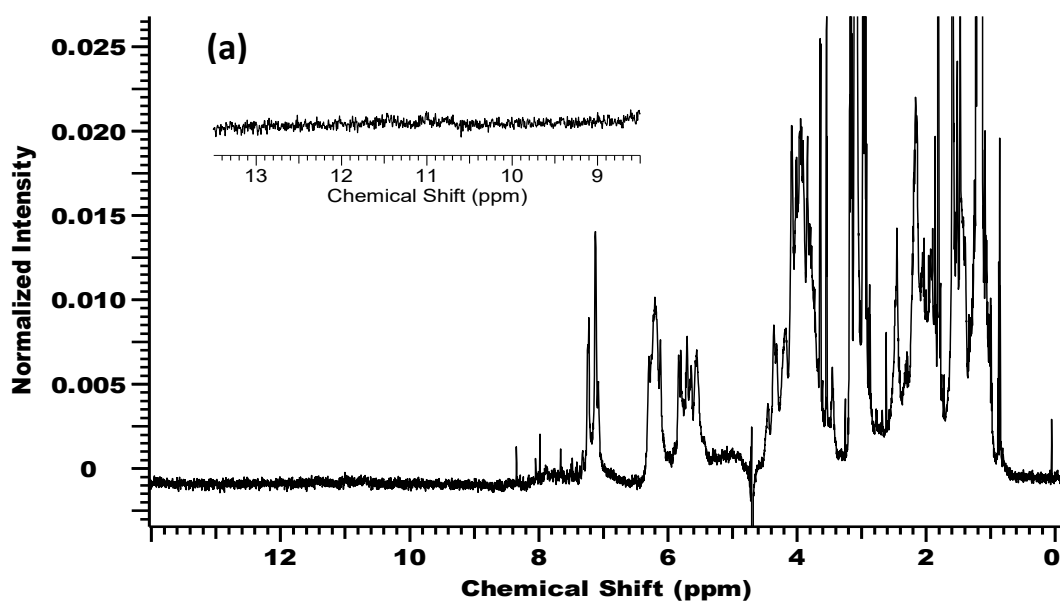
HPLC chromatogram of TBA oligomer



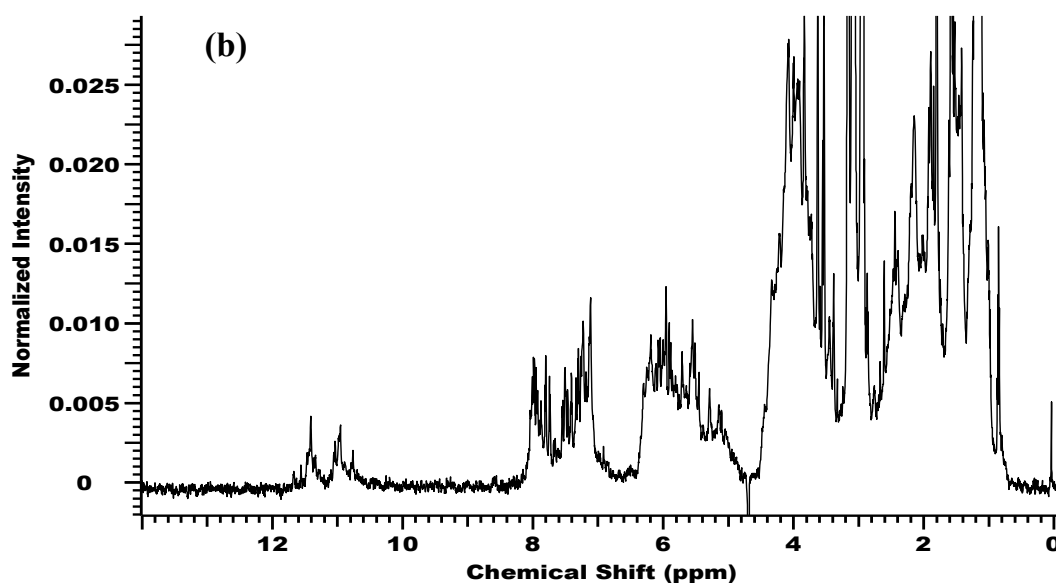
HPLC chromatogram of *iso*TBA oligomer



MALDI-TOF spectra of TBA oligomer

MALDI-TOF spectra of *iso*TBA oligomer $^1\text{H}$  NMR spectrum of *iso*TBA (200  $\mu\text{M}$ ) in 90:10  $\text{H}_2\text{O}:\text{D}_2\text{O}$





$^1\text{H}$  NMR spectrum *iso*TBA (200  $\mu\text{M}$ ) in the presence of  $\text{Sr}^{2+}$  ions (100 mM)

### 2.13 References

- (1) Bugaut, A.; Balasubramanian, S. A Sequence-Independent Study of the Influence of Short Loop Lengths on the Stability and Topology of Intramolecular DNA G-Quadruplexes. *Biochemistry* **2008**, *47* (2), 689–697
- (2) Gatto, B.; Palumbo, M.; Sissi, C. Nucleic Acid Aptamers Based on the G-Quadruplex Structure: Therapeutic and Diagnostic Potential. *Curr. Med. Chem.* **2009**, *16* (10), 1248–1265
- (3) Murat, P.; Balasubramanian, S. Existence and Consequences of G-Quadruplex Structures in DNA. *Curr. Opin. Genet. Dev.* **2014**, *25* (1), 22–29.
- (4) Neidle, S. The Structures of Quadruplex Nucleic Acids and Their Drug Complexes. *Curr. Opin. Struct. Biol.* **2009**, *19* (3), 239–250.
- (5) Kelly, J. A.; Feigon, J.; Yeates, T. O. Reconciliation of the X-Ray and NMR Structures of the Thrombin-Binding Aptamer d(GGTTGGTGTGGTTGG). *J. Mol. Biol.* **1996**, *256* (3), 417–422.
- (6) Kankia, B. I.; Marky, L. A. Folding of the Thrombin Aptamer into a G-Quadruplex with  $\text{Sr}^{2+}$ : Stability, Heat, and Hydration. *J. Am. Chem. Soc.* **2001**, *123* (44), 10799–10804.
- (7) Esposito, V.; Russo, A.; Vellecco, V.; Bucci, M.; Russo, G.; Mayol, L.; Virgilio, A.; Galeone, A. Thrombin Binding Aptamer Analogues Containing Inversion of Polarity

- Sites Endowed with Antiproliferative and Anti-Motility Properties against Calu-6 Cells. *Biochim. Biophys. Acta Gen. Subj.* **2018**, *1862* (12), 2645–2650.
- (8) Scuotto, M.; Riviuccio, E.; Varone, A.; Corda, D.; Bucci, M.; Vellecco, V.; Cirino, G.; Virgilio, A.; Esposito, V.; Galeone, A.; Borbone, N.; Varra, M.; Mayol, L. Site Specific Replacements of a Single Loop Nucleoside with a Dibenzyl Linker May Switch the Activity of TBA from Anticoagulant to Antiproliferative. *Nucleic Acids Res.* **2015**, *43* (16), 7702–7716.
- (9) Pasternak, A.; Hernandez, F. J.; Rasmussen, L. M.; Vester, B.; Wengel, J. Improved Thrombin Binding Aptamer by Incorporation of a Single Unlocked Nucleic Acid Monomer. *Nucleic Acids Res.* **2011**, *39* (3), 1155–1164.
- (10) Saccà, B.; Lacroix, L.; Mergny, J. L. The Effect of Chemical Modifications on the Thermal Stability of Different G-Quadruplex-Forming Oligonucleotides. *Nucleic Acids Res.* **2005**, *33* (4), 1182–1192.
- (11) Gunjal, A. D.; Fernandes, M.; Erande, N.; Rajamohanan, P. R.; Kumar, V. A. Functional IsoDNA Aptamers: Modified Thrombin Binding Aptamers with a 2'-5'-Linked Sugar-Phosphate Backbone (IsoTBA). *Chem. Commun.* **2014**, *50* (5), 605–607.
- (12) Aher, M. N.; Erande, N. D.; Fernandes, M.; Kumar, V. A. Unimolecular antiparallel G-quadruplex folding topology of 2'-5'-isoTBA sequences remains unaltered by loop composition. *Org. Biomol. Chem.* **2015**, *13*, 11696–11703.
- (13) Hazel, P.; Huppert, J.; Balasubramanian, S.; Neidle, S. Loop-Length-Dependent Folding of G-Quadruplexes. *J. Am. Chem. Soc.* **2004**, *126* (50), 16405–16415.
- (14) Patel, P. K.; Bhavesh, N. S.; Hosur, R. V. Cation-Dependent Conformational Switches in d-TGGCGGC Containing Two Triplet Repeats of Fragile X Syndrome: NMR Observations. *Biochem. Biophys. Res. Commun.* **2000**, *278* (3), 833–838.
- (15) Hardin, C. C.; Henderson, E.; Watson, T.; Prosser, J. K. Monovalent Cation Induced Structural Transitions in Telomeric DNAs: G-DNA Folding Intermediates. *Biochemistry* **1991**, *30*, 4460–4472.
- (16) Balagurumoorthy, P.; Brahmachari, S. K.; Mohanty, D.; Bansal, M.; Sasisekharan, V. Hairpin and Parallel Quartet Structures for Telomeric Sequences. *Nucleic Acids Res.* **1992**, *20* (15), 4061–4067.
- (17) Strahan, G. D.; Keniry, M. A.; Shafer, R. H. NMR Structure Refinement and Dynamics of the  $K^+$ -[d(G<sub>3</sub>T<sub>4</sub>G<sub>3</sub>)]<sub>2</sub> Quadruplex via Particle Mesh Ewald Molecular Dynamics Simulations. *Biophys. J.* **1998**, *75*, 968–981.
- (18) Venczel, E. A.; Sen, D. Parallel and Antiparallel G-DNA Structures from Complex

- Telomeric Sequence \*. *Biochemistry* **1993**, 32, 6220–6228.
- (19) Miyoshi, D.; Nakao, A.; Sugimoto, N.; Technology, H. Structural Transition of (G<sub>4</sub>T<sub>4</sub>G<sub>4</sub>) from Antiparallel to Parallel G-Quartet Induced by Divalent Cations. *Nucleic Acids Res.* **2001**, 2 (1), 259–260.
- (20) Majhi, P. R.; Shafer, R. H. Characterization of an Unusual Folding Pattern in a Catalytically Active Guanine Quadruplex Structure. *Biopolymers* **2006**, 82 (6), 558–569.
- (21) Gait, M. J. *Oligonucleotide Synthesis : A Practical Approach*; Rev. repr. ed.; Oxford : IRL press, **1984**, 217.
- (22) Gray, D. M.; Wen, J.-D.; Gray, C. W.; Reppes, R.; Reppes, C.; Raabe, G.; Fleischhauer, J. Measured and Calculated CD Spectra of G-Quartets Stacked with the Same or Opposite Polarities. *Chirality*, **2008**, 20, 431–440.
- (23) Karsisiotis, A. I.; Hessari, N. M. A.; Novellino, E.; Spada, G. P.; Randazzo, A.; Webba Da Silva, M. Topological Characterization of Nucleic Acid G-Quadruplexes by UV Absorption and Circular Dichroism. *Angew. Chemie. Int. Ed.* **2011**, 50 (45), 10645–10648.
- (24) Mergny, J.; Phan, A.; Lacroix, L. Following G-Quartet Formation by UV-Spectroscopy. *FEBS Lett.* **1998**, 435, 74–78.
- (25) Mergny, J. L.; Li, J.; Lacroix, L.; Amrane, S.; Chaires, J. B. Thermal Difference Spectra: A Specific Signature for Nucleic Acid Structures. *Nucleic Acids Res.* **2005**, 33 (16), 1–6.
- (26) Largy, E.; Marchand, A.; Amrane, S.; Gabelica, V.; Mergny, J. L. Quadruplex Turncoats: Cation-Dependent Folding and Stability of Quadruplex-DNA Double Switches. *J. Am. Chem. Soc.* **2016**, 138 (8), 2780–2792.
- (27) Zhu, J.; Fleming, A. M.; Burrows, C. J. The RAD17 Promoter Sequence Contains a Potential Tail-Dependent G-Quadruplex That Downregulates Gene Expression upon Oxidative Modification. *ACS Chem. Biol.* **2018**, 13 (9), 2577–2584.
- (28) Tua, A.; Modi, Y. S.; Patel, D. J. Propeller-Type Parallel-Stranded G-Quadruplexes in the Human c-Myc Promoter. *J. Am. Chem. Soc.* **2004**, 126 (28), 8710–8716.
- (29) Zhou, B.; Liu, C.; Geng, Y.; Zhu, G. Topology of a G-Quadruplex DNA Formed by C9orf72 Hexanucleotide Repeats Associated with ALS and FTD. *Sci. Rep.* **2015**, 5 , 1–7.
- (30) Zhou, B.; Geng, Y.; Liu, C.; Miao, H.; Ren, Y.; Xu, N.; Shi, X.; You, Y.; Lee, T.; Zhu, G. Characterizations of Distinct Parallel and Antiparallel G-Quadruplexes Formed by

- Two-Repeat ALS and FTD Related GGGGCC Sequence. *Sci. Rep.* **2018**, *8* (1), 1–7.
- (31) Piette, M.; Desmet, B.; Dams, R. Determination of Strontium in Human Whole Blood by ICP-AES. *Sci. Total Environ.* **1994**, *141* (1–3), 269–273.
- (32) Pejović-Milić, A.; Stronach, I. M.; Gyorffy, J.; Webber, C. E.; Chettle, D. R. Quantification of Bone Strontium Levels in Humans by in Vivo X-Ray Fluorescence. *Med. Phys.* **2004**, *31* (3), 528–538.
- (33) Specht, A. J.; Mostafaei, F.; Lin, Y.; Xu, J.; Nie, L. H. Measurements of Strontium Levels in Human Bone In Vivo Using Portable X-Ray Fluorescence (XRF). *Appl. Spectrosc.* **2017**, *71* (8), 1962–1968.
- (34) D’Haese, P. C.; Van Landeghem, G. F.; Lamberts, L. V.; Bekaert, V. A.; Schrooten, I.; De Broe, M. E. Measurement of Strontium in Serum, Urine, Bone, and Soft Tissues by Zeeman Atomic Absorption Spectrometry. *Clin. Chem.* **1997**, *43* (1), 121–128.
- (35) Ying, R. Extraction and Analysis of Strontium in Water Sample Using a Sr<sup>2+</sup> Selective Polymer as the Absorbent Phase. *Int. J. Anal. Chem.* **2015**, 1–5.
- (36) Chen, Z.; Tan, L.; Hu, L.; Luan, Y. Superior Fluorescent Probe for Detection of Potassium Ion. *Talanta* **2015**, *144*, 247–251.
- (37) Zhang, D.; Yin, L.; Meng, Z.; Yu, A.; Guo, L.; Wang, H. A Sensitive Fluorescence Anisotropy Method for Detection of Lead (II) Ion by a G-Quadruplex-Inducible DNA Aptamer. *Anal. Chim. Acta.* **2014**, *812*, 161–167.
- (38) Ma, D. L.; Wang, W.; Mao, Z.; Kang, T. S.; Han, Q. Bin; Chan, P. W. H.; Leung, C. H. Utilization of G-Quadruplex-Forming Aptamers for the Construction of Luminescence Sensing Platforms. *Chempluschem* **2017**, *82* (1), 8–17.
- (39) Lomidze, L.; Kelley, S.; Gogichaishvili, S.; Metreveli, N.; Musier-Forsyth, K.; Kankia, B. Sr<sup>2+</sup> Induces Unusually Stable d(GGGTGGGTGGGTGGG) Quadruplex Dimers. *Biopolymers* **2016**, *105*, 811–818.
- (40) Leung, K. H.; Ma, V. P. Y.; He, H. Z.; Chan, D. S. H.; Yang, H.; Leung, C. H.; Ma, D. L. A Highly Selective G-Quadruplex-Based Luminescent Switch-on Probe for the Detection of Nanomolar Strontium(II) Ions in Sea Water. *RSC Adv.* **2012**, *2* (22), 8273–8276.
- (41) Qu, K.; Zhao, C.; Ren, J.; Qu, X. Human Telomeric G-Quadruplex Formation and Highly Selective Fluorescence Detection of Toxic Strontium Ions. *Mol. Biosyst.* **2012**, *8* (3), 779–782.
- (42) For Detection Limit Calc: ICH Harmonised Tripartite Guideline, Q2(R1): Validation of Analytical Procedures. *Text Methodol.* **2005**, 11.

## **Chapter 3**

**Iso-rTBA: the 2'-5'-linked  
functional RNA equivalent of the  
Thrombin binding aptamer**

### 3.1 Introduction

Guanosine-rich sequences have a high proclivity to fold into G-quadruplex structures. Such quadruplex sequences play important roles in cell regulatory processes.<sup>1</sup> Although DNA quadruplexes have been extensively researched, RNA structures have received little attention, despite the fact that RNA is capable of forming stable G-quadruplexes. By appropriately altering nucleobases in G-quadruplexes, the chemical and biological features of G-quadruplexes could be better understood.<sup>2</sup> In general, RNA G-quadruplexes are more stable than their DNA counterparts. This observation could be explained by the preference of RNA quadruplexes for parallel quadruplexes.<sup>3</sup> The thrombin-binding aptamer (TBA),<sup>4</sup> discovered through SELEX, is a promising anticoagulant that progressed to clinical trials<sup>5</sup> because of its non-toxic nature and ability to delay blood clotting. The need for such non-toxic and economically viable alternatives to traditional anticoagulants such as heparin is being felt again, in the light of the COVID-19 pandemic, where treatment recommendations include the use of low-dose anticoagulants in COVID-19 hospitalized patients to prevent thrombosis.<sup>6</sup>

The well-studied TBA 5'-GGTTGGTGTGGTTGG was chosen for our study, with a 2'-5'-linked RNA backbone to get 5'-r(GGUUGGUGUGGUUGG)-2' (iso-rTBA). The 3'-5'-linked rTBA was earlier reported to form a multimolecular G-quadruplex in a parallel folding topology,<sup>1,7</sup> as observed with most other RNA G-quadruplexes, while TBA itself is known to fold into a unimolecular antiparallel G-quadruplex.<sup>8</sup> Our research group earlier reported an isoTBA oligomer wherein the natural 3'-5'-phosphodiester backbone linkages were replaced by the isomeric 2'-5'-phosphodiester linkages and showed that it could fold into a unimolecular antiparallel G-quadruplex structure, similar to that observed for TBA and also effect anti-coagulation.<sup>9</sup>

### 3.2 Rationale and objectives of the present work

The 2'-5'-backbone in isoTBA leads to an extended backbone with sugars predominantly adopting the N-type pucker,<sup>10</sup> while in iso-rTBA, this would lead to a compact backbone with sugars preferring the S-type pucker (Figure 1). Until now, predominantly parallel G-quadruplexes have been reported for RNA.<sup>1</sup> Some studies attribute this to the preferred *anti*-conformation about the glycosidic bond and the C3'-*endo* (N-type) sugar pucker in rG;<sup>7,11</sup> the *syn/anti*-glycosidic conformation of guanines is an important factor in deciding the G-quadruplex structural fold<sup>12</sup> (Figure 2). Recently, in contrast to previous reports stating that rG residues favor *anti*-conformation in parallel RNA G-quadruplexes, both rG (*syn*) and

rG (anti) have been observed in RNA crystal structures,<sup>13</sup> where an antiparallel orientation of strands was observed for the human telomeric sequence containing 8-bromoguanosine.<sup>13</sup>

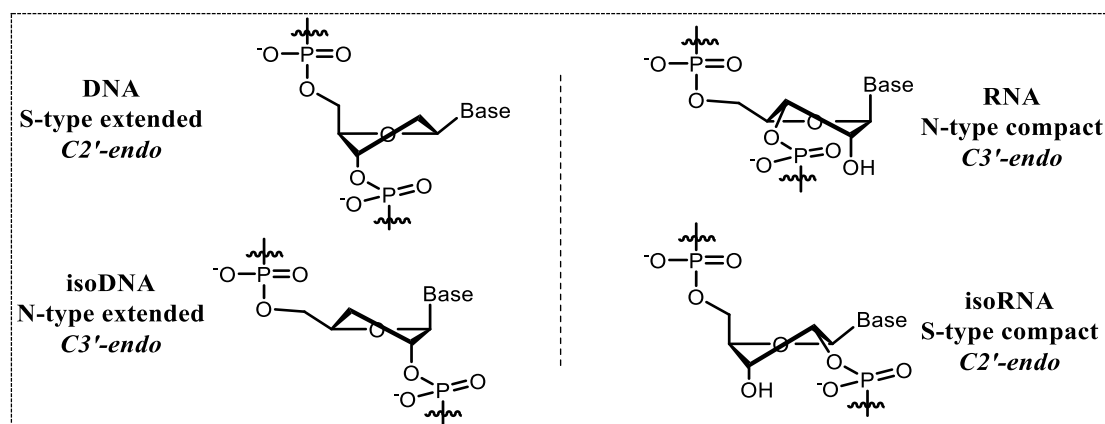


Figure 1. The preferred sugar pucker in native DNA and RNA Vs. those in 2'-5'-linked isoDNA and isoRNA.

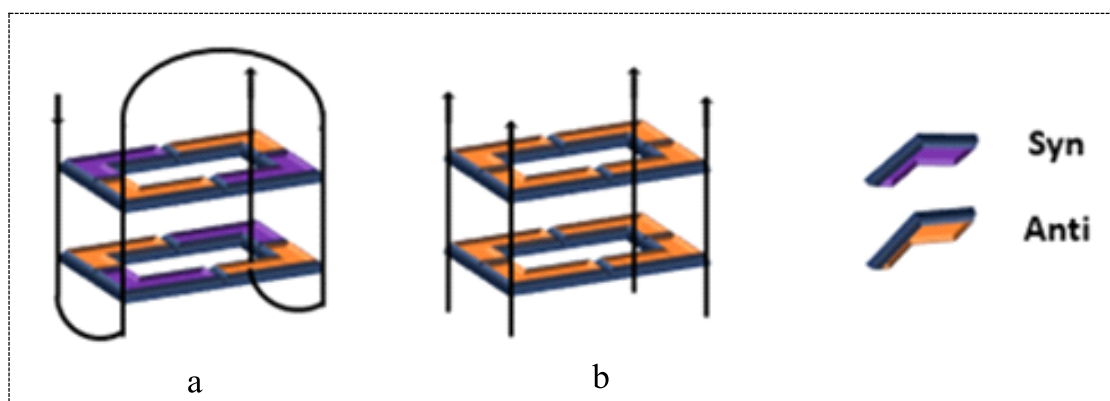


Figure 2. A schematic representation of (a) a unimolecular G-quadruplex with antiparallel orientation of strands and alternating *syn-anti* conformation of guanine residues about the glycosidic bond and (b) a multimolecular G-quadruplex with all-*anti* conformation of guanine residues. *Syn*- and *anti*-conformations of guanine are represented in purple and orange colour respectively.

Sugar puckering plays an important role in quadruplex topology. DNA has sugars with an S-type extended C2'-endo conformation, while isoDNA has sugars with an N-type extended C3'-endo conformation. Similarly, RNA has sugars with N-type compact C3'-endo conformation, while isoRNA has sugars in S-type compact C2'-endo conformation (Figure 1). Since DNA and iso RNA show similar sugar puckering, it was hypothesized that they could show a similar topology for the TBA pentadecamer. Also, the 2'-5'-rTBA (GGUUGGUGUGGTUUGG) backbone provides a more economically viable possibility, as the protected phosphoramidite building blocks are more readily economically available.

### 3.3 Synthesis of TBA, isoTBA oligomers, their purification and characterization

3'-5'-phosphodiester-linked TBA and 2'-5'-phosphodiester-linked iso-rTBA oligonucleotides were synthesized using commercially available protected 2'-deoxyguanosine-3'-phosphoramidite, 2'-deoxythymidine-3'-phosphoramidite, 3'-tBDsilyl-uridine-2'-phosphoramidite, and 3'-tBDsilyl-guanosine-2'-phosphoramidite by standard  $\beta$ -cyanoethyl phosphoramidite chemistry by solid-phase synthesis.<sup>14</sup> For iso-rTBA, universal columns from Bioautomation and an extended coupling time of 10 s were used. Subsequent to post-synthetic cleavage of protecting groups and cleavage from the support, HPLC purification yielded pure oligonucleotides that were characterized by MALDI-TOF analysis (Table 1). The general scheme for solid-phase oligonucleotide synthesis is explained in Chapter 1, Scheme 1.

Table 1. TBA and iso-rTBA oligomers.

Sr.No.	Sequence name	Sequence	MALDI TOF Mass (Da)	
			M <sub>calcd.</sub>	M <sub>obsd.</sub>
1	TBA	5'-d(GGTTGGTGTGGTTGG)-3'	4726	4731
2	Iso-rTBA	5'-r(GGUUGGUGUGGUUGG)-2'	4881	4882

### 3.4 G-quadruplex formation and topology using circular dichroism spectroscopy

CD spectroscopy is a valuable and widely-used technique to evaluate the formation and conformations of G-quadruplexes. A maximum at ~260 nm with a minimum at ~240 nm may be attributed to the stacking of successive guanines with the same (both *syn* or both *anti*) glycosidic bond angle and is thus a characteristic of parallel quadruplexes.<sup>15, 16</sup> There is thus, no clear signal at ~290 nm in these quadruplexes. On the other hand, antiparallel quadruplexes display a maximum at ~290 nm and a minimum at ~260 nm, which arises as a result of guanines with different glycosidic bond angles stacking on each other.<sup>16</sup> The quadruplex-forming ability and stability of iso-rTBA were studied by CD spectroscopy. The CD spectrum of 2'-5'-iso-rTBA displayed positive bands at ~295 nm and ~240 nm, and a negative band at ~260 nm (Figure 3) in the presence of K<sup>+</sup> ions, indicating a characteristic antiparallel G-quadruplex topology, as observed for TBA. This was an exciting observation, as 3'-5'-linked rTBA was reported earlier to present as a parallel G-quadruplex,<sup>1,7</sup> as also observed in our study (Figure 3).



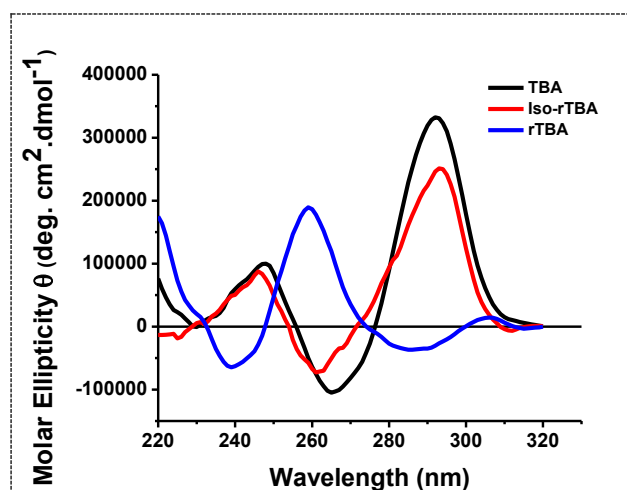


Figure 3. CD spectrum of TBA, rTBA, iso-rTBA taken at a concentration of 5  $\mu\text{M}$  in 10 mM potassium phosphate buffer (pH 7.2) containing 100 mM KCl.

### 3.4.1 G-quadruplex thermal stability evaluation by circular dichroism

The temperature-dependent change in the amplitude of the CD signal at 295 nm for antiparallel quadruplexes was followed to evaluate the stability of the G-quadruplexes. The CD melting data are indicated in Table 2, and the melting plots are shown in Figure 4.

Table 2. CD-melting data of oligomers.

Oligomer	CD $T_m$ ( $^{\circ}\text{C}$ ), $\text{K}^+$ , 295 nm	CD $T_m$ ( $^{\circ}\text{C}$ ), thrombin, 295 nm
iso-rTBA	52	29
TBA	50	22
isoTBA	29	< 10 <sup>Ref.9</sup>
rTBA	54 <sup>Ref.1</sup>	nd

The iso-rTBA quadruplex ( $T_m = 52$   $^{\circ}\text{C}$ ) was also found to be more stable than TBA ( $T_m = 50$   $^{\circ}\text{C}$ ), and isoTBA ( $T_m = 29$   $^{\circ}\text{C}$ ) and comparable to the multimolecular parallel rTBA G-quadruplex (54  $^{\circ}\text{C}$ ).<sup>1</sup> Thus, iso-rTBA forms a very stable antiparallel G-quadruplex in the presence of  $\text{K}^+$  ions.

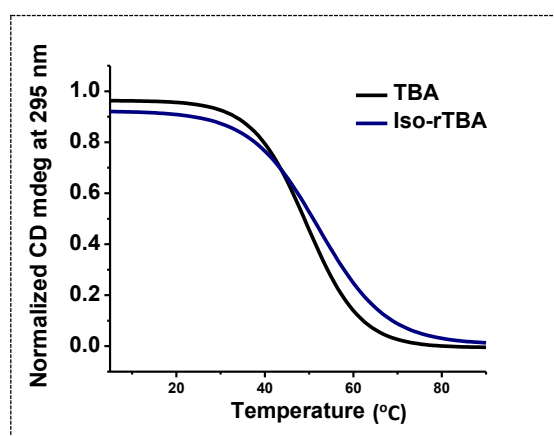


Figure 4. CD melting plots for TBA and iso-rTBA.

### 3.5 UV-Thermal Difference Spectra (TDS) and TDS factors

The thermal difference spectra (TDS) can be generated from the UV absorbance scans recorded at temperatures higher and lower than that of the melting point of the quadruplexes. TDS were obtained by subtracting the spectral scan of the sample at temperatures below (i.e., 10 °C) from that above (i.e., 90 °C) the melting temperatures. The characteristic negative at 295 nm and positive at 275 nm, that are typically seen in the TDS of G-quadruplexes<sup>17,18</sup> were observed also for iso-rTBA (Figure 5a).

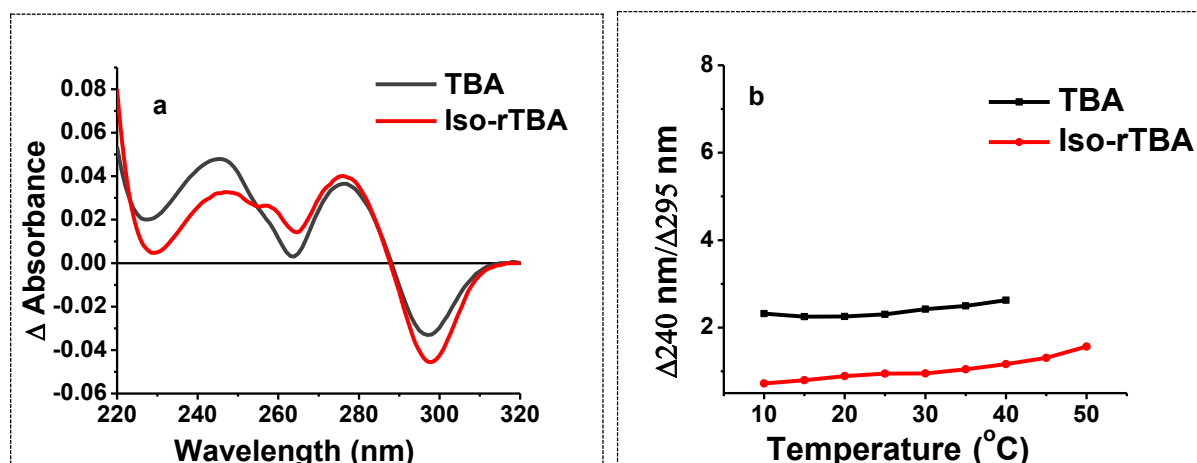


Figure 5. (a) UV-TDS (b) TDS factors of TBA and iso-rTBA in the presence of  $K^+$  ions.

The analysis of TDS factors may be used to effectively differentiate parallel and antiparallel quadruplexes. Thus, parallel quadruplexes typically contain guanosines of the same (either all *syn* or all *anti*) glycosidic bond angle, while antiparallel quadruplexes contain guanosines with differing *syn* or *anti* glycosidic bond angles in every quartet of the quadruplex. TDS factors of magnitude  $\geq 4$  imply the existence of parallel quadruplexes, while a magnitude

of  $\leq 2$  signifies antiparallel quadruplexes.<sup>16</sup> The TDS factor is the absolute value of the ratio of  $\Delta A_{240\text{nm}}/\Delta A_{295\text{nm}}$ , where  $\Delta A$  is the difference, at a given  $\lambda$ , between the absorbance above (e.g., 90 °C) and at a given temperature,  $T$ , below the melting temperature (where  $T = 5$  °C, 10 °C, ..., etc., up to the melting temperature,  $T_m$ ). The TDS factors for TBA and iso-rTBA in the presence of  $K^+$  ions were plotted as absolute values of  $\Delta A_{240\text{nm}}/\Delta A_{295\text{nm}}$  and are depicted in Figure 5b. For both TBA and iso-rTBA, the TDS factor  $\leq 2$  signifies antiparallel quadruplexes.

### 3.6 Hysteresis and concentration-dependence studies

The stable antiparallel G-quadruplex formation was observed with iso-rTBA in the presence of  $K^+$  ions. In order to confirm the molecularity of the iso-rTBA quadruplex, the UV plots during heating and subsequent cooling were analyzed for hysteresis in comparison to TBA, in the presence of  $K^+$  ions. Negligible hysteresis ( $\Delta T_m \approx 2$  °C, Table 3 and Figure 6) was observed, indicative of a unimolecular complex for TBA and iso-rTBA. Further, when the UV- $T_m$  measurements were carried out at a higher strand concentration of 20  $\mu\text{M}$  (Figure 6b), no appreciable differences were observed ( $\Delta T_m = +2$  to  $-2$  °C), again confirming the unimolecularity of the quadruplex. The data are listed in Table 3. This study thus constitutes the first report of a unimolecular antiparallel G-quadruplex for the TBA sequence with an RNA backbone, albeit 2'-5'-linked.

Table 3. UV- $T_m$  data of TBA and iso-rTBA.

Strand conc ( $\mu\text{M}$ )	TBA				Iso-rTBA			
	$T_m$ (heat) °C	$T_m$ (cool) °C	$\Delta T_m$ (20 $\mu\text{M}$ - 5 $\mu\text{M}$ ) °C	$\Delta T_m$ (heat- cool) °C	$T_m$ (heat) °C	$T_m$ (cool) °C	$\Delta T_m$ (20 $\mu\text{M}$ - 5 $\mu\text{M}$ ) °C	$\Delta T_m$ (heat- cool) °C
5	51	50	+2	+1	49	51	-1	-2
20	49	-		-	48	50		-2

Experiments were recorded at 295 nm at varying strand concentrations in 10 mM potassium phosphate buffer (pH 7.2) containing 100 mM KCl.

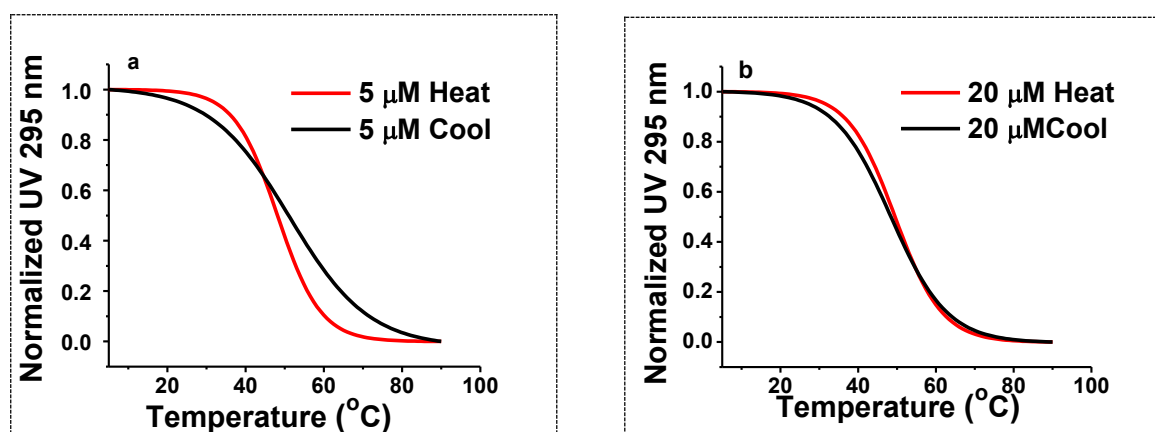


Figure 6. Normalized UV plots for heating and cooling cycles of iso-rTBA taken at 5  $\mu\text{M}$  (a) and 20  $\mu\text{M}$  (b) concentration, monitored at 295 nm. Buffer: 10 mM potassium phosphate buffer, pH 7.0, containing 100 mM KCl.

### 3.7 NMR study

The resonances of the imino protons of hydrogen-bonded guanines in the G-tetrads of G-quadruplexes typically appear between 10.5 to 12.0 ppm in the  $^1\text{H}$  NMR spectrum.<sup>19,20</sup> As observed for TBA and isoTBA,<sup>9</sup> comparable imino proton chemical shifts were observed for iso-rTBA as well (Figure 7b), indicative of the hydrogen-bonded G-quadruplex. Unlike isoTBA, where the  $^1\text{H}$  NMR spectrum did not show any imino proton resonances in this region in the absence of added cations,<sup>9</sup> some signals were observed for iso-rTBA (Figure 7a), although these were different from those observed in the presence of  $\text{K}^+$  ions (Figure 7b), and were spread over a wider chemical shift range. This could be a consequence of the different types of hydrogen-bonded structures observed with and without  $\text{K}^+$  ions, as also evident from the corresponding CD scans (Figure 8).

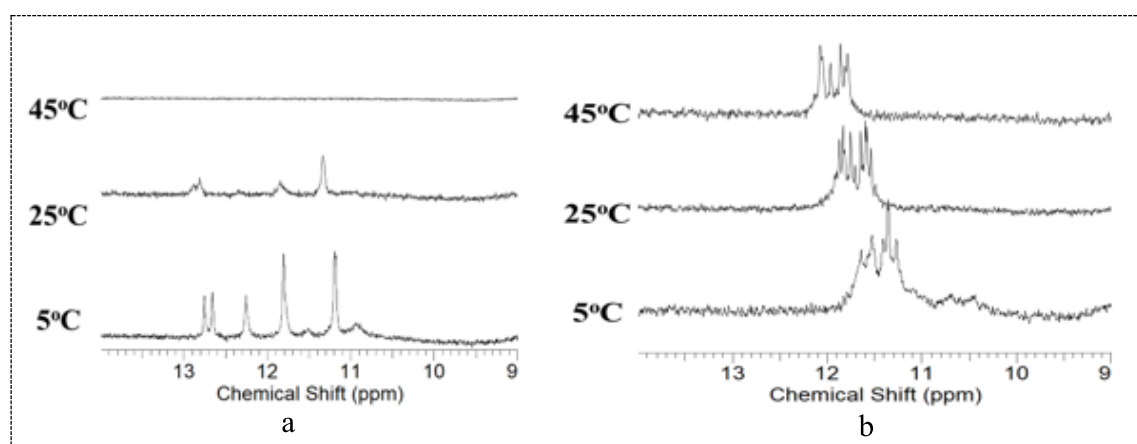


Figure 7. Imino proton region of the  $^1\text{H}$  NMR spectrum of a) iso-rTBA in the absence of  $\text{K}^+$  ions. b) Iso-rTBA in the presence of  $\text{K}^+$  ions. Spectra were recorded at 5  $^\circ\text{C}$ , 25  $^\circ\text{C}$ , and 45  $^\circ\text{C}$  for a strand concentration of 200  $\mu\text{M}$  in 90:10 v/v  $\text{H}_2\text{O}:\text{D}_2\text{O}$ .

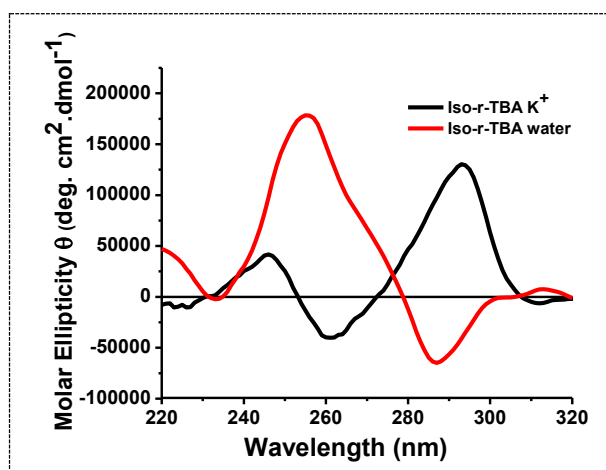


Figure 8. CD spectrum of iso-rTBA in water (absence of added cations) and in 10 mM potassium phosphate buffer, pH 7.2, containing 100 mM KCl.

In the absence of  $K^+$  ions, at low temperature narrow signals as well as some broad signals were observed, extending to  $\sim 13.0$  ppm indicating the presence of Watson-Crick type base pairs and other non-canonical, random aggregates. Temperature-dependent changes in the  $^1H$  NMR spectra show that in the absence of  $K^+$  ions, the imino signals disappear at higher temperature ( $45^\circ C$ ), indicating disruption of hydrogen-bonded structures. In the presence of  $K^+$  ions, two sets of imino signals were present at low temperature, one being very weak and broad relative to the other. This is indicative of multiple G-quadruplex conformations or simple aggregation of G-rich strands at high concentrations. At  $25^\circ C$ , the weaker signals disappeared, and a single set of narrow imino peaks equal to the number of guanines in the sequence were observed indicating a single dominant quadruplex conformation.<sup>21</sup> Further heating resulted in diminishing imino signal intensity as the temperature approached the melting temperature of iso-rTBA, as observed in the CD and UV-melting studies. The imino peaks become sharper and shift downfield on going from  $5^\circ C$  to  $45^\circ C$ , while the other less stable structures get eliminated. The observation of two sets of imino signals at low temperature, suggests the possibility of the existence of aggregated species at low temperature, their dis-aggregation near  $25^\circ C$ , followed by the initiation of quadruplex melting at higher temperatures. The aggregated species suggested by these studies is probably a consequence of much higher concentration of oligomer used ( $200\ \mu M$ ) in NMR work. Higher-order G-quadruplex structures formed by end-to-end or lateral association have been reported at millimolar concentrations typically employed for NMR studies,<sup>22</sup> which were not observed at micromolar concentrations used in UV and CD studies.

### 3.8 Thrombin binding study

Thrombin, as previously reported by Baldrich and O'Sullivan,<sup>23</sup> can act as a molecular chaperone for TBA folding. Nagatoishi and co-workers demonstrated<sup>24</sup> that, in the presence of thrombin but absence of any cation, TBA forms an antiparallel G quadruplex at low temperatures, which can be monitored using the CD amplitude at 295 nm.

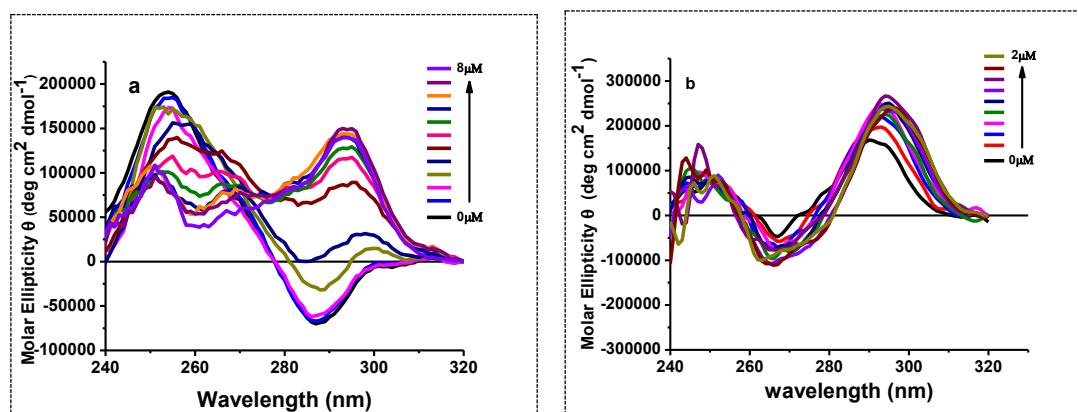


Figure 9. Changes in the CD signal of iso-rTBA and TBA (5  $\mu\text{M}$ ) upon addition of thrombin in water.

The thrombin-binding ability and affinity were studied by CD experiments when increasing amounts of thrombin were added to an aqueous solution of iso-rTBA. The drastic changes observed included a decrease in intensity of 255 nm maximum and 287 nm minimum, and a concomitant appearance and increase in the intensity of maximum at 295 nm (Figure 9a). Thus, the interaction of thrombin with iso-rTBA and its chaperone action inducing an antiparallel topology in iso-rTBA was strongly evident. In comparison, when thrombin was added to TBA, an increase in the maximum near 295 nm was observed, together with a shift towards 300 nm (Figure 9b), as reported earlier for this oligomer.<sup>23,24</sup> The stability of the thrombin complex with iso-rTBA ( $T_m = 29\text{ }^\circ\text{C}$ ) was higher than TBA iso-rTBA ( $T_m = 22\text{ }^\circ\text{C}$ ) (Table 2 and Figure 10).

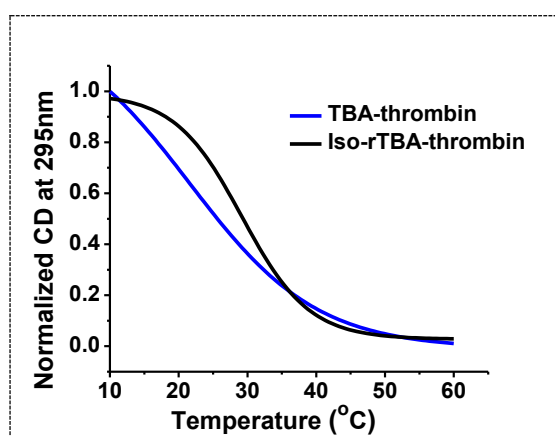


Figure 10. CD melting plots of TBA and iso-rTBA in complex with thrombin.

When the experiment was performed in the presence of  $K^+$  ions, there was negligible change in the CD spectrum of the pre-formed antiparallel iso-rTBA G-quadruplex (Figure 11a), and the complex melted at a temperature that was similar to that of the iso-rTBA quadruplex with  $K^+$  ions in the absence of thrombin (Table 2, Figure 11b).

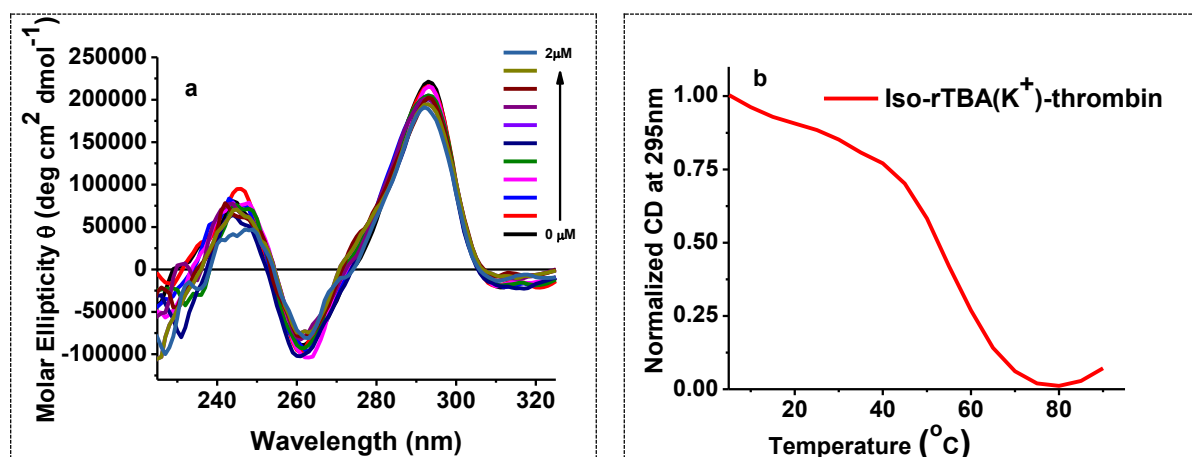


Figure 11. a) Thrombin binding monitored by CD spectra for iso-rTBA and b) CD melting plot of iso-rTBA-thrombin in the presence of  $K^+$  ions.

### 3.9 CD saturation binding curves for TBA and iso-rTBA with thrombin

The  $K_d$  for complexes of thrombin with TBA and iso-rTBA were calculated from the CD saturation binding curves (Figure 12), obtained by titrating solutions of the TBA/iso-rTBA oligomers with thrombin. The  $K_d$  value for thrombin with iso-rTBA ( $3.4 \times 10^{-6}$  M) was found to be one order of magnitude higher than for TBA ( $3.8 \times 10^{-7}$  M) while iso-rTBA was found to bind to 4 molecules ( $n$ ) of thrombin, compared to 1 molecule in the case of TBA, and a 4-fold higher concentration of thrombin was required for the CD signal to reach saturation with iso-rTBA in comparison to TBA (Table 4).

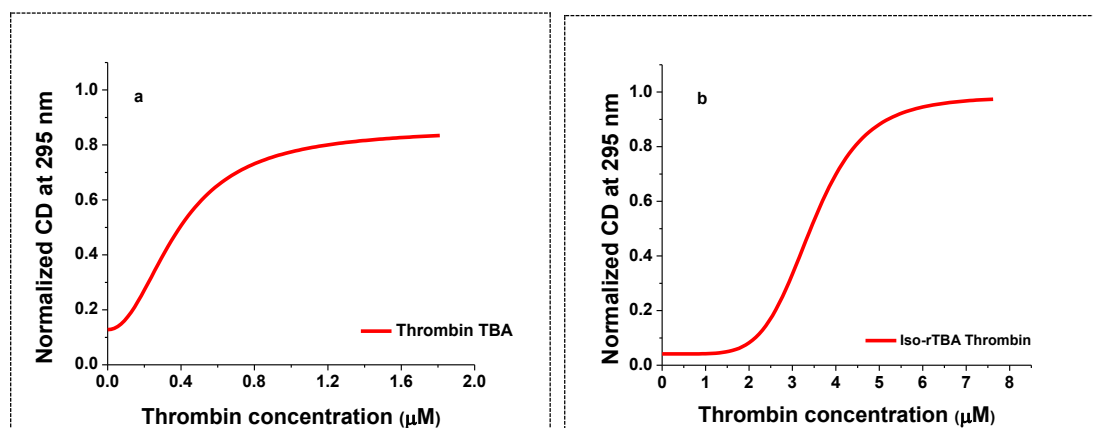


Figure 12. CD saturation binding curves for (a) TBA and (b) iso-rTBA with thrombin

$K_d$  and  $n$  were calculated using the formula

$$\theta = \frac{[L]}{[L] + K_d}$$

$$\log\left(\frac{\theta}{1-\theta}\right) = n \log[L] - \log[K_d]$$

Where,  $\theta$  is the normalized CD amplitude at 295 nm,  $[L]$  is the ligand (thrombin) concentration and  $K_d$  is the dissociation constant, which is equivalent to  $1/K_a$ .

**Table 4. Calculation of  $K_d$  and  $n$**

Oligomer	$K_d$	$n$
TBA	$3.8 \times 10^{-7}$ M	1
Iso-rTBA	$3.4 \times 10^{-6}$ M	4

### 3.10 Anti-clotting study

Thrombin converts fibrinogen to fibrin, which causes coagulation.<sup>25</sup> A clotting assay was used to assess the effect of thrombin binding on the anti-thrombin activity of the modified oligomers, and the inhibitory effect on thrombin-catalyzed fibrin polymerization (thrombin time/clotting time) was measured at 37 °C. Iso-rTBA was added to a solution of thrombin in saline and the time required for clotting was measured at 37 °C. The results are summarized in Figure 13. The anti-clotting effect of iso-rTBA (clotting time 70.9 s) was found to be similar to TBA (clotting time 77.6 s) and isoTBA (clotting time 73.4 s). Thus, not only was the RNA backbone of iso-rTBA able to fold into an antiparallel quadruplex, but iso-rTBA was also able to effect anticoagulation to almost the same level as TBA and isoTBA.



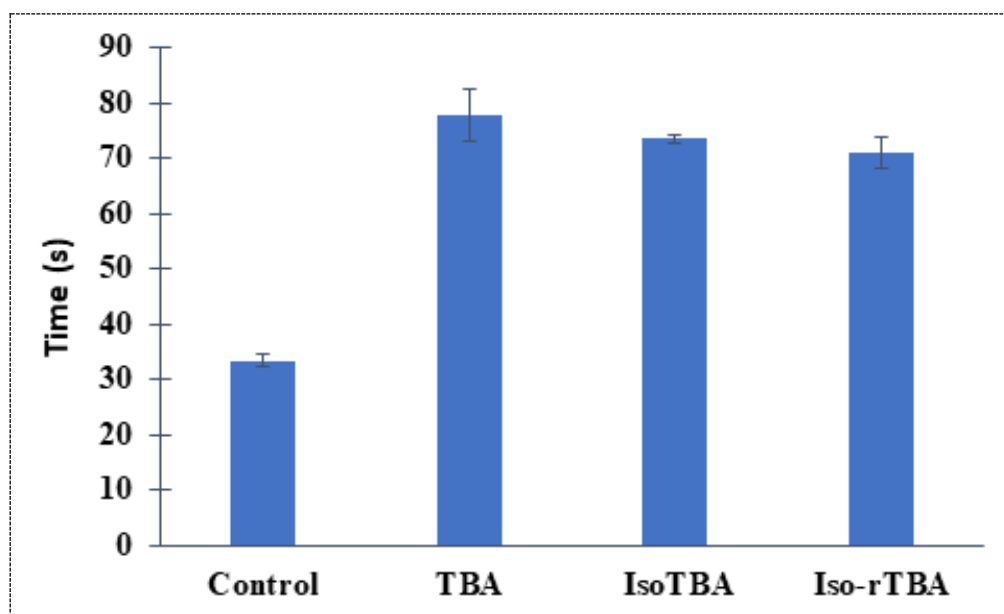


Figure 13. Anticlotting activity measured by comparing the thrombin-catalyzed fibrin polymerization time. Experiments were performed in saline at 37 °C and repeated at least three times independently. The error bars indicate the standard deviation of these measurements.

### 3.11 Nuclease stability study

The stability of iso-rTBA to degradation by nucleases RNase A and snake venom phosphodiesterase was assessed in comparison to TBA.

#### 3.11.1 Stability to RNase A

The stability of iso-rTBA to hydrolysis by RNase A was estimated in comparison to TBA and a random sequence RNA 12mer (Figure 14). As expected, TBA, being a DNA oligomer, was resistant to hydrolysis by RNase A. On the other hand, the RNA 12mer was rapidly hydrolysed, with a half-life of 1.5 min. In contrast, iso-rTBA was extremely stable and remained intact even after prolonged exposure of 12 h, behaving similar to TBA, even though it has a ribose backbone as in RNA. The stability to RNase is a significant advantage for this oligomer over other RNA oligomers/aptamers and significantly increases its potential for biological applications.

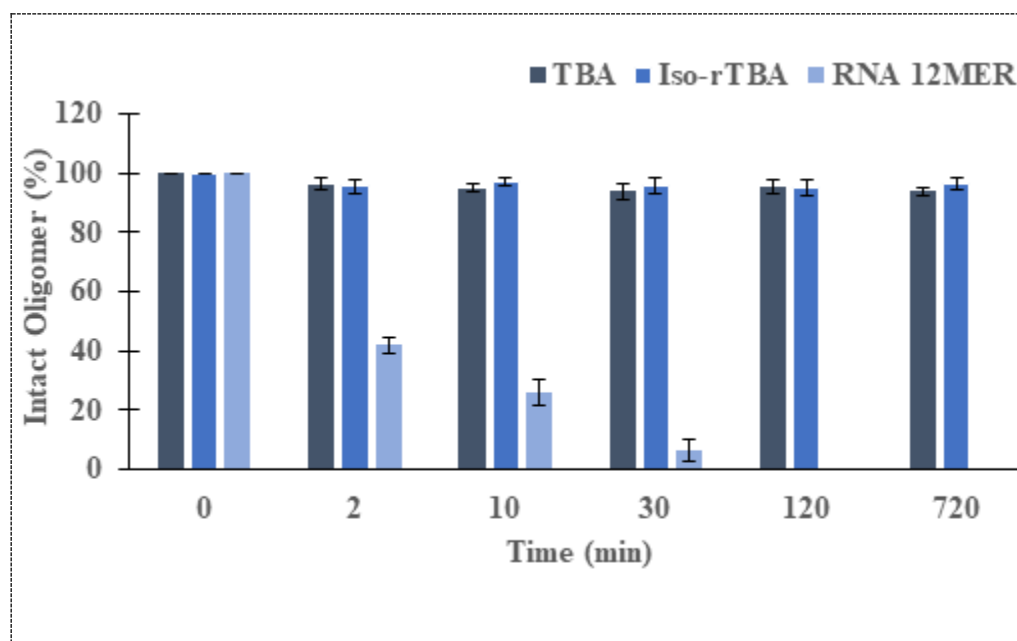


**Figure 14.** Stability of oligomers TBA, iso-rTBA and a random RNA 12mer to hydrolysis by RNase A. Oligomers were taken at a concentration of 7.5  $\mu$ M in 50 mM MOPS buffer at pH 7.0. RNase A (0.05 U) was added, and aliquots were withdrawn at successive time intervals and analyzed by HPLC to quantify the intact oligomer present.

### 3.11.2 Stability to snake venom phosphodiesterase (SVPD)

The stability of iso-rTBA to nuclease digestion was further tested by exposure to snake venom phosphodiesterase (SVPD) from *Crotalus adamanteus* (3' exonuclease) to test the enzymatic stability of the modified aptamer. The study was carried out at 37 °C and the percent oligomer remaining intact at successive time intervals was monitored by RP-HPLC (Figure 15). Although both oligomers were finally hydrolysed by SVPD, iso-rTBA was clearly more resistant to the enzyme, with a half-life of 1.9 min, Vs. TBA with a half-life of 0.8 min; 4 % intact iso-rTBA was still observed after 30 min, while TBA was completely consumed within 10 min. This superior resistance of iso-rTBA to enzymatic hydrolysis by nucleases clearly makes it appealing for applications in biological systems.

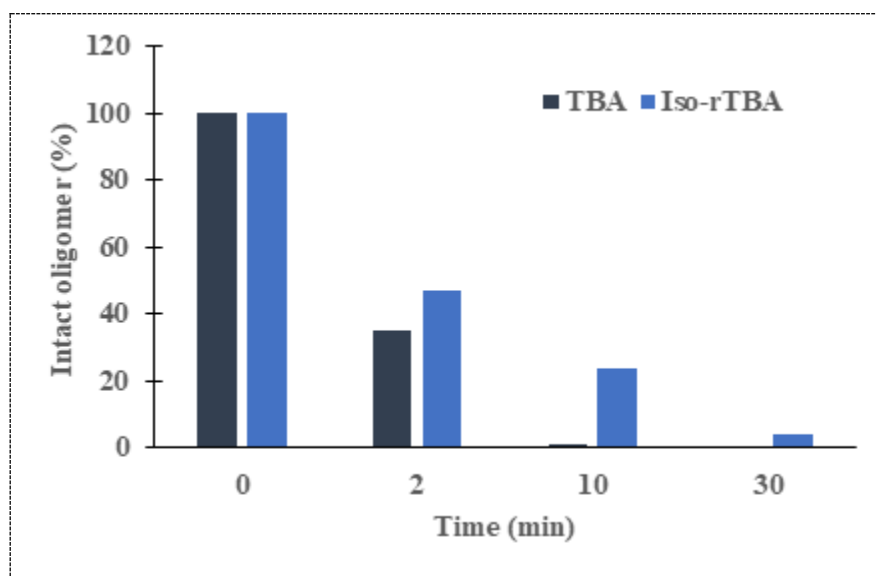


**Figure 15.** Stability of iso-rTBA and TBA (7.5  $\mu$ M each) to degradation by SVPD (0.015 U) at 37 °C. Buffer: 100 mM Tris-HCl (pH 8.5) containing 15 mM MgCl<sub>2</sub>, 100 mM NaCl.

### 3.12 Conclusions

In this Chapter, we have shown that iso-rTBA, a G-rich RNA with a 2'-5'-linked backbone, is able to fold into an antiparallel G-quadruplex, unlike most RNA quadruplexes (including rTBA), that adopt a parallel topology. Further, this unimolecular antiparallel iso-rTBA quadruplex is able to inhibit clotting, similar to TBA, and also resist degradation by nucleases. This highlights the flexibility and versatility of the 2'-5'-backbone, and its ability to adopt functional topologies, irrespective of whether the sugar is ribose or deoxyribose. The 2'-5'-RNA backbone also provides a more economically viable possibility, as the protected phosphoramidite building blocks are more readily and economically available. We believe that this study would open up possibilities for the application and study of the 2'-5'-isoRNA backbone in other DNA aptameric sequences for enhanced properties without compromising their functional ability. This report thus constitutes an important and easily implementable development in this area.

### 3.13 Experimental

#### 3.13.1 Oligonucleotide synthesis, purification and characterization

3'-5'-linked TBA and 2'-5'-linked iso-rTBA were synthesized in-house on a Bioautomation Mermade-4 DNA synthesizer employing  $\beta$ -cyanoethyl phosphoramidite chemistry. The 2'-deoxy-3'-phosphoramidites were obtained from ChemGenes and 3'-TBDMS-protected 2'-phosphoramidites, from Glen Research. Universal columns procured from Bioautomation were used for 2'-5'-linked oligomer synthesis. Oligonucleotides were

cleaved from the solid support by treating with aqueous ammonia at 60° C for 6h and then concentrated. Post-synthesis, deprotection of the TBDMS group was achieved by treatment with triethylamine trihydrofluoride for 2h, followed by purification.

### 3.13.2 HPLC analysis

Oligonucleotides were purified by RP-HPLC on a C18 column using a Waters system (Waters Delta 600e quaternary solvent delivery system, 2998 photo-diode array detector and Empower2 chromatography software. An increasing gradient of acetonitrile in 0.1 M triethyl ammonium acetate (pH 7.0) was used. The molecular weight of all oligonucleotides was verified by MALDI-TOF analysis.

### 3.13.3 CD experiments

CD spectra were recorded on a Jasco J-815 CD spectrometer equipped with a Jasco PTC-424S/15 peltier system. 5 mm path-length quartz cuvettes were used for a sample volume of 2 ml and strand concentration of 5  $\mu\text{M}$  in tris buffer (10 mM, pH 7.2) containing 100 mM KCl. Oligomers in buffer were annealed by heating at 95 °C for 5 min, then slowly cooled to room temperature followed by refrigeration for 3 to 4 h before use. Spectral scans over a range of 320 nm to 200 nm were collected as accumulations of 3 scans at a scanning rate of 100 nm  $\text{min}^{-1}$ . CD melting was performed by monitoring CD intensity at 295 nm against temperature over the range 5–90 °C at a heating rate of 3 °C per min.

### 3.13.4 UV experiments

UV-absorbance scans of the TBA and iso-rTBA oligomers were recorded using 10 mm pathlength quartz cells on an Analytik Jena SPECORD® 200 plus spectrometer equipped with a peltier-controlled temperature controller and at a scanning speed of 5 nm  $\text{sec}^{-1}$ . The TBA and iso-rTBA oligomers (5  $\mu\text{M}$  strand concentration) were annealed in tris buffer (10 mM, pH 7.2), containing 100 mM of the appropriate cations. The oligomer concentration was calculated on the basis of absorbance from molar extinction coefficients of the corresponding nucleobases of DNA. Thermal difference spectra (TDS) were obtained by subtracting the UV-absorbance spectral scan of the sample at temperatures below (i.e., 10 °C) from that above (i.e., 90 °C) the melting temperature ( $T_m$ ). The TDS factor is the absolute value of the ratio of  $\Delta A_{240\text{nm}}/\Delta A_{295\text{nm}}$ , where  $\Delta A$  is the difference, at a given  $\lambda$ , between the absorbance above (e.g., 90 °C) and at a given temperature, T, below the melting temperature (where T = 5 °C, 10 °C,...) etc. upto the melting temperature,  $T_m$ .

### 3.13.5 NMR experiments

$^1\text{H}$  NMR spectra were acquired at 700 MHz and 4 °C using a Bruker AV 700 NMR spectrometer operating at 700.13 MHz for  $^1\text{H}$  using a 5mm BBFO probe. The raw data were processed with a Gaussian function for improvement of signal to noise ratio. Temperature during the measurements was controlled by means of a Bruker BVT 3000 unit. HPLC-purified iso-rTBA was taken at 200  $\mu\text{M}$  concentration in 90:10 v/v  $\text{H}_2\text{O}:\text{D}_2\text{O}$  with or without 100 mM KCl.

### 3.13.6 Anticlotting measurements

Clotting time experiments were performed at 37 °C on a Start-Max (Stago) coagulation analyzer. Each experiment was repeated at least thrice; the standard deviation was  $\pm 1$  s. Each commercial reagent was re-constituted according to the manufacturer's protocol. Bovine thrombin (Tulip Diagnostics, 0.1 NIH unit) was incubated with TBA or iso-rTBA as applicable and specified at 0.25  $\mu\text{M}$  oligomer concentration for 1.5 min before addition to fibrinogen from human plasma (Aldrich, 3.5  $\mu\text{M}$ ). The clotting time (s) was measured as the time taken upon addition of thrombin till the polymerization of fibrin.

### 3.13.7 Stability of oligonucleotides to cleavage by RNase A

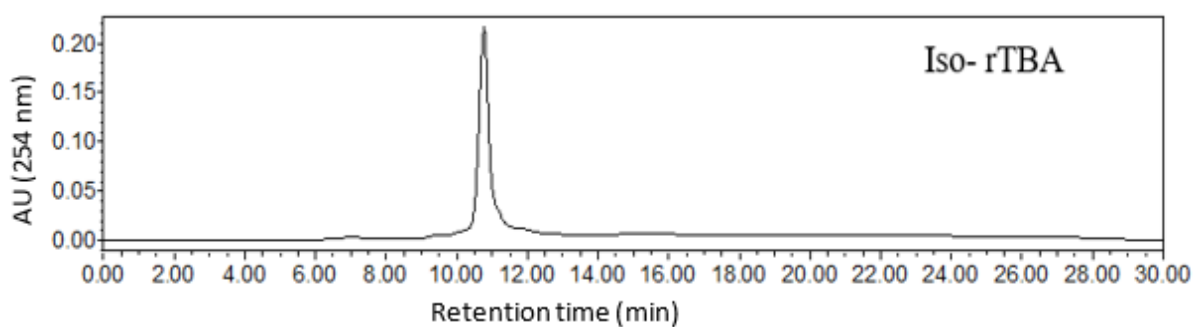
The reactions were performed in 1.5 ml plastic tubes with screw cap immersed in a water bath at 37 °C. Incubation was carried out in 50 mM MOPS buffer at pH 7. The samples were prepared by adding the oligonucleotides (iso-rTBA, 3'-5'-r(CUGAAAUCGGUU) random RNA or TBA at 7.5  $\mu\text{M}$  concentration) to a solution of the RNase enzyme (0.05 U) in MOPS buffer. Aliquots were collected at specific times after initiation of reaction, the enzyme was inactivated by heating at 90 °C for 3 min to stop the reaction, and samples were analyzed by HPLC to determine the quantity of oligonucleotide remaining intact at each time point.

### 3.13.8 SVPD stability study

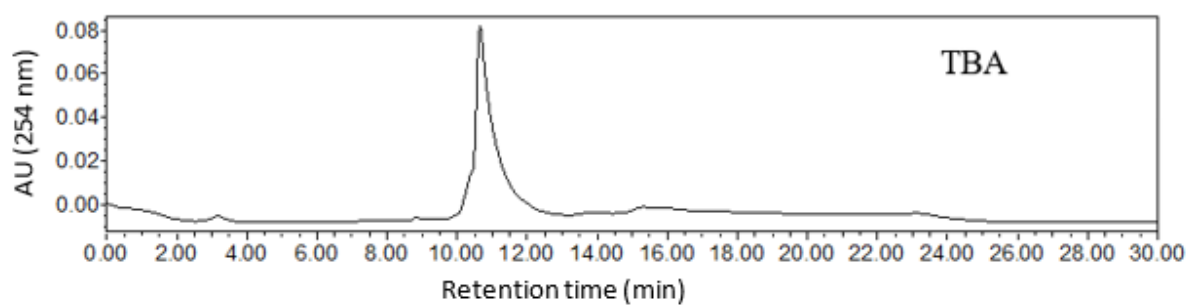
TBA and iso-rTBA (7.5  $\mu\text{M}$ ) were carried out at 37 °C in 100 mM Tris-HCl buffer (pH 8.5) containing 15 mM  $\text{MgCl}_2$ , 100 mM NaCl, and SVPD (0.015 U). Aliquots were removed at successive time intervals, heated at 90 °C for 3 min to inactivate the nuclease, and analyzed by RP-HPLC to measure the percentage of oligonucleotides remaining intact.

## 3.14 Appendix B

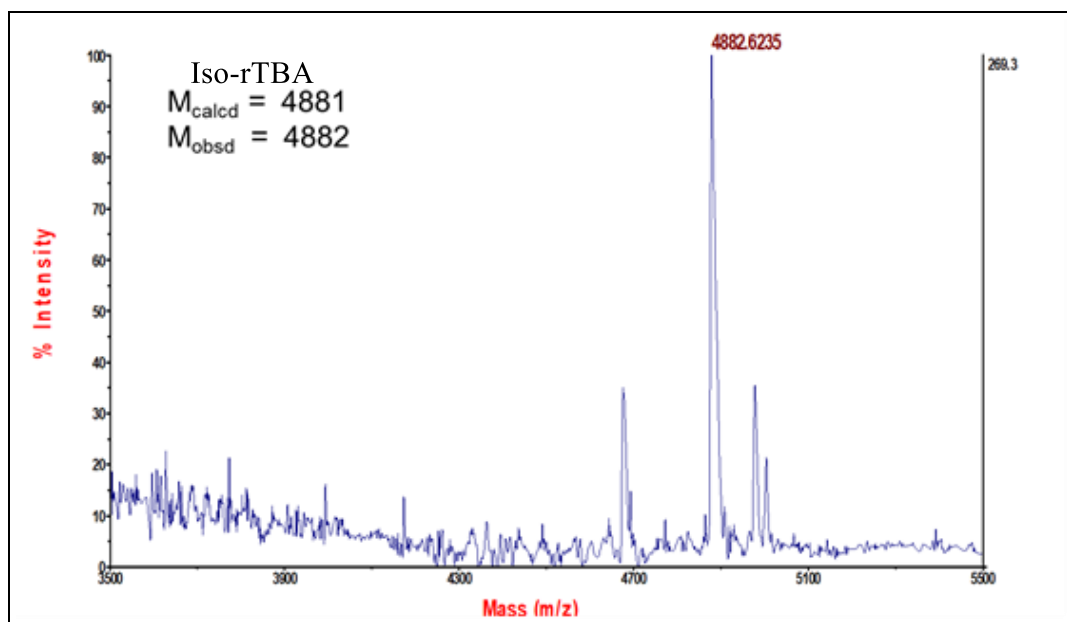
Description	Page No.
HPLC chromatogram of iso-rTBA oligomer	73
HPLC chromatogram of TBA oligomer	73
MALDI-TOF spectrum of iso-rTBA	74
MALDI-TOF spectrum of TBA	74



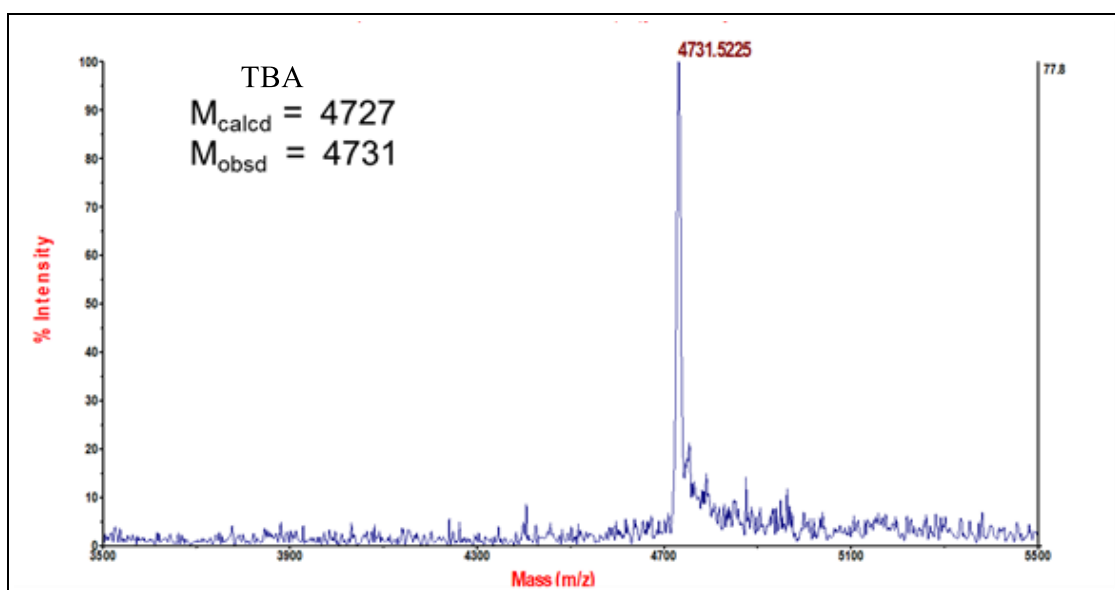
HPLC chromatogram of iso-rTBA oligomer



HPLC chromatogram of TBA oligomer



MALDI-TOF spectrum of iso-rTBA



MALDI-TOF spectrum of TBA

### 3.15 References

- (1) Joachimi, A.; Benz, A.; Hartig, J. S. A Comparison of DNA and RNA Quadruplex Structures and Stabilities. *Bioorg. Med. Chem.* **2009**, *17* (19), 6811–6815.
- (2) Saccà, B.; Lacroix, L.; Mergny, J. L. The Effect of Chemical Modifications on the Thermal Stability of Different G-Quadruplex-Forming Oligonucleotides. *Nucleic Acids Res.* **2005**, *33* (4), 1182–1192.
- (3) Liu, H.; Matsugami, A.; Katahira, M.; Uesugi, S. A Dimeric RNA Quadruplex Architecture Comprised of Two G : G ( : A ) : G : G ( : A ) Hexads , G : G : G : G Tetrads and UUUU Loops. *J. Mol. Biol.* **2002**, *322* (5), 955–970.
- (4) Bock, L. C.; Griffin, L. C.; Lantham, J. A.; & E. H. V.; Toole, J. J. Selection of Single-Stranded DNA Molecules That Bind and Inhibit Human Thrombin. *Nature* **1992**, *355*, 564–566.
- (5) Becker, R. C.; Povsic, T.; Cohen, M. G.; Rusconi, C. P.; Sullenger, B. Nucleic Acid Aptamers as Antithrombotic Agents: Opportunities in Extracellular Therapeutics. *Thromb. Haemost.* **2010**, *103* (3), 586–595.
- (6) (a) <https://www.covid19treatmentguidelines.nih.gov/therapies/antithrombotic-therapy>  
(b) Godino, C.; Scotti, A.; Maugeri, N.; Mancini, N.; Fominskiy, E.; Margonato, A.; Landoni, G. Antithrombotic therapy in patients with COVID-19? Rationale and Evidence. *Int. J. Cardiol.* **2021**, *324*, 261–266.
- (7) Tang, C.; Shafer, R. H. Engineering the Quadruplex Fold : Nucleoside Conformation Determines Both Folding Topology and Molecularity in Guanine Quadruplexes. *J. Am. Chem. Soc.* **2006**, *128*, 5966–5973.
- (8) Schultze, P.; Macaya, R. F.; Feigon, J. Three-Dimensional Solution Structure of the Thrombin-Binding DNA Aptamer d(GGTTGGTGTGGTTGG). *J. Mol. Biol.* **1994**, *235* (5), 1532–1547.
- (9) Gunjal, A. D.; Fernandes, M.; Erande, N.; Rajamohanan, P. R.; Kumar, V. A. Functional IsoDNA Aptamers: Modified Thrombin Binding Aptamers with a 2'-5'-Linked Sugar-Phosphate Backbone (IsoTBA). *Chem. Commun.* **2014**, *50* (5), 605–607.
- (10) Sheng, J.; Li, L.; Engelhart, A. E.; Gan, J.; Wang, J.; Szostak, J. W. Structural Insights into the Effects of 2'-5' Linkages on the RNA Duplex. *Proc. Natl. Acad. Sci.* **2014**, *111*



- (8), 3050–3055.
- (11) Agarwala, P.; Pandey, S.; Maiti, S. The Tale of RNA G-Quadruplex. *Org. Biomol. Chem.* **2015**, *13*, 5570–5585.
- (12) Keniry, M. A. Quadruplex Structures in Nucleic Acids. *Biopolym.* **2001**, *56*, 123–146.
- (13) Xiao, C.; Ishizuka, T.; Xu, Y. Antiparallel RNA G-Quadruplex Formed by Human Telomere RNA Containing 8-Bromoguanosine. *Sci. Rep.* **2017**, *7*, 1–8.
- (14) Gait, M. J. *Oligonucleotide Synthesis : A Practical Approach*; Rev. repr. ed.; Oxford : IRL press, **1984**.
- (15) Gray, D. M.; Wen, J.-D.; Gray, C. W.; Repges, R.; Repges, C.; Raabe, G.; Fleischhauer, J. Measured and Calculated CD Spectra of G-Quartets Stacked with the Same or Opposite Polarities. *Chirality* **2008**, *20*, 431–440.
- (16) Karsisiotis, A. I.; Hessari, N. M. A.; Novellino, E.; Spada, G. P.; Randazzo, A.; Webba Da Silva, M. Topological Characterization of Nucleic Acid G-Quadruplexes by UV Absorption and Circular Dichroism. *Angew. Chemie Int. Ed.* **2011**, *50* (45), 10645–10648.
- (17) Mergny, J.; Phan, A.; Lacroix, L. Following G-Quartet Formation by UV-Spectroscopy. *FEBS Lett.* **1998**, *435*, 74–78.
- (18) Mergny, J. L.; Li, J.; Lacroix, L.; Amrane, S.; Chaires, J. B. Thermal Difference Spectra: A Specific Signature for Nucleic Acid Structures. *Nucleic Acids Res.* **2005**, *33* (16), 1–6.
- (19) Aviñó, A.; Mazzini, S.; Ferreira, R.; Gargallo, R.; Marquez, V. E.; Eritja, R. The Effect on Quadruplex Stability of North-Nucleoside Derivatives in the Loops of the Thrombin-Binding Aptamer. *Bioorg. Med. Chem.* **2012**, *20* (14), 4186–4193.
- (20) Lim, K. W.; Amrane, S.; Bouaziz, S.; Xu, W.; Mu, Y. Structure of the Human Telomere in  $K^+$  Solution : A Stable Basket-Type G-Quadruplex with Only Two G-Tetrad Layers. *J. Am. Chem. Soc.* **2015**, *14*, 4301–4309.
- (21) Sun, H.; Xiang, J.; Zhou, Q.; Yang, Q.; Xu, G.; Tang, Y. Temperature-Sensitive Supramolecules Self-Assembled by G-Quadruplex DNA. *Int. J. Biol. Macromol.* **2010**, *46* (1), 123–125.

- (22) Abu-Ghazalah, R. M.; Rutledge, S.; Lau, L. W. Y.; Dubins, D. N.; MacGregor, R. B.; Helmy, A. S. Concentration-Dependent Structural Transitions of Human Telomeric DNA Sequences. *Biochemistry* **2012**, *51* (37), 7357–7366.
- (23) Baldrich, E.; Sullivan, C. K. O. Ability of Thrombin to Act as Molecular Chaperone , Inducing Formation of Quadruplex Structure of Thrombin-Binding Aptamer. *Anal. Biochem.* **2005**, *341*, 194–197.
- (24) Nagatoishi, S.; Tanaka, Y.; Tsumoto, K. Circular Dichroism Spectra Demonstrate Formation of the Thrombin-Binding DNA Aptamer G-Quadruplex under Stabilizing-Cation-Deficient Conditions. *Biochem. Biophys. Res. Commun.* **2007**, *352* (3), 812–817.
- (25) Mann, K. G.; Jenny, R. J.; Krishnaswamy, S. Cofactor Proteins in the Assembly and Expression of Blood Clotting Enzyme Complexes. *Annu. Rev. Biochem.* **1988**, *57*, 915–956.

## **Chapter 4**

**Replacement of loop residues in**

**TBA by an abasic**

**ethylene glycol spacer: Effect on**

**stability, structure and function**

## 4.1 Introduction

G-quadruplexes are highly ordered folded structures with various folding topologies and molecularities.<sup>1</sup> The thrombin binding aptamer (TBA)<sup>2</sup> is one such DNA sequence comprising 15 nucleotides, i.e., 5'-GGTTGGTGTGGTTGG-3' and is a result of *in vitro* selection targeted towards thrombin. NMR and X-ray crystal studies show that TBA folds in an intramolecular, anti-parallel fashion with a chair-like conformation consisting of two G-quartets linked by three loops- two TT loops and one TGT loop.<sup>2-4</sup> Although this sequence exhibits anticoagulant effects, it falls short due to its early degradation *in vivo*.<sup>5</sup> To overcome this problem while increasing the anti-clotting effect, many nucleotide and backbone modifications have been reported.<sup>6</sup> Among the studies that involved replacing the loop residues by abasic units, those that introduced a dibenzyl linker,<sup>7</sup> anthraquinone units,<sup>8</sup> tetrapeptides,<sup>9</sup> 3-carbon abasic spacer,<sup>10</sup> anthracene groups,<sup>11</sup> and azobenzene derivatives<sup>12</sup> (Figure 1). An enhancement in the thermal stability of the resulting quadruplexes was reported for the dibenzyl linker,<sup>7</sup> double anthraquinone units,<sup>8</sup> single anthracene substitution at T9,<sup>11</sup> C3-spacer,<sup>10</sup> and selected azobenzene substitutions.<sup>12</sup> The dibenzyl and C3-spacer were also found to increase the clotting time.<sup>7,10</sup> Nuclease stability studies were not reported. The increased flexibility offered by the simplest among these, i.e., the abasic 3-carbon spacer, at position T7, resulted in significant improvement in thermal stability and thrombin clotting time.<sup>10</sup>

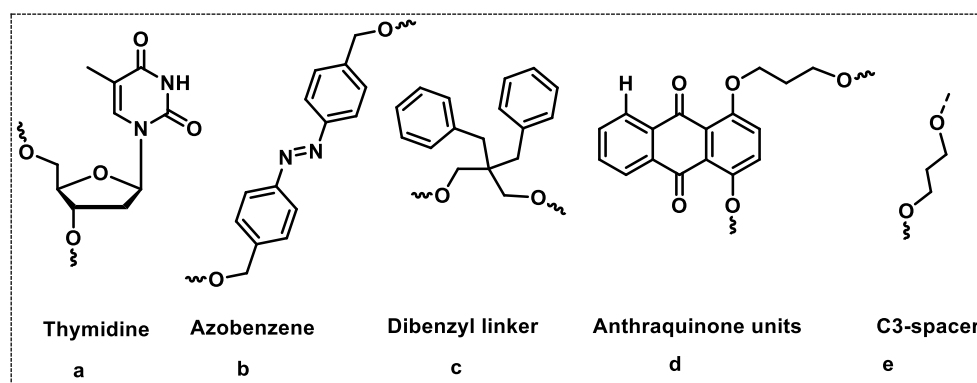
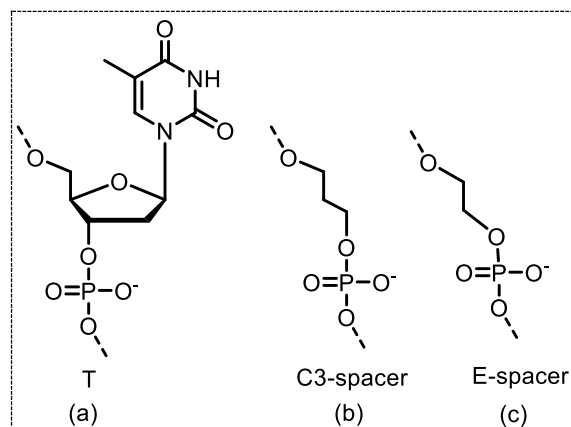


Figure 1. (a) thymidine (T) residue in comparison to (b) azobenzene (c) dibenzyl linker (d) anthraquinone units and (e) abasic propyl (C3) linker.

## 4.2 Rationale and objectives of the present work

Ethylene glycol linkages are known in oligonucleotides.<sup>13</sup> The U1 snRNA sequence was modified with ethylene glycol linkage in the phosphate region, which resulted in increased binding affinity for snurportin-1 than unmodified U1snRNA.<sup>14</sup>



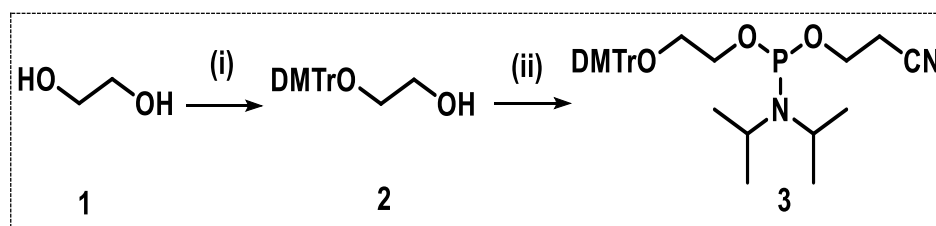
**Figure 2.** (a) thymidine (T) residue in comparison to (b) abasic propyl (C3) linker and (c) proposed abasic ethylene glycol (E) spacer.

We envisioned the synthesis of abasic spacer units derived from ethylene glycol (Figure 2) as replacement of loop residues in an attempt to further simplification and arrive at a minimal spacer unit that would preferably retain or improve the stability and anticoagulant properties of TBA. This new E spacer was incorporated at single or double positions in the T<sup>3</sup>T<sup>4</sup> and T<sup>7</sup>G<sup>8</sup>T<sup>9</sup> loops of TBA, as the TT and TGT loops are reported to be implicated in the interaction and subsequent inhibition of thrombin.<sup>15,16</sup>

### 4.3 Synthesis of ethylene glycol spacer phosphoramidite

The abasic ethylene glycol spacer phosphoramidite was synthesized employing simple chemical transformations as outlined in Scheme 1. Accordingly, commercially available ethylene glycol was converted to the mono-DMTr-protected compound **2** on treatment with DMTr chloride in the presence of DMAP with pyridine as a solvent in 60% yield. Further, reacting compound **2** with 2-cyanoethyl-*N,N*-diisopropylchlorophosphine in CH<sub>2</sub>Cl<sub>2</sub> gave the phosphoramidite **3** in 64% yield. Compound **3** was further used as the protected monomer for oligonucleotide synthesis.

**Scheme 1.** Synthesis of ethylene glycol phosphoramidite



**Reagents and conditions:** (i) DMTrCl (0.1 equiv.), DMAP (0.01equiv.), dry pyridine, 2h, r.t., 60% (ii) 2-Cyanoethyl-*N,N*-diisopropylchlorophosphine (2 equiv.), EtN(*i*Pr)<sub>2</sub> (4 equiv.), dry CH<sub>2</sub>Cl<sub>2</sub>, 1h, r.t., 64%

#### 4.4 Synthesis of TBA, and modified TBA oligomers, their purification, and characterization

TBA and modified TBA oligonucleotides containing E spacer units incorporated at pre-determined positions were synthesized using commercially available protected 2'-deoxythymidine-3'-phosphoramidite and 2'-deoxy-guanosine-3'-phosphoramidite by standard  $\beta$ -cyanoethyl phosphoramidite chemistry<sup>17</sup>, using an increased coupling time of 150 s for this unit. The synthesized oligomers were cleaved from the solid support using aqueous ammonia, purified by RP-HPLC, and characterized by MALDI-TOF spectrometry. The general scheme for solid-phase oligonucleotide synthesis is explained in Chapter 1, Scheme 1. The synthesized oligomeric sequences and their MALDI-TOF characterization data are listed in Table 1.

Table 1: Synthesized TBA and modified oligomers.

Sr.no.	Sequence	Sequence name	MALDI TOF Mass (Da)	
			M <sub>calcd.</sub>	M <sub>obsd.</sub>
1	TBA- T <sub>E</sub> <sup>3</sup>	GG <u>E</u> TGGTGTGGTTGG	4546	4587 ([M] + K <sup>+</sup> )
2	TBA- T <sub>E</sub> <sup>4</sup>	GGT <u>E</u> GGTGTGGTTGG	4546	4586 ([M] + K <sup>+</sup> )
3	TBA- T <sub>E</sub> <sup>7</sup>	GGTTGG <u>E</u> GTGGTTGG	4546	4582 ([M] + K <sup>+</sup> )
4	TBA- T <sub>E</sub> <sup>9</sup>	GGTTGGTGE <u>G</u> GGTTGG	4546	4587 ([M] + K <sup>+</sup> )
5	TBA- T <sub>E</sub> <sup>3</sup> T <sub>E</sub> <sup>4</sup>	GG <u>E</u> <u>E</u> GGTGTGGTTGG	4364	4372
6	TBA- T <sub>E</sub> <sup>7</sup> T <sub>E</sub> <sup>9</sup>	GGTTGG <u>E</u> GE <u>G</u> GGTTGG	4364	4371
7	TBA	GGTTGGTGTGGTTGG	4727	4731

E = ethylene glycol

The E units were introduced either at single positions or as double replacements of T residues in the T<sup>3</sup>T<sup>4</sup> and T<sup>7</sup>G<sup>8</sup>T<sup>9</sup> loops. TBA oligonucleotides T<sub>E</sub><sup>3</sup>, T<sub>E</sub><sup>4</sup>, T<sub>E</sub><sup>7</sup>, and T<sub>E</sub><sup>9</sup> represent single substitutions of T at positions 3, 4, 7, and 9, respectively, while oligonucleotides T<sub>E</sub><sup>3</sup>T<sub>E</sub><sup>4</sup> and T<sub>E</sub><sup>7</sup>T<sub>E</sub><sup>9</sup> represent double substitutions in the loop regions at positions indicated by the numbers.

#### 4.5 G-quadruplex formation and stability by circular dichroism spectroscopy

CD spectra of TBA oligomers singly substituted with E (T<sub>E</sub><sup>3</sup>, T<sub>E</sub><sup>4</sup>, T<sub>E</sub><sup>7</sup>, and T<sub>E</sub><sup>9</sup>) were characterized by high amplitude, positive maxima at 295 nm and 240 nm, and minima at 260

nm, in comparison to TBA oligomers bearing two E substitutions ( $T^3_E T^4_E$  and  $T^7_E T^9_E$ ; Figure 3a), where the lowest amplitude was observed for  $T^7_E T^9_E$ . In the presence of  $Na^+$ , all the modified oligomers displayed CD signals of lower amplitude and differing in their maxima/minima when compared to TBA (Figure 3b).

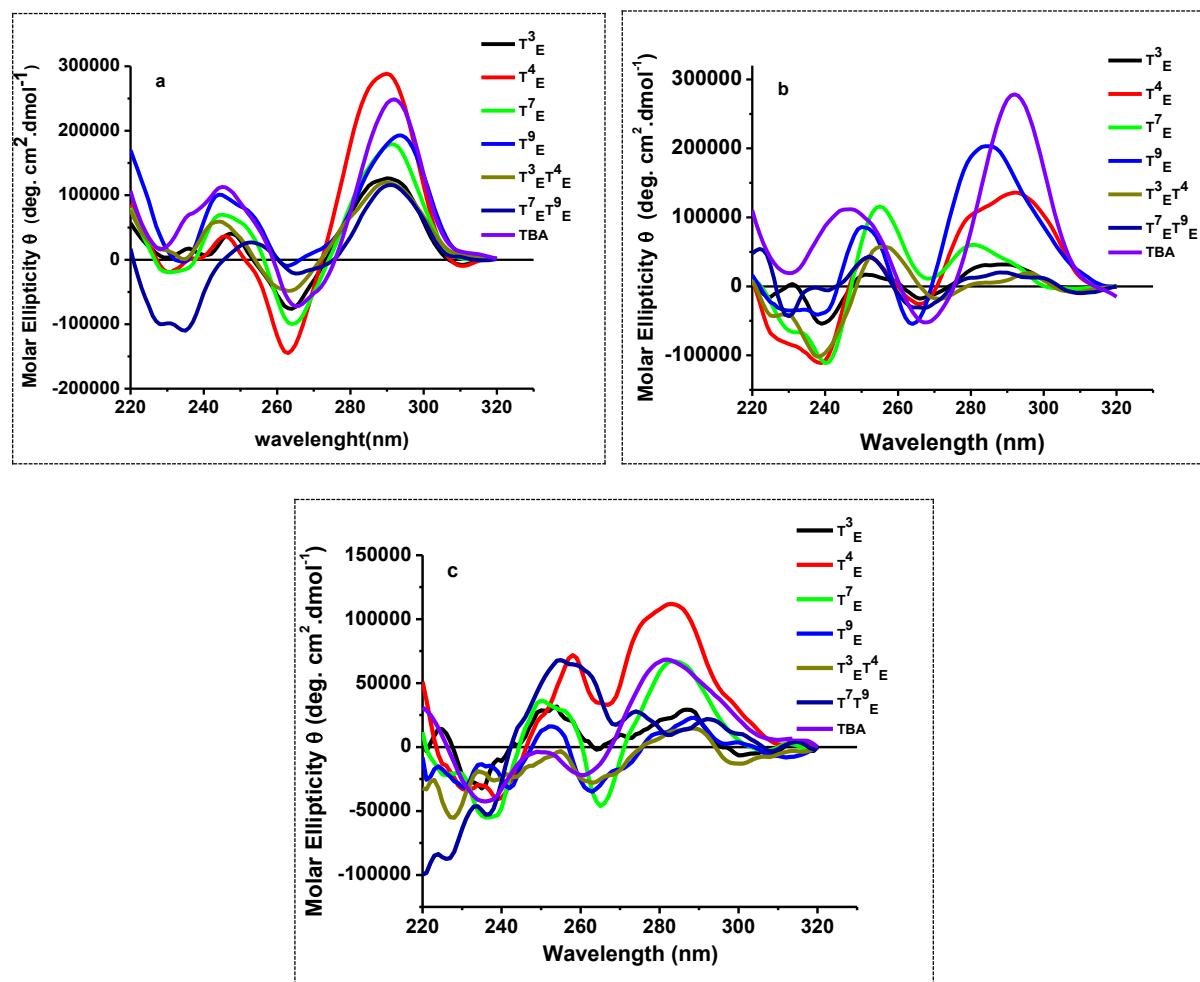


Figure 3. CD spectral scans at 4 °C of oligomers (a) in potassium phosphate buffer (10 mM, pH 7.2) containing 100 mM KCl; (b) Sodium phosphate buffer (10 mM, pH 7.2) containing 100 mM NaCl; (c) in water.

The observed spectra of the E-containing oligomers were similar to those in presence of  $Na^+$  even in the absence of any added ions (Figure 3c), thus suggesting that  $Na^+$  ions may not have a significant effect on the quadruplex-forming ability of the E-TBA oligomers. Since a CD spectrum can be used to distinguish between parallel and anti-parallel quadruplex folding topologies, where a parallel quadruplex shows maxima typically at 260 nm and an anti-parallel quadruplex at 295 nm,<sup>18</sup> it can be concluded that the E-modified oligomers fold into anti-parallel quadruplexes in the presence of  $K^+$  ions (Figure 3a). In the presence of  $Na^+$  ions,  $T^4_E$  and  $T^9_E$  showed signals characteristic of anti-parallel conformation, while the CD spectra of

the other oligomers were inconclusive (Figure 3b). In the absence of any cations,  $T^3_E$ ,  $T^7_E$ ,  $T^9_E$  and  $T^3_ET^4_E$  oligomers showed no conclusive CD pattern, while  $T^4_E$  and  $T^7_ET^9_E$  showed a completely different folding pattern (Figure 3b).

#### 4.6 Raman spectroscopy

Depending on the direction of the strands and the conformation of the guanine nucleobases about the glycosidic bond, they can be classed as parallel and antiparallel. All guanines in the parallel structure are *anti*, although in the antiparallel structure, they alternate between *syn* and *anti*. TBA and modified oligomer were incubated at room temperature in presence  $K^+$  ion. The spectra showed Raman bands associated with the quadruplex structure<sup>19</sup> (Figure 4, Table 2).

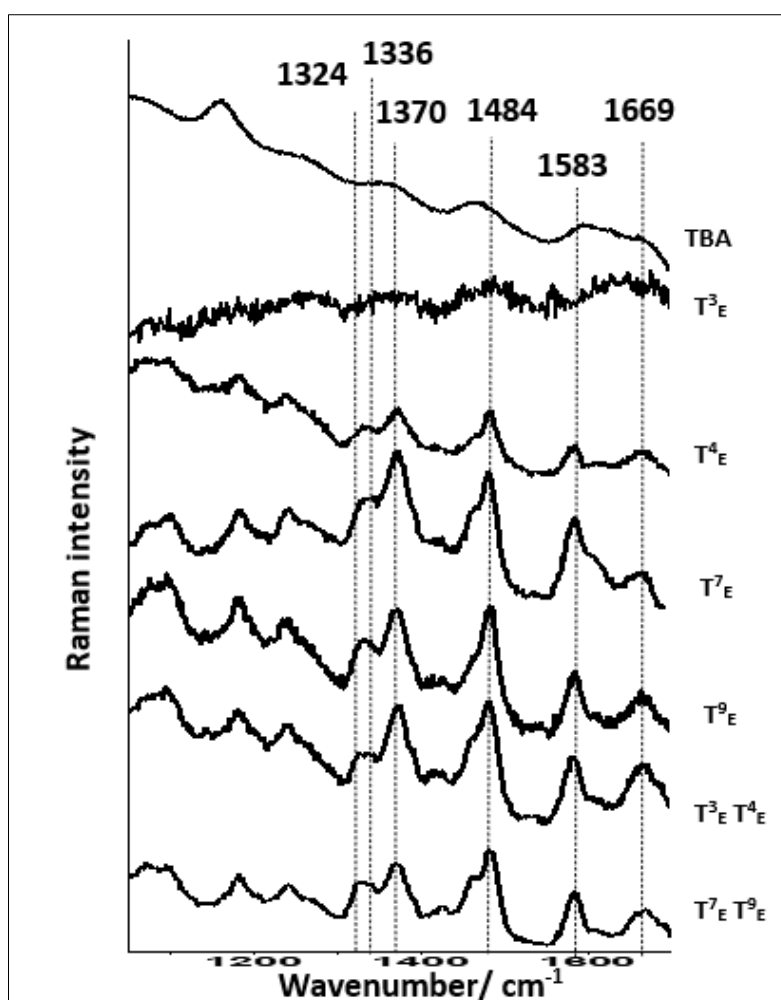


Figure 4. Raman spectra for the E-containing oligomers in comparison to TBA, with the characteristic signals from G-quadruplexes marked.



Table 2. Raman spectra signals and assignments.

Raman spectrum marker ( $\text{cm}^{-1}$ )	Assignment
$\sim 1324$	dG C2'-endo/syn,
$\sim 1336$	dG C2'-endo/anti,
$\sim 1370$	dT, dG C2'-endo/syn
$\sim 1484$	C8=N7-H2 deformation; dG-N7-H2 strong Hoogsteen H-bond
$\sim 1583$	dG; N2H interbase H-bond
$\sim 1669$	C6=O6 of Guanine

dG marker bands were observed at  $\sim 1324 \text{ cm}^{-1}$  and  $\sim 1336 \text{ cm}^{-1}$ , corresponding to the dG C2'-endo/syn and dG C2'-endo/anti conformations respectively.<sup>20</sup> The signal at  $\sim 1370 \text{ cm}^{-1}$  corresponds to dT, dG C2'-endo/syn.<sup>21</sup> The N7 and H2 deformation of the guanine tetrad is attributed to the band approximately at  $1484 \text{ cm}^{-1}$ .<sup>22</sup> It was also seen that the intensity of the  $1669 \text{ cm}^{-1}$  band (showing hydrogen-bond formation) in all oligomers was lower than the  $1583 \text{ cm}^{-1}$  band,<sup>19</sup> owing to the strong hydrogen-bond formation between O6 and H1, suggesting the quadruplex form's prevalence.

#### 4.7 G-quadruplex thermal stability using UV and CD spectroscopy

Denaturation profiles and melting temperature ( $T_m$ ) can be monitored by UV and CD spectroscopy at varying temperatures. The stability of the G-quadruplexes in the presence of  $\text{K}^+$  and  $\text{Na}^+$  ions was monitored by the temperature-dependent change in the amplitude of the UV and CD signal at  $295 \text{ nm}$ .

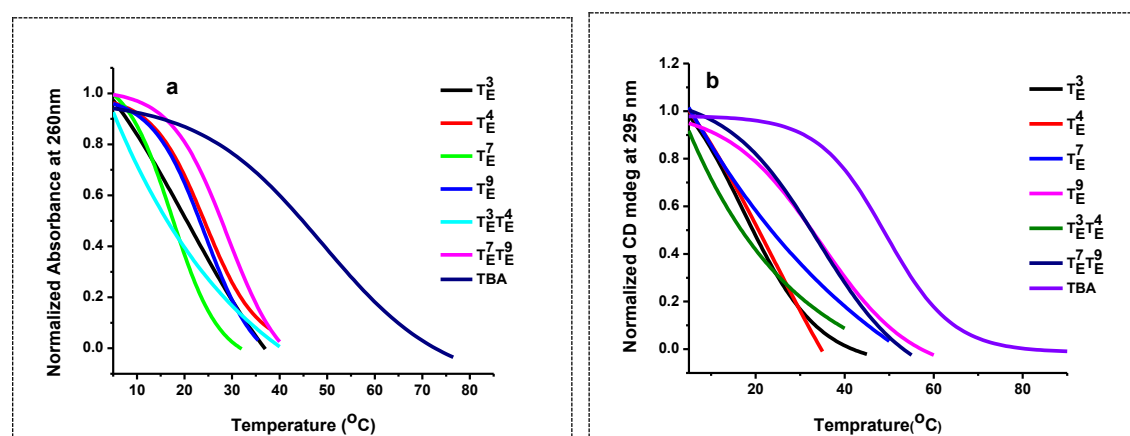


Figure 5. (a) UV  $T_m$  plots; (b) CD  $T_m$  plots of TBA oligomers in potassium phosphate buffer (10 mM, pH 7.2) containing 100 mM KCl.

The melting temperature of the quadruplexes estimated by UV and CD spectroscopy indicated that the **E** unit has a destabilizing effect on the thermal stability of TBA ( $\Delta T_m > -15$  °C; Figure 5(a) and 5(b) and Table 3). The  $T^3_E T^4_E$  oligomer, in particular, was largely destabilized and melted below 20°C. Thus, the shorter **E** unit had a negative effect on the thermal stability of the resulting quadruplexes, in comparison to the one carbon longer C3-spacer,<sup>10</sup> where a stabilizing effect was reported.

**Table 3. CD- and UV-melting data of TBA oligomers.**

No.	Oligomer	CD $T_m$ (°C)	UV $T_m$ (°C)
1	TBA	49	48/49 <sup>a</sup>
2	$T^3_E/(TBA-SP3)^{10}$	17	20/55 <sup>a</sup>
3	$T^4_E$	22	24
4	$T^7_E/(TBA-SP7)^{10}$	15	17/55 <sup>a</sup>
5	$T^9_E$	25	24
6	$T^3_E T^4_E$	nd	nd
7	$T^7_E T^9_E$	33	29
8	$(TBA-SP12)^{10}$	-	55 <sup>a</sup>

The experiments were performed in potassium phosphate buffer (10 mM, pH 7.2) containing 100 mM KCl with a strand concentration of 5  $\mu$ M and a heating rate of 3 °C/min. Each experiment was performed at least thrice and is accurate to  $\pm 1$  °C.<sup>a</sup> sodium cacodylate (10 mM, pH 7.0) containing 100 mM KCl.

#### 4.8 Evaluation of G-quadruplex topology by UV-Thermal Difference Spectra (TDS)

The thermal difference spectra (TDS) can be generated from the UV absorbance scans by subtracting the scan recorded at temperatures higher than- from that at a temperature lower than the melting point ( $T_m$ ) of the quadruplexes. The UV-TDS signature for a G-quadruplex structure<sup>23</sup> consists of a negative band centered at  $\sim 295$  nm, with positive bands at  $\sim 273$  nm and  $\sim 242$  nm.

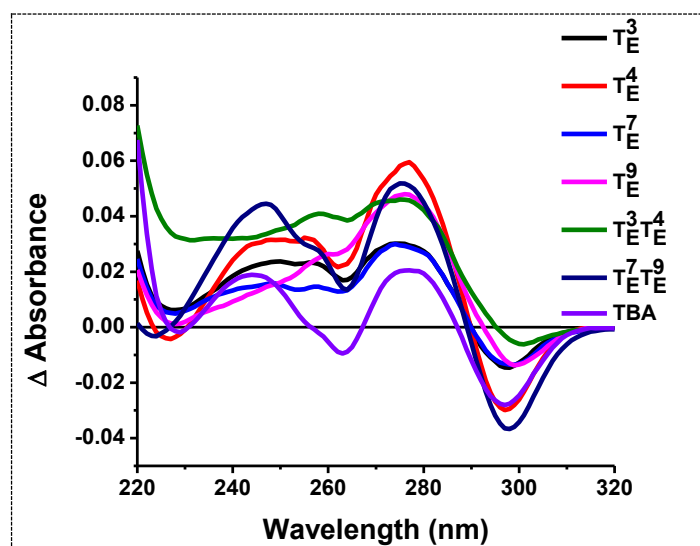


Figure 6. UV-TDS of TBA oligomers.

It was observed for TBA, and was also seen for the E-substituted oligomers (Figure 6), indicating quadruplex formation for all these oligomers. The UV-TDS spectrum of  $T^3E^4E$  showed a low-intensity negative band near 295 nm and poorly defined peaks around 273 nm and 242 nm, in comparison to the other oligomers, probably indicative of a weaker, imperfectly formed quadruplex in this case, in accordance with data from the melting studies.

#### 4.9 Nuclease stability study

##### 4.9.1 Endonuclease stability

The stability of the E-containing oligomers was tested against S1 nuclease from *Aspergillus oryzae*. As the modified units are at internal positions in the oligomer, S1 nuclease, a non-specific endonuclease was chosen for evaluation. The formation of the G-quadruplex structure is itself also reported to shield oligonucleotides from rapid nuclease degradation.<sup>24</sup>

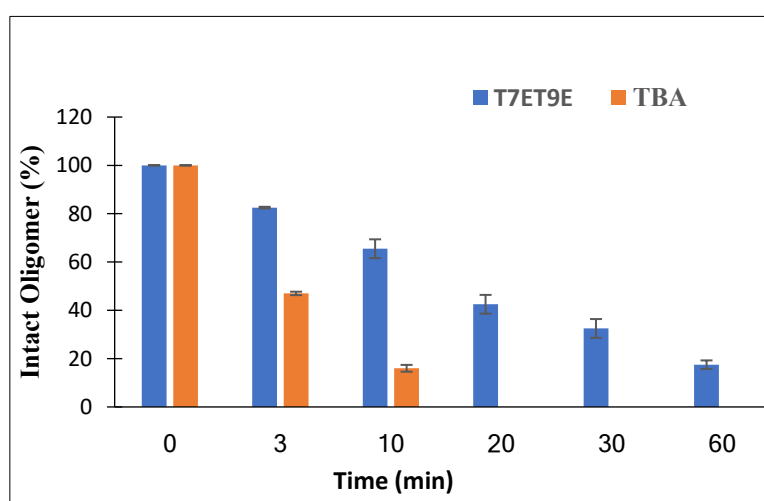


Figure 7. S1 Nuclease stability study of  $T^7E^9E$  in comparison to TBA at 37 °C. S1 nuclease (89 U/mL) was added to the oligomer (7.5  $\mu$ M) in reaction buffer (pH 4.5) containing 0.05 M sodium acetate, 0.28 M NaCl, and 4.5 mM ZnSO<sub>4</sub>.

The stability of  $T^7E^9$  as a representative oligomer against nuclease degradation was studied in comparison to TBA. The stability of the oligomers was monitored by measuring the peak area in the HPLC chromatograms at successive time intervals upon treatment with S1 nuclease. From Figure 7, it is evident that  $T^7E^9$  bearing two E units, with a half-life of nearly 15 min, was much stabler than TBA ( $t_{1/2} < 3$  min).

#### 4.9.2 Serum stability study

The serum stability of selected oligonucleotides ( $T^7E^9$  Vs. TBA) was assessed on exposure to 10% fetal bovine serum (FBS). Aliquots of the oligomer removed at successive time-points were analysed by polyacrylamide gel electrophoresis (PAGE). A portion of the  $T^7E^9$  oligomer was found to be intact even after 6 h, while the control TBA oligomer was digested entirely at this time-point (Figure 8).

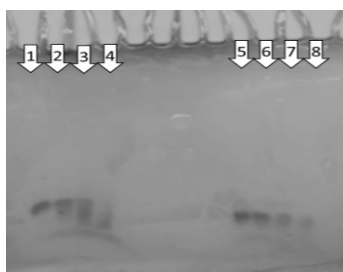
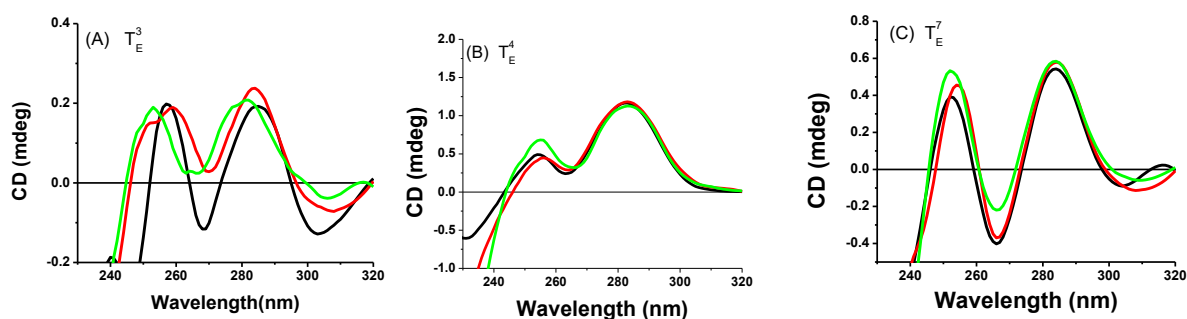
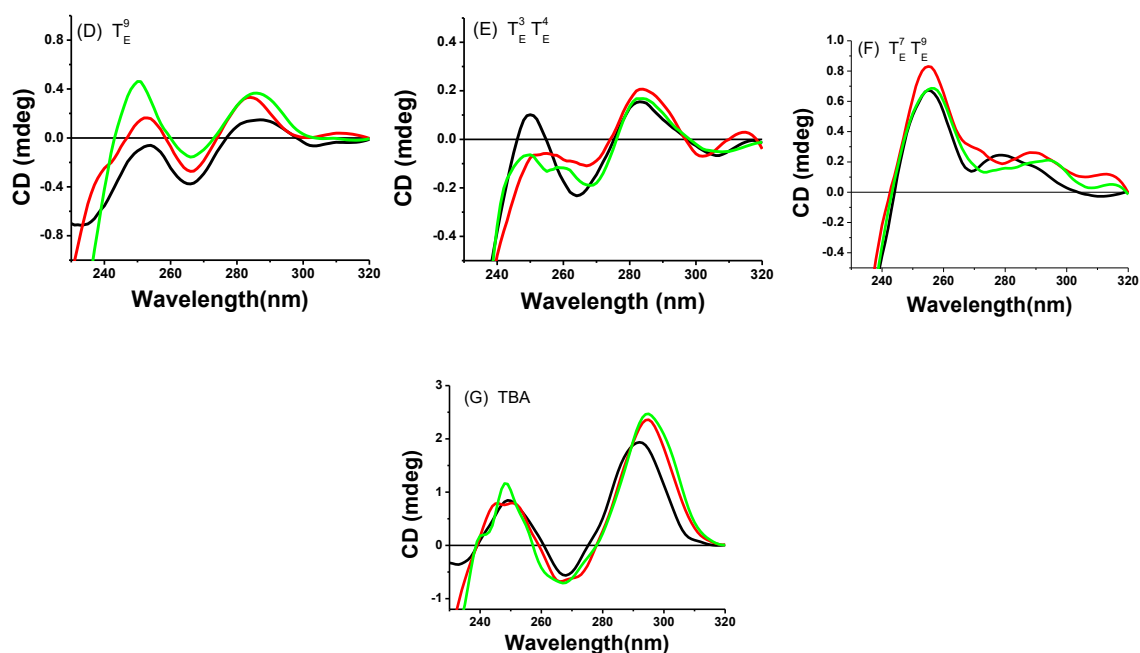


Figure 8. Stability assay upon treatment with fetal bovine serum analyzed by polyacrylamide gel electrophoresis. Lanes 1-4: TBA at 0 h, 1 h, 3 h and 6 h respectively; lanes 5-8:  $T^7E^9$  at 0 h, 1 h, 3 h and 6 h respectively. The gel was visualized by UV-shadowing.

#### 4.10 Thrombin binding and inhibition

The chaperone effect of thrombin,<sup>18</sup> evident from the increasing CD amplitude at 295 nm, confirmed the binding of the oligomers containing single E substitutions (Figure 9). This effect was not observed for  $T^3E^4$  and  $T^7E^9$ , indicating very poor binding to thrombin for these oligomers.





**Figure 9.** CD scans of oligomers (5  $\mu\text{M}$ ) upon incremental addition of thrombin. (A)  $\text{T}^3\text{E}$ , (B)  $\text{T}^4\text{E}$ , (C)  $\text{T}^7\text{E}$ , (D)  $\text{T}^9\text{E}$ , (E)  $\text{T}^3\text{E}\text{T}^4\text{E}$ , (F)  $\text{T}^7\text{E}\text{T}^9\text{E}$  and (G) TBA. Black: 0.2  $\mu\text{M}$  thrombin; red: 0.4  $\mu\text{M}$  thrombin; green: 0.8  $\mu\text{M}$  thrombin.

Thrombin transforms fibrinogen to fibrin, and that leads to coagulation.<sup>25</sup> The effect of thrombin binding on the anti-thrombin activity of the modified oligomers was assessed by carrying out a clotting assay, and the inhibitory effect on thrombin-catalyzed fibrin polymerization (thrombin time/clotting time) was measured at 37 °C. The thrombin reagent was pre-incubated with the oligomer before addition to fibrinogen-containing saline. Since TBA is known to slow down coagulation,<sup>26</sup> a thrombin time assay involving the conversion of fibrinogen to fibrin in the presence of thrombin was performed to evaluate the anticoagulant activity of the oligomers (Figure 10). The four variants containing single **E** spacers, namely  $\text{T}^3\text{E}$ ,  $\text{T}^4\text{E}$ ,  $\text{T}^7\text{E}$ , and  $\text{T}^9\text{E}$ , showed thrombin inhibitory effects (clotting time ranging from 53 s to 65 s), although slightly lower than TBA (76 s), whereas oligomers  $\text{T}^3\text{E}\text{T}^4\text{E}$  and  $\text{T}^7\text{E}\text{T}^9\text{E}$  bearing two **E** units each, with clotting times of 47 s and 40 s respectively, showed even lower anti-thrombin effects and only a slight delay in the coagulation process. The highest anticoagulant effect was observed with  $\text{T}^9\text{E}$ , with a 65 s clotting time, a delay of 31 s in comparison to the control (34 s clotting time) when no oligomer was added.

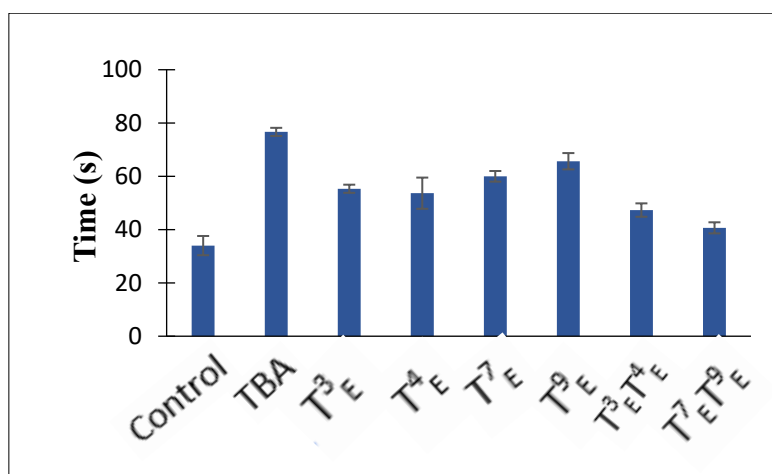


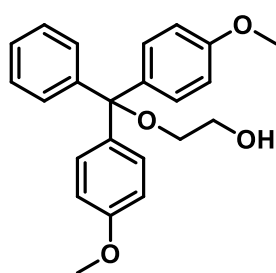
Figure 10. Clotting time measured as the time required for fibrin polymerization upon the addition of thrombin to fibrinogen in the presence of added oligomers. control: clotting time in the absence of any added oligomer.

#### 4.11 Conclusions

In this Chapter, our studies with a 2-carbon **E** spacer have shown that single replacement of loop residues by **E** spacer are tolerated better than two. Although a beneficial effect on the nuclease stability and half-life of the oligomers was observed, the lower thermal stability and anti-clotting effect were observed with the 2-carbon **E** spacer compared to the 3-carbon spacer unit suggests that this shorter backbone is less tolerated in TBA.

#### 4.12 Experimental section

##### 4.12.1 Synthetic procedures and spectral data



**2-(bis(4-methoxyphenyl)(phenyl)methoxy)ethan-1-ol (2):** Ethylene glycol **1** (5.00 g, 80.64 mmol) and dimethoxytrityl chloride (DMTr-Cl) (2.72 g, 08.64 mmol) were dissolved in pyridine (100 mL) containing DMAP (0.098 g, 0.86 mmol) as the catalyst, and the reaction mixture was stirred at room temperature. After 2 h, TLC indicated the consumption of the starting material. Removal of solvents yielded a yellowish sticky solid, which was taken up in  $\text{CH}_2\text{Cl}_2$  and given a saturated  $\text{NaHCO}_3$  wash. The organic layer was dried over sodium sulfate, and the solvent was evaporated in vacuo to get a pale-yellow solid foam, which was purified by chromatography on silica gel (pre-neutralized with  $\text{Et}_3\text{N}$ ). Compound **2** eluted in 20% EtOAc/ petroleum ether. Yield: 1.74 g, 60%.

**Mol. Formula** :  $\text{C}_{23}\text{H}_{24}\text{O}_4$

**Exact Mass (calcd)** : 364.17

**HRMS (obsd)** : 387.15 (M + Na<sup>+</sup>)

**<sup>1</sup>H NMR**

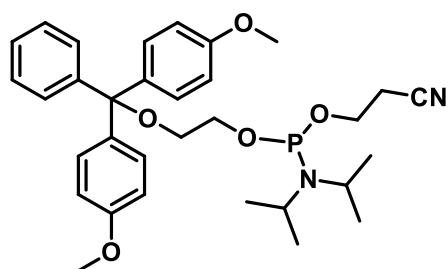
(200MHz, CDCl<sub>3</sub>) : δH (ppm) 3.25 (t, *J* = 4.61 Hz, 2H), 3.73 (b, 2H), 3.78 (s, 6H), 6.81–6.85 (m, 4H), 7.24–7.43 (m, 9H).

**<sup>13</sup>C NMR**

(125MHz, CDCl<sub>3</sub>) : δC (ppm) 158.4, 144.8, 136.0, 129.9, 128.1, 127.7, 126.7, 113.0, 86.0, 64.5, 62.3, 55.1.

**<sup>13</sup>C-DEPT**

(125MHz, CDCl<sub>3</sub>) : δC (ppm) (CH/CH<sub>3</sub>): 55.5, 113.07, 126.07, 127.78, 128.10, 129.99 (CH<sub>2</sub>): 62.33, 64.59.



**2-(bis(4-methoxyphenyl) (phenyl)methoxy) ethyl(2-cyanoethyl) diisopropylphosphoramidite (3).**

Compound **2** (0.125 g, 0.34 mmol) was dissolved in dry dichloromethane (5.0 mL). Diisopropylethylamine (DIPEA) (0.23 mL, 1.37mmol) was added to the ice-cooled solution under an argon atmosphere followed by 2-cyanoethyl *N,N*-diisopropyl chlorophosphine (0.16 mL, 0.68 mmol). After stirring the reaction mixture at room temperature for 1 h, TLC indicated complete consumption of the starting material. CH<sub>2</sub>Cl<sub>2</sub> was added to dilute the reaction, and the organic layer was washed with NaHCO<sub>3</sub> and water and then dried over sodium sulfate. Removal of solvents in vacuo afforded the crude product that was purified by column chromatography on silica gel (pre-neutralized by Et<sub>3</sub>N). The pure compound **3** was eluted by a mixture of 15 % EtOAc/ petroleum ether containing 0.5% Et<sub>3</sub>N. Yield 0.220 g, 64%.

**Mol. Formula** : C<sub>32</sub>H<sub>41</sub>N<sub>2</sub>O<sub>5</sub>P

**<sup>31</sup>P NMR**

(161 MHz, CDCl<sub>3</sub>) : δ(ppm) 148.51 ppm.

#### 4.12.2 Synthesis of Oligonucleotides

Oligonucleotides were synthesized by  $\beta$ -cyanoethyl phosphoramidite chemistry on a Bioautomation Mermade-4 DNA synthesizer. The phosphoramidites were obtained from Innovasynth Technologies India Ltd. For the E modified units, increased coupling time of 150 s was used. Oligonucleotides were cleaved from the solid support by treatment with 25% aq. ammonia. They were purified by RP-HPLC (Waters Delta 600e quaternary solvent delivery system, 2998 photodiode array detector, and Empower2 chromatography software) on a C18 column using an increasing gradient of acetonitrile in 0.1 M triethylammonium acetate (pH 7.0). Their purity was reassessed by analytical HPLC, and they were characterized by MALDI-TOF mass spectrometry. The oligomer concentration was calculated by absorbance measurements using the molar extinction coefficients of the corresponding DNA nucleobases.

#### 4.12.3 CD Experiments

For CD experiments, the TBA oligomers were taken at a strand concentration of 5  $\mu$ M. Potassium phosphate buffer (10 mM, pH 7.2) was used, which contained 100 mM KCl. Oligomers were annealed by heating at 90  $^{\circ}$ C for 2 min, slowly cooled to room temperature, and refrigerated at  $\sim$ 4 $^{\circ}$ C for 3 h before the start of the experiments. CD spectra were recorded in a 2 mm path length cuvette using a resolution of 1 nm, bandwidth of 1 nm, the sensitivity of 20 mdeg, response of 1 s, and a scan speed of 100 nm/min. Three scans were accumulated for each sample. CD melting was performed by monitoring the CD intensity at 295 nm over a temperature range of 5–90  $^{\circ}$ C. To study the chaperone effect of thrombin, bovine thrombin (Tulip Diagnostics) was added to the oligomers (5 $\mu$ M) at 5  $^{\circ}$ C in 0.2  $\mu$ M increments, and the CD scans were recorded.

#### 4.12.4 Raman measurements

Raman spectroscopy measurements were recorded at laboratory temperature on an HR 800 Raman spectrophotometer (Jobin Yvon, HORIBA, France) equipped with an achromatic Czerny–Turner type monochromator (800 mm focal-length) with silver-treated mirrors. Monochromatic radiation emitted by a He–Ne laser (633 nm), operating at 20 mW, was used, with an accuracy of  $\pm$ 1  $\text{cm}^{-1}$ , equipped with a thermoelectrically cooled (with Peltier junctions), multi-channel, spectroscopic grade CCD detector (1024  $\times$  256 pixels of 26 microns) with the dark current lower than 0.002 electrons  $\text{pixel}^{-1} \text{ s}^{-1}$ . An objective of 50 $\times$  LD (Long distance) magnification was used to collect the signal from the samples. Silicon reference was used for the calibration. To enhance the intensity of spectra, surface enhanced Raman spectroscopy (SERS) was used for all the samples. To achieve the SERS effect, two drops of each specimen



(100  $\mu\text{M}$  strand concentration in water containing 100 mM KCl; 2  $\mu\text{l}$  each, one drop after the other) were dropped on aluminum foil and air-dried at laboratory temperature for 20-30 min. The Raman signal was obtained with exposure time and acquisition time of 5 s and 10 s, respectively in the region from 200 to 3000  $\text{cm}^{-1}$  with a resolution of  $\pm 1 \text{ cm}^{-1}$ .

#### 4.12.5 UV Experiments

UV-absorbance scans of TBA and E-substituted TBA oligomers were recorded using 10 mm pathlength quartz cells on an Analytik Jena SPECORD® 200 plus spectrometer equipped with a peltier-equipped temperature controller and at a scanning speed of 5  $\text{nm sec}^{-1}$ . The oligomers were taken at a strand concentration of 5  $\mu\text{M}$ . Potassium phosphate buffer (10 mM, pH 7.2) was used, which contained 100 mM KCl. Before starting the experiments, oligomers were annealed by heating at 90  $^{\circ}\text{C}$  for 2 min, slowly cooled to room temperature, and refrigerated at  $\sim 4^{\circ}\text{C}$  for 3 h. Thermal difference spectra (TDS) were obtained by subtracting the UV-absorbance spectral scan of the sample at temperatures below, from that above the melting temperature ( $T_m$ ).

#### 4.12.6 Nuclease stability study

The S1 nuclease stability was monitored by RP-HPLC. TBA and  $\text{T}^7\text{E}^9\text{T}^9\text{E}$  (7.5  $\mu\text{M}$  each) were exposed to S1 nuclease (89 U/mL) at 37  $^{\circ}\text{C}$  in reaction buffer (pH 4.5) containing 0.05 M sodium acetate, 0.28 M NaCl, and 4.5 mM  $\text{ZnSO}_4$ . Aliquots were removed at successive time intervals, heated at 90  $^{\circ}\text{C}$  for 3 min to stop the activity of the nuclease, and analyzed by RP-HPLC to measure the percentage of oligonucleotides remaining intact. A graph of percent intact oligomer Vs. time was plotted to get an idea of the stability of the oligomer to nuclease action.

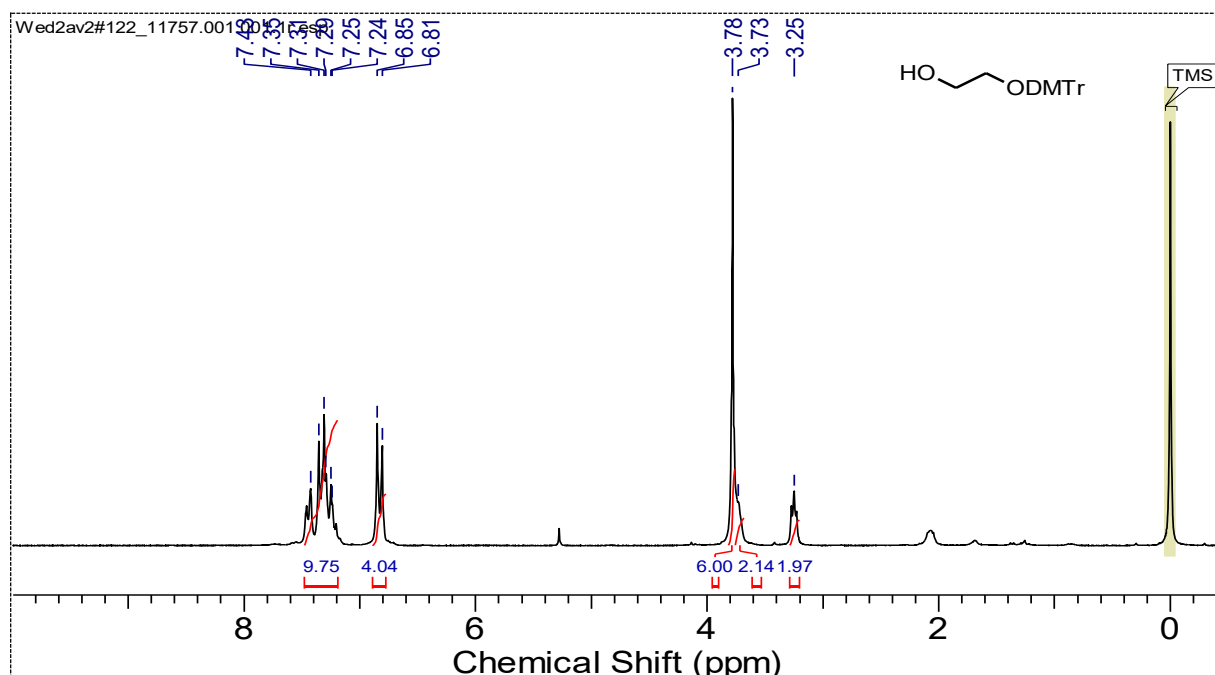
Fetal bovine serum stability study was conducted in 10% fetal bovine serum (FBS) diluted with Dulbecco's Modified Eagle's Medium (DMEM) at 37  $^{\circ}\text{C}$ . TBA or  $\text{T}^7\text{E}^9\text{T}^9\text{E}$  (320  $\mu\text{M}$ , 20  $\mu\text{l}$ ) was evaporated to dryness under reduced pressure and then re-suspended in 10% FBS (500  $\mu\text{l}$ ), followed by incubation at 37  $^{\circ}\text{C}$ . After 0, 1, 3, and 6 h, 125  $\mu\text{l}$  aliquots of samples were collected and stored at  $-20^{\circ}\text{C}$  for at least 30 min. The samples were evaporated to dryness, and then 5  $\mu\text{l}$  of gel loading buffer and 5  $\mu\text{l}$  of autoclaved water were added. 5  $\mu\text{l}$  of the mixture was used for polyacrylamide gel electrophoresis (PAGE), which was carried out at room temperature using 20% polyacrylamide gel in  $1 \times$  TBE buffer (Tris-borate-EDTA). The degradation patterns on the gel were visualized by UV shadowing.

#### 4.12.7 Thrombin time assay.

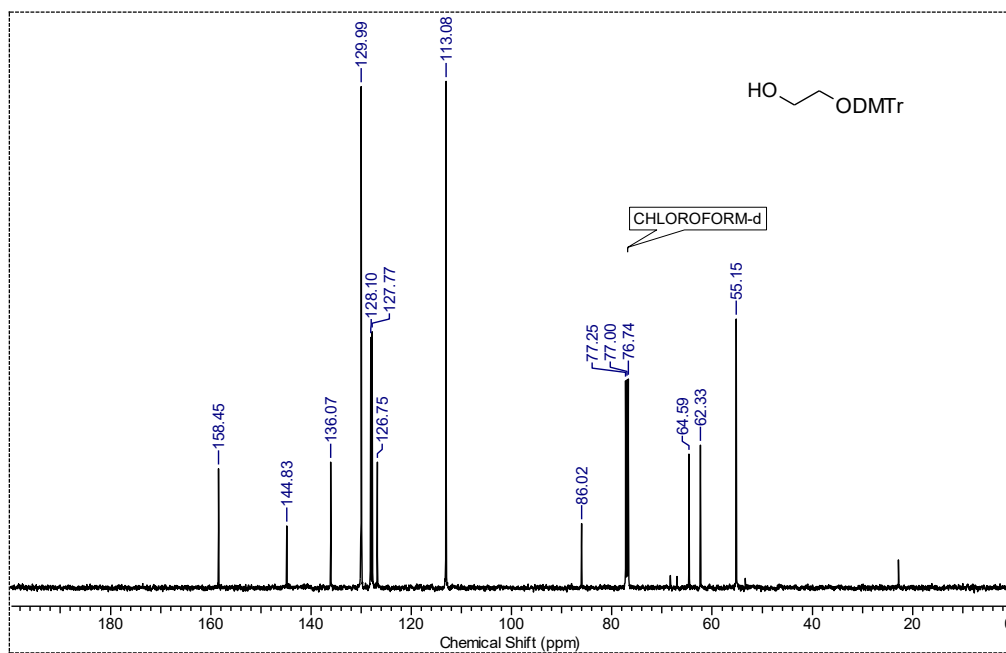
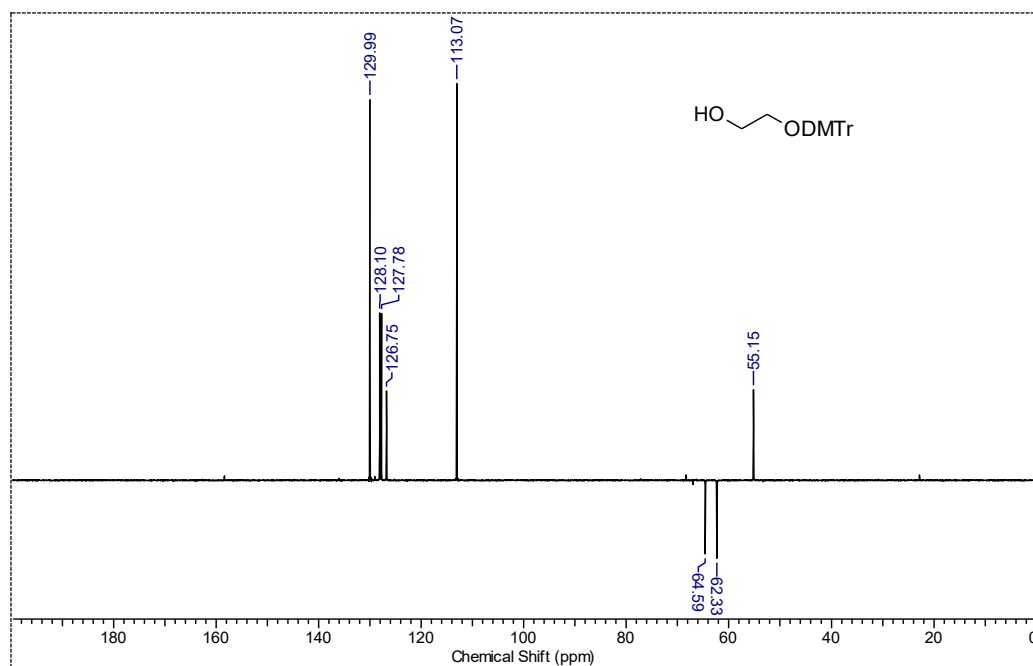
The inhibitory activity of the TBA oligomers on the thrombin-catalyzed conversion of fibrinogen to fibrin was assessed by a thrombin time assay. The time for clot formation at 37°C was measured on a START Max coagulation analyzer (Stago). Each experiment was repeated at least three times; the standard deviation ranged between  $\pm 1$  s to  $\pm 5$  s. Bovine thrombin (Tulip Diagnostics, 0.1 NIH unit) was pre-incubated with the TBA oligomer taken at a 0.25  $\mu\text{M}$  concentration for 2 min before adding fibrinogen from human plasma (3.5  $\mu\text{M}$ , Aldrich) and measurement of clotting time.

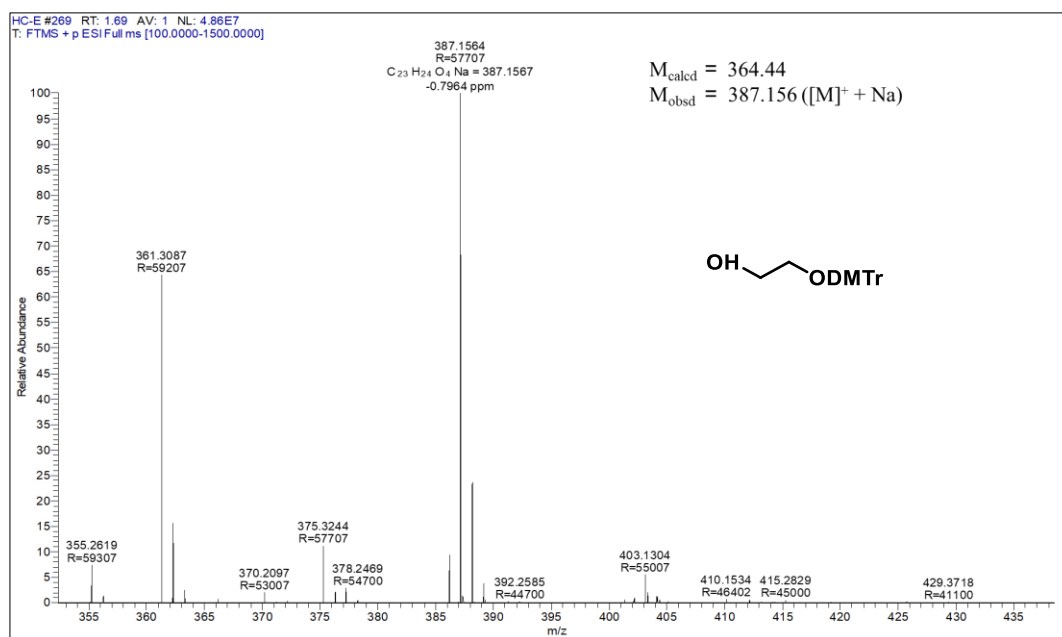
#### 4.13 Appendix C

Descriptions	Page Number
Compound 2: $^1\text{H}$ , $^{13}\text{C}$ , DEPT NMR and HRMS	92-94
Compound 3: $^{31}\text{P}$ NMR	94
HPLC chromatogram of modified TBA oligomers	95-96
MALDI-TOF spectra of modified TBA oligomers	96-98

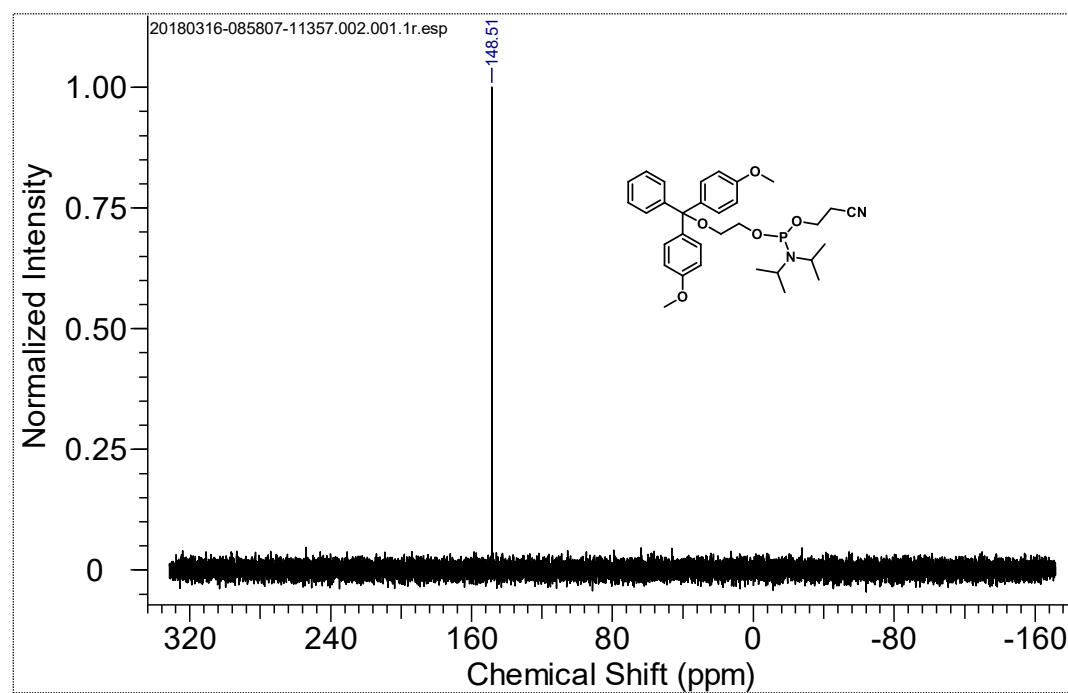


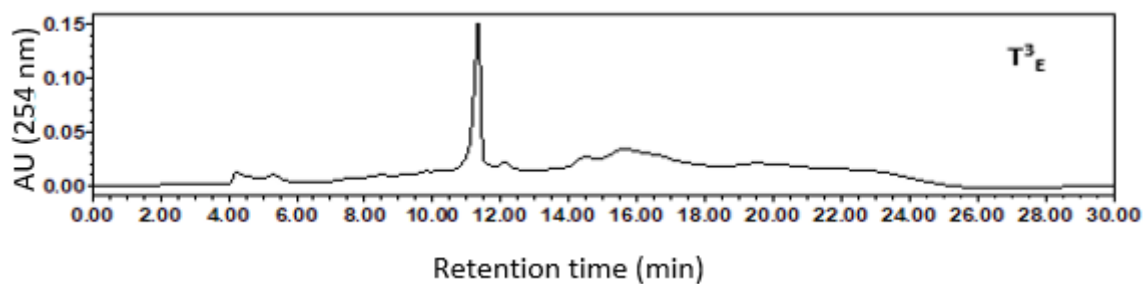
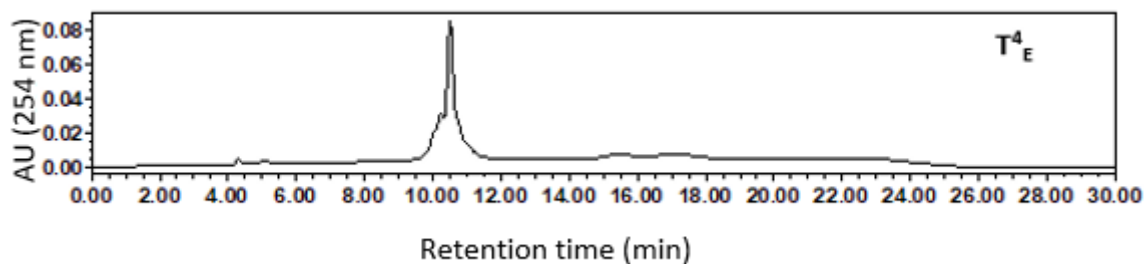
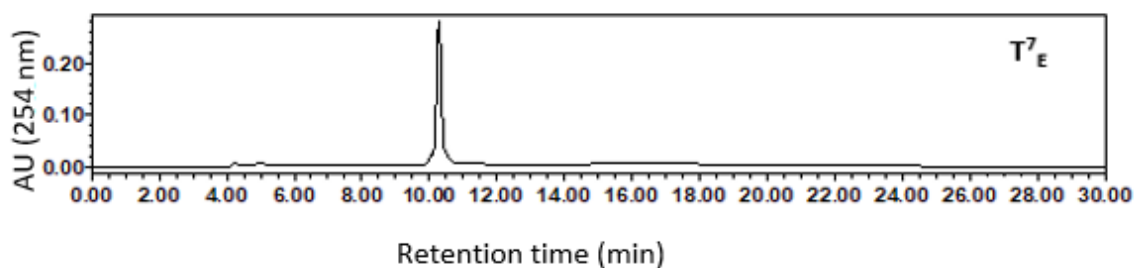
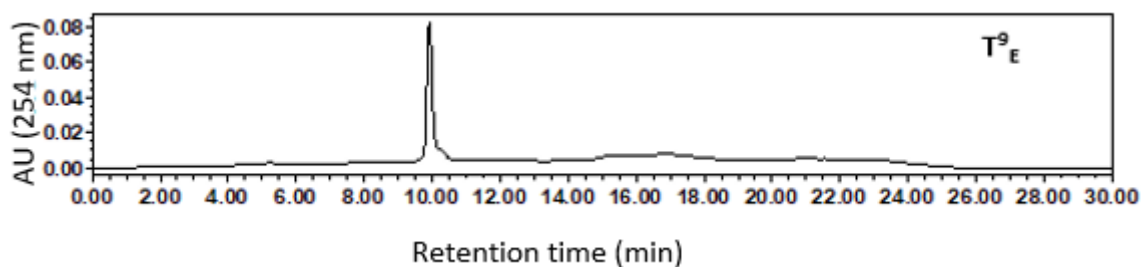
$^1\text{H}$  NMR compound no.2

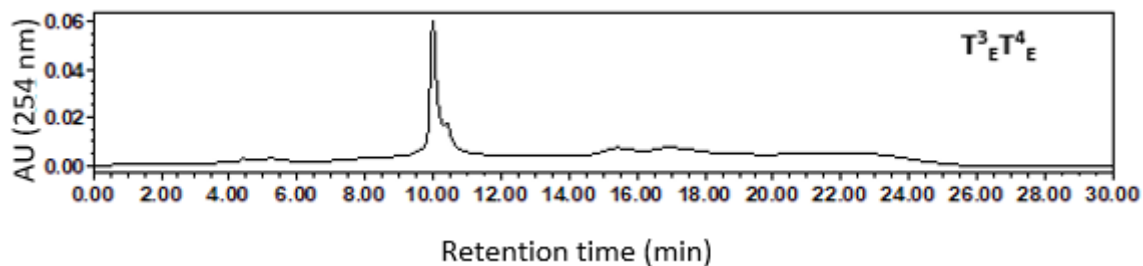
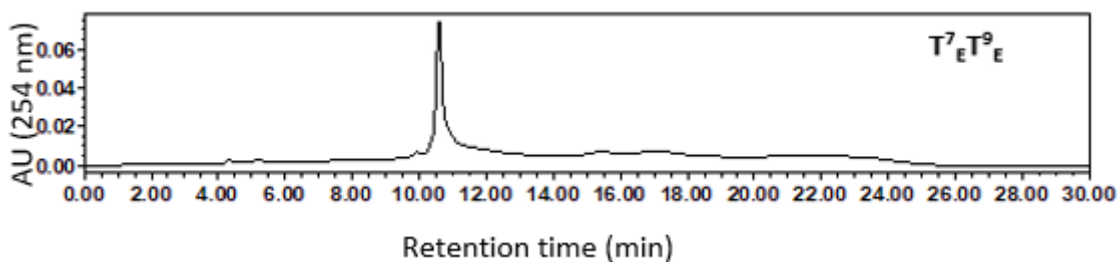
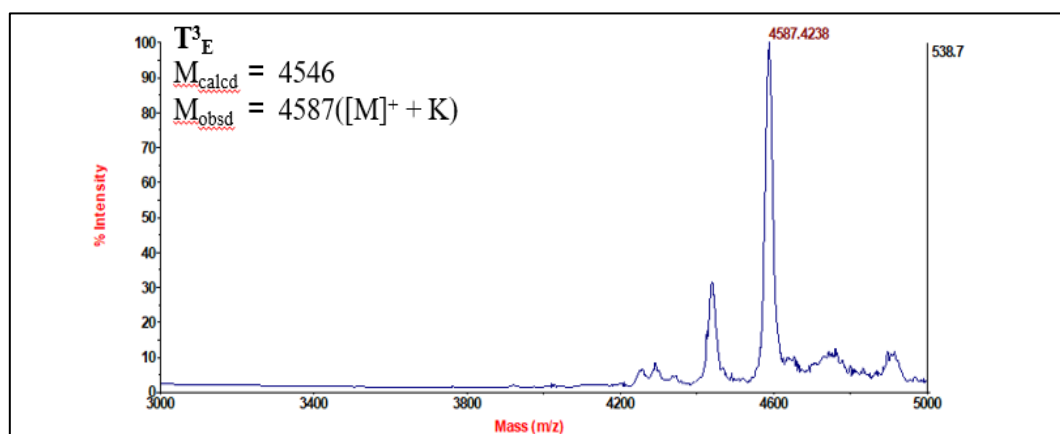
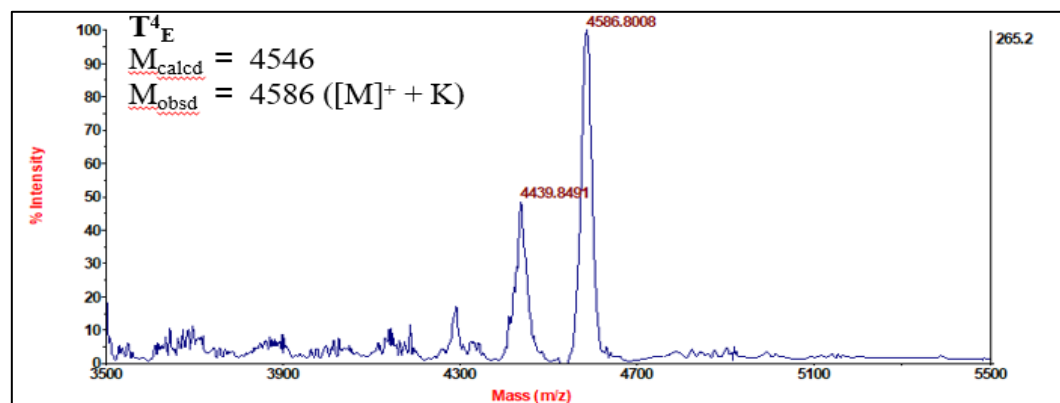
**<sup>13</sup>C NMR compound no.2****<sup>13</sup>C DEPT Compound no.2**

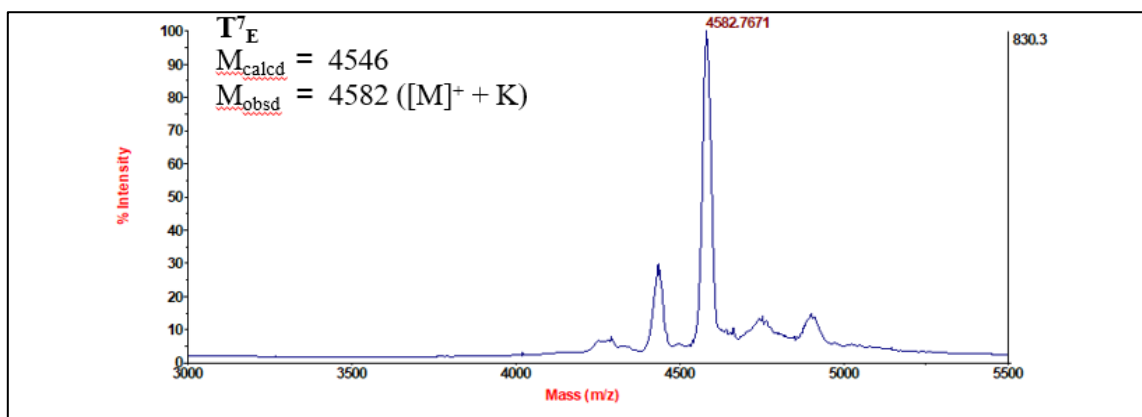
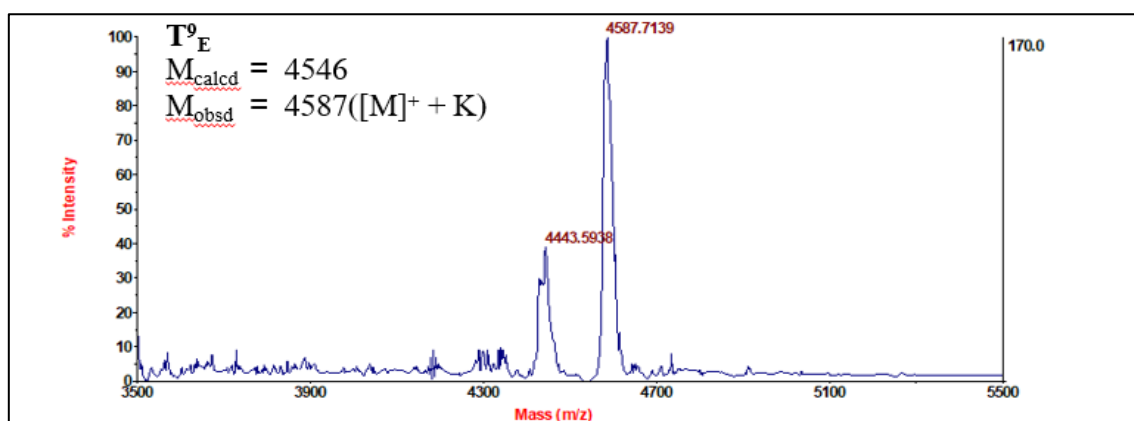
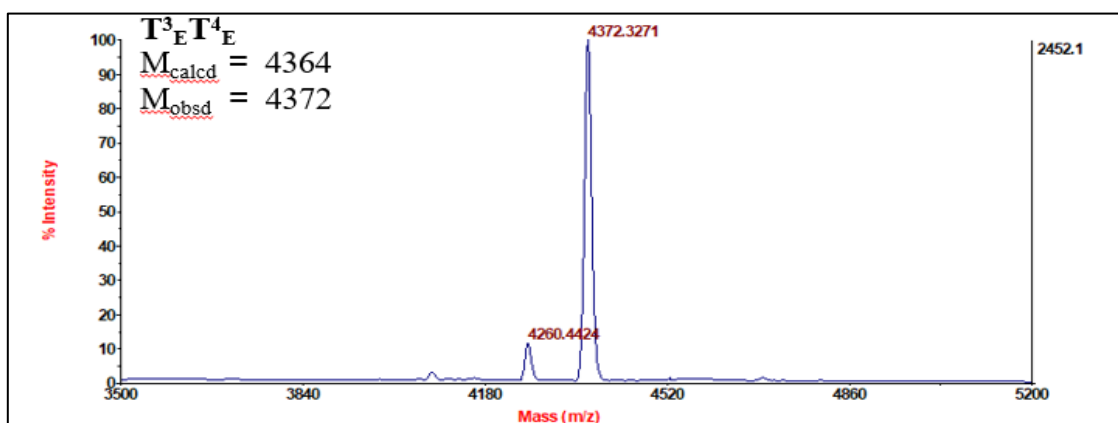


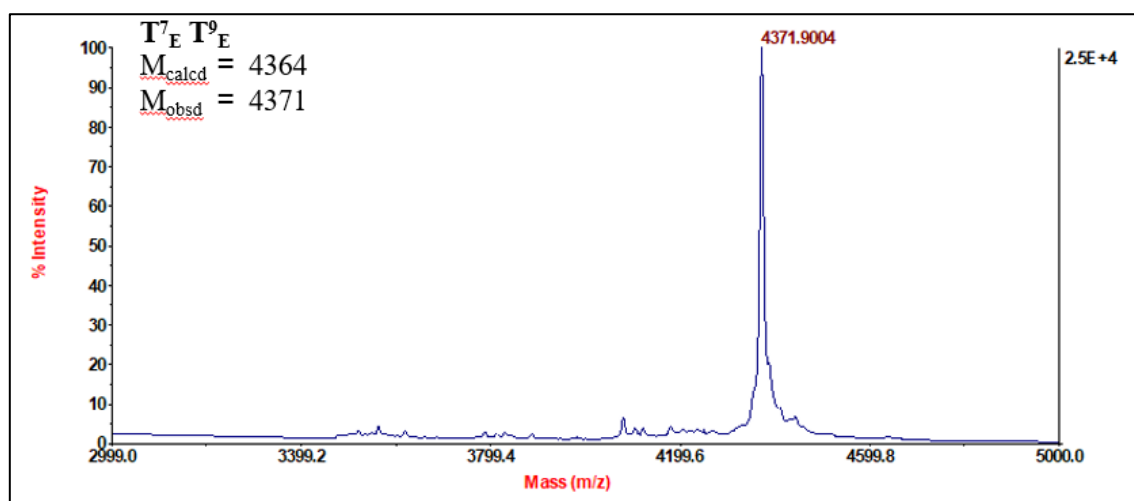
HRMS Compound no.2

 $^{31}\text{P}$  NMR Compound no.3

**HPLC chromatogram of  $T^3_E$** **HPLC chromatogram of  $T^4_E$** **HPLC chromatogram of  $T^7_E$** **HPLC chromatogram of  $T^9_E$**

HPLC chromatogram of  $T^3_E T^4_E$ HPLC chromatogram of  $T^7_E T^9_E$ MALDI-TOF spectra of  $T^3_E$ MALDI-TOF spectra of  $T^4_E$

MALDI-TOF spectra of  $T^7_E$ MALDI-TOF spectra of  $T^9_E$ MALDI-TOF spectra of  $T^3_E T^4_E$

MALDI-TOF spectra of  $T^7 E T^9 E$ 

#### 4.14 References

- (1) Burge, S.; Parkinson, G. N.; Hazel, P.; Todd, A. K.; Neidle, S. Quadruplex DNA: Sequence, Topology and Structure. *Nucleic Acids Res.* **2006**, *34* (19), 5402–5415.
- (2) Bock, L. C.; Griffin, L. C.; Lantham, J. A.; & E. H. V.; Toole, J. J. Selection of Single-Stranded DNA Molecules That Bind and Inhibit Human Thrombin. *Nature* **1992**, *355*, 564–566.
- (3) Kelly, J. A.; Feigon, J.; Yeates, T. O. Reconciliation of the X-Ray and NMR Structures of the Thrombin-Binding Aptamer d(GGTTGGTGTGGTTGG). *J. Mol. Biol.* **1996**, *256* (3), 417–422.
- (4) Macaya, R. F.; Schultze, P.; Smith, F. W.; Roe, J. A.; Feigon, J. Thrombin-Binding DNA Aptamer Forms a Unimolecular Quadruplex Structure in Solution. *Proc. Natl. Acad. Sci. U. S. A.* **1993**, *90* (8), 3745–3749.
- (5) Lancellotti, S.; De Cristofaro, R. Nucleotide-Derived Thrombin Inhibitors: A New Tool for an Old Issue. *Cardiovasc. Hematol. Agents Med. Chem.* **2009**, *7* (1), 19–28.
- (6) Avino, A.; Fabrega, C.; Tintore, M.; Eritja, R. Thrombin Binding Aptamer, More than a Simple Aptamer: Chemically Modified Derivatives and Biomedical Applications. *Curr. Pharm. Des.* **2012**, *18* (14), 2036–2047.
- (7) Scuotto, M.; Riviuccio, E.; Varone, A.; Corda, D.; Bucci, M.; Vellecco, V.; Cirino, G.; Virgilio, A.; Esposito, V.; Galeone, A.; Borbone, N.; Varra, M.; Mayol, L. Site Specific Replacements of a Single Loop Nucleoside with a Dibenzyl Linker May Switch the



- Activity of TBA from Anticoagulant to Antiproliferative. *Nucleic Acids Res.* **2015**, *43* (16), 7702–7716.
- (8) Gouda, A. S.; Amine, M. S.; Pedersen, E. B. Synthesis of New DNA G-Quadruplex Constructs with Anthraquinone Insertions and Their Anticoagulant Activity. *Helv. Chim. Acta* **2016**, *99* (2), 116–124.
- (9) Bose, T.; Kumar, V. A. Critical Role of Select Peptides in the Loop Region of G-Rich PNA in the Preferred G-Quadruplex Topology and Stability. *Tetrahedron* **2017**, *73* (12), 1534–1540.
- (10) Aaldering, L. J.; Poongavanam, V.; Langkjær, N.; Murugan, N. A.; Jørgensen, P. T.; Wengel, J.; Veedu, R. N. Development of an Efficient G-Quadruplex-Stabilised Thrombin-Binding Aptamer Containing a Three-Carbon Spacer Molecule. *ChemBioChem* **2017**, *18* (8), 755–763.
- (11) Ali, A.; Bullen, G. A.; Cross, B.; Dafforn, T. R.; Little, H. A.; Manchester, J.; Peacock, A. F. A.; Tucker, J. H. R. Light-Controlled Thrombin Catalysis and Clot Formation Using a Photoswitchable G-Quadruplex DNA Aptamer. *Chem. Commun.* **2019**, *55* (39), 5627–5630.
- (12) Mo, M.; Kong, D.; Ji, H.; Lin, D.; Tang, X.; Yang, Z.; He, Y.; Wu, L. Reversible Photocontrol of Thrombin Activity by Replacing Loops of Thrombin Binding Aptamer Using Azobenzene Derivatives. *Bioconjug. Chem.* **2019**, *30* (1), 231–241.
- (13) Gerard, R.; Cook, A. F.; Rudolph, M. J.; Fathi, R. United States Patent. 6,008,398, 1999.
- (14) Ohkubo, A.; Kondo, Y.; Suzuki, M.; Kobayashi, H.; Kanamori, T.; Masaki, Y.; Seio, K.; Nagai, K.; Sekine, M. Chemical Synthesis of U1 SnRNA Derivatives. *Org. Lett.* **2013**, *15* (17), 4386–4389.
- (15) Padmanabhan, K.; Padmanabhan, K. P.; Ferrara, J. D.; Sadler, J. E.; Tulinsky, A. The Structure of  $\alpha$ -Thrombin Inhibited by a 15-Mer Single-Stranded DNA Aptamer. *J. Biol. Chem.* **1993**, *268* (24), 17651–17654.
- (16) Krauss, I. R.; Merlino, A.; Randazzo, A.; Novellino, E.; Mazzarella, L.; Sica, F.; Ii, F.; Cintia, V.; Napoli, I.; Istituto, I.; Chimiche, S.; Bioimmagini, B.; Mezzocannone, V.; Napoli, I.; Chimica, D. High-Resolution Structures of Two Complexes between Thrombin and Thrombin-Binding Aptamer Shed Light on the Role of Cations in the Aptamer Inhibitory Activity. *Nucleic Acids Res.* **2012**, *40* (16), 8119–8128.

- (17) Gait, M. J. *Oligonucleotide Synthesis : A Practical Approach*; Rev. repr. ed.; Oxford : IRL press, **1984**.
- (18) Tang, C.; Shafer, R. H. Engineering the Quadruplex Fold : Nucleoside Conformation Determines Both Folding Topology and Molecularity in Guanine Quadruplexes. *J. Am. Chem. Soc.* **2006**, *128*, 5966–5973.
- (19) Miura, T.; Thomas, G. J. Structural Polymorphism of Telomere DNA: Interquadruplex and Duplex-Quadruplex Conversions Probed by Raman Spectroscopy. *Biochemistry* **1994**, *33* (25), 7848–7856.
- (20) Krafft, C.; Benevides, J. M.; Thomas, G. J. Secondary Structure Polymorphism in *Oxytricha Nova* Telomeric DNA. *Nucleic Acids Res.* **2002**, *30* (18), 3981–3991.
- (21) Palacký, J.; Mojzeš, P.; Kejnovská, I.; Michaela Vorlíčková. Does Raman Spectroscopy Recognize Different G-quadruplex. *J. Raman Spectrosc.* **2020**, *51*, 301–312.
- (22) Pagba, C. V.; Lane, S. M.; Wachsmann-Hogiu, S. Raman and Surface-Enhanced Raman Spectroscopic Studies of the 15-Mer DNA Thrombin-Binding Aptamer. *J. Raman Spectrosc.* **2010**, *41* (3), 241–247.
- (23) Mergny, J. L.; Li, J.; Lacroix, L.; Amrane, S.; Chaires, J. B. Thermal Difference Spectra: A Specific Signature for Nucleic Acid Structures. *Nucleic Acids Res.* **2005**, *33* (16), 1–6.
- (24) Cao, Z.; Huang, C. C.; Tan, W. Nuclease Resistance of Telomere-like Oligonucleotides Monitored in Live Cells by Fluorescence Anisotropy Imaging. *Anal. Chem.* **2006**, *78* (5), 1478–1484.
- (25) Mann, K. G.; Jenny, R. J.; Krishnaswamy, S. Cofactor Proteins in the Assembly and Expression of Blood Clotting Enzyme Complexes. *Annu. Rev. Biochem.* **1988**, *57*, 915–956.
- (26) Jensen, T. B.; Henriksen, J. R.; Rasmussen, B. E.; Rasmussen, L. M.; Andresen, T. L.; Wengel, J.; Pasternak, A. Thermodynamic and Biological Evaluation of a Thrombin Binding Aptamer Modified with Several Unlocked Nucleic Acid (UNA) Monomers and a 2'-C-Piperazino-UNA Monomer. *Bioorg. Med. Chem.* **2011**, *19* (16), 4739–4745.

# **Chapter 5**

**Synthesis of 2'-thiopropyl  
thymidine nucleoside,  
conformation studies, and  
incorporation into the Thrombin  
binding aptamer (TBA)**

## 5.1 Introduction

Chemically modified nucleic acids have been studied extensively in the development of therapeutics,<sup>1</sup> and increase in DNA affinity as a result of modification can be expected to play an essential role in improving the efficacy of putative oligonucleotide therapeutics. Sugar modifications are particularly attractive because they dramatically improve the physical and chemical properties of oligonucleotides. Substitutions at the 2'-position of the sugar in nucleosides have been explored in literature for various applications, including increasing the nuclease resistance properties of the derived oligonucleotides. There are reports of 2'-OMe<sup>2,3</sup> and 2'-F<sup>4,5</sup> 2'-N modifications,<sup>6,7</sup> while reports of 2'-S-derivatives are very rare. Among the 2'-S-derivatives, 2'-SCH<sub>3</sub>, 2'-SCH<sub>2</sub>CH<sub>3</sub>, and 2'-SCH<sub>2</sub>CH<sub>2</sub>CH<sub>3</sub><sup>8</sup> (Figure 1a) are known at the nucleoside level. Sugars containing the highly electronegative fluoro- substituent at 2'-position is known to favor the N-type pucker, suggesting that 2'-fluoro-nucleosides are good mimics for RNA. In contrast, 2'-S substituents prefer a high 2'-*endo* (80% S-type) conformation,<sup>9</sup> more than that found in 2'-deoxynucleosides (65% S-type), suggesting that it is more suited for DNA than RNA. However, the reported literature was confined to nucleosides, and oligonucleotides were not reported. 2'-SCF<sub>3</sub> modification destabilized RNA duplexes,<sup>10</sup> probably as a result of the S-type sugar pucker. However, when the 2'-SCF<sub>3</sub>-modified nucleoside was incorporated in the loop region of an RNA hairpin, it increased thermal stability compared to the unmodified RNA hairpin.<sup>10</sup>

Replacement of G2 position of TBA with 6-thioguanine (Figure 1b) resulted in complete inhibition of the G-quadruplex formation due to the decreased electronegativity of sulfur vs. oxygen, leading to weaker interactions with cations and water molecules.<sup>11</sup> Replacement of thymine by 4-thiodeoxy-uridine (Figure 1c) in the thrombin binding aptamer at loop positions resulted in more potent inhibition of thrombin-induced fibrin clotting, and platelet activation; the T<sub>3</sub>, T<sub>7</sub>, T<sub>9</sub>, and T<sub>13</sub> replacements provided a modified aptamer 2-fold more efficient in inhibiting thrombin than native TBA.<sup>12</sup> Phosphorothioate (Figure 1e) modified TBA with modifications in the G-tetrad backbone or that of the loop residues and a sequence completely modified with thiophosphoryl bonds was reported.<sup>13</sup> Increased *T<sub>m</sub>* values were observed for a single substitution in the loops, whereas the insertion of phosphorothioate linkages in the G-tetrad forming regions led to decreased G-quadruplex stability. In all the modified sequences, the anticoagulant activity was lower than that of unmodified TBA, but there was about 3-fold increased resistance to nuclease degradation in serum than the unmodified aptamer.<sup>13</sup> Introduction of alkylated phosphothioester (Figure 1f) bonds in the TBA sequence,<sup>14</sup> led to less stable G-quadruplex structures than the parent aptamer .

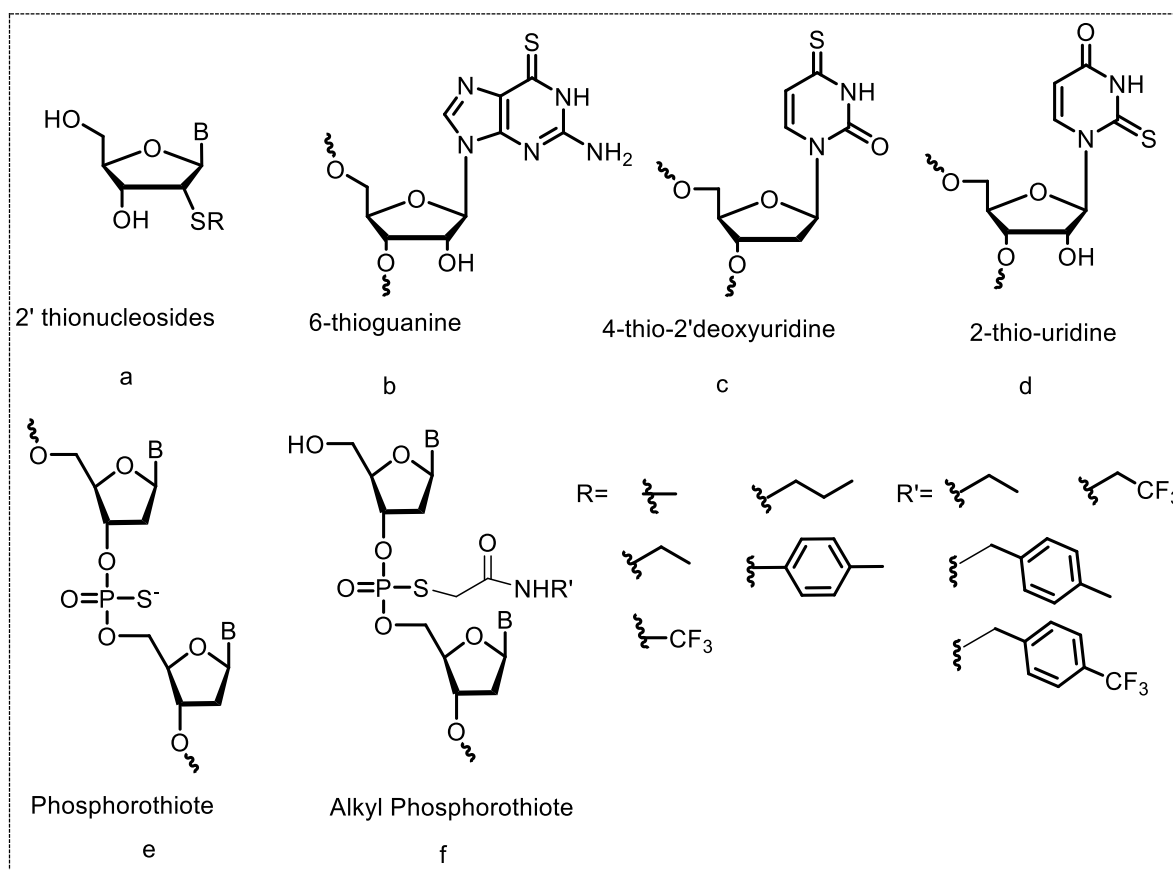


Figure 1. Thio modifications in nucleosides or TBA.

## 5.2 Rationale, design, and objectives of the present work

The main challenges to applying therapeutic oligonucleotides *in vivo* are extending the practical molecular lifetime by minimizing extra- and intracellular nuclease degradation. Phosphorothioates are among the most successful backbone alternatives to reduce the susceptibility to various extra- and intracellular nucleases. However, undesirable side-effects, mainly involving non-specific binding to proteins such as albumin, can lead to associated toxic effects that limit their application.<sup>15</sup> Substitutions at the 2'-position of the sugar in nucleosides have been explored in literature for various applications, including increasing the thermal stability, binding to ligands / protein, nuclease resistance properties of the derived oligonucleotides.<sup>16</sup> The 2'-SCF<sub>3</sub> modification destabilized RNA duplexes, probably as a result of the S-type sugar pucker. However, when the 2'-SCF<sub>3</sub>-modified nucleoside was incorporated in the loop region of an RNA hairpin, it increased thermal stability compared to the unmodified RNA hairpin.<sup>10</sup> 2'-modifications, are known to be resistant to nuclease cleavage.<sup>16</sup> Of the reported 2'-thio substituents, only 2'-SCF<sub>3</sub> has been reported at the oligonucleotide level, and none of these modifications are reported in G-quadruplexes.

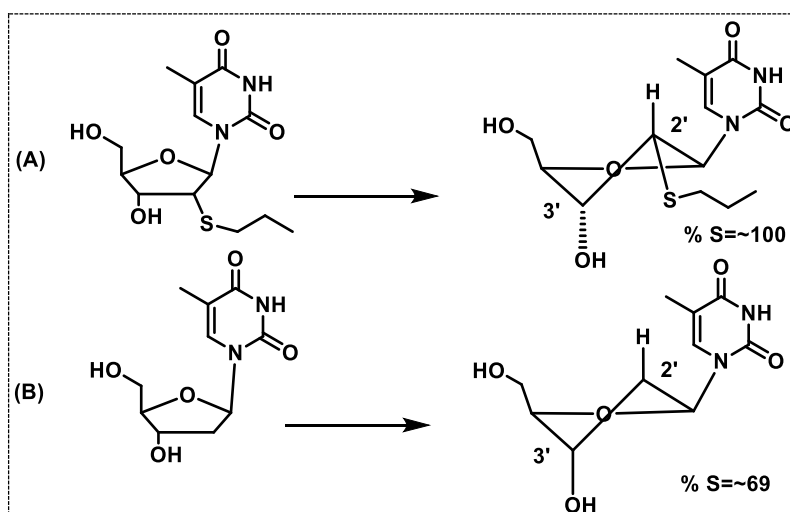


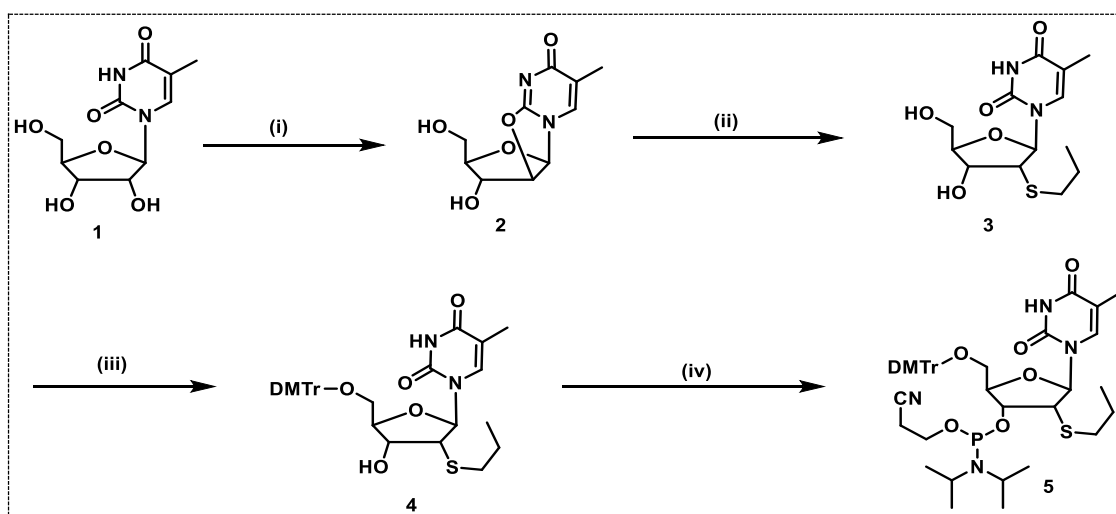
Figure 2. Sugar conformation in (A) 2'-thiopropyl-modified thymidine and (B) thymidine.

Reagents  $\text{SCH}_3$  are in gases state, and  $\text{SCH}_2\text{CH}_3$  volatile in nature, therefore, we chose to synthesize the selected 2'-thiopropyl derivative of thymidine, and study the effect of their incorporation into oligonucleotides at the structural and functional levels. It would increase % S pucker conformation as compare to thymidine, from this result will be utilized for conversion to its phosphoramidite derivative for further use in solid-phase oligonucleotide synthesis.

### 5.3 Synthesis of 2'-thiopropyl-thymidine phosphoramidite

2, 2'-anhydroribothymidine **2** was prepared from the commercially available ribothymidine **1**, by heating with diphenyl carbonate in dry DMF at 150 °C using catalytic amount of  $\text{NaHCO}_3$ . Compound **3** was prepared from 2, 2'-anhydro ring opened of compound **2** by employing 4 equivalents of thiopropyl and  $\text{N}^1, \text{N}^1, \text{N}^3, \text{N}^3$ -tetramethylguanidine in dry DMF at 75 °C. Protection of the primary hydroxyl group in compound **3** was achieved using DMTr-Cl and a catalytic amount of 4-dimethylaminopyridine (DMAP) in dry pyridine to obtain compound **4**. The 2'-thiopropyl derivative **4** was converted to its phosphoramidite derivative by treatment with 2-cyanoethyl-N,N-diisopropylchlorophosphine and N,N-diisopropylethylamine in dry DCM.<sup>8</sup> (Scheme 1).

## Scheme 1: Synthesis of 2'-thiopropylthymidine phosphoramidite



**Reagents and conditions:** (i)  $\text{Ph}_2\text{CO}_3$  (1.3 equiv.),  $\text{NaHCO}_3$  (0.1 equiv.) dry DMF, 150 °C, 0.5 h, 90-92% (ii)  $\text{CH}_3\text{CH}_2\text{CH}_2\text{SH}$  (4 equiv.)  $\text{N}^1, \text{N}^1, \text{N}^3, \text{N}^3$ -tetramethylguanidine (4 equiv.), dry DMF, 75 °C, 5 h, 63-68% (iii) DMTr-Cl (1.2 equiv.), DMAP (0.1 equiv.) dry pyridine, r.t., 2 h, 80% (iv) 2-cyanoethyl- $\text{N}$ , $\text{N}$ -diisopropylchlorophosphine (2 equiv.),  $\text{EtN}(\text{iPr})_2$  (4 equiv.), dry  $\text{CH}_2\text{Cl}_2$ , r.t., 4 h, 70-72%.

5.4 Study of sugar pucker using  $^1\text{H}$  NMR  $J_{1'2'}$  coupling constant

The S- and N-type conformations of natural and modified sugar moieties of nucleosides exist in equilibrium in solution. A coupling constant value between 6-9 Hz represents the S-type sugar pucker, whereas a lower  $J$  value between 0-3 Hz is characteristic of the N-type sugar pucker. The conformation of a nucleoside can be determined from the coupling constants of the sugar ring protons in the  $^1\text{H}$  NMR spectrum. The sugar conformation of 2'-thiopropylthymidine nucleoside was compared with those in DNA and RNA (Table 1) based on the homonuclear  $3J_{\text{H}1'-\text{H}2'}$  coupling constants. The % S conformation of the nucleoside unit was calculated from the value of  $\text{H}1'-\text{H}2'$  NMR coupling constants as earlier reported,<sup>17</sup> and according to both Equation. The relevant portion of the  $^1\text{H}$  NMR spectrum is shown in Figure 3.

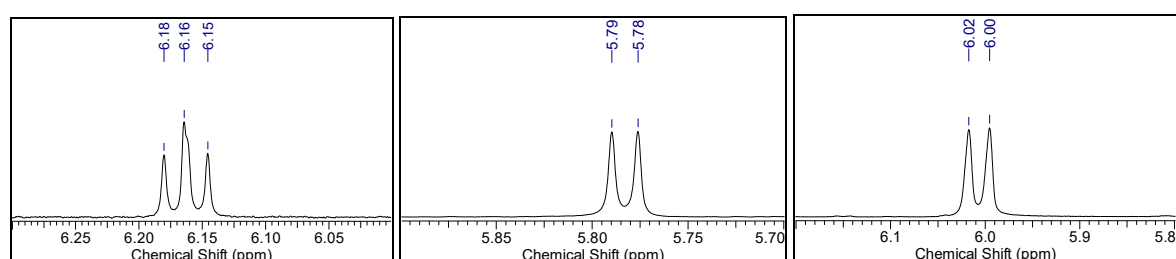


Figure 3. Relevant portion  $^1\text{H}$  NMR spectrum thymidine, uridine, 2-thiopropylthymidine

$$S (\%) = 100 \times (J_{1'2'} - 1)/6.9 \dots \dots \dots (1)$$

$$S (\%) = 100 \times (\sum J_{\text{H}1'} - 9.8)/5.9 \dots \dots \dots (2)$$

**Table 1. Conformation of nucleosides using H1'-H2' coupling constants from <sup>1</sup>H NMR spectra.**

Sr. No.	Nucleoside	$J_{H1'-H2'/H2''}$ (Hz)	% S
1	thymidine	7.5/6.3	69
2	uridine	5.5	65
3	2'-thiopropylthymidine	8.0	101

### 5.5 Synthesis of TBA and modified TBA variants, their purification and characterization

The modified monomer, 2'-thiopropyl thymidine (Figure 2), was incorporated instead of thymidine at the loop positions T<sub>3</sub>, T<sub>4</sub>, T<sub>7</sub>, T<sub>9</sub>, T<sub>12</sub>, T<sub>13</sub>, T<sub>3</sub>T<sub>4</sub> and T<sub>7</sub>T<sub>9</sub> respectively to get oligomers **TBA-t3**, **TBA-t4**, **TBA-t7**, **TBA-t9**, **TBA-t12**, **TBA-t3**, **TBA-t3t4** and **TBA-t7t9** respectively. All the TBA variants (Table 2) were synthesized on a Bioautomation MM4 DNA synthesizer using commercially available protected 2'-deoxy-thymidine-3'-phosphoramidite and 2'-deoxy-guanosine-3'-phosphoramidite by standard β-cyanoethyl phosphoramidite chemistry<sup>18</sup> using re-coupling for modified nucleotides. The synthesized oligonucleotides were cleaved from the solid support by aq. ammonia treatment at 65 °C for 6h. RP-HPLC purification of the synthesized oligomers was done, and their integrity was confirmed by MALDI-TOF mass spectrometric analysis. The general scheme for solid-phase oligonucleotide synthesis is explained in Chapter 1, Scheme 1. RP-HPLC confirmed the synthesized oligomeric sequences; their MALDI-TOF characterization data are listed in Table 2.

**Table 2. Synthesized TBA variants.**

Sr.no.	Sequence name	Sequence details	MALDI-TOF Mass (Da)	
			M <sub>calcd.</sub>	M <sub>obsd.</sub>
1	<b>TBA-t3</b>	GG <sub>t</sub> TGGTGTGGTTGG	4801	4840 ([M] + K <sup>+</sup> )
2	<b>TBA-t4</b>	GGT <sub>t</sub> TGGTGTGGTTGG	4801	4839 ([M] + K <sup>+</sup> )
3	<b>TBA-t7</b>	GGTTGG <sub>t</sub> TGTGGTTGG	4801	4838 ([M] + K <sup>+</sup> )
4	<b>TBA-t9</b>	GGTTGGTGT <sub>t</sub> GGTTGG	4801	4839 ([M] + K <sup>+</sup> )
5	<b>TBA-t12</b>	GGTTGGTGTGG <sub>t</sub> TGG	4801	4839 ([M] + K <sup>+</sup> )
6	<b>TBA-t13</b>	GGTTGGTGTGGT <sub>t</sub> GG	4801	4840 ([M] + K <sup>+</sup> )
7	<b>TBA-t3t4</b>	GG <sub>tt</sub> TGGTGTGGTTGG	4872	4921 ([M] + K <sup>+</sup> )
8	<b>TBA-t7t9</b>	GGTTG <sub>t</sub> G <sub>t</sub> GGTTGG	4872	4929 ([M] + K <sup>+</sup> )

t = 2'-thiopropyl thymidine



## 5.6 G-quadruplex formation and stability

The impact of the 2'-thiopropyl-modified units on the structural topology of TBA can be studied by CD spectroscopy. TBA is known to form an antiparallel G-quadruplex in the presence of  $K^+$  ions; the CD spectrum of TBA shows a CD maximum at 295 nm and a minimum at 265 nm, which are characteristic of antiparallel G-quadruplexes.<sup>19</sup>

### 5.6.1 G-quadruplex topology

In the presence of potassium ions, the CD spectra of the TBA variants displayed the characteristic signals corresponding to the antiparallel G-quadruplex topology known for TBA. All the variants showed maxima at  $\sim 295$  nm and minima at  $\sim 265$  nm (Figure 4a). When the CD spectra were recorded in water, in the absence of any added cations, the variants TBA-t3t4, TBA-t7t9 bearing two modified units each, failed to show any significant signal, indicating the inability of these variants to fold into any kind of structure in the absence of cations. The other variants that contain only one modified unit showed signals resembling those observed for TBA (Figure 4b).

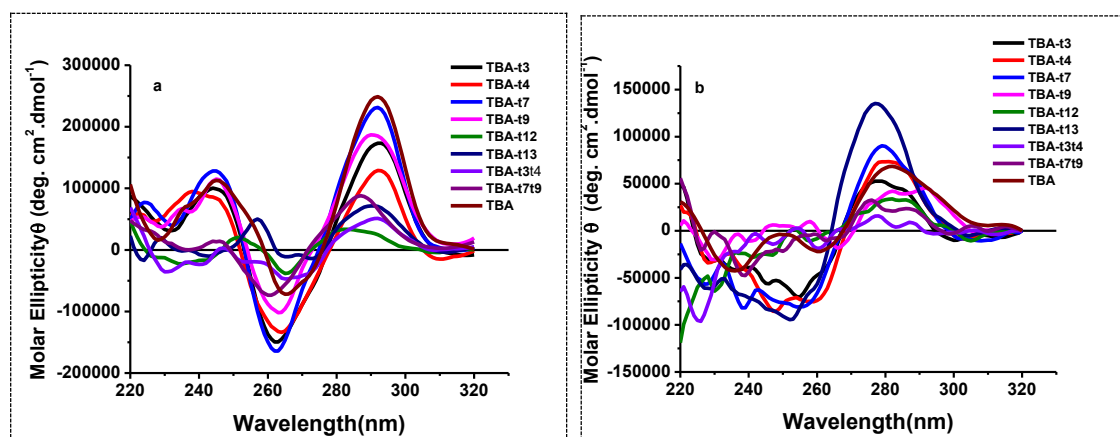


Figure 4. CD spectra of TBA and variants (5  $\mu$ M), recorded at 4  $^{\circ}$ C; a) In 10 mM potassium-phosphate buffer, pH 7.2, containing 100 mM KCl; b) in water, in the absence of any added cations.

### 5.6.2 G-quadruplex thermal stability using UV Spectroscopy

Denaturation – renaturation profiles and melting temperature ( $T_m$ ) can be monitored by UV spectroscopy by varying the temperature. The temperature-dependent changes in the UV absorbance at 295 nm were monitored to assess the stability of G-quadruplexes in the presence of  $K^+$  ions for all the variants in comparison to TBA. The results were compared with native TBA. In comparison to TBA ( $T_m = 49$   $^{\circ}$ C), all the oligomers, were destabilized to a large extent ( $\Delta T_m = -17$   $^{\circ}$ C to  $-29$   $^{\circ}$ C). The altered sugar pucker in the modified TBA could be the reason for the observed lower stability. The TBA-t4, TBA-t9, TBA-t12, TBA-t7t9 variants, in

particular, were largely destabilized and melted near 20°C. The results are summarized in Table 3, and the melting plots are shown in Figure 5. Thus, insertion of the 2'-thiopropyl thymidine units was found to be unfavorable with respect to quadruplex stability.

**Table 3: UV- $T_m$  values of TBA and variants.**

Sr. No.	Oligomer	UV $T_m$ (°C)
1	TBA-t3	25
2	TBA-t4	20
3	TBA-t7	24
4	TBA-t9	21
5	TBA-t12	20
6	TBA-t13	32
7	TBA-t3t4	nd
8	TBA-t7t9	20
9	TBA	49

UV  $T_m$  of TBA and variants oligomers in potassium phosphate buffer (10 mM, pH 7.2) containing 100 mM KCl.

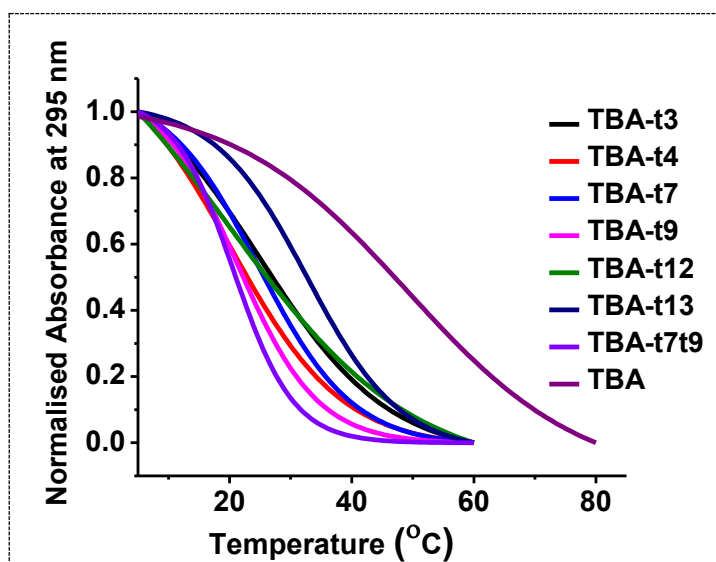


**Figure 5.** UV melting profiles of TBA and variants at a strand concentration of 5  $\mu$ M in 10 mM potassium phosphate buffer (pH 7.2) containing 100 mM KCl.

### 5.6.3 G-quadruplex in the presence of thrombin

Thrombin can act as a molecular chaperone for the folding of TBA, as has been reported previously by Baldrich and O'Sullivan.<sup>20</sup> Nagatoishi and co-workers<sup>21</sup> showed that TBA forms an antiparallel G-quadruplex in the presence of thrombin and in the absence of any cation, which can be monitored through the CD amplitude at 295 nm. In our earlier studies chap 3, we observed that the TBA sequence was also able to attain the folded G-quadruplex topology by the chaperone activity of thrombin. Therefore, we carried out CD experiments with thrombin, which was added incrementally to the individual oligomers at 4 °C. With the incremental addition of thrombin to modified TBA, we observed a slight change in the CD signal amplitude

(Figure 6). In particular, TBA-t3, TBA-t7, TBA-t12 showed CD signal changes, consistent with the chaperone action of thrombin, while for the other variants, no significant changes in the CD signal were observed.

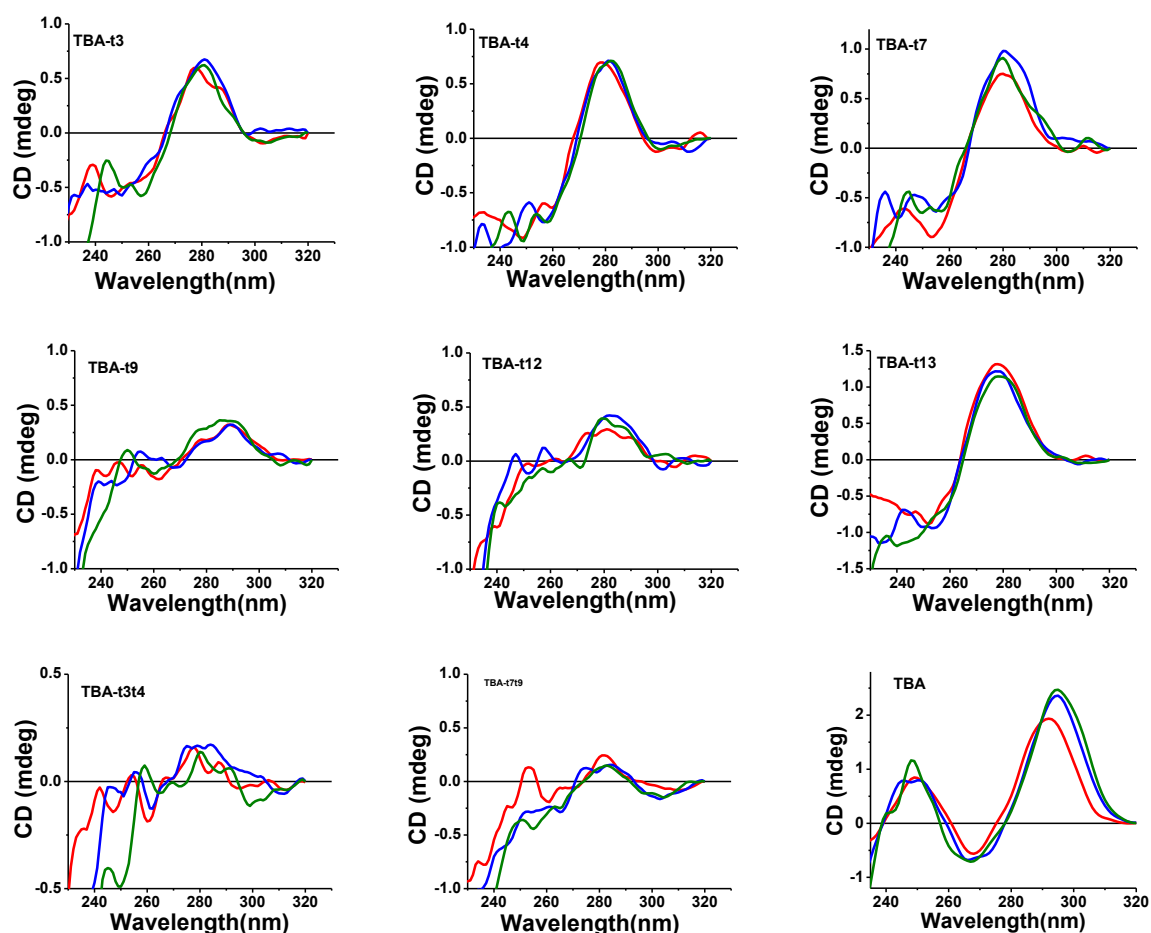
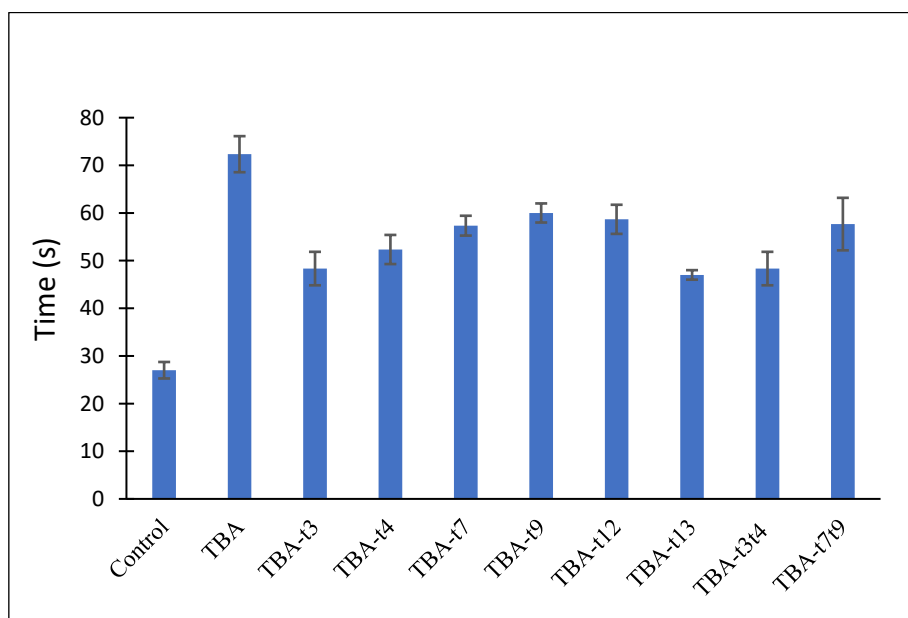


Figure 6. Changes in CD signal showing the chaperone effect of thrombin on TBA and variants. red: 0.2  $\mu\text{M}$  thrombin; blue: 0.4  $\mu\text{M}$  thrombin; green: 0.8  $\mu\text{M}$  thrombin.

### 5.7 Antithrombin effect of modified aptamers

Thrombin transforms fibrinogen to fibrin, and that leads to coagulation.<sup>22</sup> The effect of thrombin binding on the anti-thrombin activity of the modified oligomers was assessed by carrying out a clotting assay, and their inhibitory effect on thrombin-catalyzed fibrin polymerization (thrombin time/clotting time) was measured at 37 °C. The thrombin reagent was pre-incubated with the oligomer before adding fibrinogen-containing saline, and the time for clotting was measured using a SStart Max Coagulation analyzer (Diagnostica Stago). The anti-thrombin activity is reflected in the additional time required for clotting in the presence of the oligomer relative to the reference in the absence of any added oligomer. Control used as TBA is known to slow down coagulation.<sup>23</sup> Oligomers TBA-t7 (57 s), TBA-t9 (60 s), TBA-t12 (58 s), and TBA-t7t9 (57 s),

showed slightly lower anti-clotting effects than TBA (clotting time 72 s, Figure 7). The highest anticoagulant effect was observed with TBA-t9, with a 60 s clotting time and a delay of 33 s compared to the control (clotting time 27 s) when no oligomer was added. The modified oligomers- TBA-t3, TBA-t4, TBA-t13 and TBA-t3t4 showed lower thrombin inhibitory effects (clotting time ranging from 47 s to 52 s).



**Figure 7. Antithrombin activity measurement.** Error bars represent the standard deviation obtained from three independent experiments. Control indicates the clotting time measured with fibrinogen and thrombin in the absence of any added oligomer.

### 5.8 Snake venom phosphodiesterase (SVPD) stability

The stability of TBA-t7 as a representative oligomer, in comparison to TBA, to nuclease digestion was tested by exposure to *Crotalus adamanteus* snake venom phosphodiesterase (SVPD, 3' exonuclease). The study was carried out at 37 °C and the percent oligomer remaining intact at successive time intervals was monitored by RP-HPLC (Figure 8). Although both oligomers were finally hydrolyzed by SVPD, TBA-t7 was more resistant to the enzyme, with a half-life of 2.6 min, in comparison to TBA ( $t_{1/2} < 2$  min).

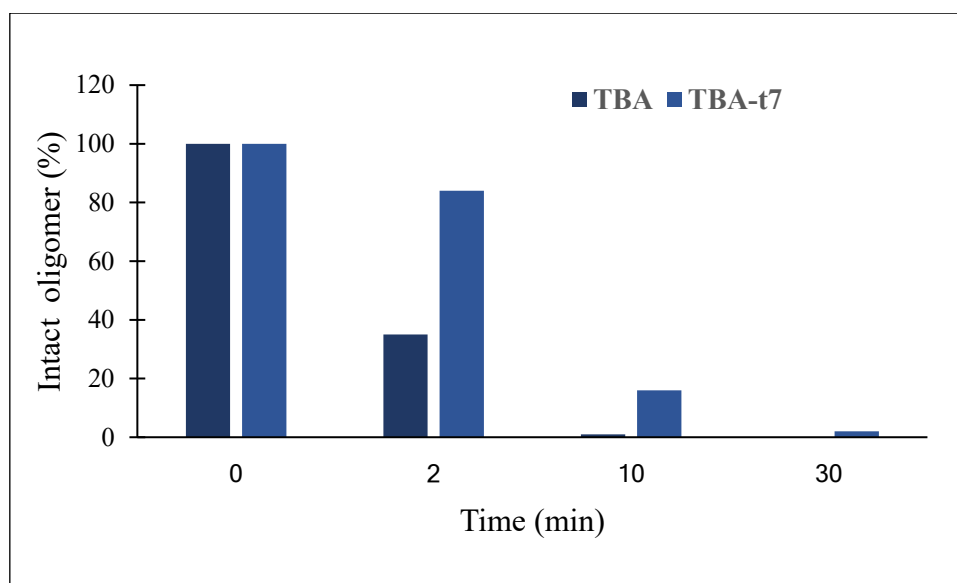


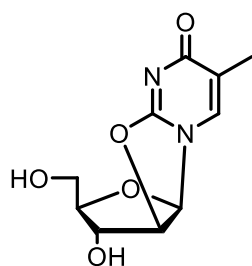
**Figure 8.** Stability of TBA and TBA-t7 (7.5  $\mu\text{M}$  each) to degradation by SVPD (0.015 U) at 37 °C. Buffer: 100 mM Tris-HCl (pH 8.5) containing 15 mM  $\text{MgCl}_2$ , 100 mM NaCl.

## 5.9 Conclusions

The sugar pucker in 2'-thiopropyl thymidine was found to be C2'-*endo* and ~100 % S-type, even more than that observed in native DNA (C2'-*endo*, 69 % S-type). TBA variants bearing this unit at selected loop positions were found to be able to form antiparallel G-quadruplexes, with a beneficial effect on the nuclease stability and half-life, although the thermal stability of the quadruplexes formed was lower than that of TBA. Some of the TBA variants, viz., TBA-t7, TBA-t9, TBA-t12 and TBA-t3t4 showed moderate anti-clotting activity, though lower than TBA.

## 5.10 Experimental section

### 5.10.1 Experimental procedures and spectral data



**2,2'-anhydroribothymidine 2:** Commercially available ribothymidine compound **1** (5.00 g, 19.37 mmol) was taken in dry DMF (100 mL) containing  $\text{Ph}_2\text{CO}_3$  (5.39 g, 25.19 mmol) and  $\text{NaHCO}_3$  (0.16 g, 1.93 mmol) as catalyst and the reaction mixture was stirred at 150°C temperature under inert atmosphere. After 30 min, TLC indicated the consumption of the starting material. Diethyl ether was then added to the reaction mixture, when pure compound **2** precipitated out as a white solid (4.1 g) in 88% yield.

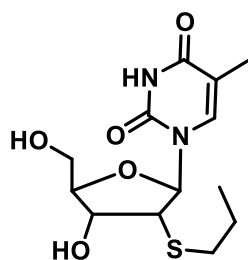
**Mol. Formula** :  $\text{C}_{10}\text{H}_{12}\text{N}_2\text{O}_5$

**Exact Mass (calcd)** : 240.07

**HRMS (obsd)** : 241.08 ( $\text{M} + \text{H}^+$ )

**<sup>1</sup>H NMR**

(200 MHz, D<sub>2</sub>O) :  $\delta$ H (ppm) 1.91 (s, 3 H) 3.51 (dd,  $J$  = 6.5 Hz, 4.2 Hz, 2 H) 4.35 (br s, 1 H) 4.62 (s, 1 H) 5.41 (d,  $J$  = 5.8 Hz, 1 H) 6.49 (d,  $J$  = 5.8 Hz, 1 H) 7.75 (s, 1 H).



**2'-deoxy 2'-(thiopropyl)-thymidine 3:** Compound **2** (3.00 g, 12.44 mmol) and N1,N1,N3,N4 tetramethylguanidine (6.2 mL, 49.70 mmol) were taken in dry DMF (60 mL), followed by addition of 1-thiopropene (4.5 mL, 49.70 mmol). The reaction mixture was stirred at 65 °C temperature for 2 h. TLC indicated consumption of the starting material. NaHCO<sub>3</sub> was added, and the reaction mixture was extracted with EtOAc, followed by drying of the organic extracts over sodium sulfate. The crude sticky compound **3** was purified by column chromatography (eluted in 25% EtOAc in petroleum ether) to give pure **3** (2.52 g) colorless foam in 64% yield.

**Mol. Formula** : C<sub>13</sub>H<sub>20</sub>N<sub>2</sub>O<sub>5</sub>S

**Exact Mass (calcd)** : 316.11

**HRMS (obsd)** : 339.09 (M + Na<sup>+</sup>)

**<sup>1</sup>H NMR**

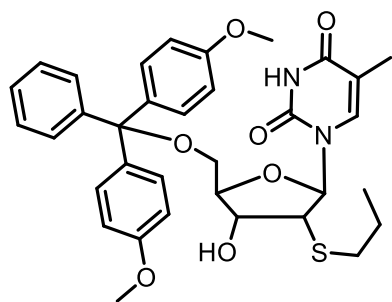
(400 MHz, DMSO-*d*<sub>6</sub>):  $\delta$ H (ppm) 0.85 (t,  $J$  = 7.3 Hz, 3 H), 1.39 -1.50 (m, 2 H), 1.79 (s, 3H), 2.42 (t,  $J$  = 7.1 Hz, 2 H), 3.39 - 3.47 (m, 1H), 3.58 (dd,  $J$  = 12.7 Hz, 4.7Hz, 2 H), 3.86 (br s, 1 H), 4.17 (br s, 1 H), 5.11 (t,  $J$  = 5.0 Hz, 1 H), 5.57(d,  $J$  = 5.3 Hz, 1 H), 6.01 (d,  $J$  = 8.0 Hz, 1 H), 7.73 (s, 1 H), 11.36 (s, 1 H)

**<sup>13</sup>C NMR**

(50 MHz, CDCl<sub>3</sub>) :  $\delta$ C (ppm) 12.4, 13.1, 23.3, 34.3, 53.0, 62.9, 71.5, 86.4, 92.8, 111.3, 138.7, 150.6, 163.7.

**<sup>13</sup>C-DEPT**

(50MHz, CDCl<sub>3</sub>) :  $\delta$ C (ppm) (CH/CH<sub>3</sub>):12.5, 13.3, 53.1, 71.7, 86.5, 92.9, 138.8 (CH<sub>2</sub>): 23.5, 34.4,63.0.


**5'-DMTr-2'-deoxy 2'-(thiopropyl)-thymidine 4:**

Compound **3** (1.00 g, 3.12 mmol) and dimethoxytrityl chloride (DMTr-Cl, 1.27 g, 3.75 mmol) was dissolved in dry pyridine (20 mL) containing DMAP (0.038 g, 0.31 mmol) as catalyst and the reaction mixture was stirred at room temperature. After 2 h, TLC indicated the consumption of the starting material. Removal of solvents yielded a yellowish sticky solid, which was taken up in  $\text{CH}_2\text{Cl}_2$  and given a saturated  $\text{Na}_2\text{HCO}_3$  wash. The organic layer was dried over sodium sulfate, and the solvent was evaporated in vacuo to get a colorless solid foam, which was purified by chromatography on silica gel (pre-neutralized with  $\text{Et}_3\text{N}$ ). Compound **4** eluted in a mixture of EtOAc in petroleum ether (30 %) as a pure colorless foam (1.56 g) in 80% yield.

**Mol. Formula** :  $\text{C}_{34}\text{H}_{38}\text{N}_2\text{O}_7\text{S}$

**Exact Mass (calcd)** : 618.24

**HRMS (obsd)** : 641.12 ( $\text{M} + \text{Na}^+$ )

 **$^1\text{H}$  NMR**

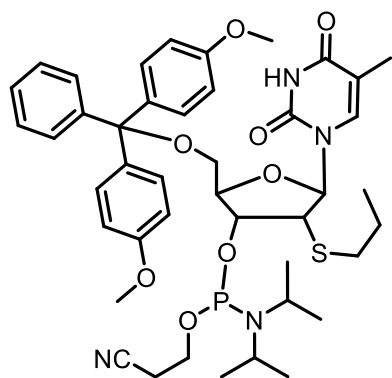
(400 MHz,  $\text{CDCl}_3$ ) :  $\delta\text{H}$  (ppm) 1.02 (t,  $J = 7.3$  Hz, 3 H), 1.39 (d,  $J = 1.1$  Hz, 3 H), 1.65 – 1.70 (m, 2 H), 2.60 (d,  $J = 1.8$  Hz, 2 H), 2.94 - 2.98 (m, 1 H), 3.40 (dd,  $J = 10.7, 2.1$  Hz, 1 H), 3.57 (dd,  $J = 10.6, 2.4$  Hz, 1 H), 3.63 (dd,  $J = 8.8, 4.9$  Hz, 1 H), 3.81 (s, 7 H), 4.23 (d,  $J = 1.7$  Hz, 1 H), 4.34 (d,  $J = 5.0$  Hz, 1 H), 6.11 (d,  $J = 8.8$  Hz, 1H), 6.85 (d,  $J = 8.6$  Hz, 4 H), 7.24 - 7.26 (m, 2 H), 7.28 - 7.34 (m, 4 H), 7.36 - 7.40 (m, 2 H), 7.66 (d,  $J = 1.1$  Hz, 1 H), 8.26 (s, 1 H).

 **$^{13}\text{C}$  NMR**

(50MHz,  $\text{CDCl}_3$ ) :  $\delta\text{C}$  (ppm) 11.6, 13.2, 23.3, 34.3, 55.3, 55.3, 63.8, 71.6, 84.7, 86.6, 87.2, 111.6, 113.2, 128.0, 130.0, 135.2, 153.2, 144.7, 150.5, 158.8, 163.6

 **$^{13}\text{C}$ -DEPT**

(50MHz,  $\text{CDCl}_3$ ) :  $\delta\text{C}$ (ppm) (CH/CH<sub>3</sub>): 11.5, 13.2, 55.2, 71.6, 84.7, 86.5, 113.2, 127.2, 127.9, 128.0, 130.0, 135.1 (CH<sub>2</sub>): 23.2, 34.3, 63.8



**5'-DMTr-2'-deoxy,2'-(thiopropyl)-thymidine -3'-phosphoramidite (5).** Compound 4 (0.5 g, 0.80 mmol) was desiccated and co-evaporated with dry  $\text{CH}_2\text{Cl}_2$  before dissolving in dry  $\text{CH}_2\text{Cl}_2$  (5.0 mL). Diisopropylethylamine (DIPEA) (0.55 mL, 3.23 mmol) was added to the ice-cooled solution under an argon atmosphere followed by 2-cyanoethyl- *N,N*-diisopropylchlorophosphine (0.38 mL, 1.62 mmol). After stirring the reaction mixture at room temperature for 4 h, TLC indicated complete consumption of the starting material.  $\text{CH}_2\text{Cl}_2$  was added to dilute the reaction, and the organic layer was washed with  $\text{NaHCO}_3$  and water and then dried over sodium sulfate. Removal of solvents in vacuo afforded the crude product that was purified by column chromatography on silica gel (pre-neutralized by  $\text{Et}_3\text{N}$ ). The pure compound was eluted by using a 1:1 mixture of  $\text{CH}_2\text{Cl}_2/\text{EtOAc}$  to give pure 5 (0.47 g) in 71% yield.

**Mol. Formula** :  $\text{C}_{43}\text{H}_{35}\text{N}_4\text{O}_8\text{PS}$

**$^{31}\text{P}$  NMR** :  $\delta\text{P}(\text{ppm})$  149.92, 150.69.  
(161 MHz,  $\text{CDCl}_3$ )

### 5.10.2 Oligonucleotide synthesis

Both TBA and modified TBA oligonucleotides were synthesized in-house on a Bioautomation Mermade-4 DNA synthesizer employing  $\beta$ -cyanoethyl phosphoramidite chemistry. The protected deoxyguanosine and thymidine phosphoramidites were obtained from ChemGenes corporation. Oligonucleotides were cleaved from the column by using aq. ammonia at  $65^\circ\text{C}$  for 6 h and then concentrated.

### 5.10.3 Purification and characterization

#### 5.10.3.1 High-performance liquid chromatography

The purity of synthesized oligonucleotides was ascertained using RP-HPLC on a C18 column using a Waters system (Waters Delta 600e quaternary solvent delivery system and 2998 photodiode array detector and Empower 2 chromatography software). An increasing gradient of acetonitrile in 0.1M triethylammonium acetate (pH 7.0) was used, and it was monitored at 260 nm. [A = 5%  $\text{CH}_3\text{CN}$  in TEAA (0.1M, pH 7); B = 30%  $\text{CH}_3\text{CN}$  in TEAA (0.1M, pH 7.0)].

#### 5.10.3.2 MALDI-TOF characterization

MALDI-TOF mass spectra were recorded on a SCIEX TOF/TOF 5800 system. A nitrogen laser (337nm) was used for desorption and ionization. The matrix used for analysis was THAP (2',



4', 6'-trihydroxyacetophenone), and diammonium citrate used as an additive. The sample was prepared by mixing 1  $\mu$ L oligomer (10-50  $\mu$ M in de-ionized H<sub>2</sub>O) with 10  $\mu$ L of THAP (0.55 M in EtOH) mixed well followed by 5  $\mu$ L diammonium citrate (0.1M in de-ionized H<sub>2</sub>O) again mixed well and then 1  $\mu$ L of the mixture was spotted on the metal plate. The metal plate was loaded to the instrument and the analyte ions were then accelerated by an applied high voltage in linear mode and detected as an electrical signal.

#### 5.10.4 CD spectroscopy experiments

CD spectra were recorded on Jasco J-815 CD spectrometer equipped with a Jasco PTC-424S/15 Peltier system. 2 mm path-length quartz cuvettes were used for a sample volume 500  $\mu$ L and strand concentration of 5  $\mu$ M in 10 mM potassium phosphate buffer (pH 7.2) containing 100 mM KCl. Oligomers prepared in buffer were annealed by heating at 90 °C for 2 min, then slowly cooling to room temperature, followed by refrigeration for 4 h before use. Spectral scans were collected at 4 °C for a wavelength range 220- 320 nm at a scanning rate of 100 nm min<sup>-1</sup>. CD melting was performed for the entire sample by monitoring the CD intensity at 295 nm against temperature over the range 5-90 °C. CD spectroscopy was also used to study the thrombin binding by TBA and modified TBA oligomers. 10  $\mu$ L of 0.5 NIH of bovine thrombin (Tulip Diagnostics) was added to the oligomers at 5 min interval, and their CD signal intensity at 295 nm was recorded with increasing thrombin concentration.

#### 5.10.5 UV experiments

UV-absorbance scans of TBA and modified TBA oligomers were recorded using 10 mm pathlength quartz cells on an Analytik Jena SPECORD® 200 plus spectrometer equipped with a peltier-equipped temperature controller and at a scanning speed of 5 nm sec<sup>-1</sup>. The oligomers were taken at a strand concentration of 5  $\mu$ M. Potassium phosphate buffer (10 mM, pH 7.2) was used, which contained 100 mM KCl. Before starting the experiments, oligomers were annealed by heating at 90 °C for 2 min, slowly cooled to room temperature, and refrigerated at ~4°C for 3 h. Thermal difference spectra (TDS) were obtained by subtracting the UV-absorbance spectral scan of the sample at temperatures below, from that above the melting temperature ( $T_m$ ).

#### 5.10.6 SVPD stability experiments

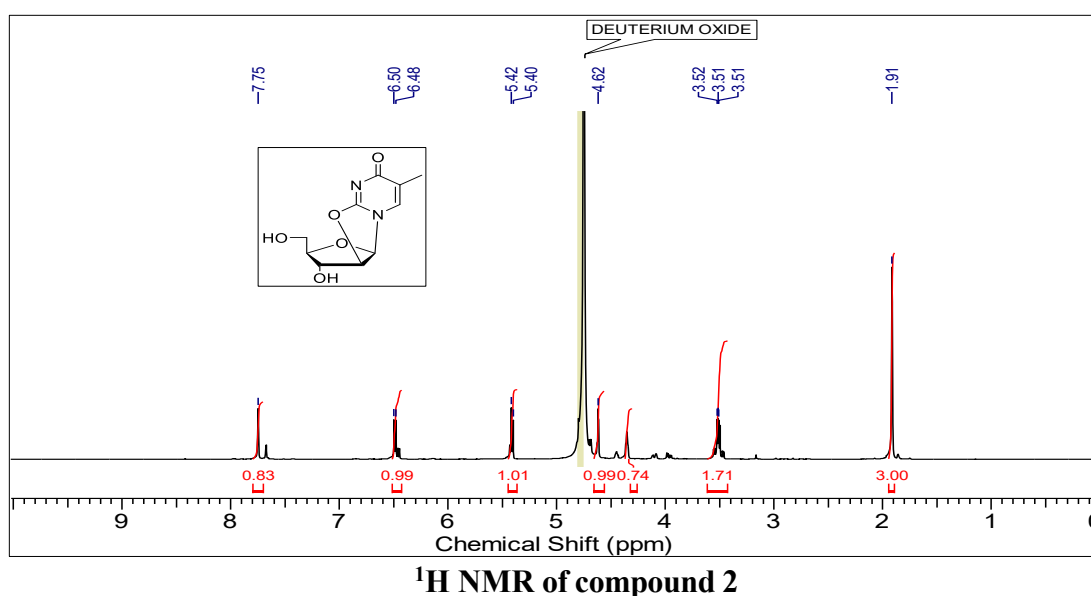
TBA and TBA-t7 (7.5  $\mu$ M) were treated with SVPD (0.015 U) at 37 °C in 100 mM Tris-HCl buffer (pH 8.5) containing 15 mM MgCl<sub>2</sub>, 100 mM NaCl. Aliquots were removed at successive time intervals, heated at 90 °C for 3 min to inactivate the nuclease, and analyzed by RP-HPLC to measure the percentage of oligonucleotides remaining intact.

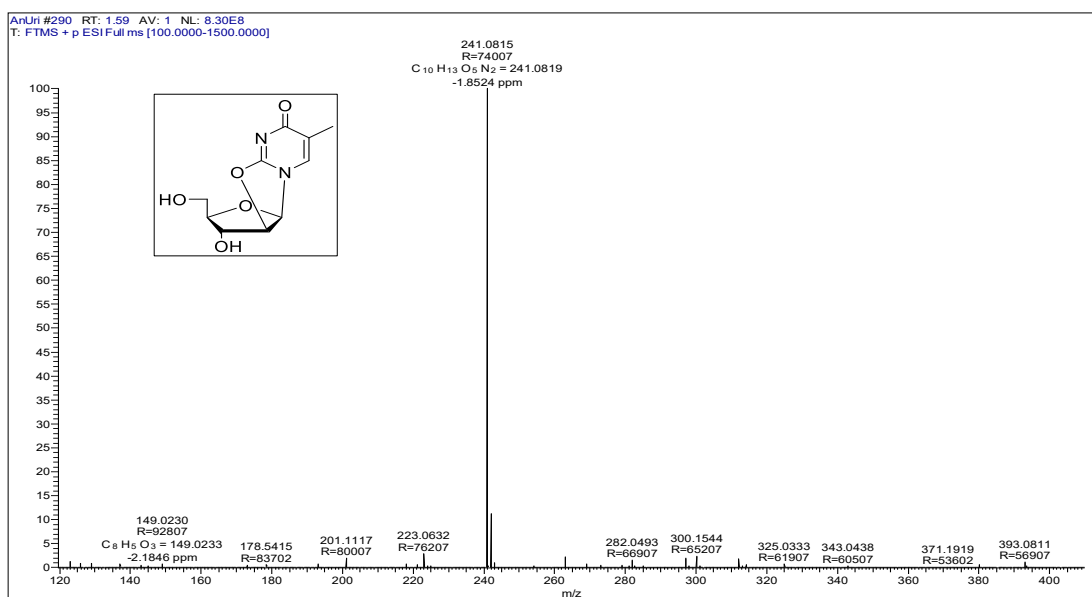
### 5.10.7 Thrombin time measurements for antithrombin effect

The inhibitory activity of the aptamers on thrombin-catalysed conversion of fibrinogen to fibrin (clotting) by TBA, modified TBA measured by thrombin time assay. The time (in seconds) for clotting at 37 °C was measured on a STart Max Coagulation analyzer (Diagnostics Stago). Each experiment was repeated at least thrice; the standard deviation was  $\pm 1$  °C. Each commercial reagent was reconstituted according to the manufacturer's protocols. Bovine thrombin (Tulip Diagnostics, 0.1 NIH unit) was pre-incubated with oligomers at 0.25  $\mu\text{M}$  concentration for 2 min before addition to fibrinogen from human plasma (2.65  $\mu\text{M}$ , Aldrich F-3897), and measurement of clotting time (thrombin time) was done according to the manufacturer's protocol.

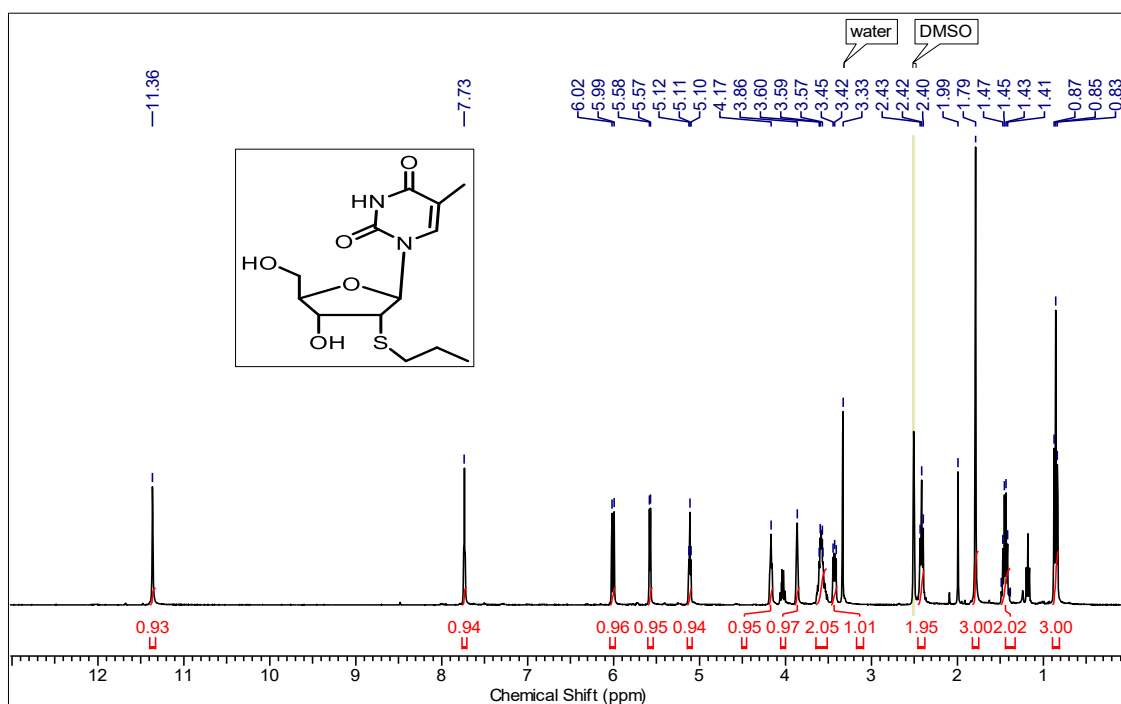
### 5.11 Appendix D

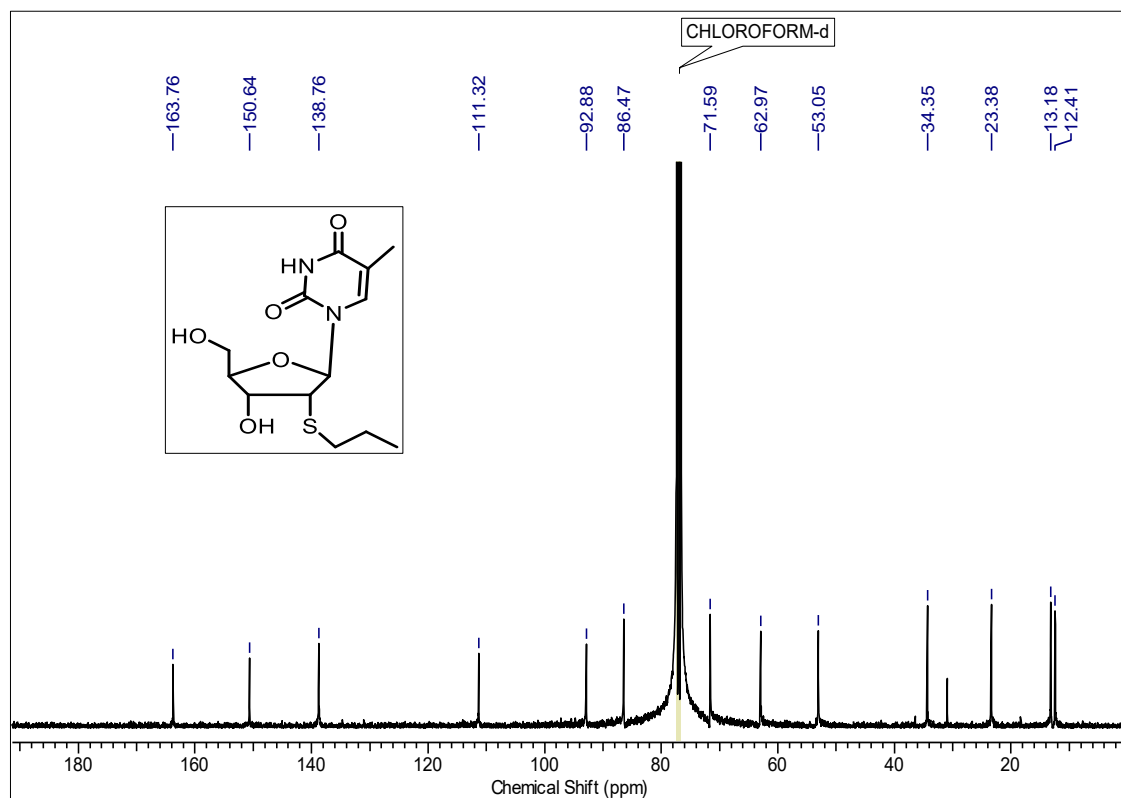
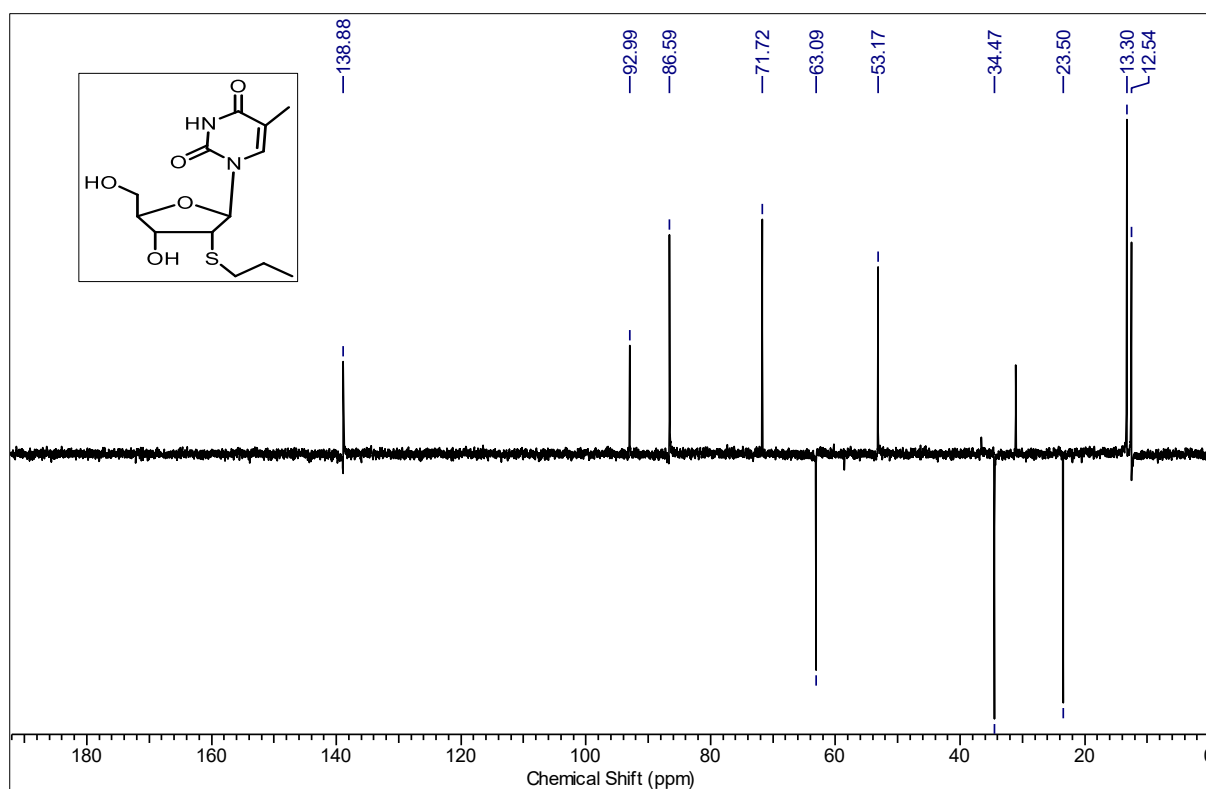
Compounds	Page Number
Compound 2: $^1\text{H}$ NMR and HRMS	115-116
Compound 3: $^1\text{H}$ , $^{13}\text{C}$ , DEPT NMR and HRMS	116-118
Compound 4: $^1\text{H}$ , $^{13}\text{C}$ , DEPT NMR and HRMS	118-120
Compound 5: $^{31}\text{P}$ NMR	120
$^1\text{H}$ NMR of Thymidine, Uridine	121
HPLC chromatogram of modified TBA oligomers	122-123
MALDI-TOF spectra of modified TBA oligomers	124-126

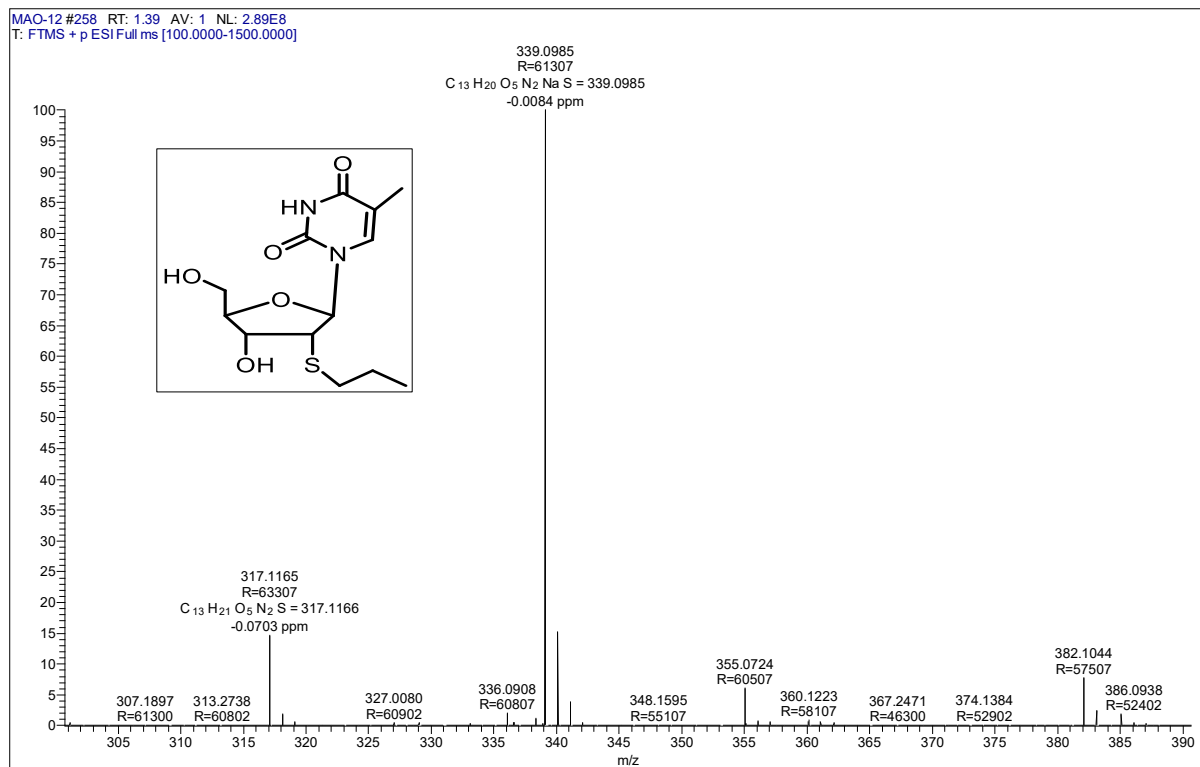




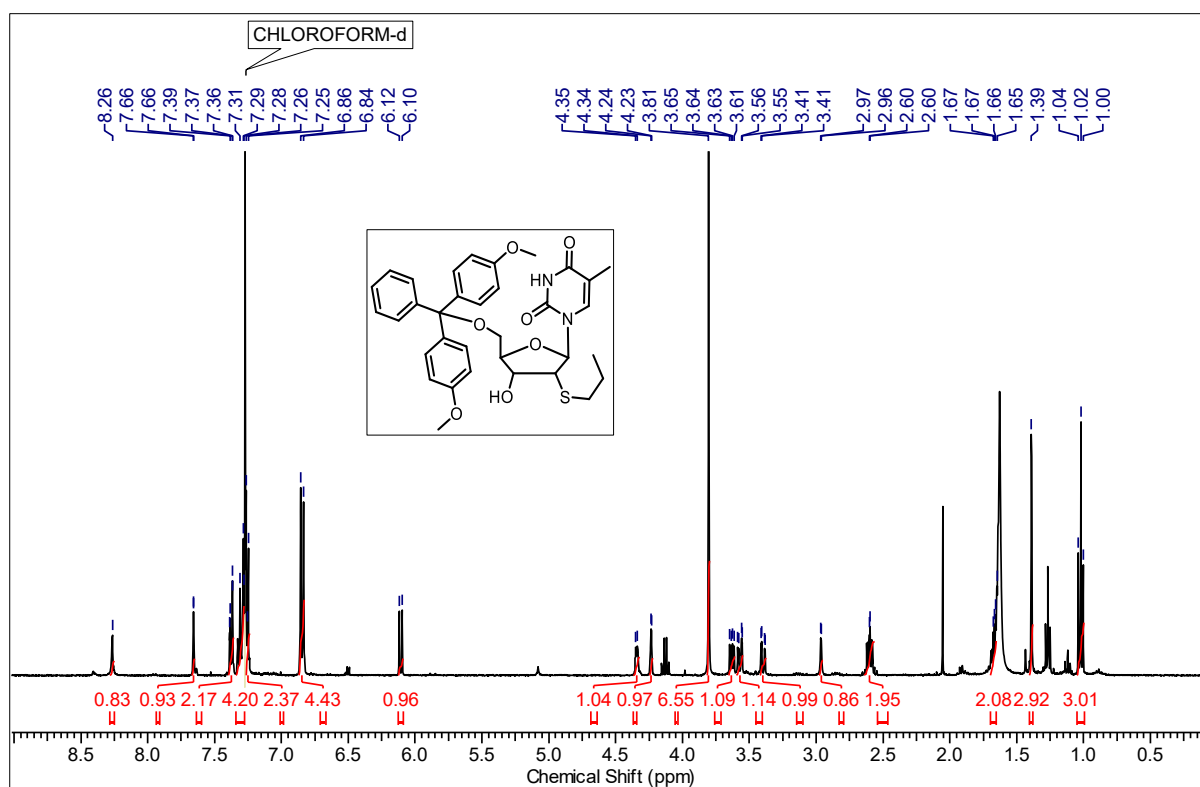
HRMS of compound 2

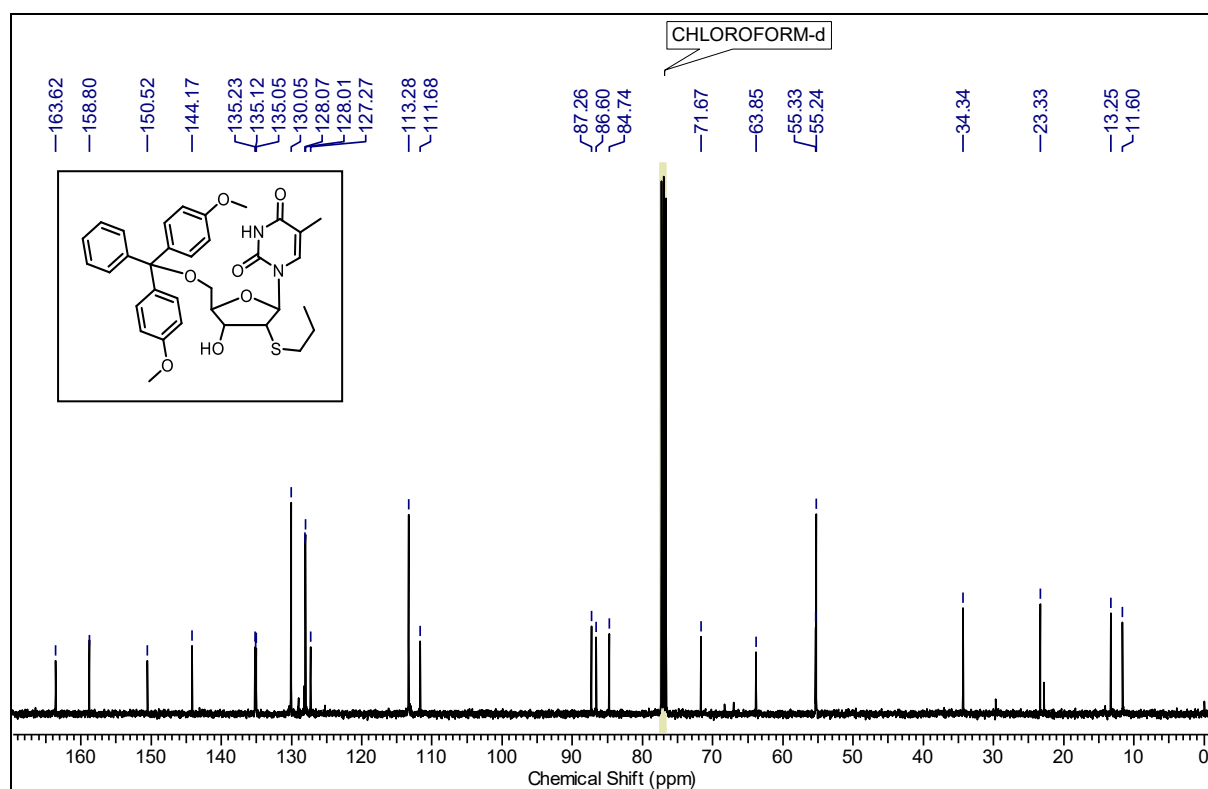
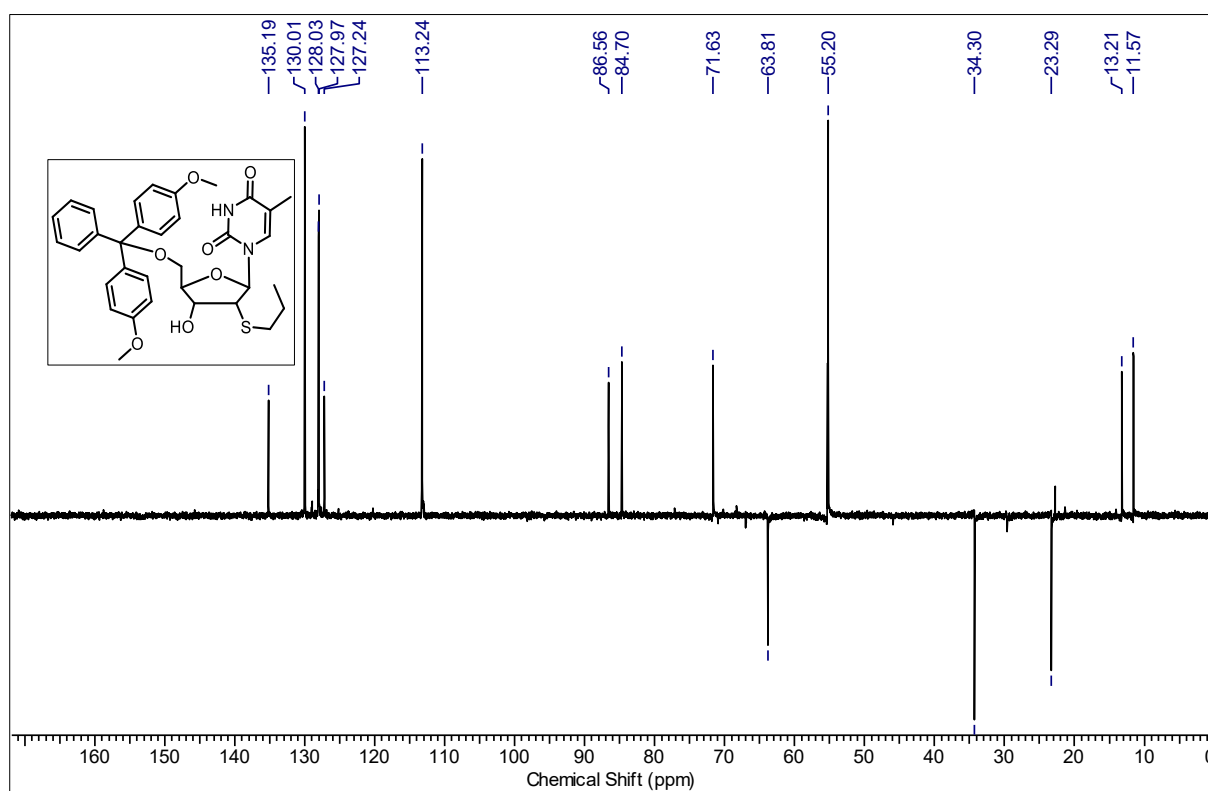
<sup>1</sup>H NMR of compound 3

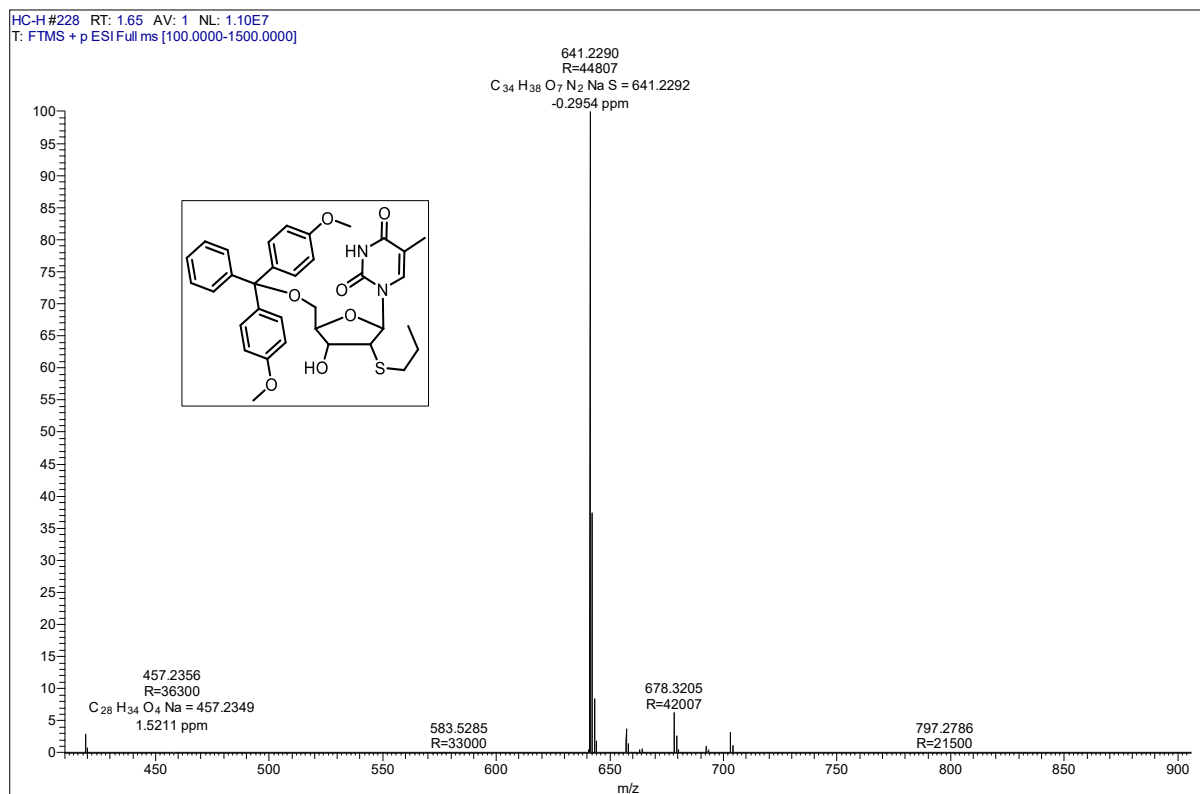
 $^{13}\text{C}$  NMR of compound 3 $^{13}\text{C}$  DEPT of compound 3



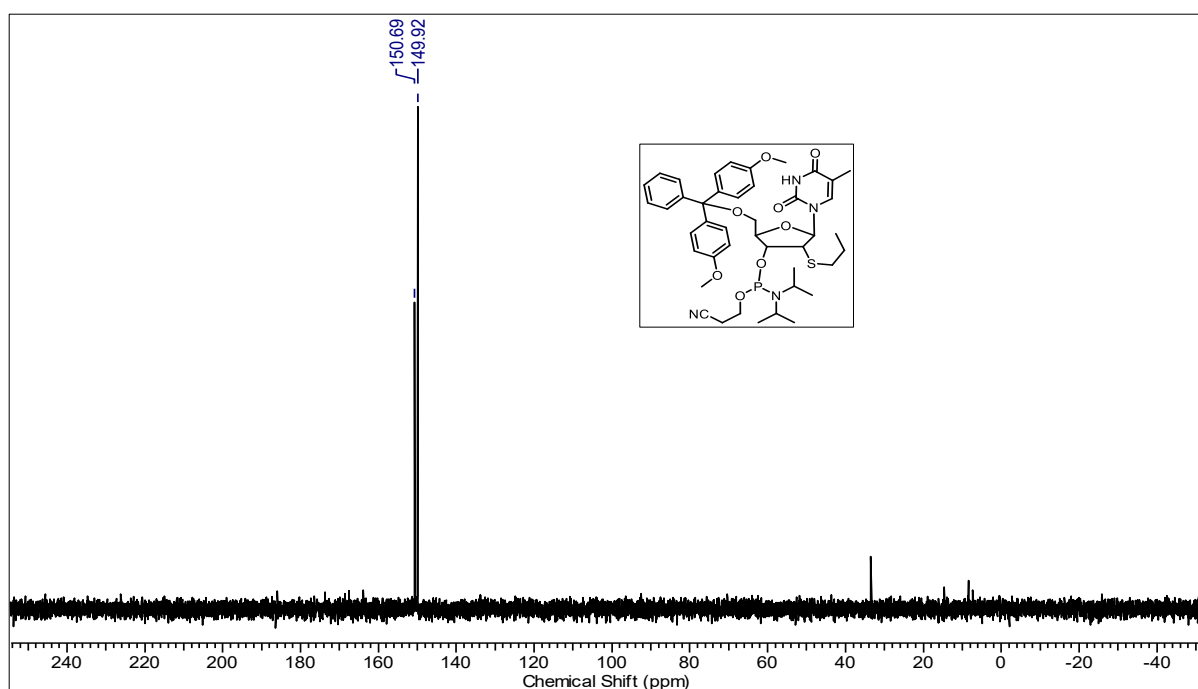
HRMS of compound 3

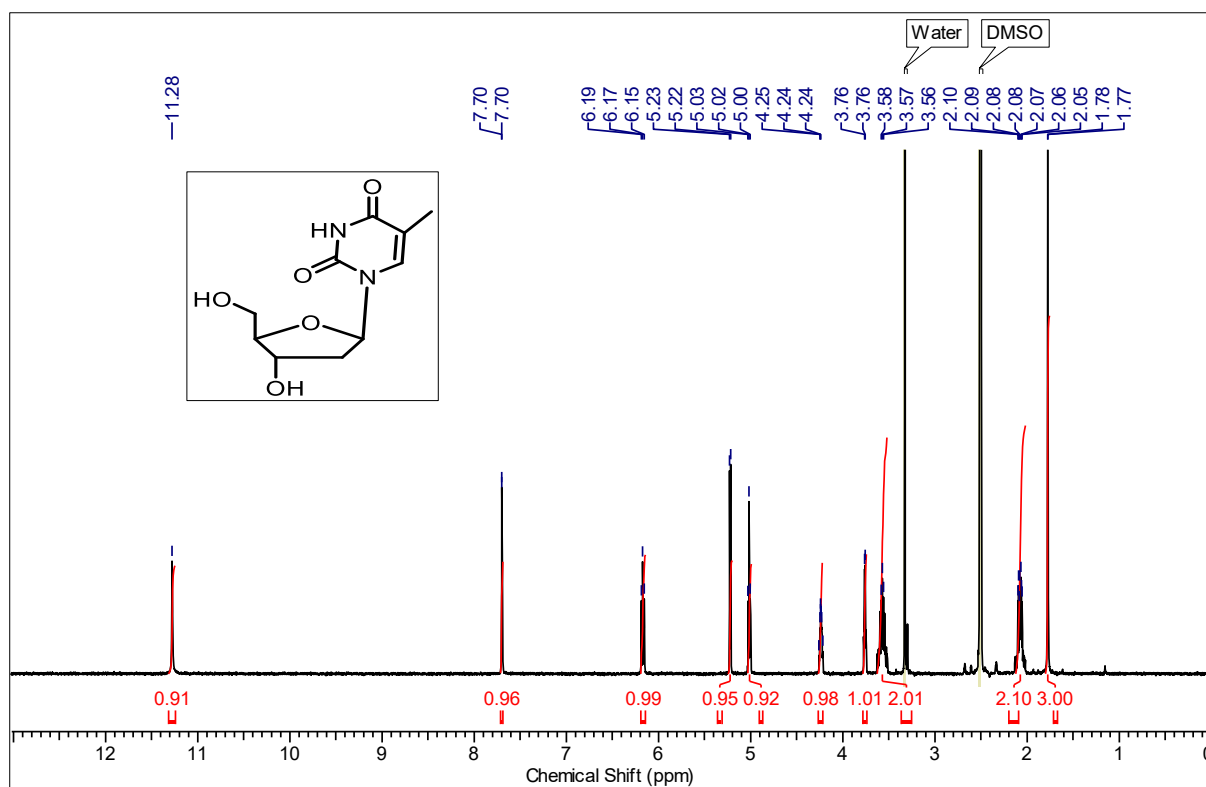
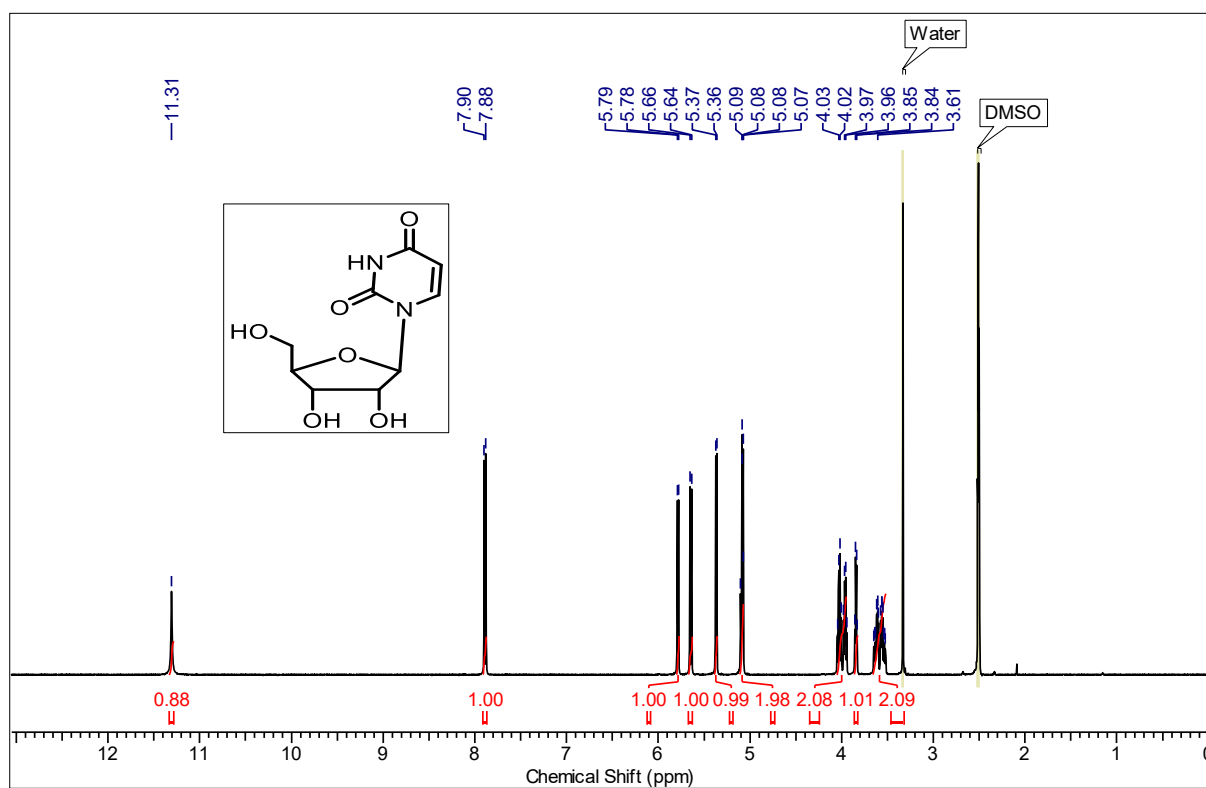
<sup>1</sup>H NMR of compound 4

 $^{13}\text{C}$  NMR of compound 4 $^{13}\text{C}$  DEPT of compound 4

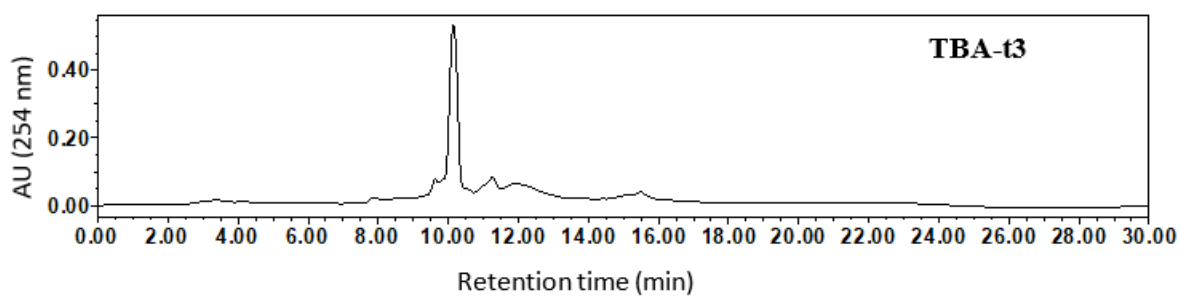


HRMS of compound 4

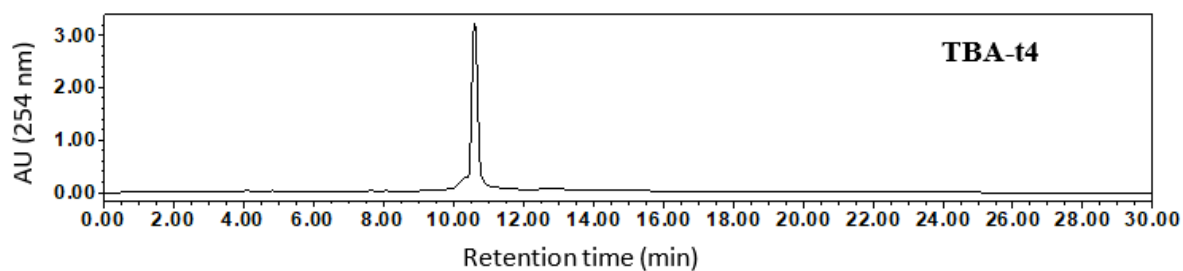
 $^{31}P$  NMR of compound 5

**<sup>1</sup>H NMR of compound Thymidine****<sup>1</sup>H NMR of Uridine**

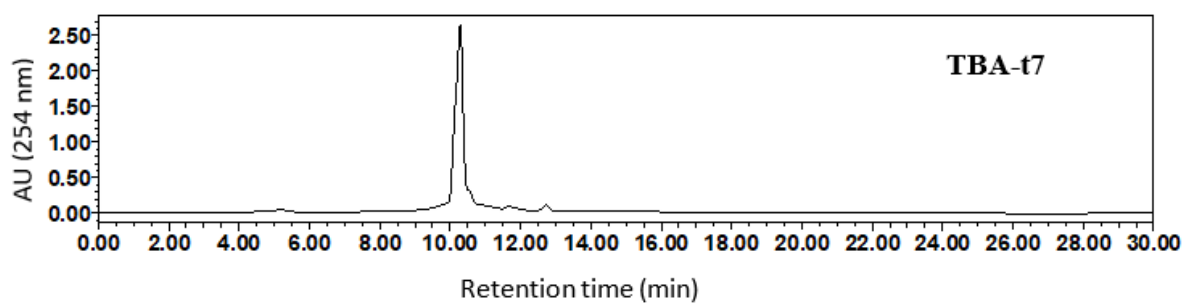




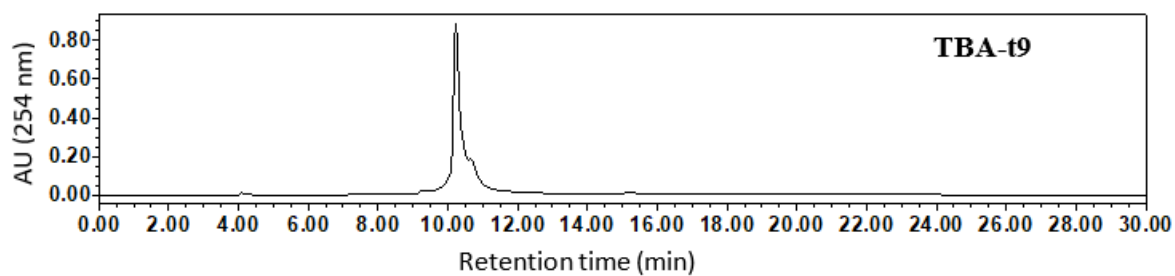
**HPLC chromatogram of TBA-t3**



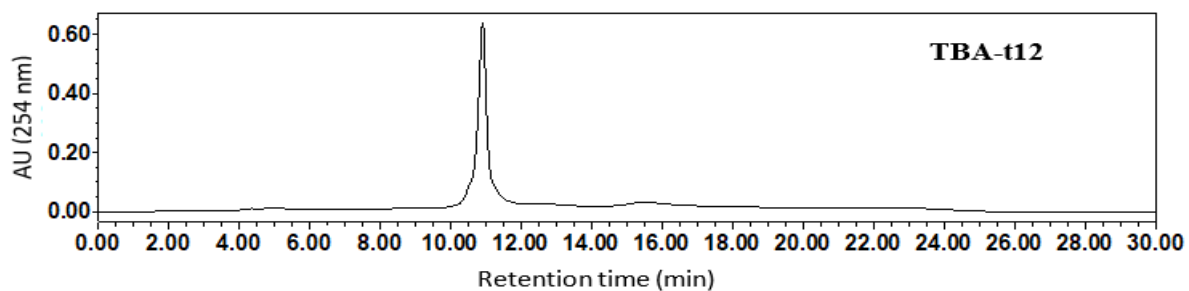
**HPLC chromatogram of TBA-t4**



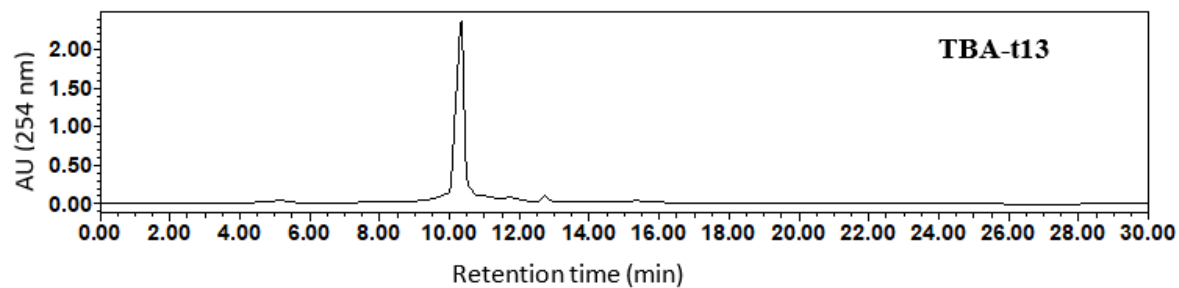
**HPLC chromatogram of TBA-t7**



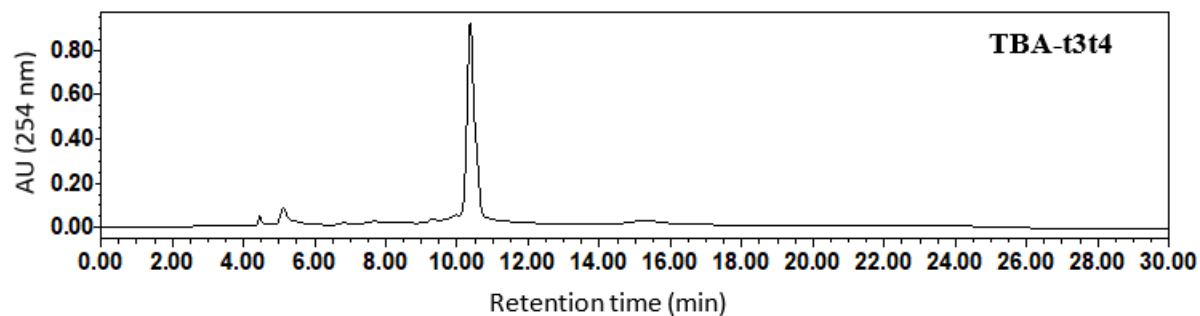
**HPLC chromatogram of TBA-t9**



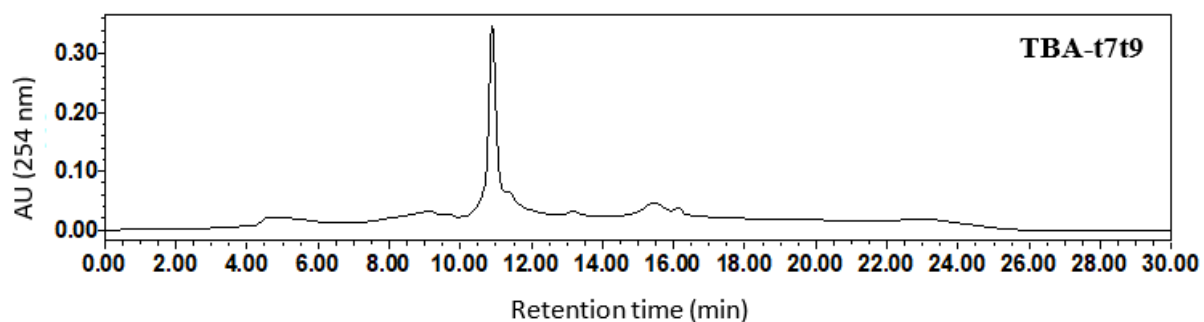
**HPLC chromatogram of TBA-t12**



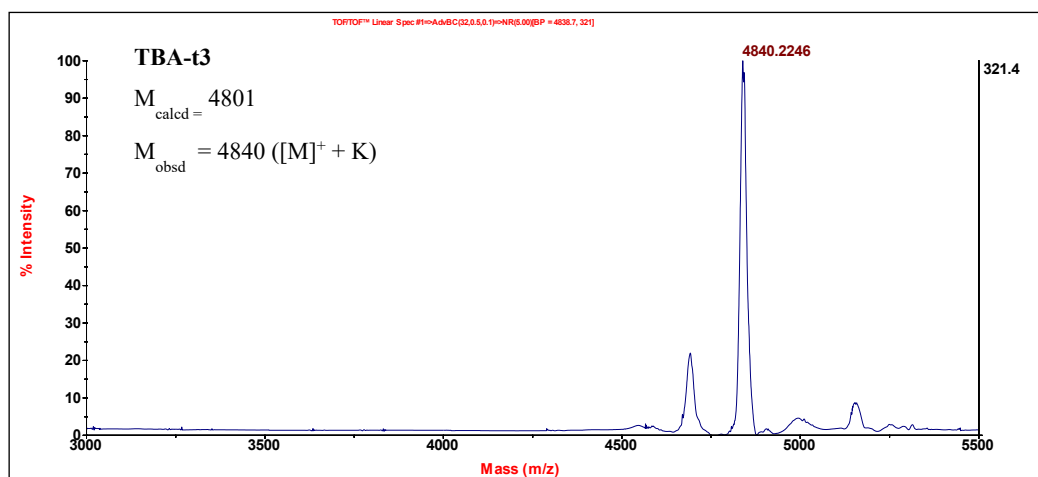
**HPLC chromatogram of TBA-t13**



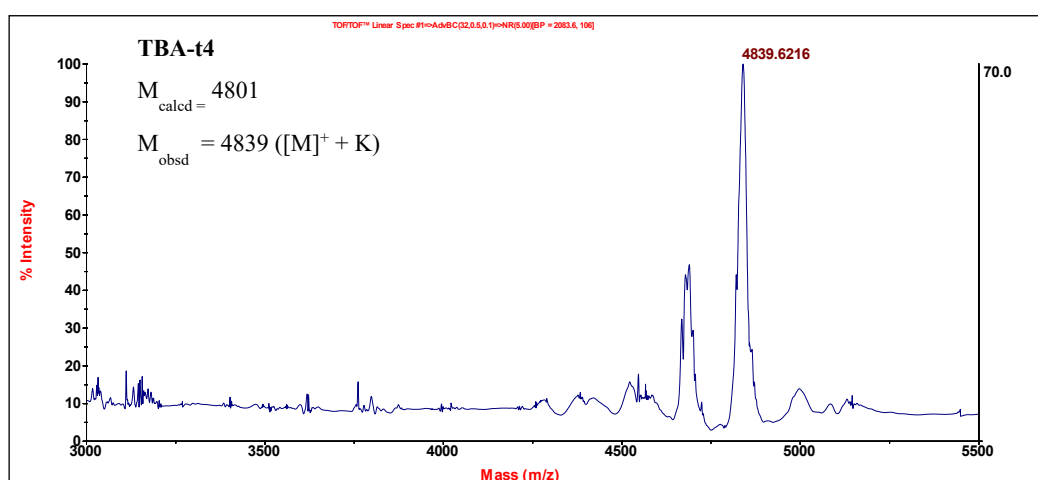
**HPLC chromatogram of TBA-t3t4**



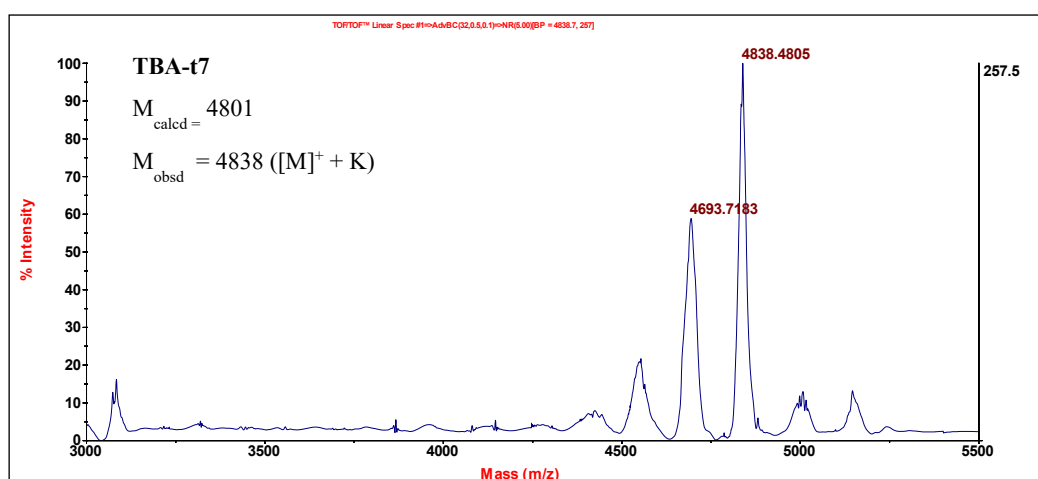
**HPLC chromatogram of TBA-t7t9**



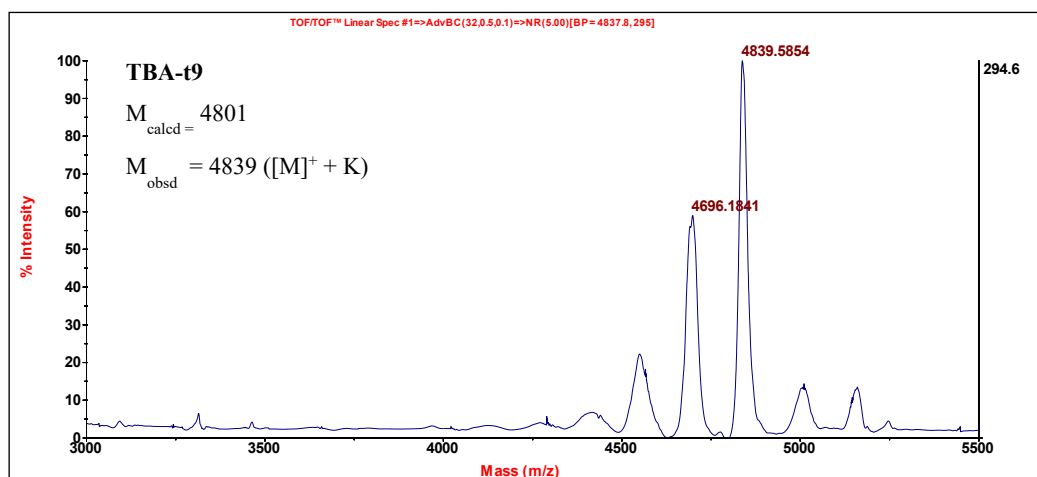
MALDI-TOF spectra of TBA-t3



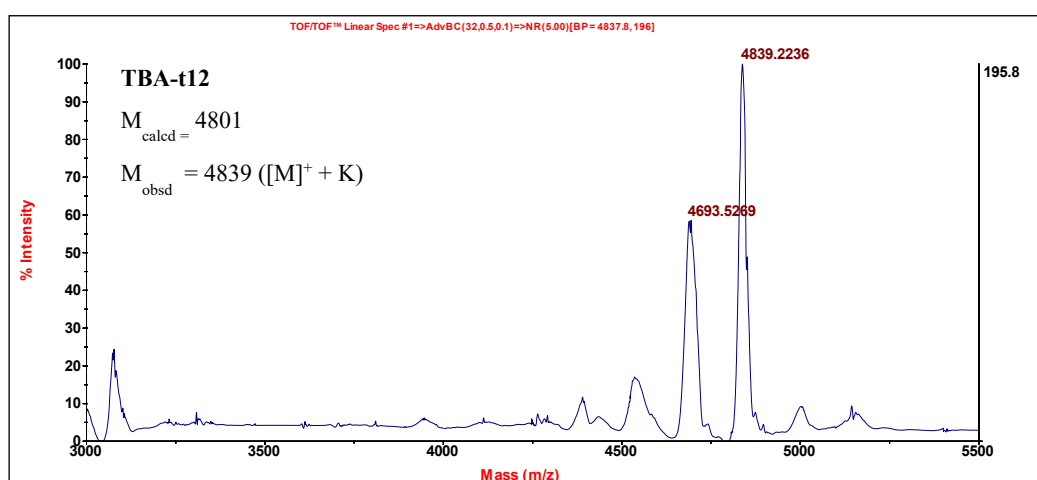
MALDI-TOF spectra of TBA-t4



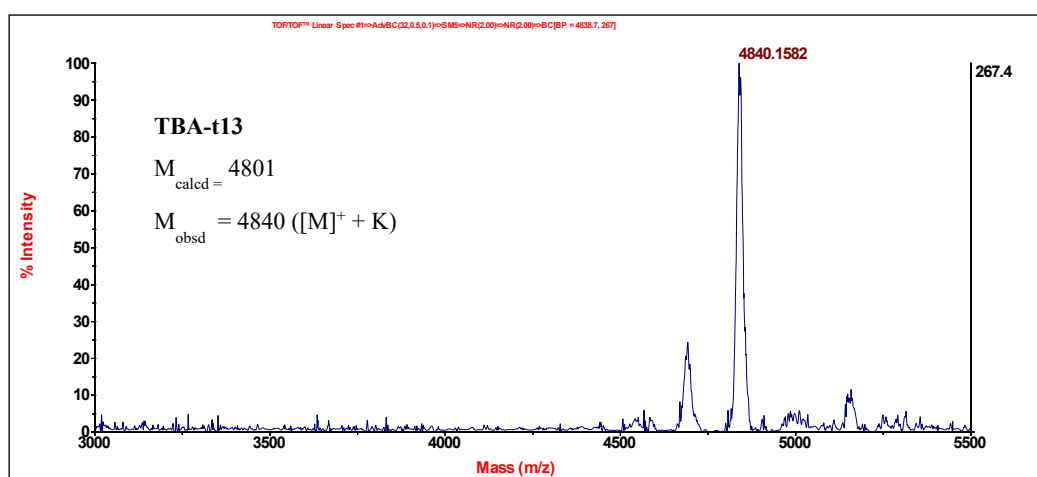
MALDI-TOF spectra of TBA-t7



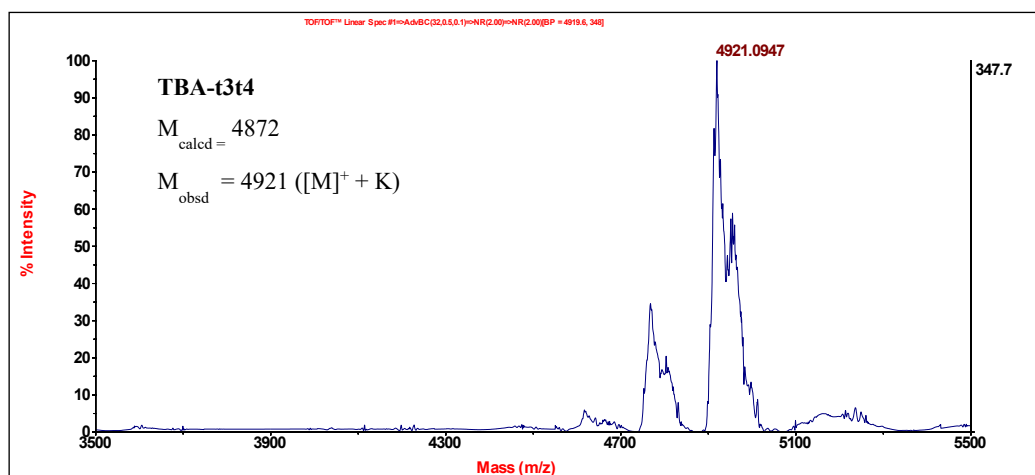
MALDI-TOF spectra of TBA-t9



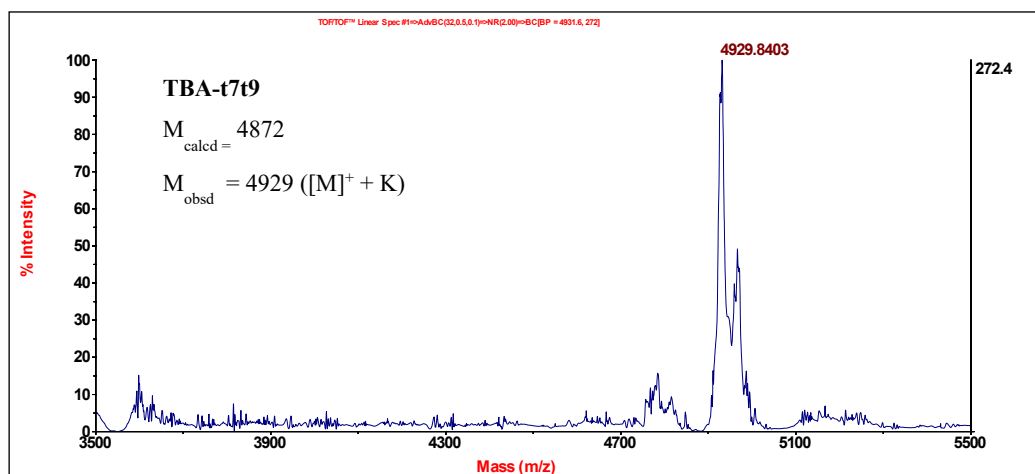
MALDI-TOF spectra of TBA-t12



MALDI-TOF spectra of TBA-t13



MALDI-TOF spectra of TBA-t3t4



MALDI-TOF spectra of TBA-t7t9

## 5.12 References

- (1) Manoharan, M. 2'-Carbohydrate Modifications in Antisense Oligonucleotide Therapy: Importance of Conformation, Configuration and Conjugation. *Biochim. Biophys. Acta Gene Struct. Expr.* **1999**, 1489 (1), 117–130.
- (2) Awachat, R.; Wagh, A. A.; Aher, M.; Fernandes, M.; Kumar, V. A. Favorable 2'-Substitution in the Loop Region of a Thrombin-Binding DNA Aptamer. *Bioorg. Med. Chem. Lett.* **2018**, 28 (10), 1765–1768.
- (3) Saccà, B.; Lacroix, L.; Mergny, J. L. The Effect of Chemical Modifications on the Thermal Stability of Different G-Quadruplex-Forming Oligonucleotides. *Nucleic Acids Res.* **2005**, 33 (4), 1182–1192.
- (4) Peng, C. G.; Damha, M. J. G-Quadruplex Induced Stabilization by 2'-Deoxy-2'-Fluoro-D-Arabinonucleic Acids (2'F-ANA). *Nucleic Acids Res.* 2007, 4977–4988.

- (5) Damha, M. J.; Noronha, A. M.; Wilds, C. J.; Trempe, J. F.; Denisov, A.; Pon, R. T.; Gehring, K. Properties of Arabinonucleic Acids (ANA & 2'-ANA): Implications for the Design of Antisense Therapeutics That Invoke RNase H Cleavage of RNA. *Nucleosides, Nucleotides and Nucleic Acids* **2001**, *20* (4–7), 429–440.
- (6) Catry, M. A.; Madder, A. Synthesis of Functionalised Nucleosides for Incorporation into Nucleic Acid-Based Serine Protease Mimics. *Molecules* **2007**, *12*, 114–129.
- (7) Hendrix, C.; Devreese, B.; Rozenski, J.; Van Aerschot, A.; De Bruyn, A.; Van Beeumen, J.; Herdewijn, P. Incorporation of 2'-Amido-Nucleosides in Oligodeoxyribonucleotides and Oligoribonucleotides as a Model for 2'-Linked Conjugates. *Nucleic Acids Res.* **1995**, *23* (1), 51–57.
- (8) Divakar, K. J.; Reese, C. B. Reaction between 2, 2'-Anhydro-1- $\beta$ -D-Arabinofuranosyluracil and Thiolate Ions. *J. Chem. Soc. Perkin Trans. 1* **1982**, *1*, 1625–1628.
- (9) Fraser, A.; Wheeler, P.; Cook, P. D.; Sanghvi, Y. S. Synthesis and Conformational Properties of 2'-Deoxy-2'-Methylthio-Pyrimidine and Purine Nucleosides: Potential Antisense Applications. *J. heterocyclic Chem.* **1993**, *30* (5), 1277–1287.
- (10) Košutic, M.; Jud, L.; Da Veiga, C.; Frener, M.; Fauster, K.; Kreutz, C.; Ennifar, E.; Micura, R. Surprising Base Pairing and Structural Properties of 2-Trifluoromethylthio-Modified Ribonucleic Acids. *J. Am. Chem. Soc.* **2014**, *136* (18), 6656–6663.
- (11) Marathias, V. M.; Sawicki, M. J.; Bolton, P. H. 6-Thioguanine Alters the Structure and Stability of Duplex DNA and Inhibits Quadruplex DNA Formation. *Nucleic Acids Res.* **1999**, *27* (14), 2860–2867.
- (12) Mendelboum Raviv, S.; Horváth, A.; Aradi, J.; Bagoly, Z.; Fazakas, F.; Batta, Z.; Muszbek, L.; Hársfalvi, J. 4-Thio-Deoxyuridylate-Modified Thrombin Aptamer and Its Inhibitory Effect on Fibrin Clot Formation, Platelet Aggregation and Thrombus Growth on Subendothelial Matrix. *J. Thromb. Haemost.* **2008**, *6* (10), 1764–1771.
- (13) Zaitseva, M.; Kaluzhny, D.; Shchylkina, A.; Borisova, O.; Smirnov, I.; Pozmogova, G. Conformation and Thermostability of Oligonucleotide d(GGTTGGTGTGGTTGG) Containing Thiophosphoryl Internucleotide Bonds at Different Positions. *Biophys. Chem.* **2010**, *146* (1), 1–6.
- (14) Yang, X.; Zhu, Y.; Wang, C.; Guan, Z.; Zhang, L.; Yang, Z. Alkylation of Phosphorothioated Thrombin Binding Aptamers Improves the Selectivity of Inhibition of Tumor Cell Proliferation upon Anticoagulation. *Biochim. Biophys. Acta Gen. Subj.* **2017**, *1861* (7), 1864–1869.

- (15) Geary, R. S.; Norris, D.; Yu, R.; Bennett, C. F. Pharmacokinetics, Biodistribution and Cell Uptake of Antisense Oligonucleotides. *Adv. Drug Deliv. Rev.* **2015**, *87*, 46–51.
- (16) Evich, M.; Spring-Connell, A. M.; Germann, M. W. Impact of Modified Ribose Sugars on Nucleic Acid Conformation and Function. *Heterocycl. Commun.* **2017**, *23* (3), 155–165.
- (17) Obika, S.; Morio, K. I.; Nanbu, D.; Imanishi, T. Synthesis and Conformation of 3'-O,4'-C-Methyleneribonucleosides, Novel Bicyclic Nucleoside Analogues for 2',5'-Linked Oligonucleotide Modification. *Chem. Commun.* **1997**, *17*, 1643–1644.
- (18) Gait, M. J. *Oligonucleotide Synthesis : A Practical Approach*; Rev. repr. ed.; Oxford : IRL press, **1984**.
- (19) Karsisiotis, A. I.; Hessari, N. M. A.; Novellino, E.; Spada, G. P.; Randazzo, A.; Webba Da Silva, M. Topological Characterization of Nucleic Acid G-Quadruplexes by UV Absorption and Circular Dichroism. *Angew. Chemie - Int. Ed.* **2011**, *50* (45), 10645–10648.
- (20) Baldrich, E.; Sullivan, C. K. O. Ability of Thrombin to Act as Molecular Chaperone , Inducing Formation of Quadruplex Structure of Thrombin-Binding Aptamer. *Anal. Biochem.* **2005**, *341*, 194–197.
- (21) Nagatoishi, S.; Tanaka, Y.; Tsumoto, K. Circular Dichroism Spectra Demonstrate Formation of the Thrombin-Binding DNA Aptamer G-Quadruplex under Stabilizing-Cation-Deficient Conditions. *Biochem. Biophys. Res. Commun.* **2007**, *352* (3), 812–817.
- (22) Mann, K. G.; Jenny, R. J.; Krishnaswamy, S. Cofactor Proteins in the Assembly and Expression of Blood Clotting Enzyme Complexes. *Annu Rev Biochem* **1988**, *57*, 915–956.
- (23) Jensen, T. B.; Henriksen, J. R.; Rasmussen, B. E.; Rasmussen, L. M.; Andresen, T. L.; Wengel, J.; Pasternak, A. Thermodynamic and Biological Evaluation of a Thrombin Binding Aptamer Modified with Several Unlocked Nucleic Acid (UNA) Monomers and a 2'-C-Piperazino-UNA Monomer. *Bioorg. Med. Chem.* **2011**, *19* (16), 4739–4745.

**List of Posters Presented with Details**

1. National Science Day **Poster presentation** at CSIR-National Chemical Laboratory, Pune (February 23-24, **2017**):

**Title: Cation-induced unprecedented parallel G-quadruplexes in 2'-5'-linked isoTBA**

**Abstract:** Guanine-rich oligonucleotides fold into guanine quadruplex (G-quadruplex) structures in the presence of certain cations. Quadruplexes can be formed from one, two or four separate strands of DNA (or RNA) and can display a wide variety of topologies, which are in part a consequence of various possible combinations of strand direction, as well as variations in loop size and sequence, we examine fundamental aspects of topology and the emerging relationships with sequence and different monovalent and divalent cation. We discovered isoTBA shows parallel G-quadruplex with  $\text{Sr}^{2+}$ .

2. **Oral presentation** at National Institute of Science Education and Research, Bhubaneswar, Odisha, India (December 22-24, **2018**)

**Title: Parallel isoTBA G-quadruplex Formation Dictated by Metal Ions**

**Abstract:** The thrombin-binding aptamer (TBA) is very widely-studied and is known to fold into a unimolecular antiparallel GQ in the presence of  $\text{K}^+$  ions. In this study, we show that in the presence of selected metal ions, iso-TBA folds into a parallel GQ, a structure that has previously never been observed for this oligomer, even in the presence of shortened loops. This observation is in contrast to that observed for the TBA.

**List of Conference Attended with Details**

International Society For Nucleosides, Nucleotides And Nucleic Acids- IS3NA Virtual Symposium on Phosphates Run the World: Chemical Biology and Applications of Nucleosides, Nucleotides and Nucleic Acids. (August 26-27, **2021**)



**List of Publications Emanating from the Thesis Work**

1. **Wagh A. A.**, Fernandes M., 2'-5'-Isomerically Linked Thrombin-Binding Aptamer (isoTBA) Forms a Stable Unimolecular Parallel G-Quadruplex in the Presence of Sr<sup>2+</sup> Ions. (*ChemistrySelect.* **2019** , 4, 10668-10673)
2. **Wagh A. A.**, Ghalawat M., Fernandes M., Replacement of Loop Residues in TBA by an Abasic Ethylene Glycol Spacer: Effect on Stability Structure and Function\*\* (*ChemistrySelect.* **2021** , 6, 10648-10650)
3. **Wagh A. A.**, Fernandes M. 2'-5'-linked RNA thrombin binding aptamer (iso-rTBA) forms a functional antiparallel G-quadruplex. (*Manuscript to be Submitted*)
4. **Wagh A. A.**, Fernandes M. Synthesis of 2'-thiopropyl thymidine nucleosides, their conformation studies, and incorporation into TBA. (*Manuscript under preparation*)

**List of Publications Non-Emanating from the Thesis Work**

1. Awachat R., **Wagh A. A.**, Aher M., Fernandes M., Kumar V. A., Favorable 2'-substitution in the loop region of a thrombin-binding DNA aptamer. (*Bioorg. Med. Chem. Lett.* **2018**, 28, 1765-1768)

## ■ Biological Chemistry &amp; Chemical Biology

# 2'-5'-Isomerically Linked Thrombin-Binding Aptamer (isoTBA) Forms a Stable Unimolecular Parallel G-Quadruplex in the Presence of Sr<sup>2+</sup> Ions

Atish A. Wagh<sup>[a, b]</sup> and Moneesha Fernandes<sup>\*[a, b]</sup>

The ability of the isomerically linked 2'-5'-phosphodiester thrombin binding DNA aptamer pentadecamer G<sub>2</sub>T<sub>2</sub>G<sub>2</sub>TGTG<sub>2</sub>T<sub>2</sub>G<sub>2</sub> (isoTBA) to fold into G-quadruplex structures in the presence of different mono- and divalent cations is reported. Strikingly, Sr<sup>2+</sup> ions cause isoTBA to fold into a stable parallel unimolecular G-quadruplex, in contrast to the antiparallel unimolecular G-quadruplex fold observed in the presence of K<sup>+</sup>. IsoTBA being advantageously more stable than TBA to nuclease degradation, may thus be useful in the selective detection of Sr<sup>2+</sup> ions, which it can sense with a detection limit of ~ 55 μM.

G-quadruplexes are formed as a consequence of stacking of successive G-quartets, that are in turn stabilized by cyclic hydrogen bonding of four guanine residues.<sup>[1]</sup> The G-quartets are further stabilized by the presence of metal ions, that are typically located between two successive G-quartets and are tightly associated through co-ordination to the guanine O6-carbonyl groups of the neighbouring planes.<sup>[2]</sup> The thrombin-binding pentadecameric aptamer (TBA), d(G<sub>2</sub>T<sub>2</sub>G<sub>2</sub>TGTG<sub>2</sub>T<sub>2</sub>G<sub>2</sub>) is very widely-studied and is known to fold into a unimolecular antiparallel G-quadruplex in the presence of K<sup>+</sup> ions.<sup>[3]</sup> This quadruplex comprises two G-quartets stacked on each other, connected by three edge-wise loops: two TT loops and one central TGT loop. The role of different cations in the formation of this structure was earlier reported.<sup>[4]</sup> Although several monovalent and divalent cations were studied, in all cases, the unimolecular antiparallel quadruplex topology was observed.<sup>[4]</sup> The stability of the resulting TBA G-quadruplexes was rationally explained to be a consequence of the ionic radii, with cations possessing an ionic radius in the range 1.3 Å to 1.5 Å leading to stabler quadruplexes compared to others, owing to a favourable fit between the two G-quartets. Such a study has not been reported with isoTBA.

A number of modifications in the sugar-phosphate backbone of TBA have been reported with a view to enhancing its properties.<sup>[5]</sup> We earlier reported an isoTBA oligomer wherein the natural 3'-5'-phosphodiester backbone linkages were replaced by the isomeric 2'-5'-phosphodiester, and showed that it could fold into a unimolecular antiparallel G-quadruplex structure, similar to that observed for TBA and also effect anti-coagulation.<sup>[6]</sup> The isomeric backbone in this oligomer leads to further enhancement in the nuclease resistance properties of the G-quadruplex and is therefore, attractive in the context of application in biological systems. Further, studies on loop-edited isoTBA oligomers<sup>[7]</sup> led to the observation that even oligomers containing the shortest loops (only one T per loop and totally 3 loop residues) retained the unimolecular antiparallel quadruplex fold, completely in contrast to the TBA oligomers, where shorter loop lengths (total number of loop residues less than 6) were found to result in multimolecular parallel quadruplexes, as reported for several other G-quadruplex sequences as well.<sup>[8]</sup> However, a change of the metal ion from K<sup>+</sup> to Sr<sup>2+</sup> during quadruplex formation was found to result in a switch of conformations from an antiparallel to a stable parallel quadruplex in the case of isoTBA. Such a unimolecular parallel quadruplex has not been reported before for any variant of TBA. The TBA RNA oligomer was reported to form a parallel quadruplex, but a multimolecular one.<sup>[9]</sup> The unique ability of Sr<sup>2+</sup> ions to induce stable unimolecular parallel G-quadruplex formation in isoTBA may be exploited in the detection of Sr<sup>2+</sup> ions, as the detection limit is in the low micromolar range.

3'-5'-phosphodiester-linked TBA and 2'-5'-phosphodiester-linked isoTBA oligonucleotides were synthesized in-house employing commercially available β-cyanoethyl phosphoramidites. Post-synthesis, they were purified by reverse-phase HPLC and their identity confirmed by MALDI-TOF mass analysis (SI, Figure S1).

CD spectroscopy is a valuable and widely-used technique to evaluate the formation and conformations of G-quadruplexes. A maximum at ~ 260 nm with a minimum at ~ 240 nm may be attributed to the stacking of successive guanines with the same (both *syn* or both *anti*) glycosidic bond angle and is thus a characteristic of parallel quadruplexes.<sup>[10,11]</sup> There is thus, no evident signal at ~ 290 nm in these quadruplexes. On the other hand, antiparallel quadruplexes display a maximum at ~ 290 nm, and a minimum at ~ 260 nm, which

[a] A. A. Wagh, Dr. M. Fernandes  
Organic Chemistry Division,  
CSIR-National Chemical Laboratory (CSIR-NCL),  
Dr. Homi Bhabha Road, Pune 411008, India  
E-mail: m.dcosta@ncl.res.in

[b] A. A. Wagh, Dr. M. Fernandes  
Academy of Scientific and Innovative Research (AcSIR),  
Ghaziabad 201002, India

Supporting information for this article is available on the WWW under  
<https://doi.org/10.1002/slct.201902005>

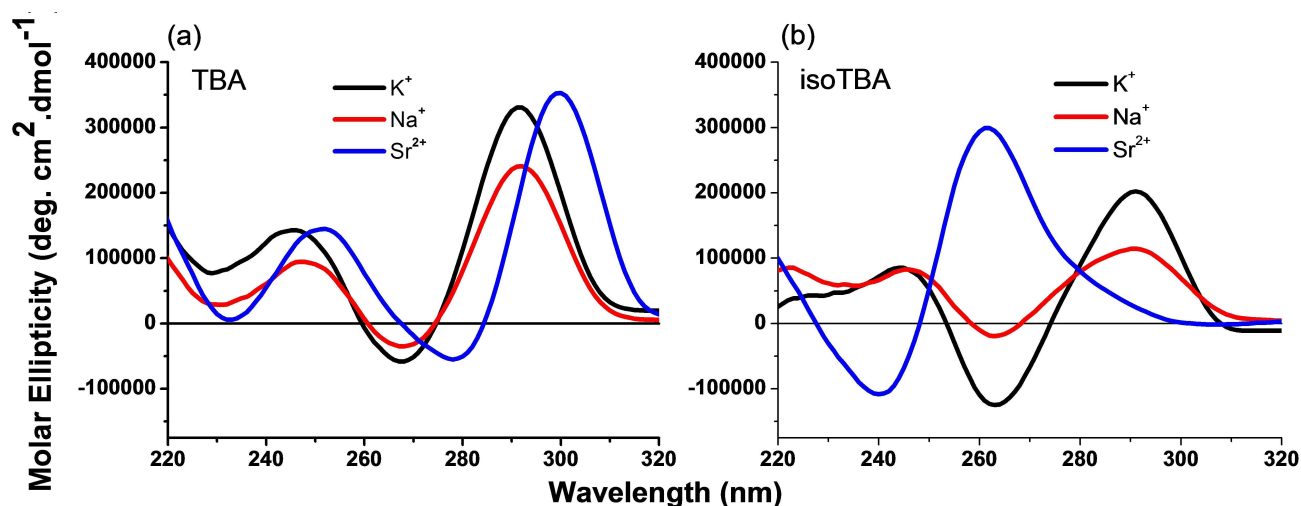


**Figure 1.** CD spectra in the presence of  $\text{Na}^+$ ,  $\text{K}^+$  or  $\text{Sr}^{2+}$  ions, of (a) TBA and (b) isoTBA. The TBA/isoTBA oligomers were taken at a concentration of  $5 \mu\text{M}$  and spectra were recorded in 10 mM Tris buffer, pH 7.2, containing 100 mM  $\text{Na}^+$ ,  $\text{K}^+$  or  $\text{Sr}^{2+}$  ions respectively at  $4^\circ\text{C}$ .

arises as a result of guanosines with different glycosidic bond angles stacking on each other.<sup>[11]</sup>

In the presence of  $\text{Na}^+$  and  $\text{K}^+$  ions, the typical antiparallel topology was observed for both, TBA and isoTBA, as reported earlier.<sup>[4,6]</sup> Both displayed maxima centered at 292 nm and minima near 260 nm. In the presence of  $\text{Sr}^{2+}$ , however, starkly contrasting spectra were observed with TBA and isoTBA. TBA displayed a CD spectrum corresponding to an antiparallel G-quadruplex, as reported earlier,<sup>[4]</sup> with a maximum at 300 nm, while the CD spectrum of isoTBA suggested a parallel G-quadruplex, with a strong maximum at 260 nm and a minimum at 240 nm (Figure 1).

Some differences were also observed in the presence of the other ions studied, but these were not so remarkable. The CD spectra of TBA in the presence of  $\text{Li}^+$ ,  $\text{Cs}^+$ ,  $\text{Mg}^{2+}$  and  $\text{Ba}^{2+}$  indicated the presence of antiparallel quadruplexes (SI, Figure S2 (a)), as reported earlier, with the 292 nm maximum red-shifted to 300 nm in presence of  $\text{Ba}^{2+}$ .<sup>[4]</sup> The CD signals of isoTBA in the presence of  $\text{Li}^+$ ,  $\text{Cs}^+$ ,  $\text{Mg}^{2+}$  and  $\text{Ba}^{2+}$ , on the other hand, were inconclusive and of very low intensity (SI, Figure S2 (b)). In the presence of other cations  $\text{Ca}^{2+}$ ,  $\text{Cr}^{3+}$  and  $\text{Mn}^{2+}$ , the CD spectrum of isoTBA was inconclusive and even in the presence of  $\text{Ca}^{2+}$ , where a slight maximum was observed around 260 nm, this was very close to the spectrum of isoTBA alone in PBS (SI, Figure S2(c)). The amplitude of the maximum was found to vary with the cation, consistent with earlier reports.<sup>[4]</sup> The observed differences in the strength of the CD signal, apparent as differential CD amplitude could be a consequence of differences in co-ordination number of the metal ions and the strength of the complex formed, which in turn also depends on the charge and ionic radius.<sup>[4]</sup> Thus, a decreased CD amplitude could result from partially unfolded structures, owing to the low thermal stability of the quadruplex. Although the magnitude of the CD band at a particular wavelength could differ, depending on the cation, all CD spectra with a common maximum showed an isoelliptic point

at 275 nm for TBA and at 280 nm for isoTBA, indicating the formation of similar type of complexes in terms of molecularity.

The thermal stability of the observed quadruplexes was assessed by temperature-dependent changes that were followed by CD and UV spectroscopy. The CD melting data are indicated in Table 1, and the melting plots are shown in the SI

**Table 1.** CD- and UV-melting data for the TBA/isoTBA quadruplexes in the presence of different cations.

Sr. No.	Cation	TBA		isoTBA	
		CD- $T_m$ ( $^\circ\text{C}$ )	UV- $T_m$ ( $^\circ\text{C}$ )	CD- $T_m$ ( $^\circ\text{C}$ )	UV- $T_m$ ( $^\circ\text{C}$ )
1	$\text{Li}^+$	$20 \pm 1$	$14 \pm 2$	nd	nd
2	$\text{Na}^+$	$22 \pm 1.5$	$21 \pm 1$	$19 \pm 0.5$	$21 \pm 1$
3	$\text{K}^+$	$49 \pm 0.5$	$51 \pm 0.5$	$29 \pm 1$	$29 \pm 1$
4	$\text{Cs}^+$	$20 \pm 0.5$	$18 \pm 1$	nd	nd
5	$\text{Mg}^{2+}$	$16 \pm 1$	$14 \pm 1$	nd	nd
6	$\text{Sr}^{2+}$	$63 \pm 1$	$61 \pm 1$	$62^a \pm 1$	$63 \pm 1$
7	$\text{Ba}^{2+}$	$57 \pm 1.5$	$53 \pm 1.5$	$26 \pm 1$	$28 \pm 1$

<sup>a</sup>measured at 260 nm. nd = not detected. Measurements were carried out using TBA/isoTBA at  $5 \mu\text{M}$  concentration, in Tris buffer (10 mM), pH 7.2, containing the respective cation (100 mM) in the form of its chloride. Experiments were repeated at least three times and the average values are listed with the standard deviations.

(Figure S3). Among the monovalent ions studied, the most stable quadruplexes were formed in the presence of  $\text{K}^+$ , where TBA melted at  $49^\circ\text{C}$  and isoTBA at  $29^\circ\text{C}$ . On the whole, the quadruplexes formed were the most stable in the presence of  $\text{Sr}^{2+}$  ( $T_m = 63^\circ\text{C}$  and  $62^\circ\text{C}$  for TBA and isoTBA respectively).

The  $T_m$  values of TBA in the presence of the other ions followed the trend as reported earlier, with  $\text{Ba}^{2+}$  also leading to stable quadruplex formation ( $T_m = 57^\circ\text{C}$ ) while the quadruplexes of isoTBA in the presence of the other cations were comparatively unstable; with  $\text{Ba}^{2+}$ , the  $T_m$  was  $26^\circ\text{C}$ , while it was  $19^\circ\text{C}$  with  $\text{Na}^+$  and not clearly detectable with  $\text{Li}^+$ ,  $\text{Cs}^+$  or

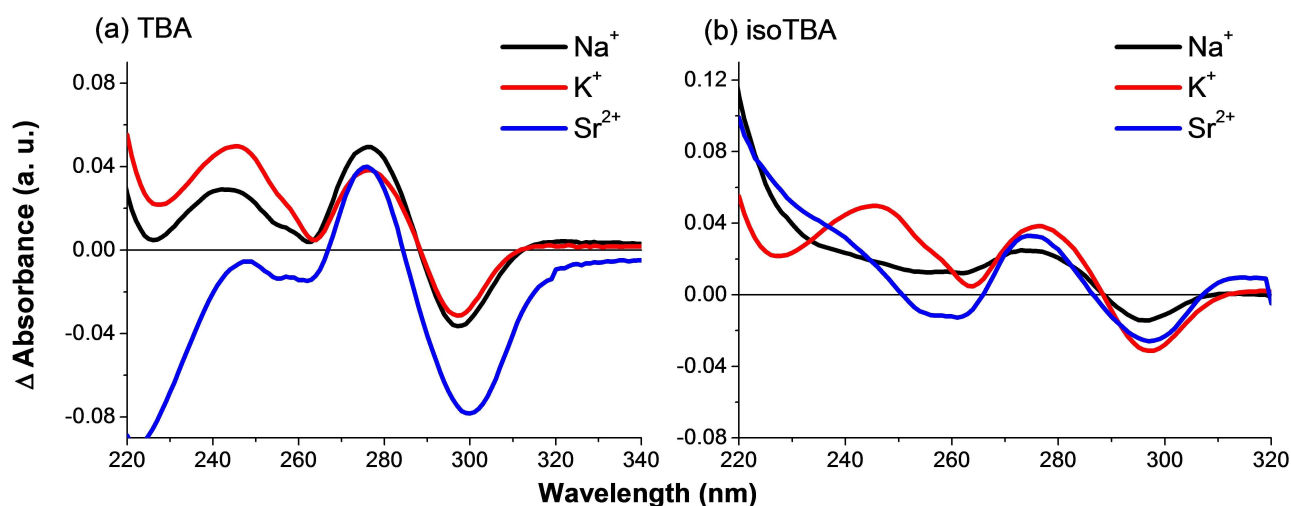


Figure 2. UV-TDS in the presence of  $\text{Na}^+$ ,  $\text{K}^+$  and  $\text{Sr}^{2+}$  for (a) TBA and (b) isoTBA.

Table 2. UV- $T_m$  data for TBA and isoTBA at 5  $\mu\text{M}$  and 20  $\mu\text{M}$  concentrations.

Cation	Strand conc ( $\mu\text{M}$ )	TBA ( $^{\circ}\text{C}$ )				isoTBA ( $^{\circ}\text{C}$ )			
		$T_m$ (heat)	$T_m$ (cool)	$\Delta T_m$ (20 $\mu\text{M}$ -5 $\mu\text{M}$ )	$\Delta T_m$ (heat-cool)	$T_m$ (heat)	$T_m$ (cool)	$\Delta T_m$ (20 $\mu\text{M}$ -5 $\mu\text{M}$ )	$\Delta T_m$ (heat-cool)
$\text{Sr}^{2+}$	5	61	61	+2	0	63	63	-2	0
$\text{Sr}^{2+}$	20	63	63	0	0	61	62	-1	-1
$\text{K}^+$	5	51	50	-2	+1	29	27	+3	+2
$\text{K}^+$	20	49 <sup>[6]</sup>	-	-	-	32	30	-	+2

$\text{Mg}^{2+}$ . The thermal stability of G-quadruplexes can also be conveniently monitored by UV-spectroscopy by measuring the temperature-dependent change in absorbance at 295 nm,<sup>[12]</sup> where transitions of other structures such as duplexes and triplexes do not interfere. The trend observed in the  $T_m$  of the quadruplexes when monitored by UV-spectroscopy, remained the same as that observed from the CD studies, and the values were in agreement with CD  $T_m$  (Table 1). Thus, both, TBA and isoTBA formed the most stable complexes in the presence of  $\text{Sr}^{2+}$  ions, with a  $T_m$  of 61  $^{\circ}\text{C}$  and 63  $^{\circ}\text{C}$  respectively.

G-quadruplex formation was further confirmed by the UV-Thermal difference spectra (TDS), that are obtained by recording the difference in UV absorption spectra above and below the melting temperature of the nucleic acid, and have been shown to be useful in the characterization of nucleic acid structures. The UV-TDS complements data obtained by CD and each nucleic acid structure has its own unique TDS. Accordingly, G-quadruplexes are characterized by a negative peak at  $295 \pm 1$  nm and positive peaks at  $273 \pm 2$  nm and  $243 \pm 1$  nm.<sup>[13]</sup> The UV-TDS for TBA and isoTBA in the presence of  $\text{Na}^+$ ,  $\text{K}^+$  and  $\text{Sr}^{2+}$  are shown in Figure 2, while the spectra with the other ions ( $\text{Li}^+$ ,  $\text{Cs}^+$ ,  $\text{Ba}^{2+}$ ,  $\text{Mg}^{2+}$ ) are depicted in the SI (Figure S4). Except in the presence of  $\text{Mg}^{2+}$ , where no negative at 295 nm was observed with isoTBA, all the UV-TDS were found to conform to the G-quadruplex signature, and displayed negative peaks near 295 nm and positive peaks near 273 nm. The positive peak near 243 nm was not as obvious for isoTBA as compared to TBA, possibly indicative of a slight change in

the stacking of nucleobases in the quadruplex as a consequence of the 2'-5'-backbone and the nature of the different cations. Thus, all the other ions led to quadruplex formation with TBA and isoTBA, albeit of low thermal stability, as evident from the CD and UV melting studies. This was also apparent from the isothermal difference spectra (IDS, Figure S4).

Since stable parallel G-quadruplex formation was observed with isoTBA in the presence of  $\text{Sr}^{2+}$  ions, in order to confirm the molecularity of the complex, the UV plots during heating and subsequent cooling were analyzed for hysteresis, in comparison to TBA and to the complexes in presence of  $\text{K}^+$  ions. Negligible hysteresis ( $\Delta T_m \approx 0^{\circ}\text{C}$ , Table 2 and Figure S5, SI) was observed, in agreement with a unimolecular complex with  $\text{Sr}^{2+}$  for TBA and isoTBA. Further, when the UV- $T_m$  measurements were carried out at a higher strand concentration, including a ten-fold excess (Figures S5, S6, SI), no appreciable differences were observed ( $\Delta T_m = +2$  to  $-2^{\circ}\text{C}$ ), and also as observed earlier for TBA and isoTBA with  $\text{K}^+$ ,<sup>[6]</sup> again suggesting the unimolecularity of the quadruplex. The data are listed in Table 2. This study, thus constitutes the first report of a unimolecular parallel G-quadruplex for TBA with an isomeric backbone, that implies the presence of three propeller loops-two TT loops and one TGT loop. This is probably more easily accommodated in the case of the 2'-5'-linked isoTBA because of the extended 7-atom backbone that allows an optimum fit of the  $\text{Sr}^{2+}$  cation between the two G-tetrads. Additional stabilization of the G-quadruplex structure through extended stacking interactions or other interactions with the loop

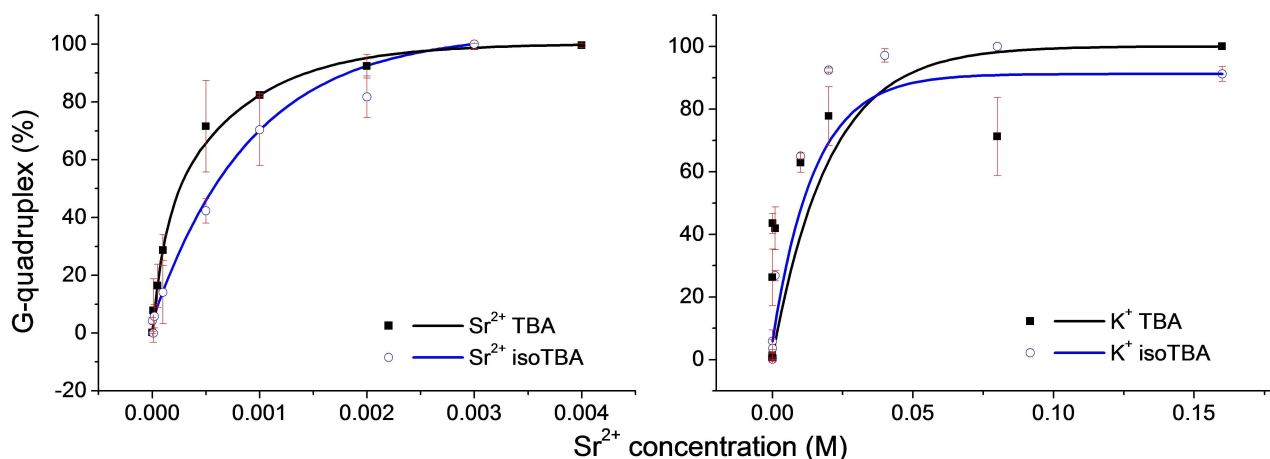


Figure 3. CD saturation binding curves for TBA and isoTBA with  $K^+$  and  $Sr^{2+}$ . The standard deviation is indicated by error bars

residues cannot be ruled out and requires more extensive evaluation through further NMR studies to be confirmed.

The  $K_d$  for complexes of  $K^+$  and  $Sr^{2+}$  with TBA and isoTBA were calculated from the CD saturation binding curves (Figure 3) obtained by titrating solutions of the TBA/isoTBA oligomers with the respective cations. The  $K_d$  value for  $Sr^{2+}$  with TBA and isoTBA was found to be one order of magnitude lower than for  $K^+$  (Table 3), indicating the higher affinity of this ion for binding to TBA/isoTBA.

Table 3. Dissociation constants for $K^+$ and $Sr^{2+}$ complexes with TBA/isoTBA.				
Oligomer	cation	$K_d$ (M)	cation	$K_d$ (M)
TBA	$K^+$	$9.54 \times 10^{-3}$	$Sr^{2+}$	$1.94 \times 10^{-4}$
isoTBA	$K^+$	$3.37 \times 10^{-3}$	$Sr^{2+}$	$9.82 \times 10^{-4}$

$K_d$  values in the table are averages that were calculated from two independent experiments.

The  $^1H$ NMR spectrum of isoTBA in the absence of any added cations (SI, Figure S7(a)) is devoid of any signals in the guanine imino proton region (10 to 12 ppm), where guanine residues typically hydrogen-bonded in a G-quadruplex are expected to appear.<sup>[14,15]</sup> In the presence of  $Sr^{2+}$  ions, broad imino proton signals were observed (Figure 4 and SI, Figure S7(b)), that have been reported in parallel G-quadruplexes.<sup>[14,16]</sup> These are in contrast to the sharp resonance signals observed for the antiparallel isoTBA G-quadruplex in the presence of  $K^+$  ions.<sup>[6]</sup> The imino proton signals for isoTBA were observed between 10.5 to 11.5 ppm in the presence of  $Sr^{2+}$ , while in the presence of  $K^+$ , they appear between 11.5 to 12.5 ppm.<sup>[6]</sup> This is similar to the observations with  $d(G_4C_2)_2$  quadruplexes, where the imino protons in the parallel quadruplex fold appeared between 10.5 to 11 ppm, while those in the antiparallel quadruplex fold appeared between 11 and

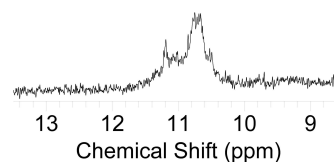


Figure 4. Imino proton region of the  $^1H$ NMR spectrum of isoTBA in the presence of  $Sr^{2+}$  ions. Spectra were recorded at 5 °C for a strand concentration of 200  $\mu$ M in 90:10 v/v  $H_2O:D_2O$ .

12 ppm.<sup>[17]</sup> This data further supports the existence of a parallel quadruplex fold for isoTBA in the presence of  $Sr^{2+}$ .

The comparative quadruplex-forming ability of TBA and isoTBA in the presence of  $K^+$  and  $Sr^{2+}$  ions was assessed by polyacrylamide gel electrophoresis. The complexes formed by isoTBA were found to have a slightly higher mobility than their TBA counterparts (Figure 5). However, no retarded bands were

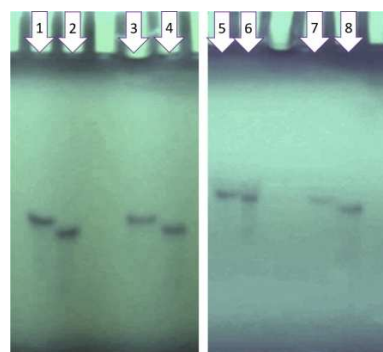
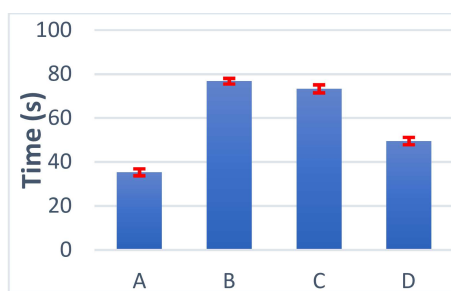


Figure 5. Non-denaturing polyacrylamide gel mobility assays of TBA and isoTBA in the presence of cations (100 mM). Lane 1 -  $Na^+$  TBA, lane 2 -  $Na^+$  isoTBA, lane 3 -  $K^+$  TBA, lane 4 -  $K^+$  isoTBA, lane 5 -  $Sr^{2+}$  TBA, lane 6 -  $Sr^{2+}$  isoTBA, lane 7 -  $Ba^{2+}$  TBA, lane 8 -  $Ba^{2+}$  isoTBA. The gel was visualized by UV-shadowing.

observed, as might be expected in the case of multimolecular complexes.<sup>[7]</sup> This further suggests that TBA and isoTBA form unimolecular quadruplexes with all the cations of the study. Further, both TBA and isoTBA are retarded to the same relative extent in the gel, suggesting complexes of the same molecularity. The complexes with  $\text{Sr}^{2+}$  were found to be slightly retarded in comparison to those in presence of  $\text{K}^+$  (SI, Figure S8); this difference may be attributed to the differences in mass and charge of the two ions.

The unique ability of isoTBA to fold into a parallel G-quadruplex in the presence of  $\text{Sr}^{2+}$  ions, and bind to it with high affinity, may be exploited in the detection of this cation. The detection limit was found to be  $\sim 55 \mu\text{M}$  (SI, Figure S9). Although this is not as low as that possible by inductively coupled plasma atomic emission spectroscopy (ICP-AES), Energy-dispersive X-ray fluorescence (EDXRF) or Zeeman atomic absorption spectrometry (Zeeman AAS), which are the methods reported for strontium detection, and where the detection limit is in the sub-micromolar range,<sup>[18–22]</sup> it offers a fairly sensitive alternative method for detection. Although G-quadruplexes are known to bind many different metal ions and some metal-binding aptamers, including TBA,<sup>[23]</sup> have also been reported,<sup>[24]</sup> there are no aptamers so far reported for  $\text{Sr}^{2+}$ , although  $\text{Sr}^{2+}$ -binding G-quadruplexes are known.<sup>[23–25]</sup> It is worth noting that the plots shown in the SI, Figure S10, were obtained by successively increasing  $\text{Sr}^{2+}$  ion concentrations in a solution of isoTBA taken in phosphate-buffered saline that contained both  $\text{Na}^+$  (137 mM) and  $\text{K}^+$  (2.7 mM) ions, both in sufficiently large excess compared to  $\text{Sr}^{2+}$  (1  $\mu\text{M}$   $\text{Sr}^{2+}$  ions, in the first case); in spite of this, the characteristic CD signature of a parallel G-quadruplex (of isoTBA +  $\text{Sr}^{2+}$ ) starts appearing. This is indicative of the selectivity and affinity of isoTBA for  $\text{Sr}^{2+}$ .

The anti-clotting activity of  $\text{Sr}^{2+}$  isoTBA was assessed in relation to TBA and isoTBA, in terms of inhibition of the thrombin-catalyzed fibrin polymerization. The anti-clotting effect was measured in terms of the additional time required for clotting in the presence of TBA/isoTBA when thrombin was added to fibrinogen. As shown in the Figure 6, the anti-clotting



**Figure 6.** Clotting time measured as the time required for fibrin polymerization upon addition of thrombin to fibrinogen. A. in the absence of TBA or isoTBA (control), B. in the presence of TBA (Standard 1), C. in the presence of isoTBA (Standard 2), and D. in the presence of  $\text{Sr}^{2+}$  isoTBA.

activity of isoTBA was severely reduced (clotting time 49 s) in the presence of  $\text{Sr}^{2+}$  ions, in comparison to TBA (clotting time

76 s) or isoTBA in the absence of  $\text{Sr}^{2+}$  ions (73 s). This may be expected, considering that the TT loops that are implicated in thrombin binding in the antiparallel TBA G-quadruplex, are not readily available for this interaction in the  $\text{Sr}^{2+}$  isoTBA unimolecular parallel G-quadruplex, as these TT loops would be propeller type. This reduced anti-clotting activity of  $\text{Sr}^{2+}$  isoTBA would be advantageous when considering the usefulness of isoTBA in  $\text{Sr}^{2+}$  detection in body fluids such as blood.

In conclusion, we have studied the effect of various alkali and alkaline earth metal cations on the G-quadruplex-forming ability of isoTBA. In contrast to all the other cations studied,  $\text{Sr}^{2+}$  was found to bind to isoTBA with high affinity and specificity and led to the formation of a parallel intramolecular quadruplex. This unique behaviour of isoTBA in the presence of  $\text{Sr}^{2+}$  together with its already reported higher resistance to nuclease-mediated degradation,<sup>[9]</sup> may be utilized in the detection of this cation in the micromolar range, which it senses with a detection limit of  $\sim 55 \mu\text{M}$ .

### Supporting Information Summary

Experimental section, HPLC chromatograms, MALDI-TOF spectra, CD, UV-TDA and UV-IDS spectra,  $K_d$  calculation,  $^1\text{H}$ NMR of isoTBA in the absence of any added cations, non-denaturing PAGE of isoTBA in presence of  $\text{K}^+$  and  $\text{Sr}^{2+}$ , detection limit calculation.

### Acknowledgements

AAW thanks UGC, New Delhi for a research fellowship. MF is grateful for a research grant from the Science and Engineering Research Board (SERB), India (EMR/2014/000481).

### Conflict of Interest

The authors declare no conflict of interest.

**Keywords:** parallel DNA G-quadruplex · 2'-5'-phosphodiester · strontium binding · thrombin-binding aptamer · unimolecular G-quadruplex

- [1] S. Balasubramanian, *Curr. Opin. Genet. Dev.* **2014**, *25*, 22–29.
- [2] S. Neidle, *Curr. Opin. Struct. Biol.* **2009**, *19*, 239–250.
- [3] J. A. Kelly, J. Feigon, T. O. Yeates, *J. Mol. Biol.* **1996**, *256*, 417–422.
- [4] B. I. Kankia, L. A. Marky, *J. Am. Chem. Soc.* **2001**, *123*, 10799–10804.
- [5] a) V. Esposito, A. Russo, V. Vellecco, M. Bucci, G. Russo, L. Mayol, A. Virfilio, A. Galeone, *Biochim. Biophys. Acta Gen. Subj.* **2018**, *1862*, 2645–2650. b) M. Scuto, E. Riviello, A. Varone, D. Corda, M. Bucci, V. Vellecco, G. Cirino, A. Virgilio, V. Esposito, A. Galeone, N. Borbone, M. Varra, L. Mayol, *Nucleic Acids Res.* **2015**, *43*, 7702–7716. c) A. Virgilio, M. Varra, M. Scuto, A. Capuozzo, C. Irace, L. Mayol, V. Esposito, A. Galeone, *ChemBioChem* **2014**, *15*, 652–655. d) L. Bonifacio, F. C. Church, M. B. Jarstfer, *Int. J. Mol. Sci.* **2008**, *9*, 422–433. e) A. Pasternak, F. J. Hernandez, L. M. Rasmussen, B. Vester, J. Wengel, *Nucleic Acids Res.* **2010**, *39*, 1155–1164. f) A. Joachimi, A. Benz, J. S. Hartig, *Bioorg. Med. Chem.* **2009**, *17*, 6811–6815. g) L. J. Aaldering, V. Poongavanam, N. Langkjær, N. A. Murugan, P. T. Jørgensen, J. Wengel, R. N. Veedu, *ChemBioChem* **2017**, *18*, 755–763. h) B. Sacca, L. Lacroix, J.-L. Mergny, *Nucleic Acids Res.* **2005**, *33*, 1182–1192. i) G. X. He, J. P. Williams, M. J. Postich, S. Swaminathan, R. G. Shea, T. Terhorst, V. S. Law, C. T. Mao, C. Sueoka, C. Coutre, N.

- Bishofberger, *J. Med. Chem.* **1998**, *41*, 4224–4231. j) A. M. Varizhuk, V. B. Tsvetkov, O. N. Tatarinova, D. N. Kaluzhny, V. L. Florentiev, E. N. Timofeev, A. K. Shcholykina, O. F. Borisova, I. P. Smirnov, S. L. Grokhovskiy, A. V. Aseychev, G. E. Pozmogova, *Eur. J. Med. Chem.* **2013**, *67*, 90–93.
- [6] A. D. Gunjal, M. Fernandes, N. Erande, P. R. Rajamohan, V. A. Kumar, *Chem. Commun.* **2014**, *50*, 605–607.
- [7] M. N. Aher, N. Erande, M. Fernandes, V. A. Kumar, *Org. Biomol. Chem.* **2015**, *13*, 11696–11703.
- [8] P. Hazel, J. Huppert, S. Balasubramanian, S. Neidle, *J. Am. Chem. Soc.* **2004**, *126*, 16405–16415.
- [9] a) C. F. Tang, R. H. Shafer, *J. Am. Chem. Soc.* **2006**, *128*, 5966–5973. b) A. Joachimi, A. Benz, J. S. Hartig, *Bioorg. Med. Chem.* **2009**, *17*, 6811–6815.
- [10] D. M. Gray, J. D. Wen, C. W. Gray, R. Repges, C. Repges, G. Raabe, J. Fleischhauer, *CHIRALITY*. **2008**, *20*, 431–440.
- [11] A. I. Karsiotis, N. M. Hessari, E. Novellino, G. P. Spada, A. Randazzo, M. Webba da Silva, *Angew. Chem. Int. Ed.* **2011**, *50*, 10645–10648.
- [12] J. L. Mergny, A. T. Phan, L. Lacroix, *FEBS Lett.* **1998**, *435*, 74–78.
- [13] J. L. Mergny, J. Li, L. Lacroix, S. Amrane, J. B. Chaires, *Nucleic Acids Res.*, **2005**, *33* (16), e138.
- [14] J. Zhu, A. M. Fleming, C. J. Burrows, *ACS Chem. Biol.* **2018**, *13*, 2577–2584.
- [15] A. T. Phan, Y. S. Modi, D. J. Patel, *J. Am. Chem. Soc.* **2004**, *126*, 8710–8716.
- [16] B. Zhou, C. Liu, Y. Geng, G. Zhu, *Sci. Rep.* **2015**, *5*, 16673.
- [17] B. Zhou, Y. Geng, C. Liu, H. Miao, Y. Ren, N. Xu, X. Shi, Y. You, T. Lee, G. Zhu, *Sci. Rep.* **2018**, *8*, 2366.
- [18] A. Pejovic-Milic, I. M. Stronach, J. Gyorffy, C. E. Webber, D. R. Chettle, *Med. Phys.* **2004**, *31*, 528–538.
- [19] A. J. Specht, F. Mostafaei, Y. Lin, J. Xu, L. H. Nie, *Appl. Spectrosc.* **2017**, *71*, 1962–1968.
- [20] P. C. D'Haese, G. F. Van Landeghem, L. V. Lamberts, V. A. Bekaert, I. Schrooten, M. E. De Broe, *Clinical Chem.* **1997**, *43*, 121–128.
- [21] R. Ying, *Int. J. Anal. Chem.* **2015**, *425084*, 5.
- [22] M. Piette, B. Desmet, R. Dams, *Sci. Total Environ.* **1994**, *141*, 269–273.
- [23] a) Z. Chen, L. Tan, L. Hu, Y. Luan, *Talanta* **2015**, *144*, 247–251. b) D. Zhang, L. Yin, Z. Meng, Z. A. Yu, L. Guo, H. Wang, *Anal. Chim. Acta.* **2014**, *812*, 161–167.
- [24] D. L. Ma, W. Wang, Z. Mao, T. S. Kang, Q. B. Han, P. W. Chan, C. H. Leung, *ChemPlusChem* **2017**, *82*, 8–17.
- [25] a) L. Lomidze, S. Kelley, S. Gogichaishvili, N. Metreveli, K. Musier-Forsyth, B. Kankia, *Biopolymers* **2016**, *105*, 811–818. b) E. Largy, A. Marchand, S. Amrane, V. Gabelica, J.-L. Mergny, *J. Am. Chem. Soc.* **2016**, *138*, 2780–2792. c) K.-H. Leung, V. P.-Y. Ma, H.-Z. He, D. S.-H. Chan, H. Yang, C.-H. Leung, D.-L. Ma, *RSC Adv.* **2012**, *2*, 8273–8276. d) K. Qu, C. Zhao, J. Ren, X. Qu, *Mol. Biosystems* **2012**, *8*, 779–782.

Submitted: May 31, 2019

Accepted: September 11, 2019

## Biological Chemistry &amp; Chemical Biology

## Replacement of Loop Residues in TBA by an Abasic Ethylene Glycol Spacer: Effect on Stability, Structure and Function\*\*

Atish A. Wagh,<sup>[a, b]</sup> Monika Ghalawat,<sup>[b, c]</sup> and Moneesha Fernandes<sup>\*[a, b]</sup>

This article describes the synthesis of ethyleneglycol (E) phosphoramidite and its incorporation into the thrombin binding aptamer (TBA) sequence at loop positions. Circular dichroism (CD) study revealed no major disturbances in the secondary structure of TBA by the abasic E unit and the derived oligomers exhibited a typical antiparallel chair-like conformation similar to that of TBA. UV and CD spectroscopy, together with anti-coagulation and HPLC studies revealed that although nuclease stability was enhanced, and anti-coagulation reasonably good, the thermal stability of the quadruplexes was adversely affected.

G-quadruplexes are highly ordered folded structures with various folding topologies and molecularities.<sup>[1]</sup> The thrombin binding aptamer (TBA)<sup>[2]</sup> is one such DNA sequence comprising 15 nucleotides i.e., 5'-GGTTGGTGTGGTTGG-3' and is a result of in vitro selection targeted towards thrombin. NMR and X-ray crystal studies show that TBA folds in an intramolecular, antiparallel fashion with a chair-like conformation consisting of two G-quartets linked by three loops- two TT loops and one TGT loop.<sup>[2-4]</sup> Although this sequence exhibits anticoagulant effects, it falls short due to its early degradation in vivo.<sup>[5]</sup> To overcome this problem while increasing the anti-clotting effect, many nucleotide and backbone modifications have been reported.<sup>[6]</sup> Among the studies that involved replacement of the loop residues by abasic units, were those that introduced a dibenzyl linker,<sup>[7]</sup> anthraquinone units,<sup>[8]</sup> tetrapeptides,<sup>[9]</sup> a 3-carbon abasic spacer,<sup>[10]</sup> anthracene groups,<sup>[11]</sup> and azobenzene derivatives.<sup>[12]</sup> An enhancement in the thermal stability of the

resulting quadruplexes was reported for the dibenzyl linker,<sup>[7]</sup> double anthraquinone units,<sup>[8]</sup> single anthracene substitution at T9,<sup>[11]</sup> C3-spacer<sup>[10]</sup> and selected azobenzene substitutions.<sup>[12]</sup> The dibenzyl and C3-spacer were also found to increase the clotting time.<sup>[7,10]</sup> Nuclease stability studies were not reported. The increased flexibility offered by the simplest among these, i.e., the abasic 3-carbon spacer, at position T7, resulted in significant improvement in thermal stability and thrombin clotting time.<sup>[10]</sup> We envisioned the synthesis of abasic spacer units derived from ethylene glycol (Figure 1) as replacement of loop residues in an attempt to further simplification and arrive at a minimal spacer unit, that would preferably retain or improve the stability and anti-coagulant properties of TBA. This E spacer was incorporated at single or double positions in the T<sup>3</sup>T<sup>4</sup> and T<sup>7</sup>G<sup>8</sup>T<sup>9</sup> loops of TBA, as the TT and TGT loops are implicated in the interaction with, and subsequent inhibition of, thrombin.<sup>[13,14]</sup>

The abasic ethylene glycol spacer phosphoramidite was synthesized employing simple chemical transformations as outlined in Scheme 1 and slight modification of earlier reported procedures.<sup>[15]</sup> Accordingly, commercially available ethylene glycol was converted to the mono-dimethoxytrityl (DMTr)-

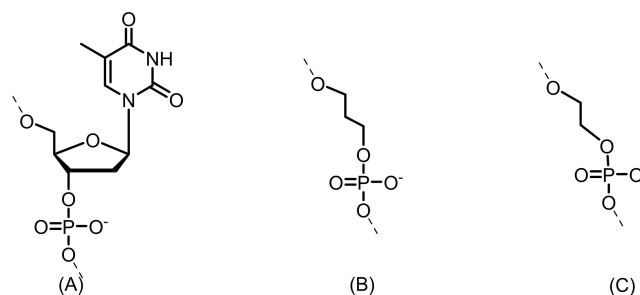
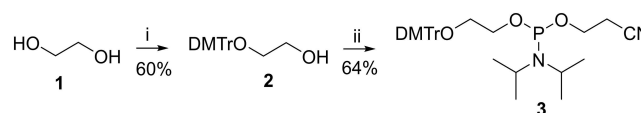


Figure 1. (A) A thymidine (T) residue in comparison to (B) abasic propyl (C3) linker<sup>[10]</sup> and (C) abasic ethyl (E) spacer of this work.



Scheme 1. Synthesis of ethylene glycol phosphoramidite. Reagents and conditions: (i) DMTrCl, DMAP, pyridine, 2 h, r.t., 60% (ii) 2-Cyanoethyl-*N,N*-diisopropylchlorophosphine, EtN(*i*Pr)<sub>2</sub>, dry CH<sub>2</sub>Cl<sub>2</sub>, 1 h, r.t., 64%.

[a] A. A. Wagh, Dr. M. Fernandes  
Organic Chemistry Division,  
CSIR-National Chemical Laboratory (CSIR-NCL)  
Dr. Homi Bhabha Road  
Pune 411008, India  
E-mail: m.dcosta@ncl.res.in

[b] A. A. Wagh, M. Ghalawat, Dr. M. Fernandes  
Academy of Scientific and Innovative Research (AcSIR)  
Ghaziabad 201002, India

[c] M. Ghalawat  
Physical and Materials Chemistry Division,  
CSIR-National Chemical Laboratory (CSIR-NCL)  
Pune 411008, India

[\*\*] TBA = thrombin binding aptamer

Supporting information for this article is available on the WWW under <https://doi.org/10.1002/slct.202102269>



protected compound **2** on treatment with DMTr-chloride in presence of 4-dimethylaminopyridine (DMAP) with pyridine as a solvent in 60% yield. Further, reacting compound **2** with 2-cyanoethyl-*N,N*-diisopropylchlorophosphine in  $\text{CH}_2\text{Cl}_2$  in presence of diisopropylethylamine gave the phosphoramidite **3** in 64% yield. Compound **3** was further used as the protected monomer for oligonucleotide synthesis.

TBA and modified TBA oligonucleotides containing E spacer units incorporated at pre-determined positions were synthesized by  $\beta$ -cyanoethyl phosphoramidite chemistry, using an increased coupling time of 150 s for this unit. The synthesized oligomers were cleaved from the solid support using aqueous ammonia, purified by RP-HPLC and characterized by MALDI-TOF spectrometry (Supporting information, Figures S4 and S5). The E units were introduced either at single positions or as double replacements of T residues in the  $\text{T}^3\text{T}^4$  and  $\text{T}^7\text{G}^9\text{T}^9$  loops. The synthesized E-containing TBA oligonucleotides are listed in Table 1. As shown, TBA oligonucleotides  $\text{T}^3_{\text{E}}$ ,  $\text{T}^4_{\text{E}}$ ,  $\text{T}^7_{\text{E}}$  and  $\text{T}^9_{\text{E}}$  represent single substitutions of T at positions 3, 4, 7 and 9 respectively, while oligonucleotides  $\text{T}^3_{\text{E}}\text{T}^4_{\text{E}}$  and  $\text{T}^7_{\text{E}}\text{T}^9_{\text{E}}$  represent double substitutions in the loop regions at positions indicated by the numbers.

CD spectra of TBA oligomers singly substituted with E ( $\text{T}^3_{\text{E}}$ ,  $\text{T}^4_{\text{E}}$ ,  $\text{T}^7_{\text{E}}$  and  $\text{T}^9_{\text{E}}$ ; Figure 2 and Supporting Information, Figure S6) were characterized by high amplitude, positive maxima at

Oligonucleotide	Sequence
TBA	GGTTGGTGTGGTTGG
$\text{T}^3_{\text{E}}$	GGETGGTGTGGTTGG
$\text{T}^4_{\text{E}}$	GGTEGGTGTGGTTGG
$\text{T}^7_{\text{E}}$	GGTTGGEGTGGTTGG
$\text{T}^9_{\text{E}}$	GGTTGGTGEGETTGG
$\text{T}^3_{\text{E}}\text{T}^4_{\text{E}}$	GGEEGGTGTGGTTGG
$\text{T}^7_{\text{E}}\text{T}^9_{\text{E}}$	GGTTGGEGETTGG

E = ethylene glycol

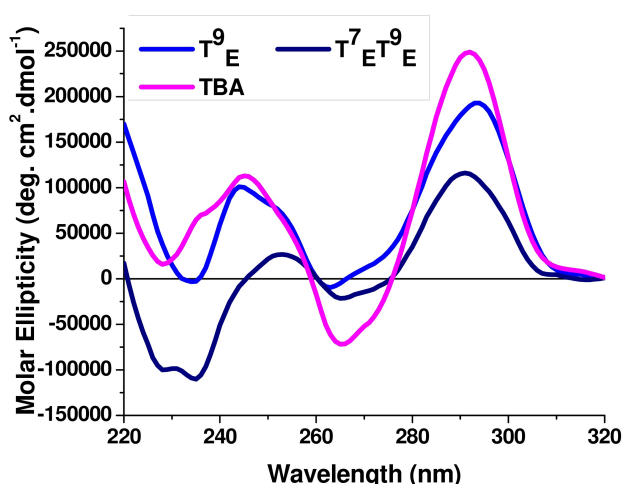


Figure 2. CD spectra of  $\text{T}^9_{\text{E}}$ ,  $\text{T}^7_{\text{E}}\text{T}^9_{\text{E}}$  and TBA oligomers taken at a conc. of 5  $\mu\text{M}$  in 10 mM potassium phosphate buffer, pH 7.2, containing 100 mM KCl, recorded at 4 °C.

295 nm and 240 nm and minima at 260 nm, in comparison to TBA oligomers bearing two E substitutions ( $\text{T}^3_{\text{E}}\text{T}^4_{\text{E}}$  and  $\text{T}^7_{\text{E}}\text{T}^9_{\text{E}}$ ; Figure 2 and Supporting Information, Figure S6), where the lowest amplitude was observed for  $\text{T}^7_{\text{E}}\text{T}^9_{\text{E}}$ . In the presence of  $\text{Na}^+$ , all the modified oligomers displayed CD signals of lower amplitude and differing in their maxima/minima when compared to TBA (Supporting Information, Figure S7). Since a CD spectrum can be used to distinguish between parallel and antiparallel quadruplex folding topologies, where a parallel quadruplex shows maxima typically at 260 nm and an antiparallel quadruplex at 295 nm,<sup>[16]</sup> it can be concluded that the E-modified oligomers fold into antiparallel quadruplexes in the presence of  $\text{K}^+$  ions (Figure 2, Supporting Information, Figure S6). In presence of  $\text{Na}^+$  ions,  $\text{T}^4_{\text{E}}$  and  $\text{T}^9_{\text{E}}$  showed signals characteristic of antiparallel conformation, while the CD spectra of the other oligomers were inconclusive (Supporting Information, Figure S7). The presence of G-quadruplexes was further confirmed by recording the Raman spectra, where signals typically observed in G-quadruplexes were seen (Supporting Information, Figure S8 and Table S1).

The melting temperature of the quadruplexes estimated by UV and CD spectroscopy, indicate that the E unit has a destabilizing effect on the thermal stability of TBA ( $\Delta T_m > -15$  °C; Supporting Information, Figure S9, S10 and Table S2). The  $\text{T}^3_{\text{E}}\text{T}^4_{\text{E}}$  oligomer, in particular, was largely destabilized and melted below 20 °C. Thus, the shorter E unit had a negative effect on the thermal stability of the resulting quadruplexes, in comparison to the one carbon longer C3-spacer,<sup>[10]</sup> where a stabilizing effect was reported.

The UV-TDS signature for a G-quadruplex structure,<sup>[17]</sup> that consists of a negative band centered at  $\sim 295$  nm, with positive bands at  $\sim 273$  nm and  $\sim 242$  nm, that was observed for TBA, was also seen for the E-substituted oligomers (Supporting Information, Figure S11), indicating quadruplex formation for all these oligomers. The UV-TDS spectrum of  $\text{T}^3_{\text{E}}\text{T}^4_{\text{E}}$  showed a low intensity negative band near 295 nm, and poorly defined peaks around 273 nm and 242 nm, in comparison to the other oligomers, probably indicative of a weaker, imperfectly formed quadruplex in this case, in accordance with data from the melting studies.

The stability of  $\text{T}^7_{\text{E}}\text{T}^9_{\text{E}}$  as a representative oligomer against nuclease degradation was studied in comparison to TBA. As the modified units are present at internal positions in the  $\text{T}^7_{\text{E}}\text{T}^9_{\text{E}}$  oligomer, S1 nuclease was chosen for the study, that is a non-specific endonuclease. The stability of the oligomers was monitored by measuring the peak area in the HPLC chromatograms at successive time intervals upon treatment with the nuclease. From Figure 3, it is evident that  $\text{T}^7_{\text{E}}\text{T}^9_{\text{E}}$  bearing two E units, with a half-life of nearly 15 min, was much stabler than TBA ( $t_{1/2} < 3$  min).

The chaperone effect of thrombin,<sup>[18]</sup> evident from the increasing CD amplitude at 295 nm, confirmed the binding of the oligomers containing single E substitutions (Supporting Information, Figure S12). This effect was not observed for  $\text{T}^3_{\text{E}}\text{T}^4_{\text{E}}$  and  $\text{T}^7_{\text{E}}\text{T}^9_{\text{E}}$ , indicative of very poor binding to thrombin for these oligomers.

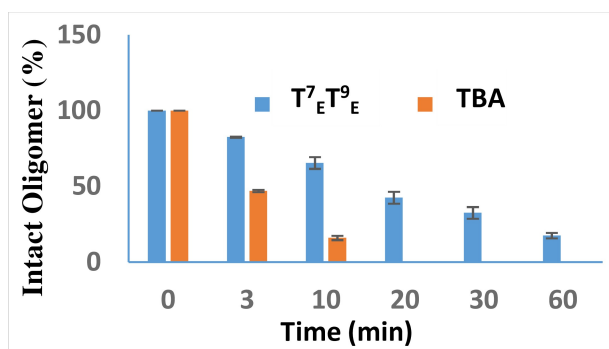


**Figure 3.** S1 Nuclease stability study of  $T^7E^9E$  in comparison to TBA. S1 nuclease (89 U/mL) at 37 °C in reaction buffer (pH 4.5) containing 0.05 M sodium acetate, 0.28 M NaCl, and 4.5 mM  $ZnSO_4$ ; oligomer concentration 7.5  $\mu$ M.

Since TBA is known to slow down coagulation, a thrombin time assay involving the conversion of fibrinogen to fibrin in the presence of thrombin was performed to evaluate the anticoagulant activity of the oligomers (Figure 4). The four variants containing single E spacers, namely  $T^3E$ ,  $T^4E$ ,  $T^7E$  and  $T^9E$ , showed thrombin inhibitory effects (clotting time ranging from 53 s to 65 s), lower than TBA (76 s), whereas oligomers  $T^3E^4E$  and  $T^7E^9E$  bearing two E units each, with clotting times of 47 s and 40 s respectively, showed even lower anti-thrombin effects and only a slight delay in the coagulation process. The highest anticoagulant effect was observed with  $T^9E$ , with a 65 s clotting time, a delay of 31 s in comparison to the control (clotting time 34 s) when no oligomer was added.

In conclusion, our studies with a 2-carbon E spacer have shown that single replacement of loop residues by E spacer are tolerated better than two. Although a beneficial effect on the nuclease stability and half-life of the oligomers was observed, the lower thermal stability and anti-clotting effect observed with the 2-carbon E spacer in comparison to the 3-carbon spacer unit (Supporting Information, Table S3) suggests that this shorter backbone is less tolerated in TBA.

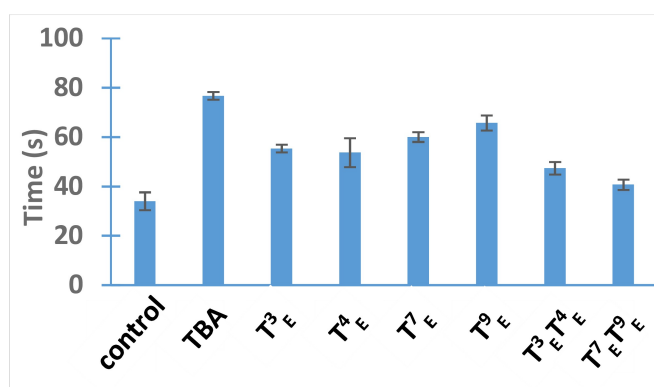


**Figure 4.** Clotting time measured as the time required for fibrin polymerization upon addition of thrombin to fibrinogen in the presence of added oligomers. control: clotting time in the absence of any added oligomer.

## Supporting Information available

Synthetic procedures, experimental details, characterization data, UV and CD data.

## Acknowledgements

Research funding from SERB (EMR/2014/000481/OC) is gratefully acknowledged. AAW thanks UGC for a research fellowship.

## Conflict of Interest

The authors declare no conflict of interest.

**Keywords:** aptamers · clotting time · ethylene glycol spacer · G-quadruplexes · nuclease stability

- [1] S. Burge, G. N. Parkinson, P. Hazel, A. K. Todd, S. Neidle, *Nucleic Acids Res.* **2006**, *34*, 5402–5415.
- [2] L. C. Bock, L. C. Griffin, J. A. Lantham, E. H. Varmaas, J. J. Toole, *Nature* **1992**, *355*, 564–566.
- [3] J. A. Kelly, J. Feigon, T. O. Yeates, *J. Mol. Biol.* **1996**, *256*, 417–422.
- [4] R. F. Macaya, P. Schultze, F. W. Smith, J. A. Roe, J. Feigon *Proc. Natl. Acad. Sci. USA* **1993**, *90*, 3745–3749.
- [5] S. Lancellotti, R. De Cristofaro, *Cardiovasc. Hematol. Agents Med. Chem.* **2009**, *7*, 19–28.
- [6] Avino, C. Fabrega, M. Tintore, R. Eritja, *Curr. Pharm. Des.* **2012**, *18*, 2036–2047.
- [7] M. Scuotto, E. Riviaccio, A. Varone, D. Corda, M. Bucci, V. Vellecco, G. Cirino, A. Virgilio, V. Esposito, A. Galeone, N. Borbone, M. Varra, *Nucleic Acids Res.* **2015**, *43*, 7702–7716.
- [8] A. S. Gouda, M. S. Amine, E. B. Pedersen, *Helv. Chim. Acta* **2016**, *99*, 116–124.
- [9] T. Bose, V. A. Kumar, *Tetrahedron* **2017**, *73*, 1534–1540.
- [10] L. J. Aaldering, V. Poongavanam, N. Langkjaer, N. A. Murugan, P. T. Jorgensen, J. Wengel, R. N. Veedu, *ChemBioChem.* **2017**, *18*, 755–763.
- [11] A. Ali, G. A. Bullen, B. Cross, T. R. Dafforn, H. A. Little, J. Manchester, A. F. A. Peacock, J. H. R. Tucker, *Chem. Commun.* **2019**, *55*, 5627–5630.
- [12] M. Mo, D. Kong, H. Ji, D. Lin, X. Tang, Z. Yang, Y. He, L. Wu, *Bioconjugate Chem.* **2019**, *30*, 231–241.
- [13] K. Padmanabhan, K. P. Padmanabhan, J. D. Ferrara, J. E. Sadler, A. Tulinsky, *J. Biol. Chem.* **1993**, *268*, 17651–17654.
- [14] I. R. Krauss, A. Merlino, A. Randazzo, E. Novellino, L. Mazzarella, F. Sica, *Nucleic Acids Res.* **2012**, *40*, 8119–8128.
- [15] M. Fontanel, H. Bazin, R. Téoule, *Nucleic Acids Res.* **1994**, *22*, 2022–2027.
- [16] C. Tang, R. H. Shafer, *J. Am. Chem. Soc.* **2006**, *128*, 5966–5973.
- [17] J. L. Mergny, J. Li, L. Lacroix, S. Amrane, J. B. Chaires, *Nucleic Acids Res.* **2005**, *33*, 1–6.
- [18] E. Baldrich, C. K. O'Sullivan, *Anal. Biochem.* **2005**, *341*, 194–197.

Submitted: June 28, 2021

Accepted: October 7, 2021